SEPTEMBER 1960 VOLUME 8 (1960) No. 3

GREGG M. SINCLAIR LIBRARY
UNIVERSITY OF HAWAII
8-7-63

NUCLEAR INSTRUMENTS & METHODS

A JOURNAL ON ACCELERATORS, INSTRUMENTATION AND TECHNIQUES IN NUCLEAR PHYSICS

EDITOR: K. SIEGBAHN - UPPSALA

LAST NUMBER OF THIS VOLUME

CONTENTS

J. J. BURGERJON and W. WEIDEMANN, The Pretoria cyclotron, Second Report 261
F. S. GOULDING, R. W. NICHOLSON and J. B. WAUGH, A double-delay-line linear amplifier employing transistors I 272
F. S. GOULDING and R. A. MCNAUGHT, A transistorized fast-slow coincidence and pulse amplitude selecting system II 282
J. B. MARION, R. J. A. LEVESQUE, C. A. LUDEMANN and R. W. DETENBECK, A versatile, high efficiency 4π neutron detector 297
E. ZACCHERONI, H. F. power meter for operation at 2.5 MW pulsed power 304
R. D. BIRKHOFF, J. M. KOHN, H. B. ELDRIDGE and R. H. RITCHIE, The spherical condenser as a high transmission particle spectrometer II. Disc source 313
G. G. EICHHOLZ, Continuous monitoring of uranium leach solutions 320

(continued on p. 3 of cover)

NORTH-HOLLAND PUBLISHING COMPANY — AMSTERDAM

NUCLEAR INSTRUMENTS AND METHODS

A journal on accelerators, instrumentation and techniques in nuclear physics

EDITOR: K. SIEGBAHN, UPPSALA

EDITORIAL BOARD:

J. B. ADAMS (CERN)
F. A. ALSINA (Buenos Aires)
E. AMALDI (Rome)
H. L. ANDERSON (Chicago)
K. T. BAINBRIDGE (Cambridge, Mass.)
P. R. BELL (Oak Ridge)
R. E. BELL (Montreal)
A. BERTHELOT (Saclay)
H. BRINKMAN (Groningen)
E. H. COOKE–YARBOROUGH (Harwell)
S. DE BENEDETTI (Pittsburgh)
M. DE HEMPTINNE (Louvain)
A. DE-SHALIT (Rehovoth)
M. DEUTSCH (Cambridge, Mass.)
S. DU TOIT (Pretoria)
B. S. DŽELEPOV (Leningrad)
W. GENTNER (Heidelberg)
P. C. GUGELOT (Amsterdam)
H. HALBAN (Paris)
O. HAXEL (Heidelberg)
P. HUBER (Basel)
S. KIKUCHI (Tokyo)
J. KOCH (Copenhagen)
M. S. KOZODAEV (Moscow)
S. LIVINGSTON (Cambridge, Mass.)
E. M. MCMILLAN (Berkeley)
M. G. MEŠČERJAKOW (Moscow)
P. B. MOON (Birmingham)
M. L. OLIPHANT (Canberra)
W. PAUL (Bonn)
A. S. RAO (Bombay)
G. SALVANI (Rome)
P. SAVIĆ (Belgrade)
P. SCHERRER (Zürich)
CH. SCHMELZER (CERN)
R. TANGEN (Oslo)
D. TAYLOR (Northampton)
V. I. VEKSLER (Moscow)
G. VON DARDEL (CERN)
O. WERNHOLM (Stockholm)
R. R. WILSON (Cornell)
S. D. WINTER (Saclay)

INSTRUCTIONS FOR CONTRIBUTORS

Contributions may be sent to the Editor, Professor K. Siegbahn, Institute of Physics, University of Uppsala, Sweden, either directly or through the intermediation of one of the members of the Editorial Board. Contributions may be written in English, French or German but should always, except for very short papers, be supplied with a brief abstract in English. Figures should be in inked original drawings or glossy prints and they should be sufficiently large. Contributors should make sure that important details in drawings and photographs will show up clearly in the diminished copy used by the publisher.

Books for review should be sent to Professor Siegbahn.

Objective and descriptive material on endeavours and product developments from the industry for the section "Spotlight on Industry" should be sent directly to the publishers, North-Holland Publishing Company, P.O. Box 103, Amsterdam.

Nuclear Instruments and Methods is published monthly. The subscription price of a volume of 360 pages is $ 17.00 (130 s), postage free.

Subscriptions should be sent to the publishers, North-Holland Publishing Company, P.O. Box 103, Amsterdam, or to any subscription-agent.

No part of this issue may be reproduced in any form, by print, photoprint, microfilm or any other means without written permission from the publisher.

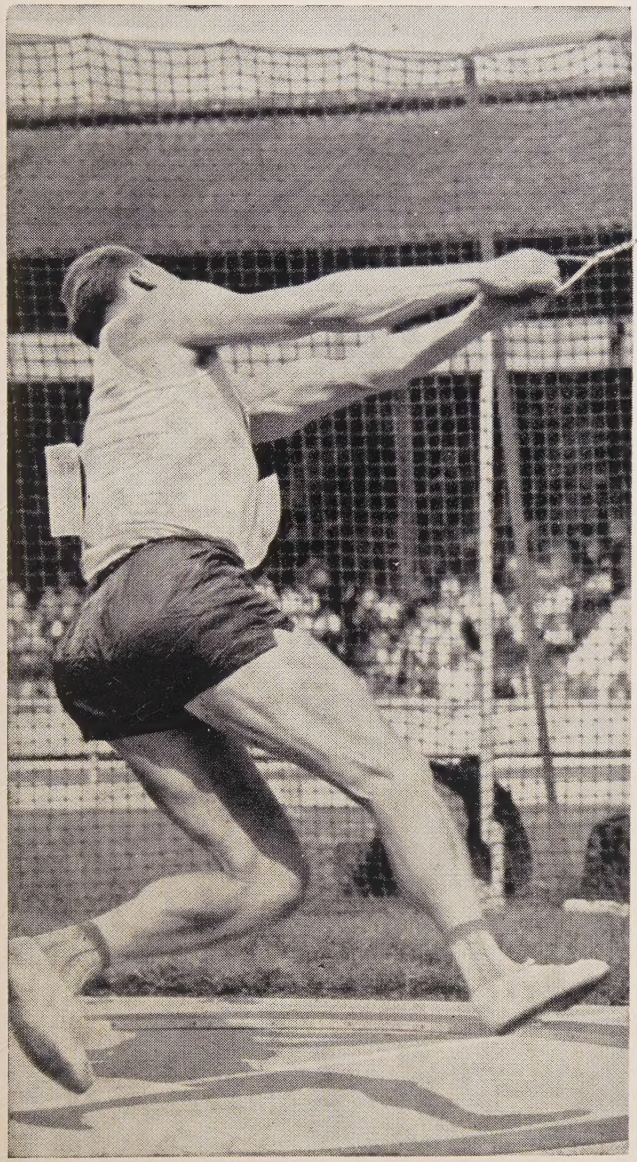

PHILIPS

The possibility of imparting through centrifugal force kinetic energy sufficient to transform a body into a projectile and hence a weapon, was known even in dim antiquity. Such a projectile in the world of to-day is, of course, of little consequence: only in the realm of athletics does exploitation of the principle to this end still survive, namely, in throwing the hammer. In nuclear physics, however, application of the same principle afforded new possibilities in the quest for attainment of very high elementary particle-speeds. Gigantic installations are now in being where, under the influence of both a magnetic and a rapidly alternating electrical field the particles are brought into a spiral trajectory and accelerated to such a degree that nuclear reactions can be triggered. Philips have for many years been constructing and supplying cyclotrons and synchrocyclotrons on a commercial basis, the 150 MeV synchrocyclotron in operation since February 1959 in the "Laboratoire Nucléaire de la Faculté des Sciences de Paris" in Orsay, France, being but one example of the Philips-made installations. This apparatus, with an internal beam current at 165 MeV of 10 micro-amps and an external beam current of more than 0.4 micro-amps measured behind the deflection magnet, occupies a unique place among the particle accelerators in operation to-day.

NBO

Applied ballistics

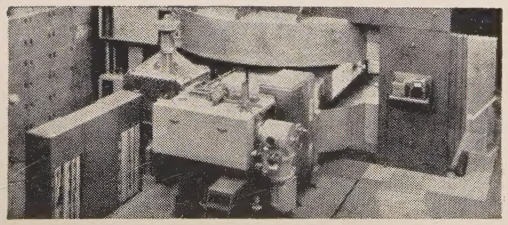

PHILIPS

N.V. PHILIPS' GLOEILAMPENFABRIEKEN EINDHOVEN - HOLLAND

nuclear equipment

Particle accelerators ● Reactor control instrumentation ● Health protection and monitoring equipment ● Radiation measuring and detection equipment ● Geiger counter tubes ● Photomultipliers ● Radio-active isotopes ● Vacuum measuring equipment ● Air and gas liquefiers.

ALL-ROUND, LOW PRICED MONITOR

Typically developed as a laboratory equipment the monitor 111-A1 combines quality and high performance with low cost.

- Completely transistorized
- Designed as portable type
- Very low count rate: 0 to 5 c.p.s. full scale
- Highest count rate: 0 to 5000 c.p.s. full scale
- Equalizing accumulators
- Automatically recharged from A.C. mains
- Priced $ 410 F.O.B. Antwerp

For further information on this and other applications in the field of "Electronics for Nucleonics" ask :

AN ITT ASSOCIATE

Bell Telephone Mfg Co

"NUCLEAR ENERGY DIVISION"
33, Berkenrodelei
HOBOKEN-Antwerp
Belgium

NORTH-HOLLAND BOOKS

Paul Ehrenfest

COLLECTED SCIENTIFIC PAPERS

XII + 632 pages

Guilders 45,00 (90s.)

This volume makes widely scattered publications readily available. All Dutch articles appear here in English; the German publications are in the original language.

Sole Agency for U.S.A.:

Interscience Publishers Inc. — New York

NORTH-HOLLAND PUBLISHING COMPANY - AMSTERDAM

FOR SCINTILLATION & PROPORTIONAL COUNTING

Non-overloading Linear Amplifiers

MODELS 108 and 108 p

* GAIN–40,000, continuously variable
* RISE TIME–0.2 microsecond
* ACCEPTS + AND — PULSES

Tremendous Dynamic Range

EXCEEDS 1,000,000 (0.1 mV to 100 V)

Excellent linearity for small pulses in the presence of tremendous overloads that paralyze other amplifiers.
Model 108 P includes precision trigger type Pulse-Height Selector.

Model 413 Mercury relay precision sliding Pulser

The one pulser that fills every need of the Nuclear Physics Laboratory
0 to 100 Volts

10 full scale ranges from 1 mV to 100 volts
Fast rise and exponential decay of 1, 3, 10. 30, and 100 microsec simulate pulses from scintillation, proportional and Geiger counters.
Incorporates both manual control and precision motor drive.
The ideal instrument for precise calibration and test of pulse-height analyzers and other nuclear instrumentation.

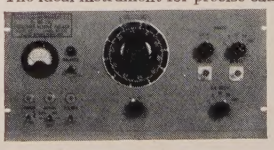

Window widths are determined AUTOMATICALLY, 10 × more ACCURATELY, 40 × FASTER than with conventional pulsers.

Model 108 Amplifier . . . . . $ 545.00
Model 108 P Amplifier (includes pulse-height selector) $ 595.00
Model 413 Precision Sliding Pulser . . . . . $ 630.00
Prices f.o.b. Silver Spring. Md.

RADIATION INSTRUMENT CO.

P.O. BOX 733 SILVERSPRING, MARYLAND, U.S.A.

256 THE TMC 256-CHANNEL PULSE ANALYSIS SYSTEM

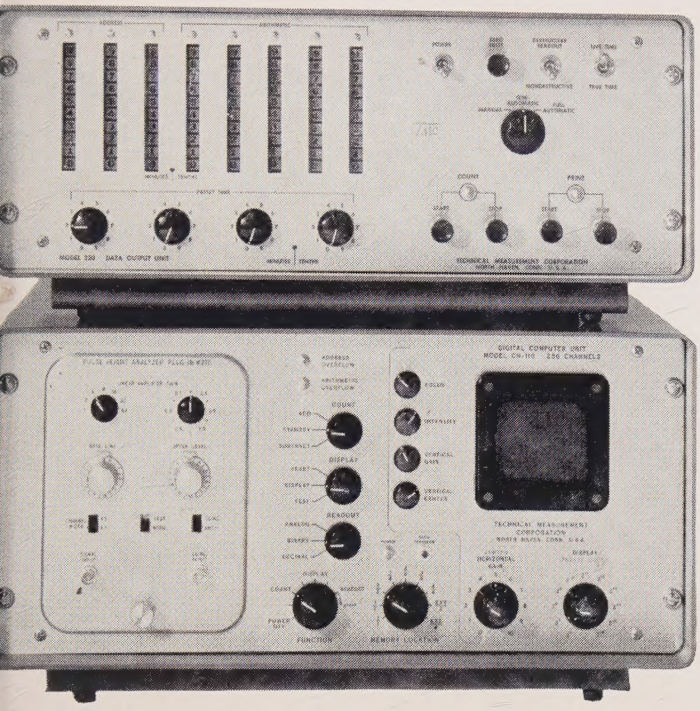

#220 DATA HANDLING UNIT usable as an active timer, event counter and readout device . . . effective or actual counting times may be selected from 0.1 to 999.9 minutes in 0.1 min. steps . . . manual, semi- or fully automatic operation, destructive and non-destructive readout.

TIME-OF-FLIGHT MEASUREMENT #211 plug-in . . . built-in delay of 0, 1, 2, 3 times address cycle . . . choice of 9 channel lengths from 0.25 to 64 μs. . . . automatic channel advance

PULSE HEIGHT ANALYSIS — #210 plug-in . . . built-in linear amplifier, pulse generator . . . 10-74 μs. dead time . . . ±0.5% linearity

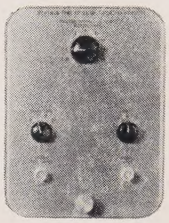

The Model CN-110 digital computer assembly . . . only 8¾" high . . . weighs 30 lbs. with plug-in . . . operates on 25 watts

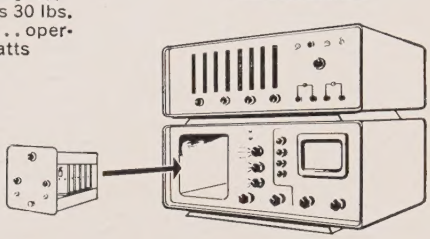

ONE BENCH-TOP INSTRUMENT . . .

Becomes a different pulse analyzer every time you change the logic

PULSED NEUTRON MEASUREMENT — #212 plug-in . . . analysis channel lengths from 10 to 2560 μs. . . . 10 μs. storage time . . . (a high speed arithmetic scaler is supplied with the CN-110 at no extra charge when the 212 unit is purchased with it)

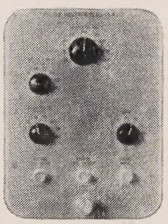

With just one CN-110 in your laboratory you have 256 channels of the pulse analysis you need — whether it's pulse height, time-of-flight, pulsed neutron or a special program. When you plug in the logic network, the instrument becomes a ready-to-use analysis system for that program. And you can change them in the time it takes to loosen a thumbscrew. Total weight is only 30 lbs., all circuits are transistorized — making this today's most versatile, compact pulse analyzer for research, field work or regular laboratory use. *They are now in production and deliveries are being made.*

THE BASIC UNIT IS A COMPLETE DIGITAL COMPUTER with all the circuitry for a 256-channel magnetic core memory and has the advantages of completely enclosed, plug-in memory . . . choice of memory sub-groups . . . pushbutton data transfer . . . instantly selected analog, binary or digital readout.

FOR DATA HANDLING, a readout instrument has been designed specifically for use with the CN-110. The compact #220 data handling unit can be used as a live-timer during data gathering and as a readout system afterward. The #220 can be used with various types of paper tape printing and punching instruments.

Other readout devices that you can use with the CN-110 include strip chart and X-Y recorders, magnetic computer tape, punched paper cards.

Write for the new 6-page bulletin which contains complete details of the CN-110 and all accessories.

TECHNICAL MEASUREMENT CORPORATION TMC 441 WASHINGTON AVE., NORTH HAVEN, CONN.

Elcor inc.
1225 W. BROAD ST.,
FALLS CHURCH, VA.

MODEL A 309
CURRENT INDICATOR AND INTEGRATOR

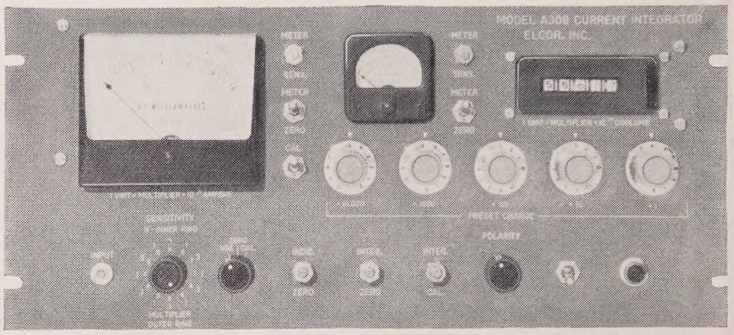

MODEL A 309 A

FEATURES

- Wide current range: 1 x 10^{-3} to 3 x 10^{-9} amp. in 12 switch settings.
- High accuracy: 1% of full scale.
- Internal calibrating current source to check proper operation.
- Front panel switch allows instrument to be used with current of either polarity.
- Pre-setting feature provides means of safeguarding against over-exposure.
- Developed especially for use with Van de Graaff and other high-voltage accelerators.
- Permits many experiments with particle accelerators that would otherwise be difficult or impossible.
- Register readout gives digital accuracy on charge measurement.

The versatility and accuracy of two instruments in one!

1. Measures currents from 1 milliampere to 3 milli-microamperes.
2. Integrates input current and registers accumulated charge.

GENERAL DESCRIPTION—The Model A309 Current Indicator and Integrator is a sensitive current indicator that also measures the total charge collected in a given length of time. Developed especially for use with high-voltage particle accelerators such as the Van de Graaff generator, the instrument is also ideally suited for other applications requiring the measurement of accumulated charge or the integration of a variable current.

The full-scale sensitivity of the instrument can be varied from 1 milliampere to 3 milli-microamperes in twelve ranges. For convenience in checking the performance and accuracy of the instrument, an internal calibrating current source is provided for each range. The accumulated charge is indicated on a 5-decimal-digit register. Any number up to 99,999 can be preset into the instrument, and upon reaching the corresponding charge a relay closes to actuate a warning device or control auxiliary equipment. In applications where X-rays are being generated, this feature affords protection against accidental over-exposure.

Input current of either polarity can be measured and integrated, and a front panel switch enables the instrument to be immediately changed from one polarity to the other. Advanced circuit techniques have been employed to achieve low input impedance, negligible drift, and a high overall accuracy and reliability.

Two models are available with the same specifications except for the method of presetting. In the Model A309A the presetting means consists of five front-panel switches. Presetting in the Model A309B is accomplished by manual adjustment of five presetting wheels that are accessible through the hinged cover of the register used in this model.

SPECIFICATIONS

1. Input current for full-scale meter deflection — 1 x 10^{-3} to 3 x 10^{-9} ampere in twelve switch settings
2. Polarity of input current — positive or negative, controlled by front-panel switch
3. Current indicating means — 4½" meter
4. Charge indicating means — 5-decimal-digit register and 2½" meter
5. Maximum charge indicating capacity — 99,999 units
   Note: Each unit is equal to one coulomb multiplied by the numerical value of the full-scale current.
6. Maximum integrating time — 28 hours
7. Integrating rate for full-scale current — 1 unit per second
8. Method of presetting:
   Model A309A — five front-panel switches
   Model A309B — five presetting wheels in register
9. Accuracy (Indicating and integrating accuracy, based on full-scale current) — 1%
10. Maximum drift — .01% per hour
11. Maximum input voltage for full-scale current — 2 millivolts
12. Minimum signal-source impedance for 1% accuracy — 1 ohm divided by numerical value of full-scale current
13. Calibration — Internal reference current provided for each current range
14. Power Input — 110–125 volts, 50-60 cps
15. Dimensions — 19" wide x 8¾" high x 13¼" deep
16. Mounting — standard 19" relay rack
17. Weight — approximately 25 lbs
18. Price: Model A309A — $1674.00
    Model A309B — $1524.00

ELCOR, — INC. • 1225 W. BROAD STREET • FALLS CHURCH, V

Telephone JEfferson 2-7718

A subsidiary of Fairfax Manufacturing Co., Inc.

Bulletin No. 24-1

One of a series of discussions on topics of particular interest to those employing radioisotopes and tracer techniques.

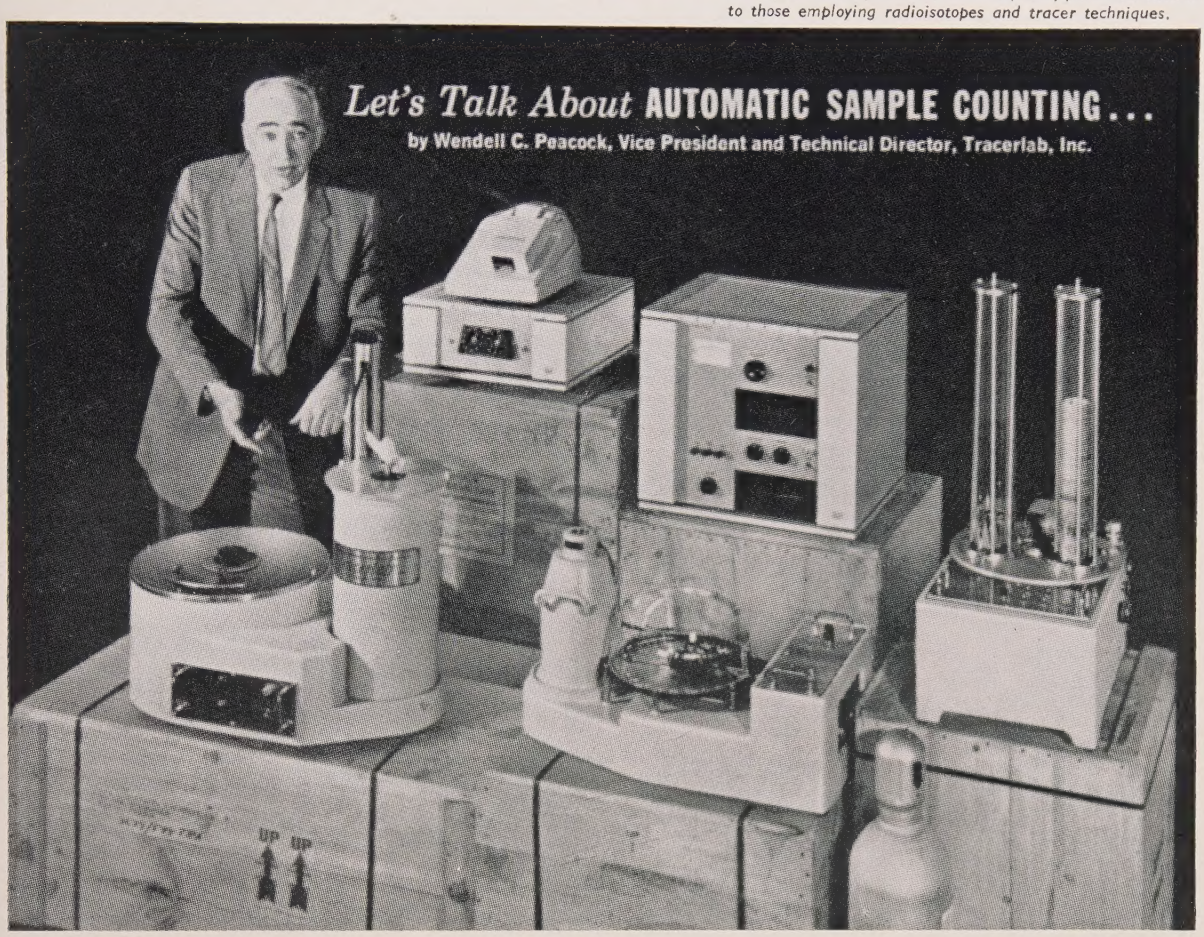

There is nothing complicated about selecting automatic sample counting equipment . . . It simply boils down to a careful analysis of your needs. When you reach the point where automatic equipment is desirable, consider all the equipment commercially available and obtain the following information:

1. Sample Capacity
2. Detection Method
3. Type of Data Printout Provided
4. Simplicity and Versatility
5. Efficiency and Reproducibility
6. Cost
7. The Experience and Reputation of the Manufacturer

Since TRACERLAB introduced the first automatic sample counter and has made most of the significant advances in this important area, it seems logical to check first with TRACERLAB for equipment to meet your requirements. For example:

1. *Sample Capacity?* Standard TRACERLAB counters will accommodate up to 50 samples on planchets, vials or test tubes. Custom-built units accommodating several hundred samples have been supplied.

2. *Detection Method?* For alpha, beta or gamma emitters in either solid or liquid form, TRACERLAB equipment employing your choice of scintillation, geiger and proportional (conventional or flow type, thin window or windowless) detectors, is available to count samples automatically.

3. *Type of Printout?* With TRACERLAB equipment it's your choice. Most users prefer the convenience of the complete sample data (sample number, count, time and count rate) provided by TRACERLAB's Auto/Computer and Auto/Printer. Records are always *complete* and an overriding preset-time, preset-count feature permits frequent insertion of background samples without excessive time delays. However, if the economy of a printing timer is desired, this is also available. And remember, whether you wish to use commercial tape punch or card punch machines, TRACERLAB systems will function smoothly and effectively with almost any system you choose.

4. *Simplicity and Versatility?* All TRACERLAB automatic sample counting systems employ the same scalers and data printers. Therefore, when you need a second automatic sample changer, a stepping chromatogram, a stepping spectrometer or manual equipment, there's no need to purchase duplicate instrumentation. What's more, you won't find any huge complex consoles with *"intergalactal"* control panels in TRACERLAB systems. They have a minimum of controls, require very little bench space, and can be serviced and maintained with ease.

5. *Efficiency and Reproducibility?* Vital points in any technical comparison. The need for high efficiency is obvious but without reproducibility an automatic sample counting system is worthless. Ask about efficiency and reproducibility and remember that TRACERLAB makes every effort to optimize both features.

6. *Cost?* Don't be misled when you price an automatic system. Be sure to include *all* of the components and accessories required for a complete functioning unit; you'll be surprised at the relatively low cost of a TRACERLAB system. The cost will be even less if you already own a Tracermatic scaler because all scalers in TRACERLAB's new line have built-in automatic capabilities.

7. *Experience and Reputation of the Manufacturer?* Remember these facts and decide for yourself. TRACERLAB not only made the first commercial automatic sample counting system, but is today the *only* company which designs and manufactures not just one or two, but a complete line of automatic sample counting systems.

In short, TRACERLAB can provide automatic sample changers and systems to meet your every requirement and, most important of all, you get everything you need from a single source.

For complete information on TRACERLAB's automatic sample changers and the complete line of TRACERLAB nuclear equipment, write for your copy of the new General Catalog F.

Tracerlab *first in radiation measurement*

Tracerlab KELEKET

TRACERLAB, INC. • 1610 Trapelo Rd., Waltham 59, Mass. • 2030 Wright Ave., Richmond, Calif.

European Office: TRACERLAB (Holland) N.V., 119 Singel, Amsterdam, Netherlands

"PLANNAIR" GAS CIRCULATION BLOWERS FOR NUCLEAR PROJECTS

The AGR 19 Fuel Element Cluster CO_2 circulator, here illustrated, provides for reliable and efficient cooling of nuclear reactors. The blower, with its 11,500 r.p.m. motor (200V 400 c/s supply), is sealed within a long pressure vessel at the opposite end to which the nuclear reaction occurs. CO_2 circulates through the tube at 285 p.s.i. A and 95°C. The blower output is 6300 lb./hour at 7.5 p.s.i. pressure differential. A secondary radial impeller gives a cooling gas circuit via a demineralised water heat exchanger coil which keeps the motor operating at below 75°C.

This is but one of several gas circulating blowers which Plannair have designed for various nuclear projects. These include a Leaky Cartridge Test Rig Air-Blower, a Sodium Loop-Nitrogen Circulator, a Helium Circulator, Air Circulators and a Nitrogen Circulator for R.3 Adam, CO_2 circulator for Fuel Element Cluster Irradiation Test Rig, Burst Fuel Element Test Rig Air-Blower.

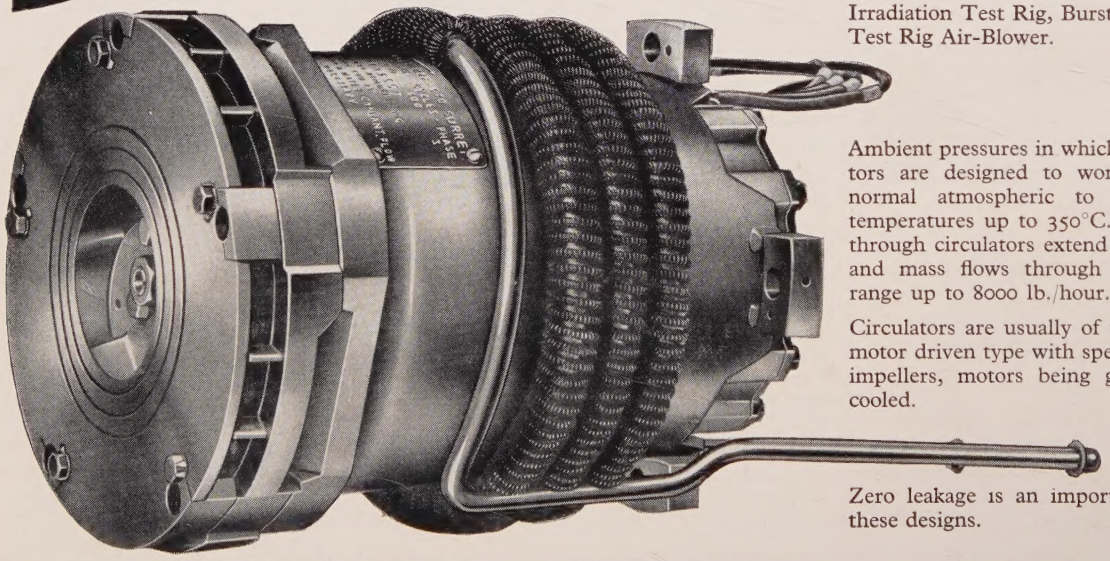

Ambient pressures in which these circulators are designed to work range from normal atmospheric to 300 p.s.i. at temperatures up to 350°C. Pressure rises through circulators extend up to 30 p.s.i. and mass flows through units cover a range up to 8000 lb./hour.

Circulators are usually of the high speed motor driven type with specially designed impellers, motors being gas and liquid cooled.

Zero leakage is an important feature of these designs.

Further details available on request.

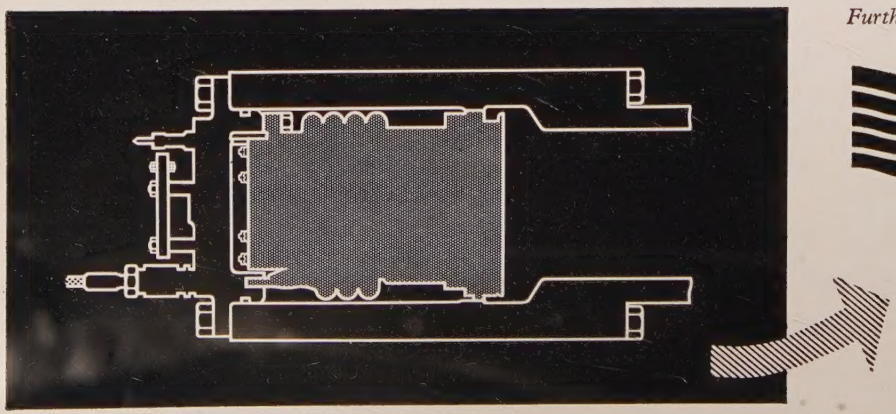

PLANNAIR

PLANNAIR LIMITED

Winfield House • Epsom Road

Leatherhead • Surrey

Tel: Leatherhead 4091/3, 2231

PLA39a

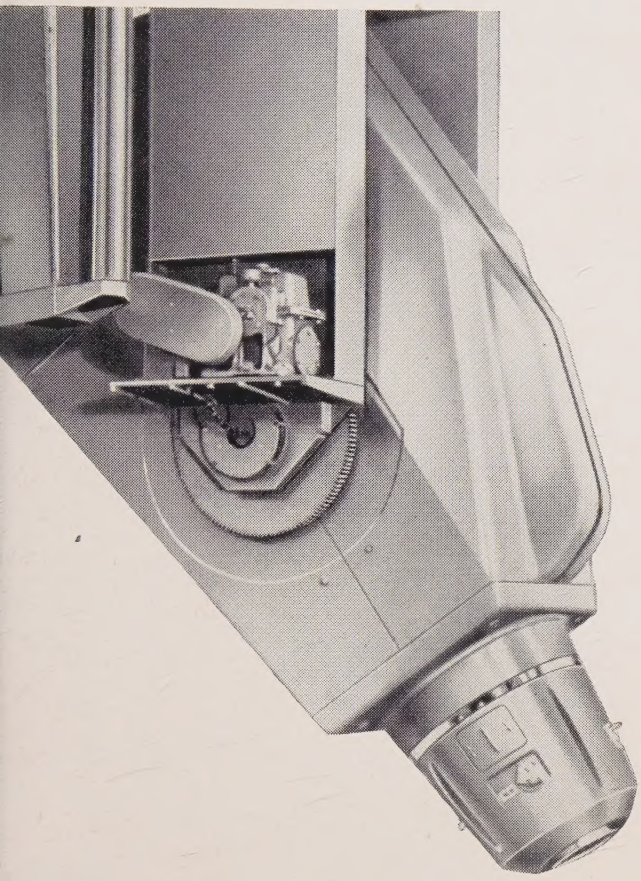

electron linear accelerators for research, industry and medicine

by Mullard Equipment Limited

Electron Linear Accelerators manufactured by Mullard Equipment Ltd. are the logical result of wide and detailed experience in this field. Machines for all types of applications are available, from the standard 4.3 MeV model to equipments specially built to meet individual requirements with electron beam energies up to 50 MeV.
The units are designed for continuous operation, ease of control and high reliability.

STANDARD MACHINE OPERATING AT 4.3 MeV

Mean power output at 500 pulses per second	850 W (electrons)
Maximum pulse repetition frequency.....	500 p.p.s.
Electron pulse length.....	1.65 microseconds
When used as an X-Ray source maximum X-Ray output is approximately.....	600 röntgens per minute at 1 metre

MULLARD EQUIPMENT LIMITED

Mullard House · Torrington Place London W.C.1 · Tel: LANgham 6633

RESEARCH Now regarded as indispensable in many research laboratories Linear Accelerators can be fitted with supplementary heads to provide X-Rays or neutrons. Present day applications include investigation of properties of irradiated materials; preservation of food; basic studies on structure of organic molecules; modification of the properties of plastics.

INDUSTRIAL RADIOGRAPHY The compact accelerator design with wide range of movements and precision positioning enables radiographs of complicated heavy metal sections to be taken with minimum setting-up times. The high X-Ray output gives short exposure time and the extremely small (2mm) focal spot gives the highest possible definition. Penetration is sufficient to radiograph steel sections up to 12 inches thick.

MEDICAL THERAPY The use of Linear Accelerators for X-Ray and Electron Medical Therapy is well established. These machines give rapid treatment times with precisely defined fields and negligible 'penumbra' effects. Skin and exit dosages are minimised.

ME 664

Eldorado

DECIMAL SCALERS FOR THE NUCLEAR PHYSICIST

100% SOLID STATE

...and Fast

Eldorado solid state all-electronic scalers count random events at a maximum rate of over one million counts per second. Resolving time is less than 1.0 microsecond. Especially well-suited for accelerator counting room service, these compact instruments weigh just 13 pounds and use ⅓ fewer transistors than comparable models. They can be used wherever the advantages of complete transistorization are important.

Eldorado offers three standard models in the SC-750 series, each with built-in regulated power supply. Two models provide full electronic storage of 10^7 and 10^8 counts. The third has 3 decades of electronic storage and a 4-digit mechanical register. Special versions can be furnished with other counting combinations and provisions for readout to a printer or tape punch.

KEY SPECIFICATIONS

SCALER	
Resolution	Better than 1.0 microsecond
Max. Counting Rate	Greater than 1 megacycle
AMPLIFIER (optional)	
Minimum Input Signal	10 millivolts
Overload Recovery	100 X, 7 microsecond
DISCRIMINATOR TYPE	Integral
RANGE	1 to 11 volts
SIZE	19 x 3¼ x 10½ inches

Eldorado can furnish scalers and counters to fit your specific application. For more details, please address Dept. 79

Eldorado Electronics

2821 Tenth Street
Berkeley 10, California

How to detect and measure α, β, γ

Choose one of these four combinations for a compact, all-purpose laboratory:

- ❶ ... or
- ❶ + ❷ ... or
- ❶ + ❸ ... or
- ❶ + ❷ + ❸

❶ PROPORTIONAL COUNTING SYSTEM

(PC-3A)

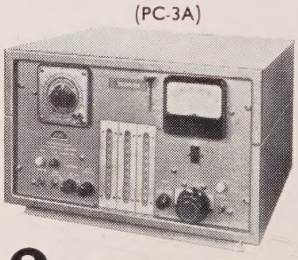

Precision detection and counting of alpha and beta-gamma activity in prepared samples. No window absorption. Full 2 pi geometry. Sample analyzed directly inside detecting chamber. High voltage and scaling systems operate with US-1 and WSC-1 shown below. Accessories optional.

❷ UNIVERSAL SHIELD

(US-1)

With beta-gamma G-M probe

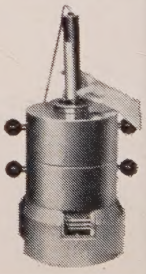

Detects gamma and beta-gamma activity in prepared flat samples. Also accepts gamma scintillation detector, mylar window G-M flow detector, and strip chromatograph scanner. Operates with PC-3A.

❸ WELL-TYPE SCINTILLATION COUNTER

(WSC-1)

Detects low-level gamma activity in test tube type samples. Also takes flat type samples. All-transistorized amplifier. Counter balanced lid. Background lower than 140 cpm. Works with any scaler. Operates with PC-3A.

WRITE FOR CATALOG

NMC

NUCLEAR MEASUREMENTS CORP.

International Office: 13 E. 40th Street, New York 16, N.Y.

Transistorized . . . . . Multichannel Analyzers

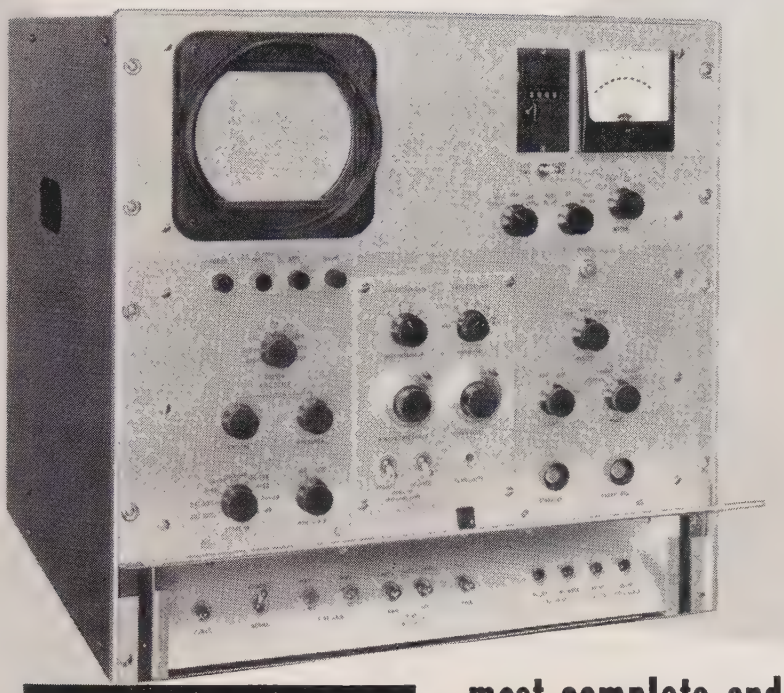

Model 34-8

200-Channel

Model 34-12

400-Channel

- automatic programming including
  - Auto-Print
  - Auto-Record
  - Auto-Transfer
- weight less than 80 pounds
- NOT microminiaturized
- ALL coincidence features
- ferrite core memory
- memory subgrouping
- 10^5 count capacity (10^6 OPT.)
- external programming
- LIVE display
- time analyzer mode
- CRYSTAL controlled live timer
- FAILSAFE channel identification
- simultaneous print and record (OPT.)
- 0.5 percent linearity
- dead time meter
- spectrum transfer circuit

most complete and available line of *TRANSISTORIZED* analyzers

FULLY TRANSISTORIZED . . . Most of the Pulse Height Analyzers produced today are transistorized units, and fully transistorized units have long been in production at RIDL. Full production of complete system RIDL transistorized multi-channel analyzers has allowed RIDL to put many units in the field and to produce additional available 200-channel Model 34-8s and 400-channel Model 34-12s. All models may be operated as **one, two** or **four** independent analyzers, or as multi-channel scalers (time analyzers). All models have **all** the best features of RIDL's best analyzers.

AUTOMATION IN THE LAB . . . RIDL designed the Model 34-8 and Model 34-12 analyzers to save valuable technical man hours through providing such features as **Auto-Print, Auto-Record** and an automatic transfer circuit. A built-in crystal-controlled Live Timer allows automatic **dead time correction.** The addition of automatic **background correction** allows final data readout without laborious manual corrections or replotting of curves.

AUTOMATIC DATA PROCESSING . . . RIDL builds on its maximum development of automatic **data gathering** and **analysis** further possibilities for **automatic data processing.** To normal printing and recording is added readout on **magnetic tape, punched tape,** and parallel or serial entry printers. This allows full control over programming, internal and external data format, and data processing. Whatever your data readout and processing needs may be, our staff is ready at all times to discuss them with you.

SIXTY DAY DELIVERY ON ANALYZERS IN ANY PART OF THE WORLD

Light weight makes AIR SHIPMENT economical.
Chicago to Europe — for example — approximately $150.00
RIDL Representatives are located in most areas of the world.
Contact the RIDL home office for prompt service in locating the sales office nearest you.

RIDL INC.

Radiation Instrument Development Laboratory, Inc.

61 EAST NORTH AVENUE • NORTHLAKE, ILLINOIS

PHONE: MUrray 1-2323 • Cable Address: RADILAB

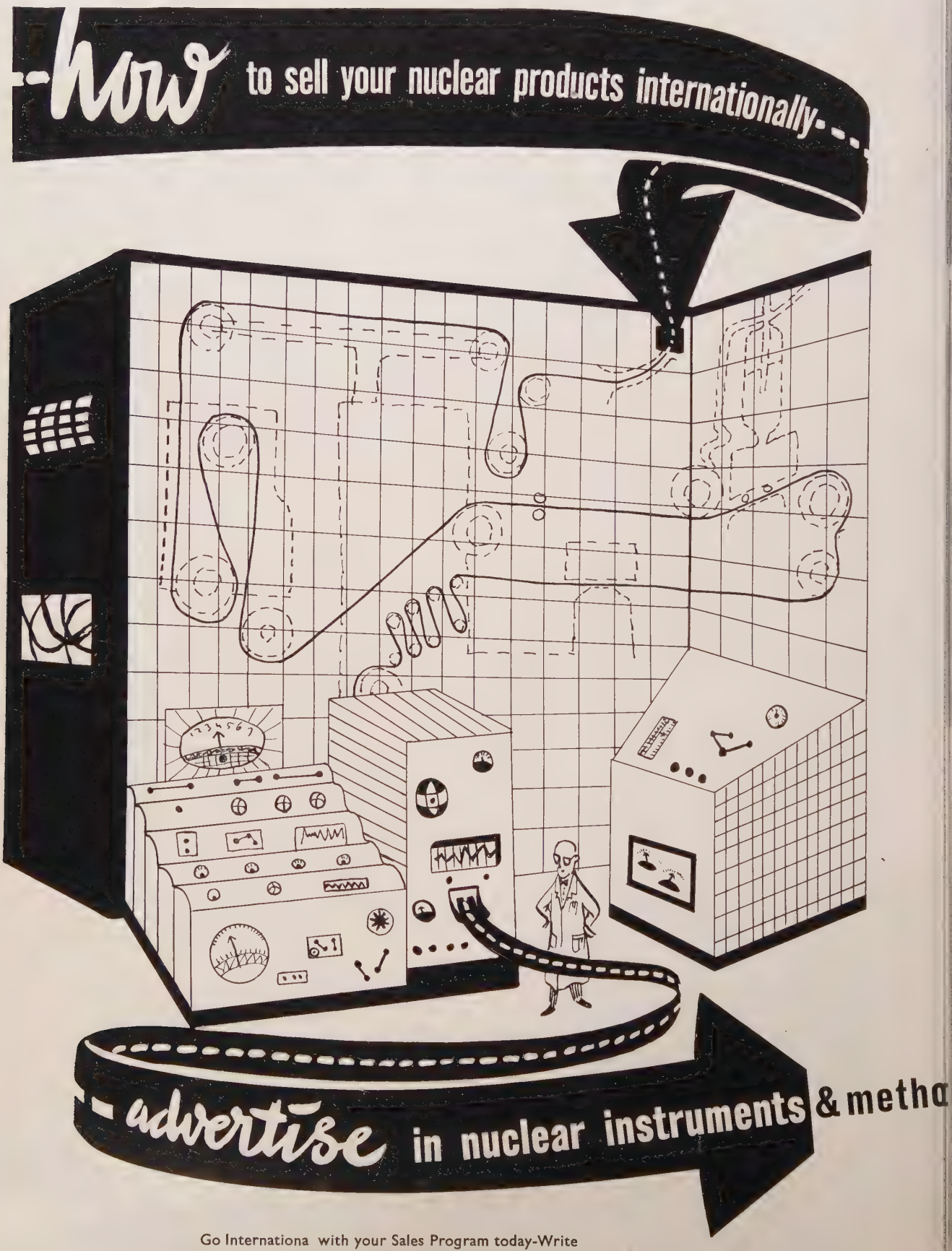

Go Internationa with your Sales Program today-Write

William F. Baars-Advertising Manager, North-Holland Publishing Company

P.O. Box 103, Amsterdam, The Netherlands

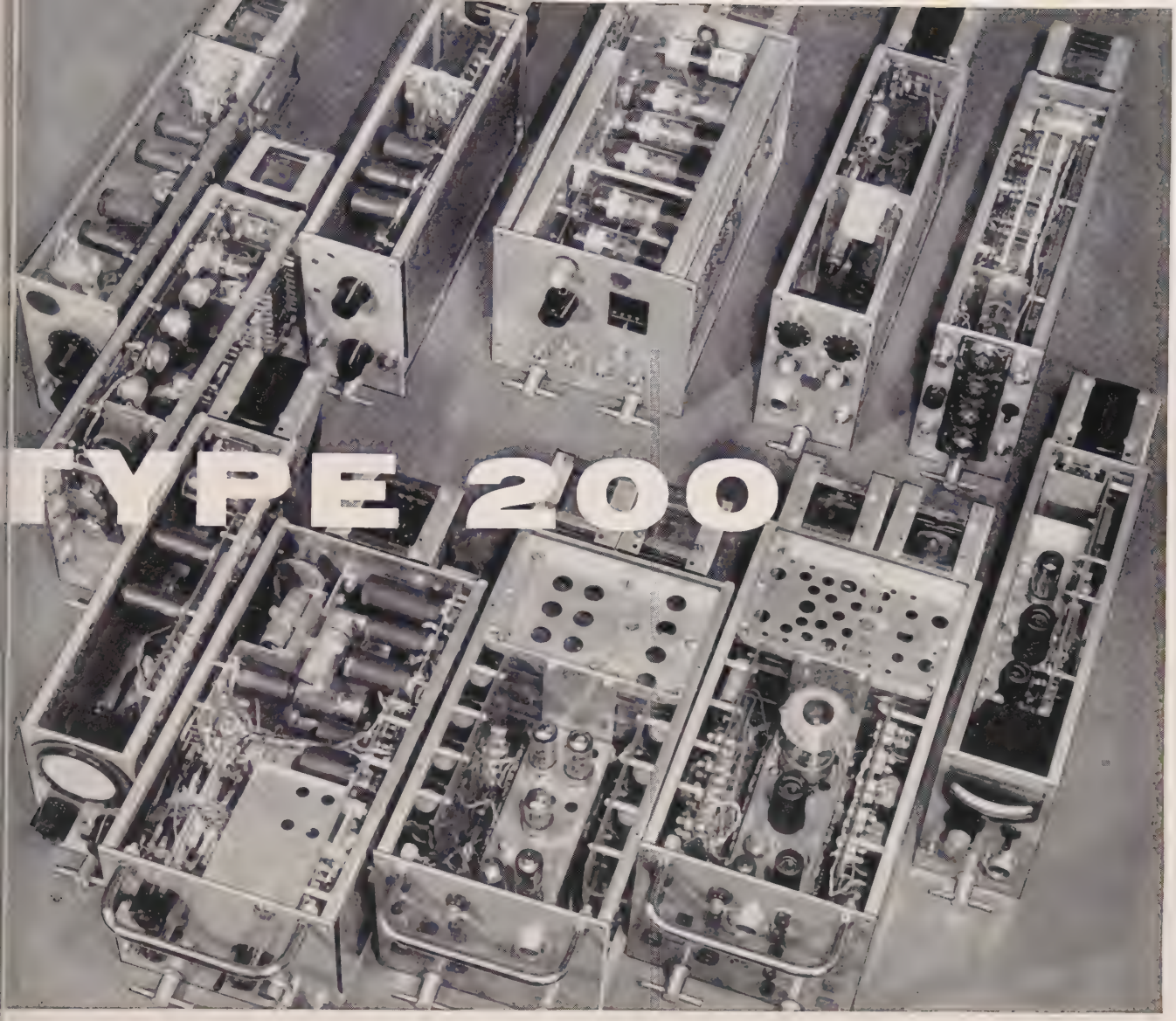

UNITIZED NUCLEONIC RANGE

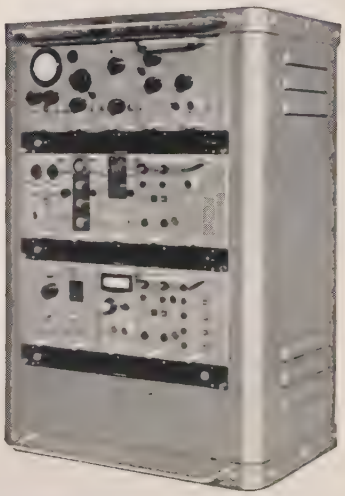

The plan behind this Type 200 equipment is to offer you a Unitized Range (already 24 units and still increasing) not only to cover every type of nucleonic counting, but one that can be added to at will, so that you get only what you want, when you want.

- **Suitable for all types of nucleonic detectors.**
- **Built to a stringent specification.**
- **Designed in conjunction with A.E.R.E. Harwell.**
- **Flexible in use—a unit for every purpose.**

Enquiries should be addressed to:—

INSTRUMENT DIVISION

HIGH CHURCH STREET · NEW BASFORD · NOTTINGHAM

ERICSSON

ERICSSON TELEPHONES LIMITED · HEAD OFFICE · 22 LINCOLN'S INN FIELDS LONDON W.C.2

NUCLEAR PARTICL

ANALYZING MAGNET

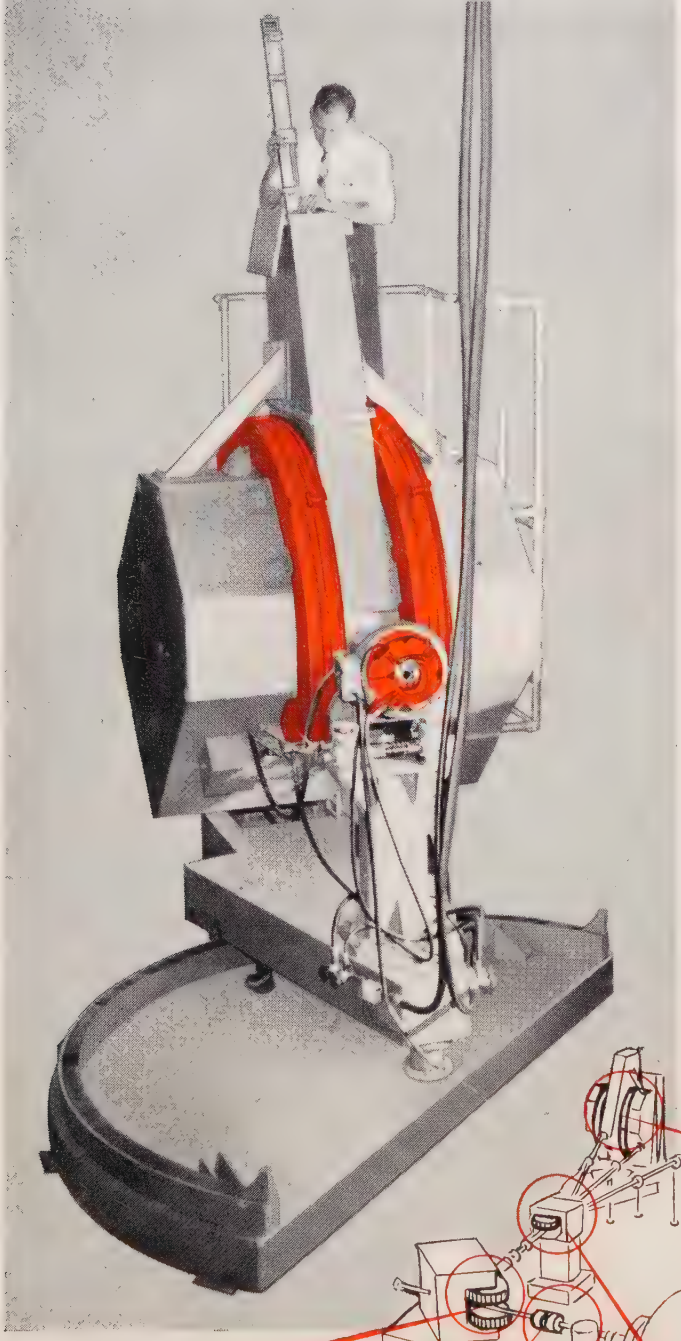

Combined Magnetic Spectrograph and Spectrometer* designed and built for Chalk River Laboratories, Atomic Energy of Canada, Ltd., for energy analysis of protons, deuterons, and alpha particles.

- Magnetic rigidity —
  Up to $B\rho$ = 865 kilogauss-cm (12- Mev tritons)
- Resolving power (spectrograph) —
  $E/\Delta E = 10^3$ or better
- Solid angle (spectrograph) —
  $\Omega = 1.4 \times 10^{-3}$ steradians (max)
- Solid angle (spectrometer) —
  $\Omega = 0.9 \times 10^{-2}$ steradians (max)
- Reaction angle —
  θ = 0 to 135 degrees
- Detector —
  Nuclear track plate and scintillation counter

*For further technical reference, see H.A. Enge, RSI **29**, 885 (1958)

TYPICAL MAGNET SYSTEM FOR 12-MEV TANDEM *Van de Graaff* ACCELERATOR

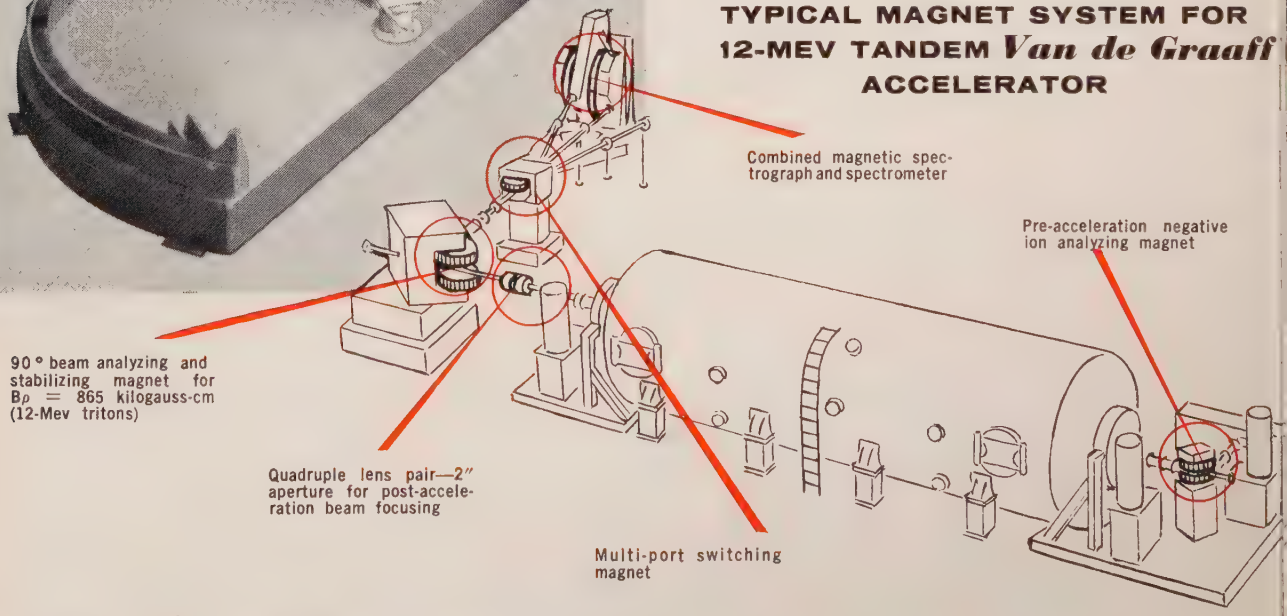
Combined magnetic spectrograph and spectrometer
Pre-acceleration negative ion analyzing magnet
90° beam analyzing and stabilizing magnet for $B\rho$ = 865 kilogauss-cm (12-Mev tritons)
Quadruple lens pair—2" aperture for post-acceleration beam focusing
Multi-port switching magnet

For detailed information on magnets and accelerators, write to Technical Sales:

HIGH VOLTAGE ENGINEERING CORPORATION

BURLINGTON, MASSACHUSETTS – U. S. A.

HIGH VOLTAGE ENGINEERING (EUROPA) N.V. AMERSFOORT, THE NETHERLANDS

NUCLEAR INSTRUMENTS AND METHODS 8 (1960) 261–271; NORTH-HOLLAND PUBLISHING CO.

THE PRETORIA CYCLOTRON

SECOND REPORT

J. J. BURGERJON† and W. WEIDEMANN††

Nuclear Physics Division, National Physical Research Laboratory,
South African Council for Scientific and Industrial Research, Pretoria

Received 15 June 1960

This report deals with improvements to the cyclotron, as well as with the extraction and external focusing of the beam. The various components, in so far as they have been subject to alterations, as well as new components, are described. The properties of both the internal and external beams are discussed in separate chapters. Throughout, reference is made to the first report[1]).

1. General

An audible and visible alarm-system was installed in the cyclotron hall and its entrances, i.e. the waterdoors and the maze-passage from the now completed experimental hall. This alarm is actuated automatically as soon as the cyclotron is potentially dangerous, i.e. when the magnet, the oscillator and the ion-source are in operation simultaneously. It has proved to be a valuable addition to the existing safety measures.

Automatic emergency lighting in all underground halls and passages was installed because of frequent power-cuts on the C.S.I.R. site.

After the completion of the cyclotron experimental hall, it was possible to instal an optical observation system. This makes possible observation of phenomena in the cyclotron hall, and particularly in the vacuum-chamber, through a water window eight feet long and a 4-inch telescope with 25 × magnification, from a radiation-free location.

The polarity of the magnet was reversed to make focusing of the external beam possible at a desired point. For this reason the beam is now accelerated in an anti-clockwise direction.

† From June 1960 at University of Manitoba, Winnipeg, Canada.

†† From August, 1960, at South African Atomic Energy Board, Pretoria.

2. The Magnetic Field

2.1. THOMAS SHIMS

It follows from the previous report that the internal beam position in relation to the geometrical median plane and the internal beam focusing were not of the high quality that would be favourable for successful deflection.

To improve both these properties, new forged pole plates with Thomas shims were fitted[2]). The plates were machined parallel to a thickness of $1\frac{5}{8}''$. This is $\frac{3}{8}''$ thinner than the old ones, to accomodate the Thomas shims, the $\frac{1}{8}''$ Rose shim and the poleface windings. The overall tolerances again are well within the $\pm 0.001''$ limit, while the geometrical positions of the plates and the shims relative to each other and to the pole pieces are fixed within $\pm 0.004''$. No external shims are used, but the $\frac{1}{4}''$ airgaps between poles and plates were filled, after external steering coils proved to be unfeasible. This lowers the generator load by some 6%. In spite of the precise geometry,

[1]) National Physical Research Laboratory. *The Cyclotron of the N. Phys. R. L. First Report.* C.S.I.R. Spec. Techn. Rep. No. E.1., Pretoria, April 1958. A condensed version of this report has been published: J. J. Burgerjon, S. J. du Toit and C. A. J. Kritzinger, The Pretoria Cyclotron., Nucl. Instr. 3 (1958) 323.

[2]) K. Boyer, Los Alamos Scientific Laboratory, U.S.A. Private communication to S. J. du Toit (1957).

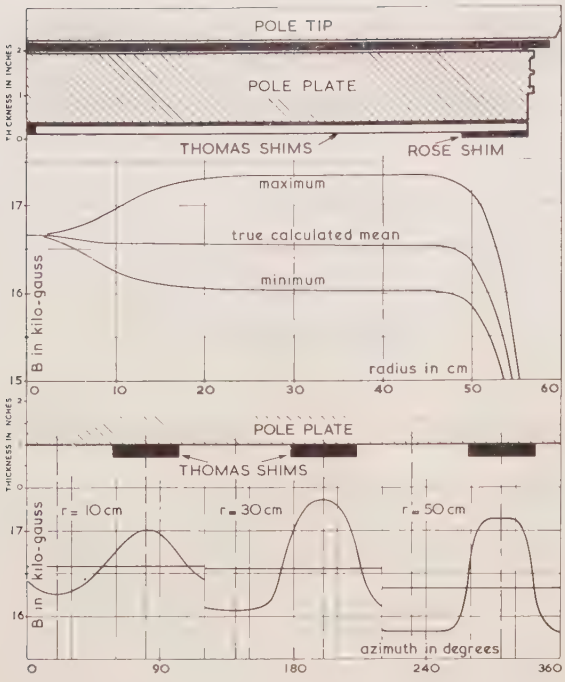

Fig. 1. Radial field plots and azimuthal field curves.

corresponding points of the azimuthally varying field differ by approximately 0.13%.

Fig. 1 shows the shimming, the radial and azimuthal field curves, while fig. 2 shows the various fringing field curves which were measured with a view to extraction calculations. At B in fig. 3 it can be seen that the centre-field versus current plot differs from the previous one because of the alterations.

2.2. POLE FACE WINDINGS

Windings on the interior side of the pole plates were fitted to make possible the choice of any gradient between + 12.7 Gauss/cm and — 14.7 Gauss/cm. As can be seen, working from the centre to the periphery, consecutive areas are surrounded by a diminishing number of turns. By varying the current through the windings it is thus possible to adjust the gradient to any desired value between these limits. The limited number of turns does not appear to have any measurable effect on the smoothness of the radial field plots, which are shown at A in fig. 3.

The water-cooled windings were constructed from $\frac{3}{8}''$ electrolytic copper tubing, flattened to $\frac{1}{8}''$, and insulated by two layers of 0.005″ fibreglass tape. As can be seen on the photograph in fig. 4, they are held in position by grooved polyethylene sectors and the copper linings that cover the whole assembly. At the maximum current of 500 A the waterflow through a coil, slightly increasing with temperature, is approximately 1 l/sec at a pressure of 3 kg/cm². In each coil about 3 kW, supplied by a 6 kW motor-generator set, is dissipated.

2.3. WIRE LOOP CHECK[3])

To determine the radial gradient of an azimuthally homogeneous field that would produce the

[3]) See also G. R. Lambertson, Use of the wire loop in locating the orbital surface of a cyclotron field, U.C.R.L. 3366

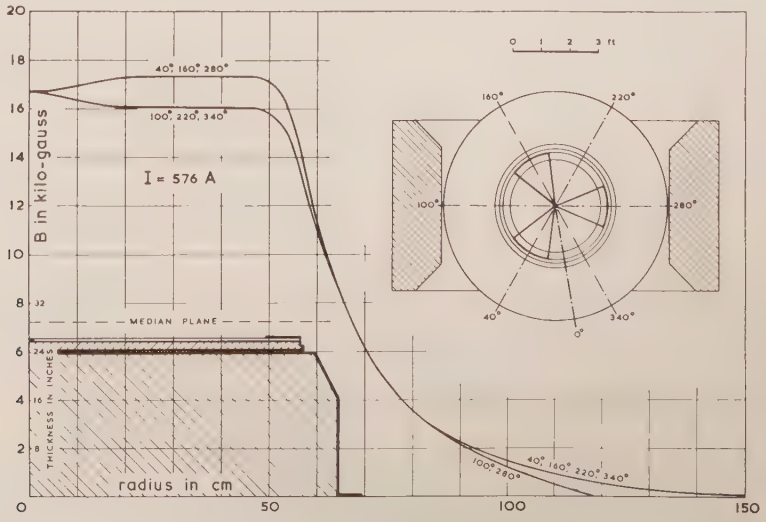

Fig. 2. Fringing field plots.

same focusing effect as the Thomas shims, the following experiment was carried out.

A thin current carrying copper wire loop was suspended by a spring in the vacuum chamber in a position 62 mm above the median plane. As the focusing forces, which act on the beam, act defocusing on the wire, the radial gradient was made focusing for the loop, i.e. positive, and then increased gradually. At a current of 115 A the loop drops, i.e. the focusing radial gradient and the defocusing effect (on the wire) of the Thomas shims are then equal. According to this experiment, the beam-focusing effect of the Thomas shims is roughly equivalent to a radial gradient of 2.2 Gauss/cm.

2.4. STABILIZATION

The galvanometer-type current stabilization of $\pm$ 0.01%, described in the previous report, proved inadequate for successful beam deflection, as the orbit position tends to change together with the degree of resonance. As the current fluctuations of short duration only

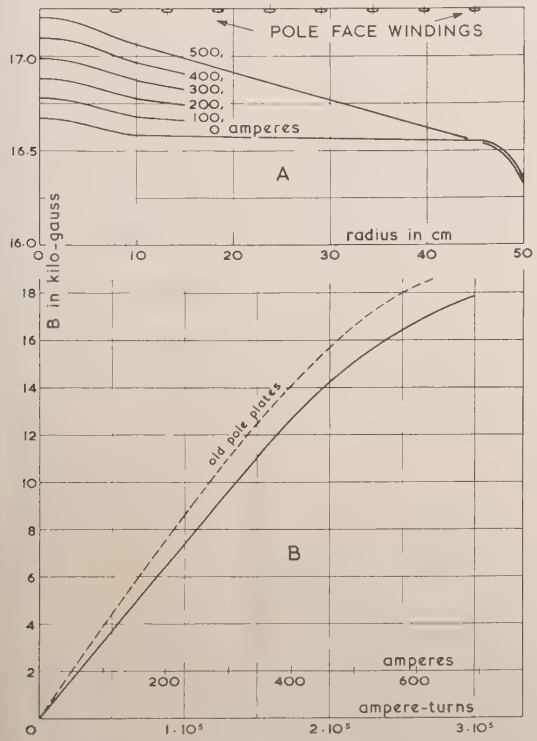

Fig. 3. A. Effect of pole face windings on mean radial field plot; B. Magnetic flux-density versus ampere-turns.

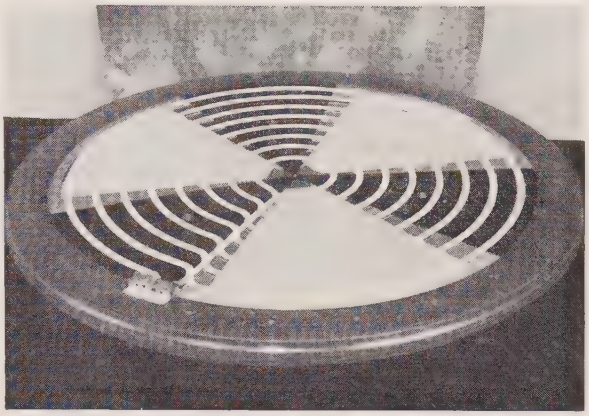

Fig. 4. Pole plate with Thomas shims, Rose shim and pole face winding.

resulted from voltage fluctuations at the output of the generator, the existing system was augmented by the addition of a short-term voltage stabilizer.

A 10 μF low-loss condensor, connected to the generator terminals through a 1 megohm resistor acts as a reference voltage, with the limitation that only fluctuations which are not long compared to the time constant of 10 seconds, are detected as voltage fluctuations across the resistor. These are amplified by a simple balanced D.C. amplifier, and the output signal is applied to one of the amplidyne field windings. The generator voltage is thus stabilized for short-term fluctuations, while the normal current stabilizer takes care of long-term current variations, due to temperature changes and possible drift of the voltage stabilizer. With this simple stabilizing arrangement, shown as a block-diagram at B in fig. 5, a drift-free stability of $\pm$ 0.002% i.e. 1 in 25 000, is easily achieved, which proved to be more than adequate.

3. The R.F. System

3.1. DEES

Considerable difficulties were experienced with the original dees, as at the time we were not able to acquire the services of a firm that was better qualified to make them. Right from the beginning the dees were not within the required tolerances, while the soldering of the cooling lines was of very poor quality, resulting in leaks.

To remedy the situation, the old dees were sawed off the dee-stems, and new dees of a much-improved design fitted by the C.S.I.R. workshops. As can be seen in fig. 6, these consist

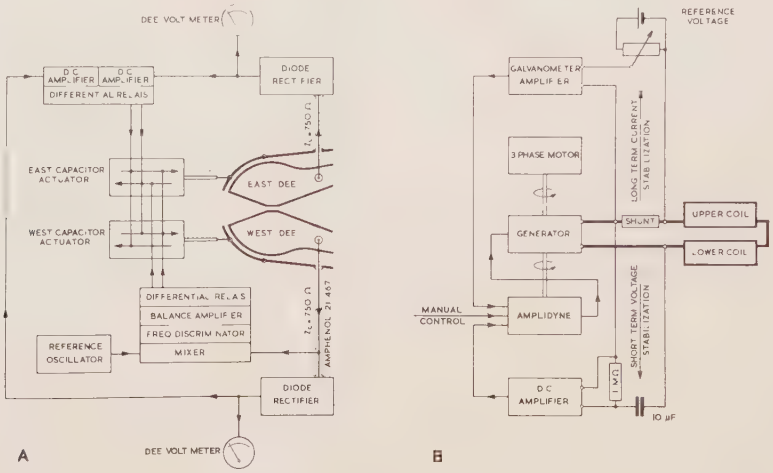

Fig. 5. A. Block diagram of R.F. stabilization; B. Block diagram of magnet stabilization.

of an aluminium backbone, which is secured to the dee-stem by a large number of screws, and onto which in turn the top and bottom lids with their soft-soldered cooling tubes are screwed.

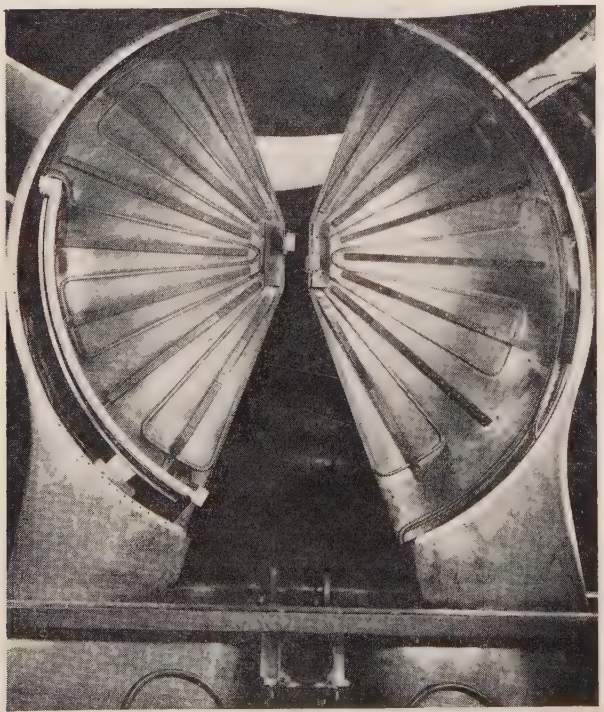

Fig. 6. The dees with the top plates removed.

This makes for superb accessibility to the septum and deflector assembly. Furthermore, the new dees are clad with carbon strips to avoid undue radioactivity. These strips also light up if hit by the beam; this can be observed through the optical system. Tolerances are within $\pm$ 1 mm. Together with the dees the construction of the trimmer condensors was improved and can now effect a frequency change of $\pm$ 1.7%.

To suit the ion source as described in Section 4, vertical feelers were slide-fitted. The first revolution is guided by an extraction plate in the dee opposite the ion source slit, and a further slit in the East dee. The relative positions of the ion source and the slits are shown in fig. 7.

3.2. STABILIZATION

Stabilization was introduced for the R.F. system for the same reason as mentioned on p. 263, and to shorten the warming-up period of the machine. A block-diagram of the system is A in fig. 5.

The ratio of the dee-voltages is stabilized by a combination D.C. amplifier, deriving its signals directly from the dee voltmeters, and actuating both trimming condensors through a differential relay. Although normally equal voltages are used, the ratio of dee voltages can be adjusted at will, and is kept within $\pm$ 0.5%.

The frequency is stabilized by heterodyning the cyclotron frequency with that of a local

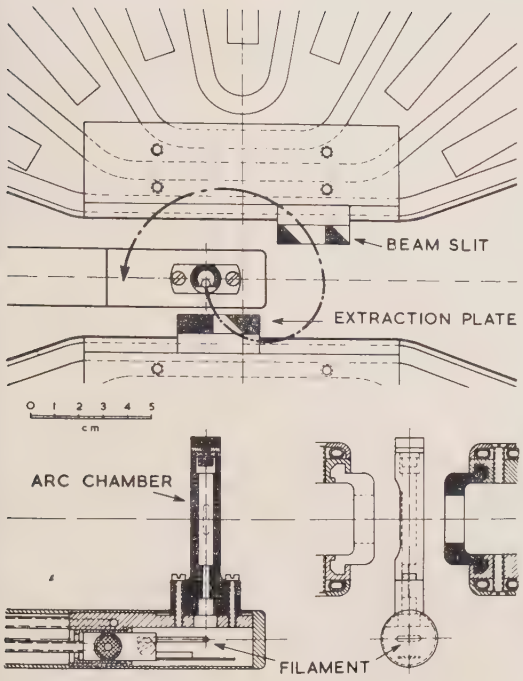

Fig. 7. The ion source and the feelers.

stable Variable Frequency Oscillator. The resultant frequency is amplified and fed into a limiter and discriminator. This F.M. detector drives a D.C. amplifier, and again both condensator plates are actuated through a differential relay. The voltage-ratio stabilizer moves the plates in opposite directions, while the frequency stabilizer moves them together. After some interplay a stable position is reached. To overcome the mechanical overshoot of the actuator motors, D.C. braking is employed. The frequency, which after the warming-up period was normally stable within only $\pm$ 0.01%, is thus also stabilized now within $\pm$ 0.002%.

4. The Ion Source

4.1. ION SOURCE PROPER

A new ion source of more advanced design was installed. The construction is shown in fig. 7, and a photograph can be seen at B in fig. 9.

Teflon insulation was used between the filament holder and the housing, and between the two halves of the filament holder. A silicone-rubber ○-ring was used to seal the water connection between the two halves. The filament holder and housing are made of a tungsten-copper alloy, while graphite was employed for the vertical tube and the reflecting anode, which are insulated from each other by a fused quartz ring.

The filament is made of 2 mm ⌀ tungsten and the reflecting plate underneath of molybdenum. Both vertical tube and filament are of uncomplicated design and can easily be made and replaced when necessary. The vertical chamber has a very long life-expectancy that is mainly limited by accidental breakage.

The filament position can be easily adjusted externally in relation to the $\frac{1}{8}$" ⌀ hole above it. Remote control is possible for the East—West and North—South directions and for tilting of the vertical tube. The output of the source is very sensitive to this last movement.

The ion source normally operates under the following conditions:

Filament Voltage	3 V
Filament Current	124 A
Filament life expectancy	30 hours
Gas flow	0.03 mm 1/sec
Arc voltage	200 V
Arc current	2.2 A .

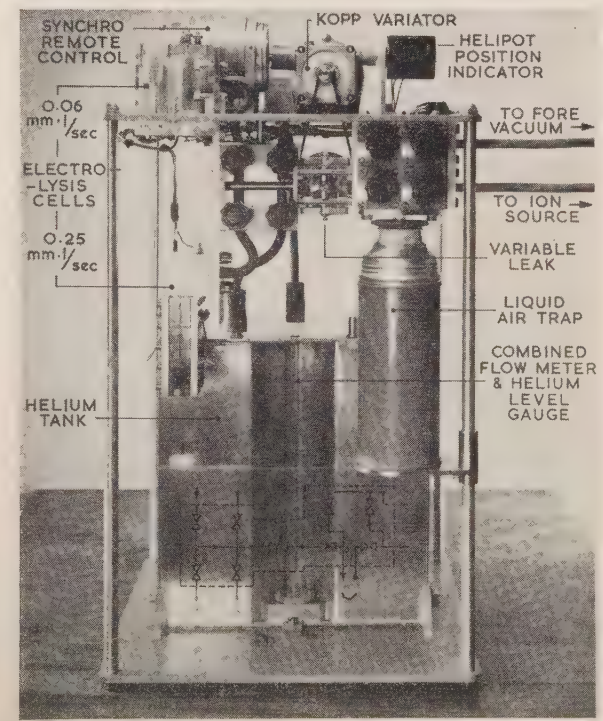

Fig. 8. The ion source gas supply.

The source produces about 2 mA of useful D^+, 1 mA of H_2^+ or 150 μA of He^{++}, as measured after one turn in the cyclotron, guided by the extraction plate in the West dee and the slit in the East dee, under R.F. conditions.

4.2. GAS SUPPLY

Using the principles described in the first report this has been reconstructed for easier maintenance and to facilitate the change-over from deuterium to hydrogen or helium gas. The apparatus is shown in fig. 8.

to suit the relative positions of the ion source, extraction plate and slit, as shown in fig. 7, a number of curves were obtained, three of which are shown at D in fig. 9. This dee-voltage, the most suitable for stable operation of the R.F. system, was kept constant during the entire experiment, and the beam current at the minimum radius, i.e. after one turn of acceleration was adjusted to 500 μA.

The top curve, taken with no current through the pole face windings, shows a very low loss of beam current at radii beyond 20 cm, proving

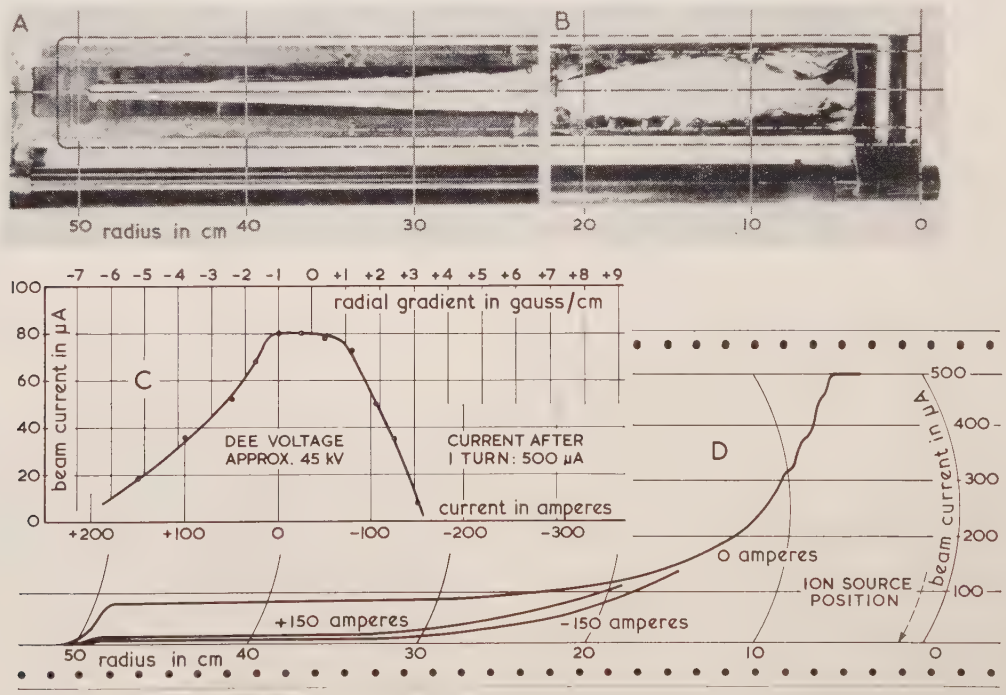

Fig. 9

A. Beam shape at large radii; B. Beam shape at small radii; C. Effect of the radial gradient; D. Radial beam current plots.

5. The Circulating Beam

5.1. RADIAL BEAM CURRENT CURVES

To obtain more knowledge about the behaviour of the internal beam, a remote controlled sliding probe target was installed in the neutral plane between the dees. In this plane, R.F. pick-up and dee-voltage unbalancing are reduced to a minimum. The target is water-cooled and 4 cm wide to ascertain interception of the total beam even at small radii.

With a dee-voltage of approximately 45 kV, that the magnetic focusing of the Thomas shims is more than adequate at these radii. At the smaller radii, however, the loss of beam is still important, due to insufficient electrostatic focusing, and the experiment indicates that improvements can be expected by placing more beam slits in the proper positions where the beam enters the dees[4]).

The behaviour of the beam is also clearly

[4]) A. H. Morton and W. I. B. Smith, Nucl. Instr. **4** (1959) 36.

illustrated by the two photographs in fig. 9. At A is shown a 0.5 mm thick lead foil that had been placed in the neutral plane between the dees, and which was "burned" away by the beam. The beam is very narrow indeed at the larger radii. The accurate vertical beam distribution at max. radius can be seen in fig. 11 (side view of stationary target). At B is shown a 0.05 mm thick aluminium foil, "burned" away by the beam in the same manner, proving the lack of sufficient focusing at smaller radii.

The photographs also show that the beam is perfectly centred in the geometric median plane between the pole faces. This other great advantage of the Thomas shims is due to the fact that mechanical inaccuracies in the position of the pole plates and shims have a much smaller effect on the position of the orbital plane, as the radii of curvature of the lines of force are orders of magnitude smaller than in a conventional radial gradient field. Thus the "median plane resistor", as described in the previous report, is no longer necessary.

5.2. EFFECT OF THE POLE FACE WINDINGS

From the abovementioned set of curves, the beam currents at maximum radius were plotted as a function of the current through the pole face windings, as shown at C in fig. 9. For positive values of the current, i.e. when this current increases the main field, the radial gradient becomes negative. In this region we observe that the beam current decreases gradually with increase of the negative radial gradient, due to increasing loss of phase of the particles with respect to the constant R.F. voltage. In the region of positive gradient, however, we see a rather abrupt decrease of the beam current, due to defocusing of the beam. It will be noted that this decrease occurs for a value of positive gradient, which was roughly predicted by the wire-loop check (see Section 2).

It is obvious from these experiments that, if this fairly low dee-voltage is used, the cyclotron performs best at approximately zero radial gradient, i.e. with the pole face windings not in use. In fact the cyclotron is always operated under these conditions, and internal currents of over 200 μA (measured calorimetrically) of 16 MeV deuterons can be easily obtained.

5.3. ORBIT POSITIONING COILS

Orbit positioning coils, placed at right angles in the $\frac{1}{4}''$ external shimming gaps, were tried in an effort to facilitate deflection. Each coil was oblong in shape, $15'' \times 25''$ across main diameters, wound of 40 turns of 2×4.5 mm copper, and insulated by polyester-resin impregnated fibreglass. Currents of up to 25 A could be sent through these coils to vary the magnetic field locally by approximately 40 gauss.

While it was possible to move the beam orbits with these coils, a strong horizontal defocusing effect was observed, probably due to the fact that the local field variations have a different effect on particles that leave the ion-source under different phase conditions, thus making a different number of traverses through the regions of stronger or weaker field.

Consequently the orbit positioning coils have been discarded, and orbit positioning is now effected by moving the ion-source only.

6. The Automatic Rotating Target

In the first report, an automatic target and its mode of operation are described. To cope with increasing beam intensities, and to facilitate irradiations where low target temperatures are imperative, a rotating automatic target was designed. This is shown in fig. 10. The mechanism

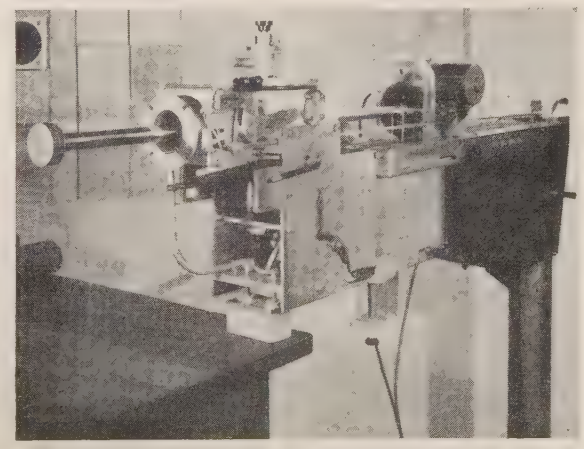

Fig. 10. The automatic rotating target.

operates on exactly the same lines as the previous one, except that the target proper is not sheared, but screwed off by a fork, which then places it in the pneumatic carrier. The blowing-out time of the coolant had to be lengthened, so that the clears the dee covers by 15 mm, and can stand up to 45 kV without sparking. However, the carbon, useful as it was in the preliminary tests, proved to be unpractical because of the heating of and consequent emission from the deflector.

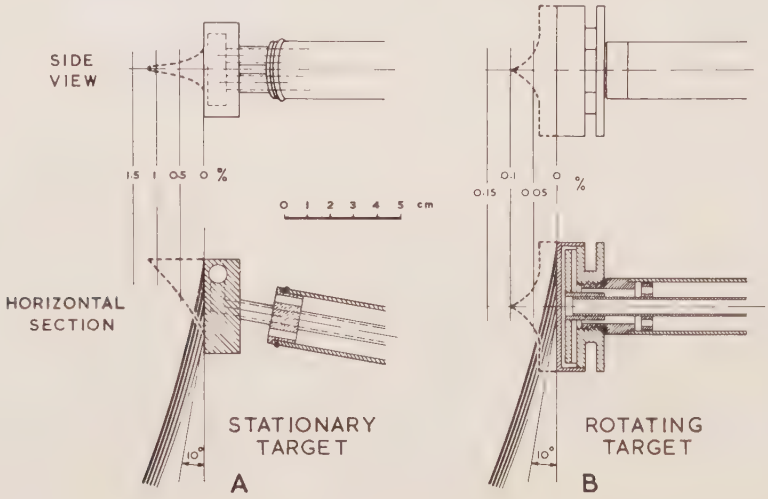

Fig. 11. A. Beam distribution on stationary target; B. Beam distribution on rotating target; The horizontal axes show percents of the *total* activity per mm².

target now reaches the hot laboratory some 80 seconds after the button is pressed.

As can be seen from fig. 11, the distribution of the beam, as measured by the activity of an irradiated target, is much more uniform than is the case with the normal stationary target. Hot spots are thus avoided. For instance, lead of 0.3 mm thickness is not damaged by 80 microamps of 16 MeV deuterons. A non-metal, such as NaCl, is first applied in a thickness of 1 mm to a $\frac{1}{16}''$ copperplate, which is then softsoldered to the target head. This sodium chloride target then can stand up to 25 microamps of 16 MeV deuterons, producing about 30 mC/h of Na^{24}.

7. The Deflecting System

7.1. DEFLECTING CHANNEL

For the first deflection tests, both septum and deflector were carbon-clad. The carbon gave a visible indication when hit by the beam, and prevented undue radioactivity. This safety-measure was welcomed when it was necessary to disassemble the channel frequently because of insulation difficulties. The 20 mm high deflector The channel was thus replaced by a metal septum and deflector of the same shape.

The deflector entrance and exit and the septum exit are adjustable without breaking the vacuum. The septum entrance can only be adjusted by disassembling the dee. The channel is shown in fig. 6 and its actual position can be seen in fig. 11.

7.2. VOLTAGE SOURCE

An old X-ray rectifier was adapted for this purpose, and can now provide 60 kV at a continuous current of 10 mA. The voltage is variable from the control room, and both current and voltage are measured from there.

The deflector is cooled by water mixed with cutting lubricant, to lubricate the gearpump used for circulating the coolant. This pump and an air-cooled radiator are on a high voltage pedestal, coupled to the drive motor by an insulating shaft. The sole electrical connection between the deflector and the high voltage pedestal is the coolant, which thus acts as a buffering resistor of 50 kΩ, to damp transients initiated by sparks in the vacuum-chamber.

8. The External Beam Focusing System

8.1. FRINGING FIELD WEDGES

As the deflected beam spreads considerably in the horizontal plane, because of the long trajectory in the fringing field, steel blocks were placed in the fringing field to act as sector magnets. Their shape and position can be seen in fig. 12.

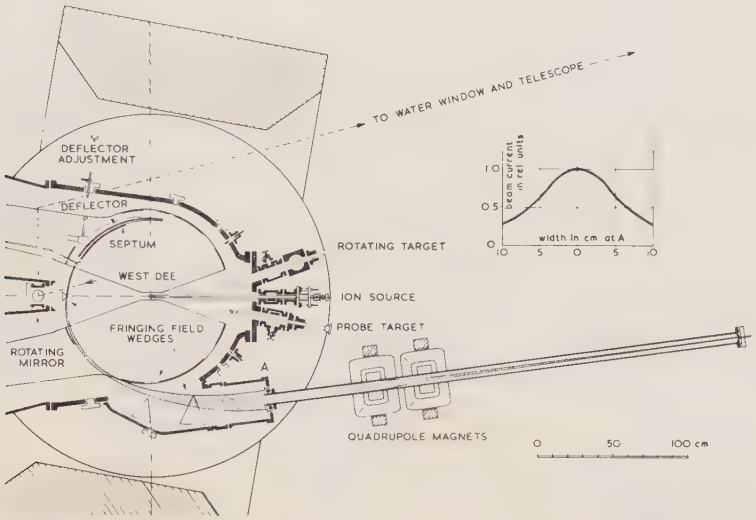

Fig. 12. The beam trajectory.

The first wedges are placed inside the vacuum-chamber and can be moved in and out without breaking the vacuum. They are 35 mm thick and 25 mm apart. The second and third sets of wedges are placed on both sides of the exit-chamber. These wedges are 200 mm thick and 85 mm apart. It is not possible to place the second wedges in the most effective position because of the shape of the exit-chamber.

8.2. QUADRUPOLE MAGNETS[5])

A $2\frac{1}{2}''$ O.D. stainless steel tube leads part of the beam through the quadrupole magnets, which are shown in Figures 12 and 13, thus accepting 60 mm of the horizontally flat beam at the end flange of the exit-chamber extension (A in fig. 12). The beam is focused at a point some 3 m away from this point, where it will be used for experiments.

[5]) See also: W. Weidemann, Nucl. Instr. 8 (1960).

Under operating conditions the magnets consume some 600 watts, which is dissipated through air-cooling at a surface temperature of 80°C. The quality of focus is not affected by varying operating conditions of the cyclotron, and is kept sufficiently constant by a current-stabilization of $\pm$ 0.5%.

9. The Deflected Beam

With the septum entrance at 49.5 cm radius, an entrance gap of 5 mm, and the septum exit at 52.0 cm with an exit gap of 12 mm, and with a deflecting voltage of approximately 40 kV,

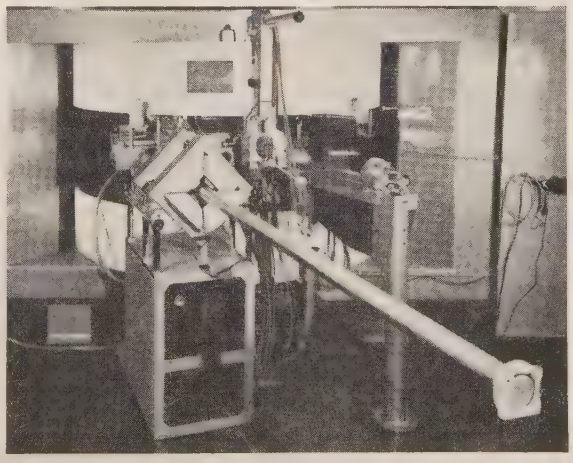

Fig. 13. North view of cyclotron.

about 24% of the beam current at maximum radius can be deflected, as measured on one of the two probes that can be inserted on either side of the rotating mirror. This situation is depicted in fig. 12. If no fringing field wedges are used, the halfwidth of the beam, where part of it enters the pipe leading to the quadrupole magnets, i.e. at point A, is considerably larger than the width of the exit-chamber extension. With the wedges in the position already described, however, the half-width is approximately 13 cm, as can also be seen in fig. 12. This information was obtained from irradiated copper plates and from a ten-target plate which could either be screwed to the exit chamber, or to its extension. Thus practically all of the beam is now confined within the side walls of the exit-chamber extension, and this is about 12% of the beam at maximum radius. Insufficient time was spent on experiments to further reduce the losses in the fringing field region, and it is clear that there is still scope for improvement.

5% of the beam current at maximum radius enters the stainless steel tube and, because of the slight divergence, only 4% enters the first quadrupole magnet, which effects horizontal focusing. Owing to the associated vertical defocusing effect of this magnet, another 1% is lost between the two quadrupole magnets, which leaves approximately 3% of the beam at maximum radius to reach the target onto which the beam is focused.

The quadrupole system, with its nett transmission of 75% confines the beam at the target area to a focus of some 4 by 6 mm, where it would otherwise have spread to approximately 6 cm by 24 cm.

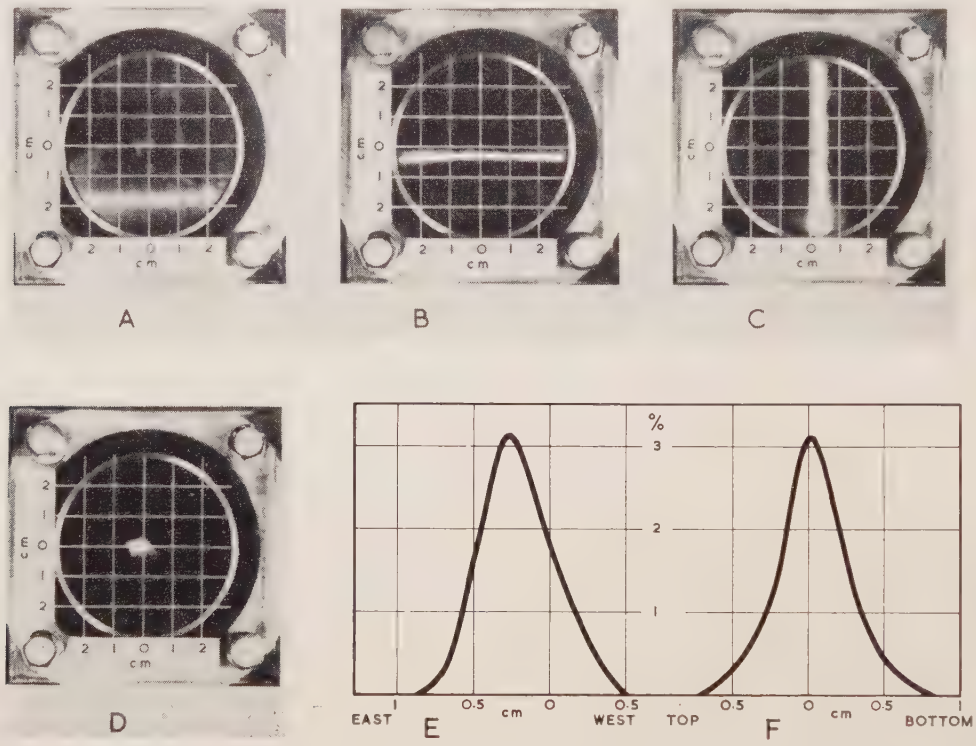

Fig. 14. The focused beam. The vertical axes of E and F show percents of the total beam current per mm².

Fig. 14 shows, A: a photograph of part of the unfocused beam directed onto a fused quartz plate, to make the beam shape visible; B: the vertically focused beam; C: the horizontally focused beam; and D: the spot focus, obtained with both quadrupoles in operation. An accurate survey of the beam distribution was made by

irradiating a copper target and measuring its activity distribution, which is shown at E and F in fig. 14.

Acknowledgements

The authors wish to extend their sincere thanks to Dr. S. J. du Toit, for his constant encouragement and interest in the work, while head of the Nuclear Physics Division of the N. Phys. R.L. After his departure in October, 1959, Dr. E. J. Marais, Director of the N. Phys. R.L., added to his already overcrowded schedule the duties of acting head of this department. Thanks are due to him for the admirable way in which he has filled this rôle.

The whole project, of course, would have been impossible without the conscientious and dedicated work of the whole cyclotron group, consisting of Messrs. Z. de Velde Harsenhorst, L. D. Bruins, P. van Vliet, K. Lubbinge and J. Kuiper. In this connection we wish to mention also the sustained and excellent craftsmanship of Messrs. A. Dekter and J. L. Liebenberg of the C.S.I.R. Workshops, who worked for the cyclotron during the period covered by this report.

Finally we would like to express our appreciation to Dr. S. M. Naudé, President of the South African Council for Scientific and Industrial Research for his personal interest in this project.

NUCLEAR INSTRUMENTS AND METHODS 8 (1960) 272–281; NORTH-HOLLAND PUBLISHING CO.

A DOUBLE-DELAY-LINE LINEAR AMPLIFIER EMPLOYING TRANSISTORS I

F. S. GOULDING, R. W. NICHOLSON and J. B. WAUGH

Atomic Energy of Canada Limited, Chalk River, Ontario, Canada

Received 20 June 1960

A transistor amplifier designed mainly for precise scintillation counter spectroscopy is described. Techniques such as double-delay-line pulse shaping and considerable negative feedback result in excellent linearity, gain stability and overload behaviour at high counting rates. An input charge of 2×10^{-13} Coulombs develops a $\pm$ 4V output pulse into a 100 Ω matched cable which feeds the Chalk River kicksorter. With 1 μsec pulse shaping lines the input equivalent R.M.S. noise is 4000 ion-pairs. Lower noise may be achieved by using shorter lines. The amplifier rise-time is 0.2 μsec (10 to 90%). Use of plug-in printed circuit boards increases the versatility of the amplifier and simplifies the adjustment procedures.

1. Introduction

The advantages of double-delay-line pulse shaping and careful control of amplifier limiting action for scintillation counter amplifiers have been appreciated for some time[1,2]) and the use of tube amplifiers employing these techniques has become common wherever high counting rates and large overload pulses are encountered. Work

[1]) E. Fairstein, Rev. Sci. Instr. **27** (1956) 475.
[2]) G. G. Kelly, I.R.E. Nat. Conv. Rec. Pt. **9** (1957) 63.

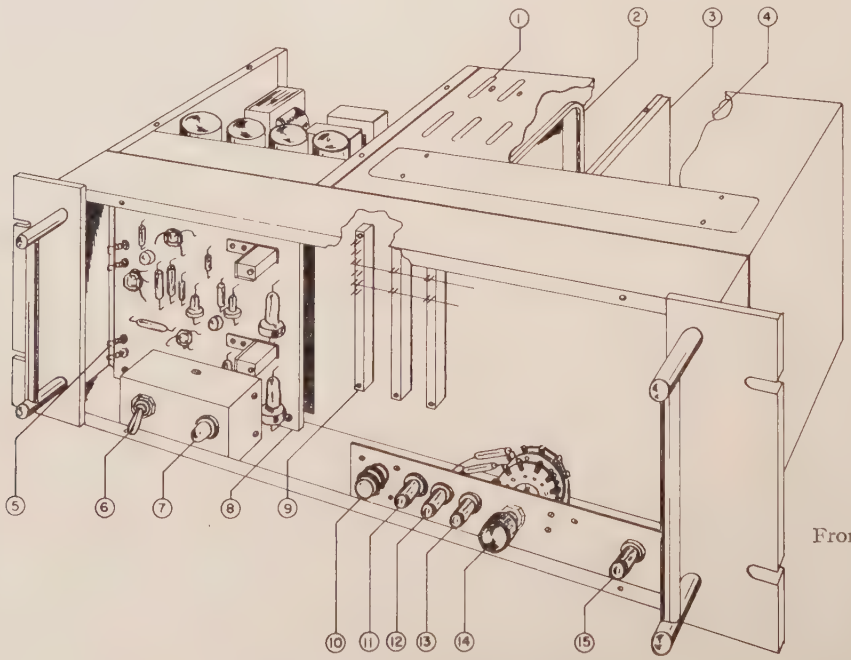

Front panel removed.

Fig. 1. Main amplifier cutaway view.

1. Louvres ventilation and adj. presets;
2. Printed card with handle;
3. Shield;
4. Back cover and card retainer;
5. Power supply to connectors;
6. Mains on/off;
7. Indicator;
8. Printed board (power supply);
9. Printed circuit connectors;
10. To head unit;
11. Input Mix;
12. Input Test;
13. Input Head;
14. Gain control;
15. Output.

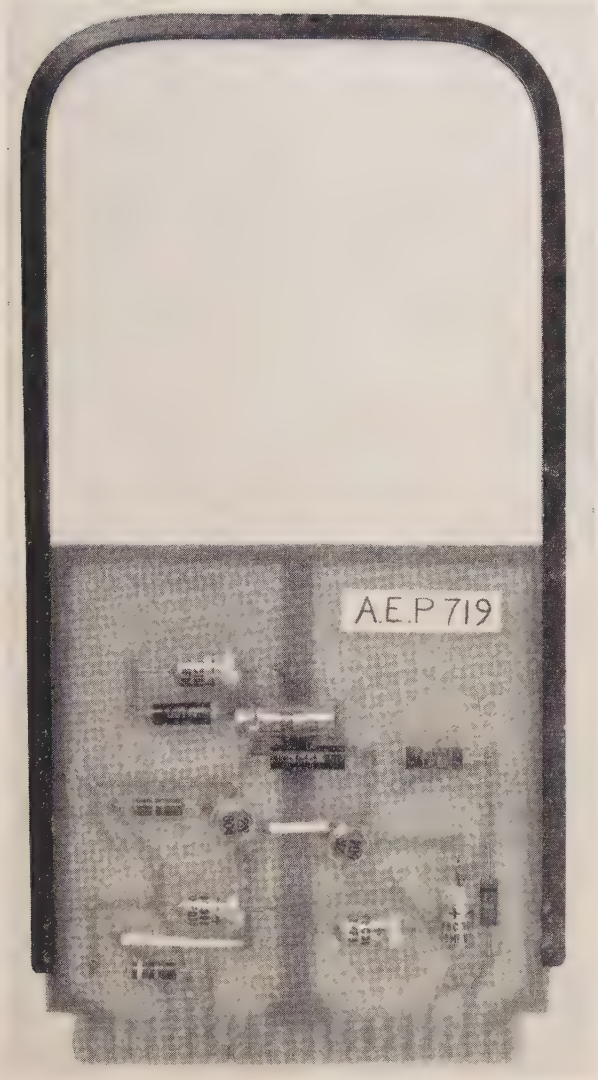

Fig. 2. Typical printed circuit unit.

at Chalk River on transistor amplifiers which started with the use of current fed-back pairs in monitoring instruments[3,4]) and continued with the development of a non-overloading amplifier for proportional counters[5]) has now culminated in the development of a transistor double-delay-line linear amplifier. Apart from the advantages of reliability, small size and low power consumption resulting from the use of transistors this amplifier is much simpler to manufacture and adjust than its tube counterparts.

The complete unit is designed for rack mounting with the head unit containing the scintillation detector, photomultiplier and head amplifier connected to the main unit by not more than 50 feet of cable. A cutaway view of the main unit with its panel removed, shown in fig. 1, illustrates the method of construction. Printed circuit units each containing a basic circuit element (current amplifier, limiter, delay line shaper and output stage) plug into the 8 printed circuit sockets shown in fig. 1. The power supply is contained on the main chassis which also includes separate shielded compartments for each of the plug-in units. Input and output connectors, gain control, power switch and indicator are mounted on a shallow sub-panel behind the main panel.

Experience has shown that the versatility of a plug-in form of construction is invaluable. The present amplifier design has evolved from a methane proportional counter amplifier design using the same base unit described by Waugh[5]) and it is likely that deficiencies which probably will be found to exist in the present design can be easily remedied by simple changes to, or

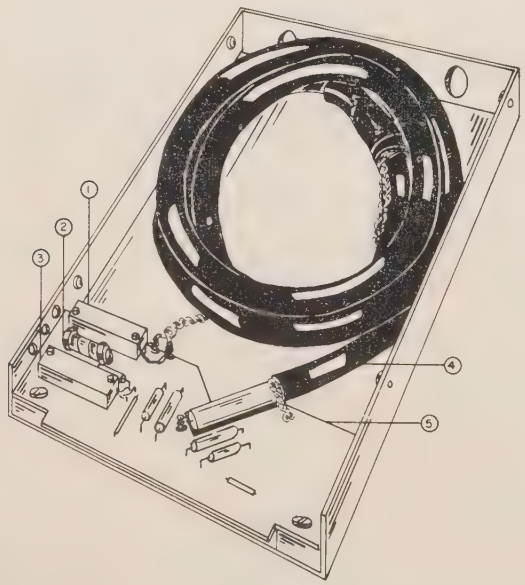

Fig. 3. Delay line pulse shaper. 1. Loss adjustment; 2. High frequency match; 3. Resistive match; 4. HH2000 Delay cable; 5. Printed card copper side down.

[3]) F. S. Goulding, Chalk River Report CREL-741 (1957).

[4]) V. H. Allen, Canadian Electronics Engineering **2** (1958) 22.

[5]) J. B. Waugh, Chalk River Report CREL-828 (1959) (to be published in Nucleonics, July, 1960).

replacement of, plug-in units with no change in the base unit.

A typical printed circuit unit is shown in fig. 2 and fig. 3 illustrates the construction of the delay line pulse shaper. We have employed printed circuits to simplify construction and also to control layout thereby obtaining reproducible results when large quantities of the units are manufactured. The printed circuit pattern is gold plated and the plug portion of the board is palladium plated. These two measures together with the choice of a good printed circuit socket have virtually eliminated dry joints and contact problems.

2. Overall Circuit Design

The amplifier design is based largely on the use of fedback pairs of transistors used as current amplifying sections. Each pair exhibits a low input impedance and high output impedance which lends itself to the inclusion of shaping lines in the outputs of stages. A detailed analysis of the frequency response of the fed-back pair has been performed by Waugh[6,7]; for the present purpose we need only note that the majority of the stages occurring in this amplifier exhibit current gain-bandwidth products of more than 30 Mc/s.

Fig. 4 shows the schematic of the complete amplifier excluding the power supply which is shown in fig. 5. The low ripple power supply which provides $\pm$ 30 V for the amplifier is conventional in design apart from the use of current controlled series transistors for overload protection.

[6]) J. B. Waugh and R. W. Nicholson, Chalk River Report CREL-829 (1959).

[7]) J. B. Waugh and R. W. Nicholson, Chalk River Report CREL-830 (1959).

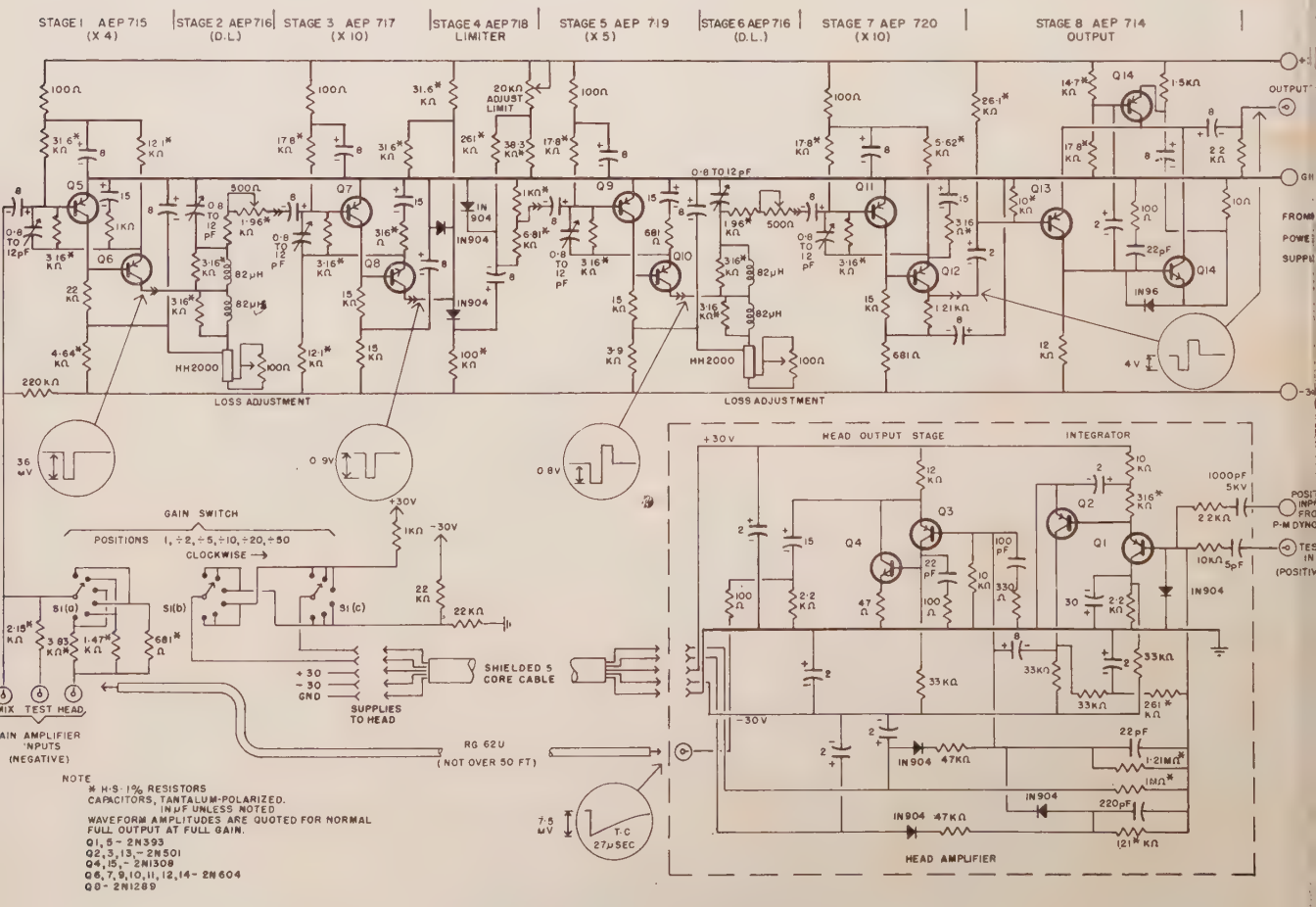
STAGE 1 AEP 715 (X 4)
STAGE 2 AEP 716 (D.L.)
STAGE 3 AEP 717 (X 10)
STAGE 4 AEP 718 LIMITER
STAGE 5 AEP 719 (X 5)
STAGE 6 AEP 716 (D.L.)
STAGE 7 AEP 720 (X 10)
STAGE 8 AEP 714 OUTPUT
LOSS ADJUSTMENT
LOSS ADJUSTMENT
HEAD OUTPUT STAGE
INTEGRATOR
GAIN SWITCH
POSITIONS 1, ÷2, ÷5, ÷10, ÷20, ÷50
CLOCKWISE →
SHIELDED 5 CORE CABLE
SUPPLIES TO HEAD
RG 62U (NOT OVER 50 FT)
HEAD AMPLIFIER
NOTE
* H·S·1% RESISTORS
CAPACITORS, TANTALUM-POLARIZED. IN μF UNLESS NOTED
WAVEFORM AMPLITUDES ARE QUOTED FOR NORMAL FULL OUTPUT AT FULL GAIN.
Q1, 5 - 2N393
Q2, 3, 13 - 2N501
Q4, 15, - 2N1308
Q6, 7, 9, 10, 11, 12, 14 - 2N604
Q8 - 2N1289

Fig. 4. Schematic of amplifier.

The supply is capable of providing up to 150 mA in each voltage line but this capability is not fully used in this amplifier which consumes

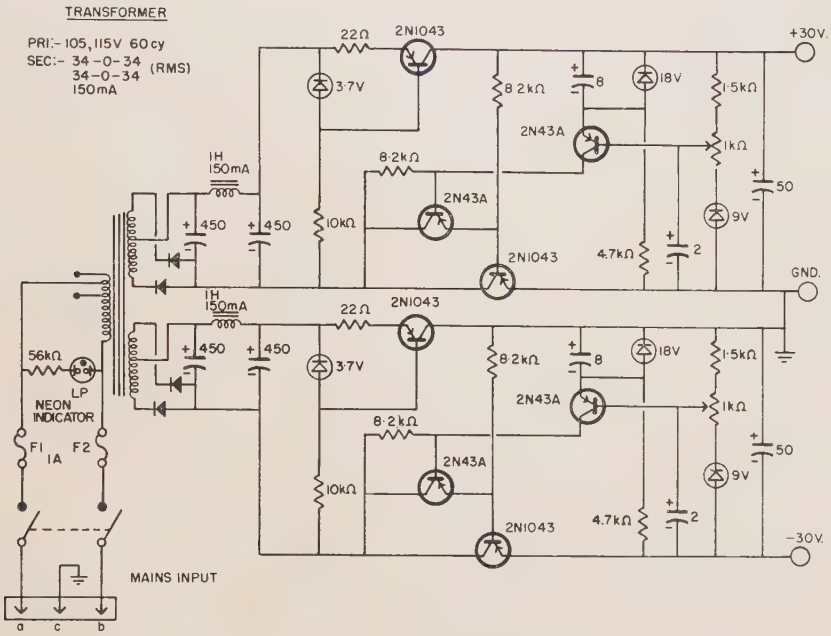

Fig. 5. Power supply schematic.

only 28 mA at ± 30 V. The design of the power supply will not be discussed further.

The block diagram shown in fig. 6 will be used in the following discussion of the general

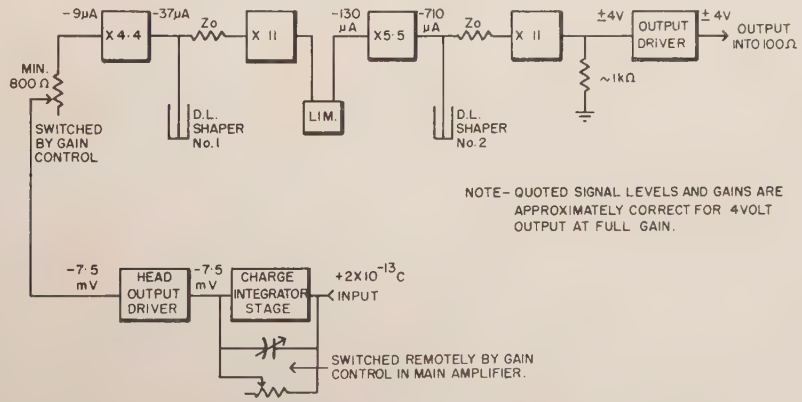

Fig. 6. Amplifier block diagram.

problems involved in the design of the amplifier. Considering the input stages first, a choice must be made between shaping short pulses in the head or integrating the detector charge in the head and feeding long pulses (i.e. with slow decay) into the main amplifier which contains the pulse shaping components. We chose the second alternative partly due to the inconvenience of including shaping lines in the head—which may well be in an inaccessible location where space is at a premium—and also due to the slight reduction in noise obtained when the shaping is done later in the amplifier. The chosen method is not without its difficulties. The greater the number of stages handling long pulses the more severe are problems due to "pile-up" at high counting rates of large overload

pulses. Also it is difficult to realise long decay times in transistor circuits due to the presence of leakage and drive currents in the input base circuit. This difficulty led to the use of the feedback integrator in preference to a more conventional emitter follower.

The input circuit is designed to accept positive pulses from the dynode of a photomultiplier. This choice was made bearing in mind the increasing use of the final anode (negative pulse) for fast coincidence purposes.

The output signal from the integrator feeds an output driver stage designed to feed 100 Ω cable linking the head to the main amplifier. For most applications where long lengths of cable are not required, matching the cable at the head end only is more satisfactory than terminating in 100 Ω at the amplifier end of the cable. This results from the fact that the driver stage would be called upon to drive a large dc current into the 100 Ω termination in the latter case if a high rate of large overload pulses were applied to the input. If very long lengths of cable are required between head and main amplifiers and if high rates of overload pulses are not present, termination at the main amplifier end of the cable would be preferred.

The signal levels involved in the head amplifier are quite small under normal operating conditions but rise to large values when the main amplifier gain is reduced by attenuation at the input. The design is based on the premise that high counting rates (up to 10^5/sec) of overload pulses equivalent to 50 times the normal maximum operating level may be present. Thus, with no attenuation at the input of the main amplifier (i.e. a series resistor of about 800 Ω) signals levels up to 0.4 V may be produced in the head by these 50 $\times$ overload pulses. At high rates changes in the operating points of the transistors result and, to minimize these, a fixed decay time constant of slightly over 25 μs is built into the integrator. With this time constant and 50 $\times$ overload pulses occurring at 10^5/sec "pile-up" effects may produce up to about 1.5 V temporary shift in operating points in the head. Attenuation at the input of the main amplifier increases this figure and, for this reason, such attenuation is limited to a factor of 5. Further reduction in the overall gain of the system is produced by increasing the value of the integrating capacitor in the head by a factor of 10. This is accomplished by using a diode arrangement in the head switched remotely from the main amplifier by changing a dc level.

The gain and configuration of the main amplifier was determined by the following considerations:

(a) The input stage should present a low impedance at its input. This allows gain to be changed by switching a series resistor and also permits mixing of signals from more than one head and from a test pulse generator.

(b) The first shaping line should be as early as possible in the amplifier.

(c) The only limiting action in the amplifier should occur before the second delay line. This is essential if the area balance of the negative and positive pulses at the output is to be preserved.

(d) The previous consideration implies that the limiter shall not affect linearity and gain in the normal linear range of the amplifier but shall limit sharply slightly above the linear range. A resistor-semi-conductor diode series combination may be shown to exhibit a change from 99% transmission to 99% attenuation (incremental) for a change of output voltage across the diode of about 300 mV. We have therefore chosen to place the limiter diode at a point in the amplifier where the normal maximum linear signal is about 1 V and the diode is biased to produce virtually complete limiting at 1.5 V.

(e) Having fixed the limiter voltage, consideration of the rise-time and stray capacities leads to a choice of resistor value in the limiter ($\sim$ 5 kΩ) and this, in turn, determines the current gain requirements preceding the limiter.

(f) Using easily available very high frequency transistors a simple output stage has been designed capable of feeding up to $\pm$ 6 V into 100 Ω cable. Fixing the normal linear output of the amplifier at $\pm$ 4 V allows the use of this stage. The Chalk River 100-channel analyzer has been modified to accept and analyze these

± 4 V signals and we have also designed discriminators with a threshold accuracy of about 0.1% of this signal.

(g) The previous consideration fixes the overall current gain of the amplifier.

(h) Allocation of gain between the head and the main amplifier is affected by various considerations but we have been guided by the desire to keep the noise due to the input circuit of the main amplifier to a small fraction of 1% of the normal operating level at that point in the system.

C_5 decoupling ac signals in this feedback loop. The current in R_{10} or R_{10} and R_{12} combined, depending upon the setting of the gain control in the main amplifier, determines the dc potential at the collector of Q_2. This is chosen to be about -11 volts. The collector of Q_1 is returned to a low voltage (-2 V) and its emitter current is kept at a low value (80 μA); these two measures ensure that Q_1 contributes a minimum of noise at the input due to its base current fluctuations. Lowest noise demands a small base current in the input transistor. The type of transistor

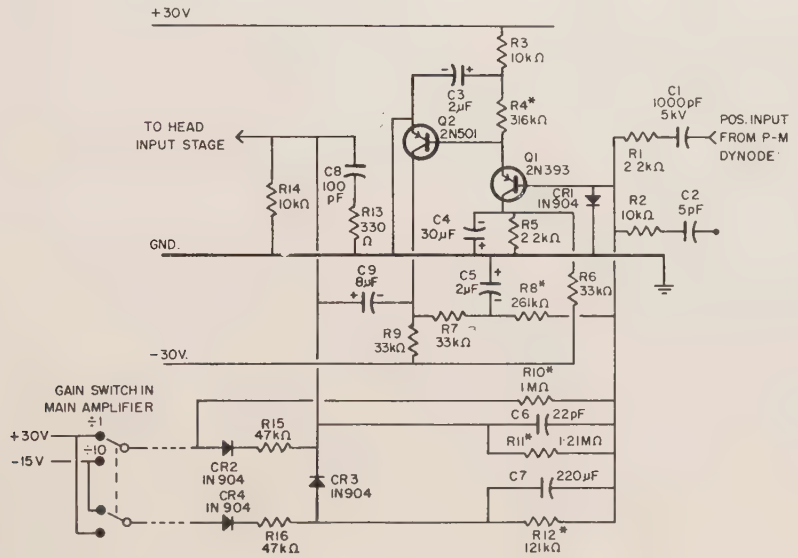

Fig. 7. Integrator-head amplifier.

3. Detailed Stage Design Considerations

In this section a brief description of the circuit of each stage is given together with an explanation of the choice of dc conditions.

3.1. HEAD AMPLIFIER-INTEGRATOR STAGE

Fig. 7 shows the integrator stage in detail and will be used in this description. In discussion of this and the following stages the complete amplifier circuit given in fig. 4 should be used to determine the relationship of any stage to others in the amplifier.

The integrator stage consists of two transistors in cascade, a grounded collector Q_1 driving a grounded emitter Q_2. The dc conditions are determined by feedback through R_7 and R_8 with chosen (2 N393) is the best available type for this position at the present time. Diode CR_1 protects Q_1 from damage when the P-M voltage is applied. It is necessary to use a good quality silicon diode in this position to keep its noise contribution small.

In addition to the input to the head from the dynode of the P-M, a test input is also provided. A voltage step of 40 mV applied to the test input simulates the normal maximum signal under full gain conditions.

When operating under full gain conditions the anode of CR_2 is returned to $+30$ V and that of CR_4 is returned to -15 V. Current therefore flows through CR_2 and R_{15} into R_{14} producing about $+5$ V across R_{14}. Diode CR_3 is then

reverse biased since R_{12} connects the anode of CR_3 to the base of Q_1 which is near ground potential. Thus the ac feedback in the integrator is only via C_6, R_{11} while C_7, R_{12} are isolated from the feedback loop. When the gain is to be reduced by a factor of 10 the anode of CR_4 is connected to $+30$ V and that of CR_2 to -15 V. CR_3 then conducts and C_7, R_{12} shunt C_6, R_{11}. In either gain position the decay time constant in the integrator remains near 25 μsec.

3.2. HEAD AMPLIFIER-OUTPUT STAGE

This stage is a transistor analogue of the White cathode follower used commonly in tube circuitry. As the output stage of the main amplifier is similar the design of this stage will be discussed later.

3.3. CURRENT AMPLIFYING STAGES

Four current amplifying feedback pairs are used in the main amplifier. These differ in detail according to the requirements as to dc conditions and gain in different parts of the unit but the basic circuits are the same and the same printed circuit wiring is used in each case. Three of the stages use two p-n-p transistors, but in stage 3 of the amplifier the second transistor of the pair is

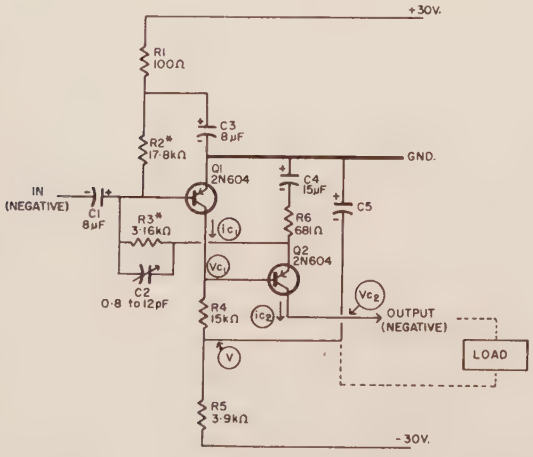

Fig. 8. Typical current amplifying stage.

an n-p-n. This is necessary to avoid overload problems in that particular stage but the basic operation is the same as the other stages. Fig. 8 shows a typical current amplifying stage.

The stage consists of two transistors in cascade, Q_1 being a grounded emitter stage while Q_2 is a grounded collector stage as far as the feedback is concerned. The output is taken from the collector of Q_2 so no phase change occurs in the stage. The current in R_2 flows in R_3 and sets up the dc conditions; thus, in this particular stage, the emitter of Q_2 and collector of Q_1 each resides at about -5 V with the collector current of Q_1 about 1 mA while that of Q_2 is about 1.5 mA. The ac current gain of the stage is given approximately by $\alpha_2 (R_6 + R_3)/R_6$ where α_2 is the emitter-collector current gain of Q_2. In modern transistors $\alpha_2 \to 1$ and tests on a number of transistors have shown that α_2 remains constant to within $\pm 0.1\%$ or better for a $\pm 10°C$ change of temperature providing that the transistor is operated under its correct conditions. The low frequency feedback factor of the stage shown in fig. 8 generally exceeds 200 resulting in excellent gain stability and constancy whatever cause of possible gain changes is considered. Transistors may be changed, voltages varied over a reasonable range and the temperature of the unit can be varied over a $\pm 10°C$ range—all producing a total gain change, in the whole amplifier, of considerably less than 1%.

Trimmer capacitor C_2 permits adjustment of the overall frequency response of the stage to produce optimum pulse shape with no overshoots on the edges of the pulse.

The load connected to the amplifying stage output depends upon its position in the main amplifier. The dc conditions in each stage are chosen to permit developing the required signal across the load without either saturating the second transistor or causing it to become

TABLE I

	V_{c1}	V	V_{c2}	i_{c1}	i_{c2}	Note
Stage 1	— 3	— 12.0	— 12.0	0.35	3.8	
Stage 3	— 5.1	— 17.5	+ 3.2	0.8	— 0.5	n-p-n in second position
Stage 5	— 5.1	— 20	— 20	1.0	1.6	
Stage 7	— 5.1	— 24	— 15	1.20	7.5	

Volts with respect to gnd. Current in mA.

non-conducting. Approximate operating conditions in the various stages shown in fig. 4 are given in table 1 in which the circuit references are the appropriate ones in fig. 8.

3.4. DELAY LINE PULSE SHAPER

Two of these units are included in the main amplifier and lines of different lengths may be plugged in depending upon the decay time of the scintillator being employed. For NaI-Tl, 1 μsec wide pulses are usually shaped. The mechanical arrangement of the delay line shaper is shown in fig. 3 and reference should be made to fig. 4 for the circuit. It is particularly important to terminate the first delay line carefully to avoid both high frequency and low frequency mismatch for, while the normal maximum signal level at the collector of Q_6 is about 40 mV and one channel of a 100-channel kicksorter corresponds to 0.4 mV at this point, 50 times overload signals produce 2 V here. Thus if recovery to less than 1 channel is required the match must be sufficiently accurate that rings, overshoots etc. are kept down to less than 1 part in 500 of the input pulse. Since the second delay line is never subjected to large overloads its matching is less critical but, for convenience, the same adjustments are included with each delay line. These adjustments and their purpose are as follows:

(a) Loss Adjustment

The integrator in the head is arranged to produce a decay time constant of 25 μsec and this waveform when fed to the usual shorted delay line would produce an overswing on the back edge of the shaped pulse. If the shaped length were 1 μsec the overswing would amount to $\frac{1}{25}$th of the pulse amplitude. In order to prevent this happening, a small variable resistance is inserted in place of the usual short circuit in the delay line shaper. Adjustment of this variable resistor alters the loss in the delay line reflected pulse and can be used to eliminate the overswing on the back edge of the shaped pulse. The slight droop on the top of the pulse produced by the 25 μsec decay time-constant is tolerable.

(b) Resistive Match

The usual variable resistor is provided to allow accurate matching at the driving end of the shaper and thereby prevent multiple reflections. Note that we are using current amplifying stages here and the following stage therefore appears in series with the termination, not in shunt as in tube amplifiers.

(c) H.F. Match-Capacity Trimmer

An attempt is made to include a filter network to match the end of the cable despite capacity loading due to the collector of the driving stage. A trimmer capacitor included at the output of the filter is found to permit adjustment to give the best high frequency match.

3.5. LIMITER STAGE

Fig. 9 shows the limiter stage. In the normal operating range diode CR_2 is conducting while CR_1 and CR_3 are reverse biased (see dc potentials shown on the diagram). Input signals appear as pulses of increasing current in the n-p-n transistor which forms the output of the previous stage. In the normal operating range these pulses share between R_1, R_2, R_3, R_6 and the series resistor R_4 feeding the next stage. Since resistor R_4 is of much lower value than the remainder most of the signal from the input of the limiter

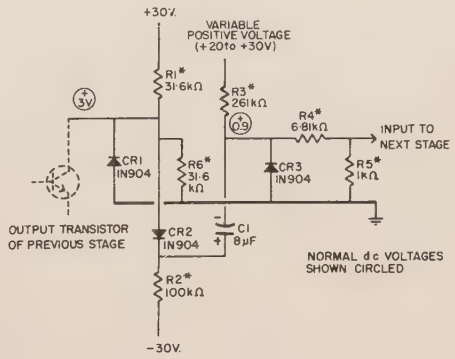

Fig. 9. Limiter stage schematic.

appears at its output. Signals slightly larger than the normal linear range cause CR_3 to conduct and this attenuates the output. As mentioned earlier, the attenuation changes from a negligible amount to a factor of 100 for a change in output

of about 300 mV so, while the circuit is completely linear (i.e. no attenuation due to CR_3) at levels below 1 V of pulse across R_4 (and CR_3), virtually complete limiting is present at 1.5 V. Adjustment of the positive voltage applied to R_3 changes the bias on CR_3 thereby changing the limit level. This adjustment is included to allow for variations between diodes used for CR_3.

When diode CR_3 conducts, CR_2 becomes non-conducting which limits the current charging C_1 during the pulse to that in R_2 (i.e. 340 μA). Were diode CR_2 not present, the largest overload pulses would produce large pulse currents in C_1 and, at high counting rates, a serious shift in the dc voltage across R_4, R_5 would result. Inclusion of CR_2 cuts this dc shift to a tolerable amount. The additional diode CR_1 serves to prevent saturation of the output transistor of the previous stage under the worst overload conditions.

3.6. OUTPUT STAGE

The circuit of the output stage is shown in fig. 10. In order to feed a 100 Ω cable with $\pm$ 6 V pulses the stage must be able to feed $\pm$ 60 mA into the load. To ensure adequate linearity of response the stage must exhibit an output impedance which changes by less than 1 Ω over the operating range. To accomplish these objectives while consuming only a small standing current a transistor version of the well known White cathode follower is used. Transistor Q_1 acts as a difference amplifier between the input and output lines and the amplified signal at the collector of Q_1 is fed to two transistors Q_2 (p-n-p) and Q_3 (n-p-n) in parallel. By using complementary transistors in this manner we ensure that one of these transistors is turned on whichever polarity of input pulse is applied to the circuit. Resistor R_4 defines the standing current in Q_1, R_8 defines the current in Q_2 and the difference between these currents flows in Q_3. Diode CR_1 protects the circuit against very large overload pulses.

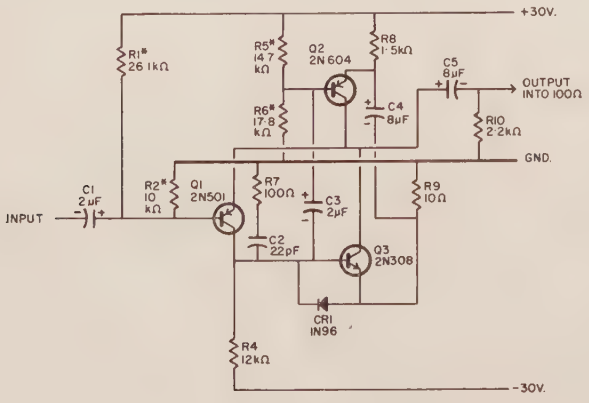

Fig. 10. Output stage schematic.

Loop stability of the circuit does not present severe difficulties as transistor Q_1 appears as a grounded base stage within the loop while Q_2 and Q_3 appear as grounded emitter stages. Since Q_1 is a very high frequency type of transistor the loop response is dominated by the time constant associated with Q_2 and Q_3. To ensure stability under all conditions R_9 is inserted in the emitter circuits of Q_2 and Q_3 thereby increasing the impedance appearing at the collector of Q_1. C_2 and R_7 then shunt this collector to roll off the loop gain at high frequencies.

The head amplifier output stage is similar but, since only negative pulses are to be handled, transistor Q_2 and the associated components are omitted.

4. Performance

4.1. GAIN STABILITY

Varying the ambient temperature over the range 25° C to 45° C produces a change in gain of less than 0.6% and varying the mains input voltage from 105 V to 125 V ac produces no measurable gain change. Gain changes at high counting rates are difficult to measure due to small shifts which occur in the kicksorter used for measurement but counting rates up to 10^5/sec of 15 times overload pulses appear to produce gain changes less than 1%. Less than 0.2% drift in the amplifier gain has been noted over a period of 1 day.

4.2. LINEARITY

The incremental gain of the amplifier (i.e. the slope of an input-output plot) is constant to within 1% over the full 4 V normal range of outputs. We have not detected any departure

from linearity under high counting rate conditions.

4.3. NOISE

The equivalent R.M.S. noise input of each of the two amplifiers tested was about 4000 ion pairs ($\sim$ 30 μV in 20 pF). At full gain this corresponds to a full width at half maximum of less than 1% on an output pulse of 4 V amplitude.

A 0.3 μsec line used in the first shaper and replacement of the second shaper by a network (1 K series, 1 K shunt) coupling from stage 5 to 7 reduced the RMS noise to 1800 ion pairs. For applications requiring low noise and short time resolution (e.g. semi-conductor junction detectors) this mode of operation is preferable to the normal double delay line mode.

4.4. OVERLOAD PERFORMANCE AT HIGH COUNTING RATES

Fig. 11 shows an example of the performance of the amplifier under these conditions. The amplifier fed a 100-channel kicksorter self-gated to reduce wastage of counting time due to noise at low levels and overload pulses at high levels. The system gain was adjusted to observe the Ba^{137} X-ray emitted by a Cs^{137} source. Curves (a) and (b) show the resulting peak under conditions where only the Cs source was present and the total counting rate above 10 keV adjusted to be 10^4 and 5×10^4 counts/second respectively. Curve (c) shows the effect of large overload pulses produced at a rate of about 5×10^4 counts/second by a Co^{60} source added to the 5×10^4 counts/second of Cs^{137}. The peak is broadened somewhat (from 24% to 28%) but there is very little shift in the peak position. A further experiment (not shown in fig. 11) showed a broadening to 32% when observing 10^4 counts/second of Cs^{137} in the presence of 10^5 counts/second of Co^{60}.

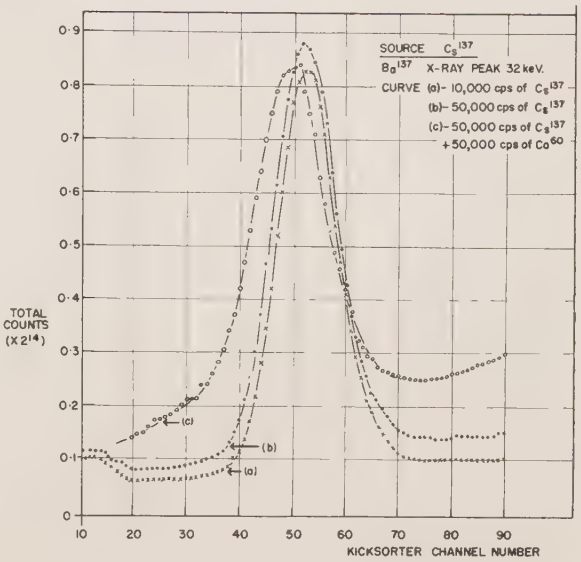

Fig. 11. Spectra at high counting rates.

Acknowledgements

This work was carried out as part of the research programme of the Physics Division of Atomic Energy of Canada Ltd. Our thanks are due to several colleagues who contributed ideas to the design. R. A. McNaught carried out some of the measurements quoted in this paper.

NUCLEAR INSTRUMENTS AND METHODS 9 (1960) 282–296; NORTH-HOLLAND PUBLISHING CO.

A TRANSISTORIZED FAST-SLOW COINCIDENCE AND PULSE AMPLITUDE SELECTING SYSTEM II

F. S. GOULDING and R. A. McNAUGHT

Atomic Energy of Canada Limited, Chalk River, Ontario, Canada

Received 20 June 1960

This paper describes a system developed for fast-slow coincidence experiments in nuclear physics and discusses the design of functional units including a low level discriminator, single or dual-channel analyzer, coincidence circuit and linear gate. The system is designed to use the ± 4 V double-delay-line shaped pulses produced by the amplifier described in the previous paper or equivalent pulses from other amplifiers. Operation with single phase pulses of similar amplitude is also possible but with reduced performance. Uncertainty of the discriminator threshold and the spurious pedestal and disturbances introduced by the linear gate are less than 10 mV under all normal operating conditions. Functional units of the system are constructed on printed circuit boards which plug into a base unit where interconnections are made between them through a programming plug. This arrangement allows the experimenter to change interconnections quickly and makes the whole system extremely versatile. The system also takes advantage of the timing accuracy of the zero cross-over of double-delay-line pulses to give a coincidence resolving time of 40 nsec while using no fast amplifiers or coincidence circuits. A technique of compensating for baseline shift at high counting rates of single phase pulses is also described.

1. Introduction

Bell, Graham and Petch[1]) introduced the technique of fast-slow coincidence systems in 1949 and, since that time, the technique has seen common use in many nuclear physics experiments. The complexity and size of the apparatus required for these experiments is alarming and, for this reason, the development described in this paper was initiated. Apart from the reliability and small size of transistor equipments there appeared to be possible technical advantages over vacuum tube circuits in the small voltage drifts in semi-conductor devices used as voltage discriminators[2]) which would allow the use of relatively low level signals. The system to be described has been designed to accept — 4 V

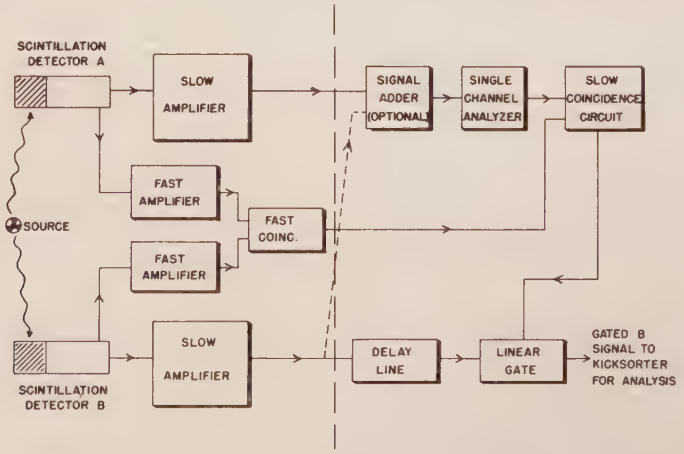

Fig. 1. Typical fast-slow coincidence and amplitude.

[1]) R. E. Bell, R. L. Graham and H. E. Petch, Canadian J. of Physics **30** (1952) 35.

[2]) F. S. Goulding and L. B. Robinson, Chalk River Report CREL-778 (1958).

signals for measurement purposes and the best operation results when ± 4 V signals from a double-delay-line amplifier such as that described in the previous paper are employed. Using these signals the timing accuracy of the zero cross-over of the pulse can be used for fast coincidence purposes[3]) thereby eliminating the need for high frequency chain type amplifiers in all but very short resolving time applications.

The arrangement shown in fig. 1 was chosen as a typical example of a fast-slow coincidence system. It was realised at the outset that many experiments involve more than two signal inputs but nearly all can be built up of dual input blocks such as that in fig. 1. A single unit as described here can accept only two signals for amplitude measurement but connections can be made to other similar units through several connectors provided on the front panel. It was also realised that the experimenter would require many arrangements of interconnections between the functional circuits. To permit this, all required inputs and outputs to and from circuit units are connected to a single programming socket on the front panel of the unit through which interconnections are made. The plug which the experimenter inserts in this socket contains a block diagram of the actual connection system appropriate to that plug.

As an additional aid to versatility of the individual functional circuit units each has been designed to present a reasonably high impedance at the input and, in the case of circuits handling linear signals, the output can drive full signal into matched 100 Ω cable. The circuits which provide logical outputs (i.e. a pulse or no pulse) produce a current output of 10 mA and will develop up to $+12$ V into the load chosen according to the application. Normally these logical outputs are terminated in 100 Ω providing $+1$ V pulses, but it is often convenient to have the higher level output available (e.g. to drive existing scalers).

The mechanical design of the unit is based on the use of a standard form of rack mounting printed circuit board base unit in use at Chalk River. A stable power supply (for the circuit details see ref.[4])) mounts on the chassis while receptacles for up to 14 printed circuit boards occupy the remainder of the chassis. In this particular unit only 8 boards are included and shields are inserted in the remaining positions to reduce electrical interaction between the units. The printed circuit boards insert from the rear of the chassis and access to the sockets for maintenance purposes is available by removing a cover plate over a cut-out in the front panel. The programming plug and discriminator bias controls are mounted on the front panel. Screened leads are used for signal connections to the programme plug to reduce interaction in the low level circuits.

2. Overall Design

The system shown in fig. 1 illustrates the functions to be performed in a fast-slow coincidence system. Signals in the "A" channel are amplitude analyzed by a single-channel analyzer which produces an output pulse to the coincidence circuit only when the "A" input pulse amplitude is within a restricted range. The fast portion of the system determines whether signals in "A" and "B" channels occur within a very short predetermined time of each other and, if so, the fast coincidence circuit feeds a pulse into the slow coincidence unit. If the slow coincidence circuit receives simultaneous inputs from the single-channel analyzer and the fast coincidence circuit it produces an output pulse which opens the linear gate for a defined time allowing the signal in the "B" channel to pass unchanged to a kicksorter for amplitude analysis.

The measurement of pulse amplitude by the single-channel analyzer cannot be completed until the input pulse has reached its peak height. This involves a time delay in measurement and equalizing delays must be inserted in the fast coincidence circuit output and in the "B" channel if the linear gate is to be opened before the "B" signal reaches it. The delay line ac-

[3]) E. Fairstein is believed to have suggested this technique in 1958.

[4]) F. S. Goulding and R. A. McNaught, Canadian Electronics Eng. 3 (1959) 28.

complishes the delay in the "B" channel and fig. 1 assumes that a circuit delay is included in the fast coincidence circuit. The final result of these operations is that the system presents to the kicksorter only those "B" signals coincident within a very short time interval with "A" signals of a selected amplitude. In one common modification of the simple system the single-channel analyzer measures the sum of "A" and "B" channel signals (dotted in fig 1).

while using no fast circuit of the type shown in fig. 1. In this unit we have chosen to limit the resolution to 40 nsec to avoid the need for accurate matching of line lengths in the amplifiers. Faster coincidences can be achieved by feeding a pulse into the unit from an external fast coincidence circuit in the manner shown in fig. 1.

Fig. 2 shows the arrangement employed in the unit. Apart from the delay line and the dual-channel analyzer each functional unit is a single

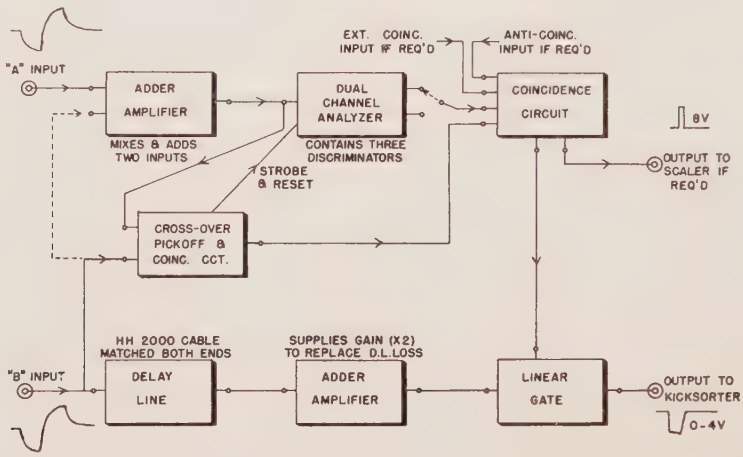

Fig. 2. Block diagram of unit.

In considering the design of a fast-slow coincidence unit the decision was made to omit the fast coincidence circuit shown in fig. 1 from the main unit and regard it as a separate unit. Where very high speed is required it is essential that wiring and construction be more carefully controlled than is possible in a versatile unit of the type to be described. Also, for many applications, no fast coincidence circuits are required to reduce chance coincidence pulses. The decision was therefore made to include circuits in the unit capable of performing functions similar to those to the right of the dotted line in fig. 1.

Use of double delay line pulses suggested the possibility of simply reducing the resolving time of the unit by including circuits capable of determining the zero cross-over of the pulses and taking a coincidence between the zero cross-over in channels A and B. By this technique it is possible to achieve coincidence resolving times of a few nanoseconds on NaI(Tl) scintillation pulses

printed circuit board. The dual-channel analyzer contains 3 discriminator boards while the delay line mounts under the chassis of the base unit. Thus 8 boards are included in the unit. The base unit is wired to bring the inputs and outputs from the boards to the programming socket where connections are made through a programme plug. Fig. 2 illustrates just one way of interconnecting the units. Mounted together with the programme plug is a row of test points which allow monitoring of all waveforms and also permit the connections shown dotted in fig. 2 to be made as required.

3. Details of Functional Circuit Units

3.1. ADDER AMPLIFIER (see fig. 3)

This is a simple circuit designed to provide the facility of algebraically adding two input signals and/or providing gain where required in the system. In fig. 2, one such unit is used in the "A" channel to add signals at input points 14, 15

while, in the "B" channel, a similar unit is used to provide gain × 2 at input 12 to make up for the signal loss due to the delay cable matched in its characteristic impedance at each end.

3.2. COINCIDENCE CIRCUIT (see fig. 4)

This circuit accepts three + 1 V inputs (12, 14, 15) which, if coincident for about 20 nsec normally result in a shaped output pulse + 10 mA,

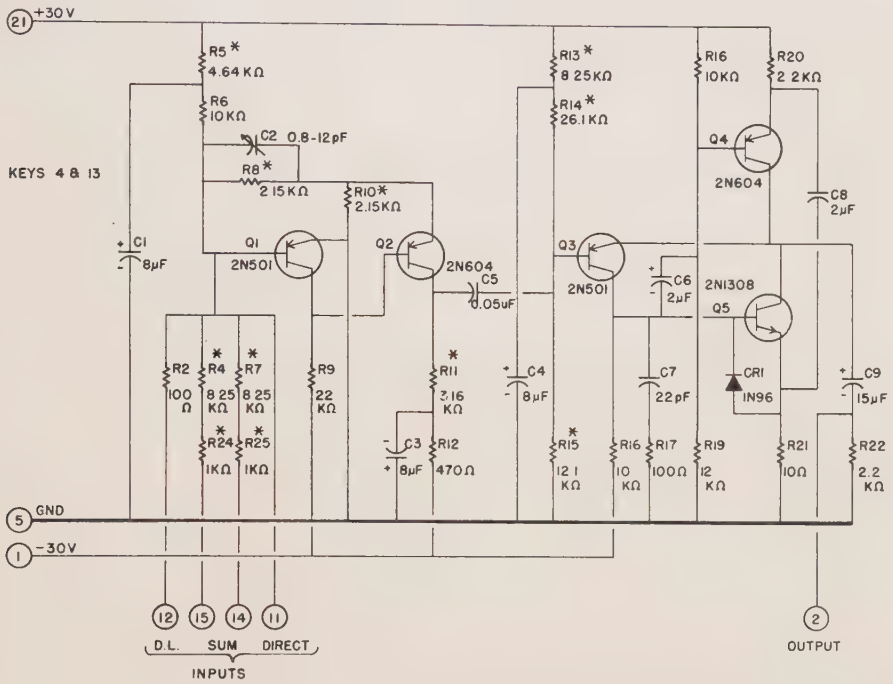

Fig. 3. Adder amplifier.

Transistors Q_1, Q_2 constitute a dc fed-back amplifier with feedback from the emitter of Q_2 to the base of Q_1. The base of Q_1 acts as a virtual ground to provide an adding point for inputs. The collector waveform of Q_2 feeds an output driver containing Q_3, Q_4 and Q_5 which will drive the full signal (up to 6 V) into a 100 Ω load if required to do so. This output stage, which is a transistor complementary-pair analogy to the well known White cathode-follower, was described in the previous paper where a similar stage is used as an output stage in the double delay line amplifier.

The delay line shown in fig. 1 is terminated in 2200 Ω at each end of the cable. The terminating resistors mount directly on the ends of the cable, the input one being *series* fed by the input signal while the *current* in the output resistor is *series* fed to the adder amplifier. Thus no stray capacity is added across the termination of the cable and excellent signal shapes result.

0.4 μsec wide. A + 1 V pulse applied to an anti-coincidence input (22) during the entire time for which the other inputs are coincident inhibits the circuit and prevents an output pulse occurring.

The resistor R_4 provides a nearly constant current of 10 mA into the emitter circuits of transistors Q_1 to Q_5. In the rest condition this current shares between the emitters of Q_2, Q_3 and Q_4 since the bases of these transistors are about 0.5 V negative with respect to the base of Q_1 and 1.6 V negative with respect to the base of Q_5. Thus nearly 10 mA flows in the common collector circuit of Q_2, Q_3 and Q_4 and produces a voltage drop of 3.8 V in R_6. Application of + 1 V input pulses to any one or two of the transistors Q_2, Q_3 and Q_4 causes no change in this situation since if, for example, Q_2 and Q_3 are turned off, Q_4 conducts all the 10 mA current. If, however, simultaneous + 1 V inputs are applied to Q_2, Q_3 and Q_4, Q_1 momentarily conducts the 10 mA, the

collector voltage of Q_2, Q_3, Q_4 falls and the negative voltage swing at these collectors is fed via C_6 to the base of Q_5, Q_5 therefore starts conducting and the positive feedback loop causes a trigger action to ensue at the end of which Q_5 is conducting all the 10 mA, its base potential swinging to about + 13 V (i.e. 1.5 V below the external capacity across pins 8–11 on the printed circuit socket.

The action of a + 1 V anti-coincidence pulse is to prevent Q_1 coming into conduction at the start of the trigger action described earlier, thereby preventing the triggering process from occurring.

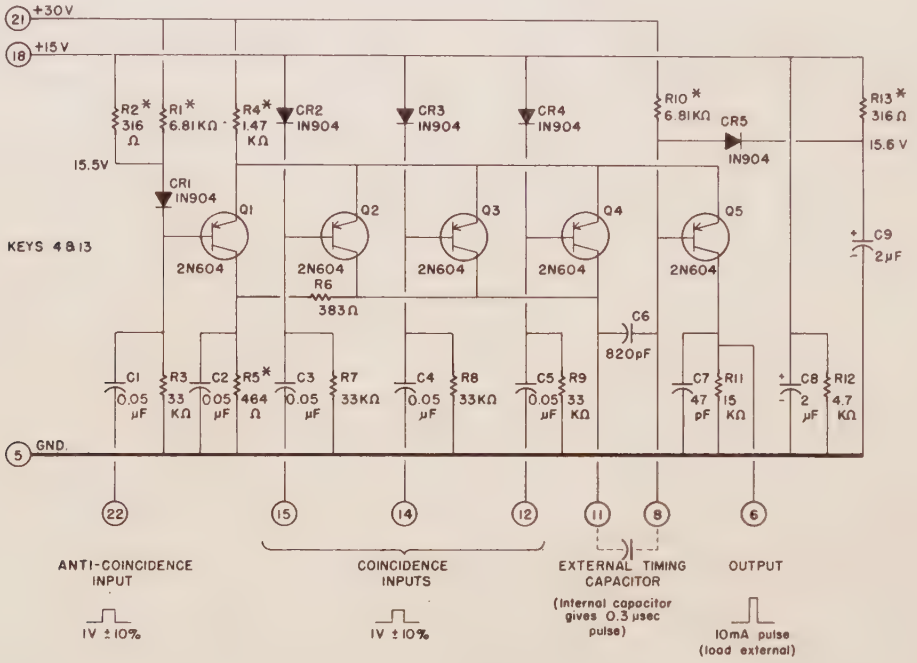

Fig. 4. Coincidence circuit.

base potentials of Q_2, Q_3 and Q_4. The trigger action is extremely fast and occupies only a few nanoseconds.

Following this action, the base of Q_5 rises as C_6 is charged by the current flowing in R_{10}. When the base potential of Q_5 approaches that of Q_2, Q_3 and Q_4 these transistors start to conduct and a regenerative action starts at the end of which the circuit has relaxed back to its rest condition. The output pulse is taken from the collector of Q_5 where a 10 mA pulse is available. This is usually used to produce + 1 V in 100 Ω for other logical units. The small capacitor C_7 prevents rapid changes in the collector voltage of Q_5 thereby reducing the slowing down in triggering which is caused by Miller effect in Q_5. The output pulse width (normally 0.4 μsec) may be increased by adding

The circuit is quite tolerant of variations in input pulse amplitude; both coincidence and anti-coincidence inputs can be varied over the range 0.6 V to 1.5 V with no effect on circuit operation.

3.3. VOLTAGE DISCRIMINATOR (see fig. 5)

The use of low level pulses in a system demands a high degree of stability in the voltage discriminators employed. In the present case we are dealing with a 4 V system and it is reasonable to demand a discriminator with a triggering threshold accuracy of about $\pm$ 4 mV under all working conditions. Since the Chalk River kick-sorter operates from negative pulses the discriminator is required to measure the negative pulses of the bi-phase waveform produced by double delay line shaping. A single semi-conductor diode is unable to achieve the required

threshold sensitivity since the voltage drop in such a diode, at constant current, exhibits a temperature coefficient of about — 2.5 mV/°C. For a ± 10°C change of temperature, a reasonable operating range, the change in threshold is

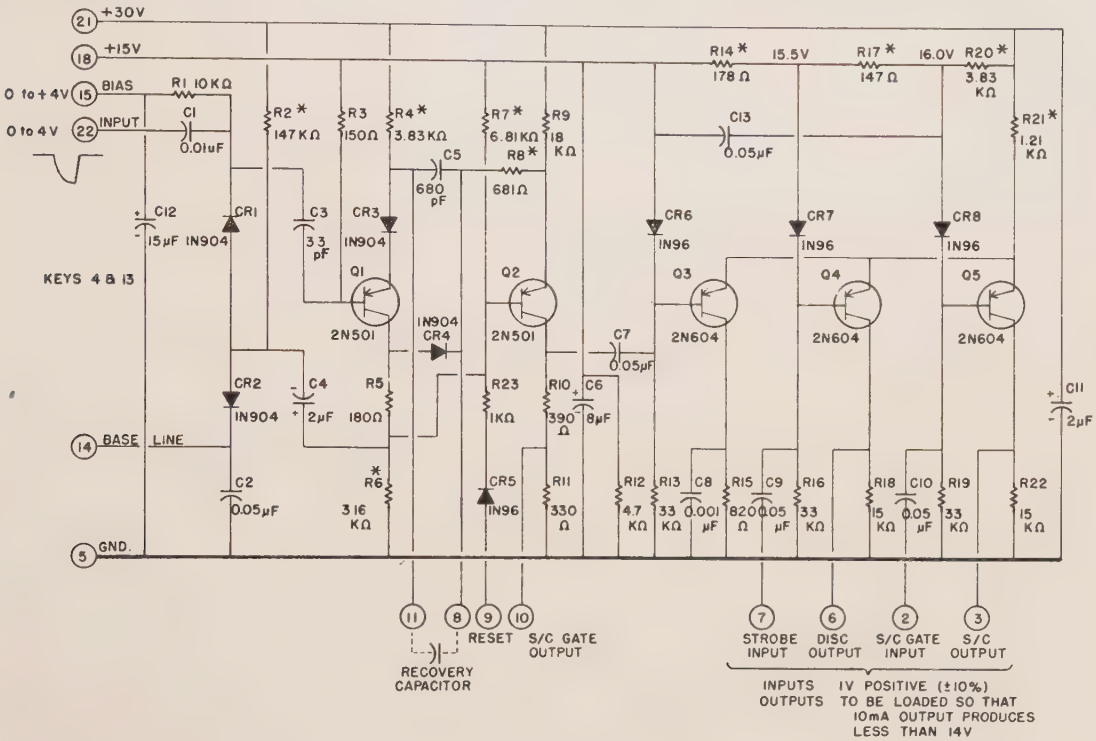

Fig. 5. Voltage discriminator.

± 25 mV. Fortunately, nearly all diodes of a given type exhibit within ± 5% the same temperature coefficient. Therefore, if the drop in one diode is balanced by the drop in another of the same type the temperature coefficient of the pair of diodes will not exceed 250 μV/°C— (i.e. ± 2.5 mV change for ± 10°C).

In the circuit shown in fig. 5, diode CR_1 is the voltage discriminator element while CR_2, operating at constant current, provides the temperature compensation for changes in CR_1. Back bias (0 to + 4V at pin 15) is applied to diode CR_1 and only when the negative pulse applied to the cathode of CR_1 exceeds the bias does CR_1 conduct and a small pulse appear across CR_2.

In a biased diode discriminator of this type a second type of temperature variation occurs. Leakage current in CR_1 flows in R_1 producing a voltage drop in R_1 which changes the effective bias on CR_1. Since the leakage current of the diode is temperature dependant the effective bias depends on temperature. To reduce this effect to negligible proportions a low leakage silicon diode type is selected for CR_1 and the value of R_1 is limited to a value where the temperature coefficient due to leakage current in CR_1 is less than ± 1 mV for ± 10°C change of temperature.

An additional source of change in threshold of a discriminator is base-line shift at the cathode of CR_1 at high pulse rates. This effect is negligible when using double delay line pulses, where the areas of positive and negative pulses are equal, but can be very serious when using single phase pulses. A circuit, to be described later, has been devised which measures the base-line of single phase pulses and the base-line determined by this circuit can be fed into pin 14 on the discriminator board. This minimises the base-line shift at high counting rates of single phase pulses. When using double delay line pulses pin 14 is grounded.

The circuit associated with transistors Q_1 and Q_2 is a trigger circuit of the type described in ref.[2]). With the values shown in fig. 5 the circuit triggers when a negative pulse of about 150 mV appears across CR_2. The triggering threshold is extremely accurate ($\sim \pm 1$ mV) as required in this application. In the rest condition, transistor Q_1 passes the current flowing in R_4 while Q_2 passes that flowing in R_9. Positive feedback is present in the circuit due to the direct coupling from the collector of Q_1 to the base of Q_2 and the coupling via C_5, R_8 between the emitters. Since both transistors are conducting in the rest condition, the circuit would be oscillating were it not for the effect of the low impedance of CR_2 shunting the collector load of Q_1 via Q_4, thereby reducing the loop gain in the trigger circuit below unity.

As seen by diode CR_2, the trigger circuit may be shown to exhibit a negative resistance roughly equal in magnitude to resistor R_8. Thus a negative pulse which feeds through CR_1 and appears across CR_2 causes current to flow into C_4 from diode CR_2; this reduces the current in CR_2 and, if the input pulse is of sufficient magnitude (about 150 mV) across CR_2, the circuit triggers. When this happens the collector voltage of Q_1 drops as Q_1 becomes non-conducting. The 7 V drop at the collector of Q_1 feeds through C_4 to the common anodes of diodes CR_1 and CR_2 holding both diodes out of conduction for the duration of the relaxation period of the trigger circuit.

Capacity feedthrough in CR_1 is partially compensated by the action of capacitor C_3 and resistor R_3. A negative input pulse causes a differentiated negative pulse at the base of Q_1 which tends to prevent the trigger circuit action to the same degree as the capacity breakthrough in CR_1 aids triggering. C_3 has been chosen to make the trigger level almost independent of signal rise time in the range 50 nsec to 0.5 μsec. During the relaxation period the emitter-base junction of Q_1 is reverse biased and C_5 charges due to the current in R_4 flowing into it. At a time determined by C_5 and shunt capacity connected externally across pins 8–11 of the printed circuit socket, Q_1 again conducts and a reverse trigger action occurs. Diode CR_4, which has previously been out of conduction, conducts and capacitor C_5 is rapidly recharged back to its original condition. The recovery time is very short amounting to less than 10% of the pulse width produced by the circuit.

The relaxation time of the circuit may be terminated prematurely by feeding a + 10 V reset pulse through diode CR_5 at any time during the relaxation period. This facility is used when two or more discriminators are cascaded to give a single or multiple channel analyzer; a common reset pulse generated by a unit to be described then ensures that all discriminators are reset at the same time.

The parts of the discriminator described so far are the only parts required in a single discriminator. However, in a system like the one described here, several discriminators arranged as single or multi-channel analyzers are used and the remaining circuitry in the discriminator unit is required to facilitate cascading discriminators for these purposes. In the case of a single-channel analyzer, an output pulse must result when the lower but not the upper discriminator fires. Furthermore since the rise time of input pulses is not in general very short the two discriminators do not fire at the same time. We therefore arrange to wait until the input pulse is known to have passed its peak amplitude then to sample the condition of the discriminators and finally reset them. The output pulse from the single-channel analyzer which appears during the sampling or strobe period is therefore delayed with respect to the input signal.

An external unit, described later, is used to generate the sample (strobe) and reset pulses. Each discriminator then contains a coincidence circuit similar to that described in the previous section of this paper which accepts inputs from the discriminator itself, from the next highest discriminator in the cascade and also the strobe pulse. The discriminator itself generates a 2.5 V positive pulse which feeds the base of normally conducting transistor Q_3 transferring the current from Q_3 to Q_4. When a (+ 1 V) strobe input

pulse is fed to the base of Q_4 the current transfers to Q_5 unless a + 1 V pulse taken from pin 10 on the next higher discriminator is present at the base of Q_5. In this case Q_4 remains in conduction when the strobe is applied. Thus the + 10 mA output pulse at the collector of Q_5 in a particular discriminator only occurs following a signal

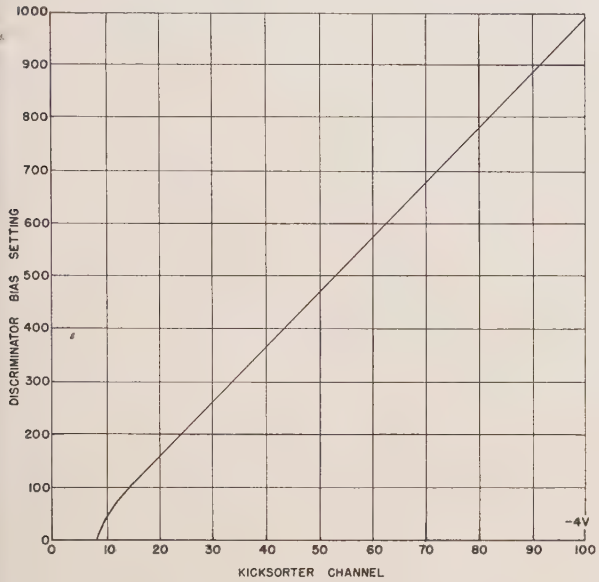

Fig. 6. Discriminator calibration curve.

whose amplitude lies between this discriminator bias and the next one in the cascade. The collector of Q_4 provides a pulse which indicates that the discriminator has fired.

Bias for the discriminators is obtained from helical potentiometers supplied with a stable voltage from a Zener reference element. The potentiometers and the Zener regulating system mount on the front panel of the complete unit. The circuit is shown together with the overall connections for the double-channel analyzer in fig. 9. The linearity of calibration of the discriminator bias control is a matter of some interest. As seen in fig. 6 the calibration is almost linear but the calibration line does not pass through the origin. This is due to the fact that a portion of the current in CR_2 in fig. 5 flows in CR_1 at low bias levels and, when CR_1 is in conduction the sensitivity is mainly determined by the threshold level of the trigger circuit containing Q_1 and Q_2.

3.4. CROSS-OVER PICK OFF AND COINCIDENCE CIRCUIT (see fig. 7)

As mentioned in the previous section cascading several discriminators to produce a multi-channel analyzer requires that a strobe pulse be developed at a time when the input pulse amplitude is known to have reached its maximum value and that a discriminator reset pulse be developed following the strobe pulse. A convenient way of determining a suitable time for the strobe pulse is to measure the zero cross-over of a double delay line pulse (see fig. 2 for pulse shape). One function of the unit to be described is to determine the cross-over of pulses fed to the dual-channel analyzer and to develop strobe and reset pulses for the discriminators in the analyzer. Transistors Q_6, Q_7 determine the cross-over while Q_9, Q_{10} and Q_{11} produce strobe and reset pulses appropriately delayed from the cross-over. Emitter-follower Q_{12} provides the reset pulse with adequate current to reset up to ten discriminators. The cross-over measuring circuit Q_6, Q_7 is duplicated in the "B" channel by Q_1, Q_2 and transistors Q_3, Q_4, Q_5 act as a fast coincidence circuit producing an output pulse at the collector of Q_5 only when crossovers in "A" and "B" channels occur within 40 nsec of each other. The diode circuits in the input of both crossover circuits limit the signal amplitude applied to the transistors to a level where reverse emitter breakdown does not occur.

The operation of the crossover measuring circuit will be described with reference to Q_1, Q_2. Double-delay-line pulses up to ± 6 V in amplitude appear at pin 3 with the negative phase of pulse preceding the positive phase. When no pulse is present the current in R_1 shares between CR_1 and CR_2, approximately 1.25 mA flowing in each. Small negative or positive pulses feed through the two diode impedances in series into the 464 Ω resistor R_4 in the base of Q_1. Large negative signals cut-off the current in CR_2 producing a maximum negative signal of about 0.6 V at the base of Q_1. Large positive signals cut-off CR_1 producing + 0.6 V at the base of Q_1. Thus small input signals appear almost

unchanged at the base of Q_1 but large signals are very effectively limited.

Q_1 and Q_2 constitute a Schmidt type circuit with an accurately controlled amount of backlash (about 150 mV). Q_2 is in conduction in the rest condition and the circuit is triggered into the opposite state when the input negative edge exceeds 150 mV. Due to the voltage movements at the base of Q_2 the retrigger action does not occur until the pulse crosses the baseline at the end of its negative excursion. Preset the base of Q_3. A similar arrangement feeds pulses at the "A" channel crossover from Q_7 to the base of Q_4. Q_3, Q_4 and Q_5 constitute a coincidence circuit of the type described earlier in the paper and, when coincident pulses occur at the bases of Q_3 and Q_4 a shaped square $+10$ mA current pulse 0.25 μsec wide is produced in the collector circuit of Q_5. As with the other coincident circuits this output (pin 6) is usually terminated in 100 Ω to give a $+1$ V pulse in another unit.

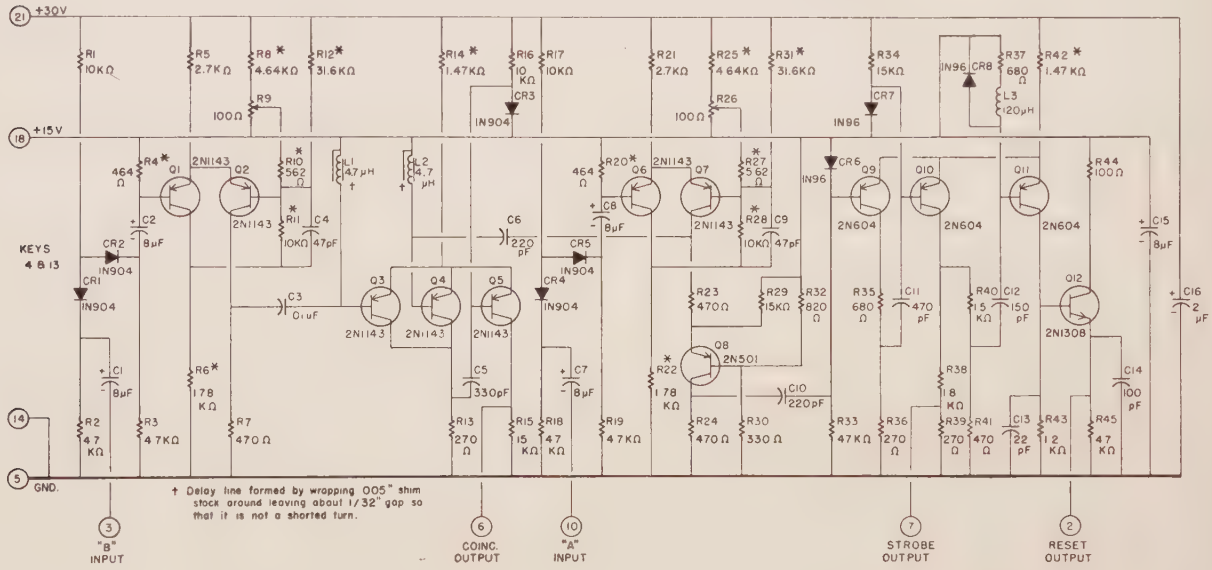

Fig. 7. Cross-over pick off and coincidence circuit.

potentiometer R_9 is provided to allow exact adjustment of the crossover trigger point since the precise trigger level is dependent upon the characteristics of the transistors. Adjustment of R_9 is conveniently carried out by feeding a 300 mV negative pulse having an exponential tail into the input and adjusting R_9 to cause the circuit retrip to occur when the tail reaches 5 mV or so (i.e. or 22 μsec if the pulse tail time constant is 5 μsec). This accuracy of measurement of the crossover ensures timing accuracy of the crossover of $\pm$ 3 nsec on NaI(Tl) pulses for a range of pulse amplitudes from 200 mV to 4 V (the range measured by the discriminators).

When the current in Q_2 turns on at the crossover point, a narrow positive pulse about 1.5 V high is shaped by the shaping network† in

The collector current of Q_7 flows in Q_8 and the back edge of the pulse at the collector of Q_8 is used to trigger a three-transistor trigger circuit which produces strobe and reset pulses for the discriminators. Q_9 is normally in conduction passing all the current (10 mA) in R_{41}. A positive pulse fed from the collector of Q_8 to the base of Q_9 via C_{10} causes Q_{10} to conduct for a period determined by capacitor C_{11} and other components in the base of Q_{10} and collector of Q_9. When Q_9 goes out of conduction its collector voltage falls. This drop in voltage feeds via C_{12} to the base of Q_{11} turning on Q_{11} for a period

† The shaping network is a 4.7 μH "National" choke surrounded by a close fitting grounded shield to give distributed stray capacity from the coil to ground. Its characteristic impedance is about 500 Ω.

determined by its base circuit. This circuit arrangement, which is an adaptation of the coincidence circuit described earlier, allows the generation of a sequence of delayed pulses at a cost of 1 transistor per delay plus 1 triggering transistor. In this case the circuit is used only to produce a + 1 V strobe pulse at pin 7 and a + 10 V produced. The sequence of delays is produced by the circuits associated with Q_3, Q_4, Q_5, Q_6 in the same way as described in the previous section.

Transistors Q_1 and Q_2 are used to determine the baseline of the input signal pulses. The discriminators then measure the pulse heights from this baseline thereby largely eliminating the

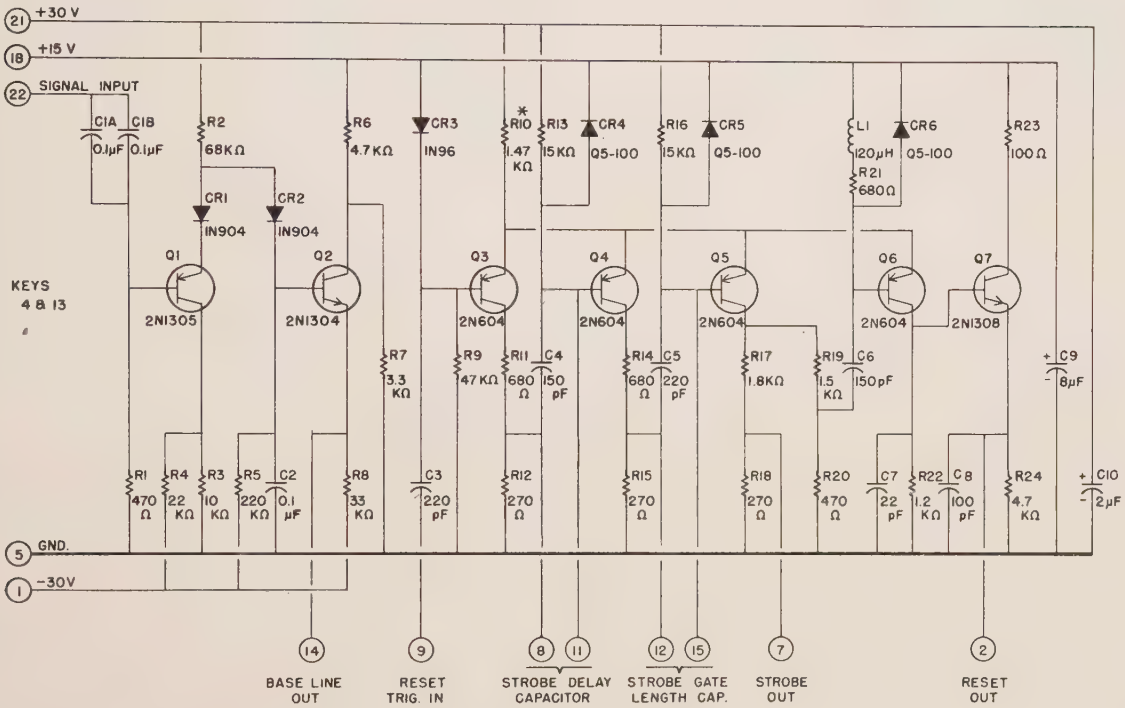

Fig. 8. Base line compensator strobe and reset circuit.

reset pulse at the collector of Q_{11} which feeds emitter-follower Q_{12} to drive the output pin 2.

3.5. BASE LINE COMPENSATOR, STROBE AND RESET CIRCUIT (see fig. 8)

Inevitably some applications of the system involve the measurement of single phase as distinct from double delay line pulses. To deal with these cases a unit has been designed which can replace the crossover measurement unit just described in these applications. This unit duplicates the functions of developing strobe and reset pulses as in the crossover pickoff unit but instead of using the input pulse zero crossover as its basic timing mark, the firing of the first discriminator is used for this purpose. A fixed delay then occurs before the strobe pulse is baseline shift effects at high pulse rates. Negative input pulses are fed to the base of Q_1 through capacitors C_{1A} and C_{1B} in parallel. At high rates the base of Q_1 moves in a positive direction between pulses since the average current flowing in C_1 must be zero. A negative pulse at the input is emitter-followed by Q_1 and, if the pulse height exceeds about 0.2 V, diode CR_2 is cut off. Capacitor C_2 prevents the cathode of CR_2 falling in potential appreciably during the pulse since C_2 can only be discharged by the small current flowing in R_5. When the negative pulse terminates, CR_2 again conducts, rapidly replacing the charge lost from C_2 during the pulse. It may be seen that a rate of 10^5 pulses/sec each 1 μsec wide causes a change of only about 15 μA in the mean current in the emitter of Q_1, CR_1 and CR_2

as compared with zero input rate. This current change in the three elements produces a total change in voltage across them of only about 5 mV. Thus the voltage across C_2 is a good replica of the baseline of the pulses at the base of Q_1. Q_2 emitter-follows the voltage at its base giving a low impedance output to serve as a baseline for the discriminators. Note that the temperature coefficient of voltage drop in Q_1 and CR_1 is balanced by that in Q_2 and CR_2 so that the output baseline is very nearly independent of temperature.

the bias dial reading is 1000 (i.e. bias control set to maximum bias). A 215 Ω resistor in series with the baseline (pin 14) to discriminator 1 causes the baseline of that discriminator to assume a potential of about + 40 mV (the voltage drop being due to the 200 μA flowing through CR_2 in the discriminator (fig. 5). Adjustable resistors in the equivalent points of the other two discriminators are set to produce the same — 4 V sensitivity in these discriminators as in 1 when the bias controls are set to maximum. These adjustments are required to compensate for

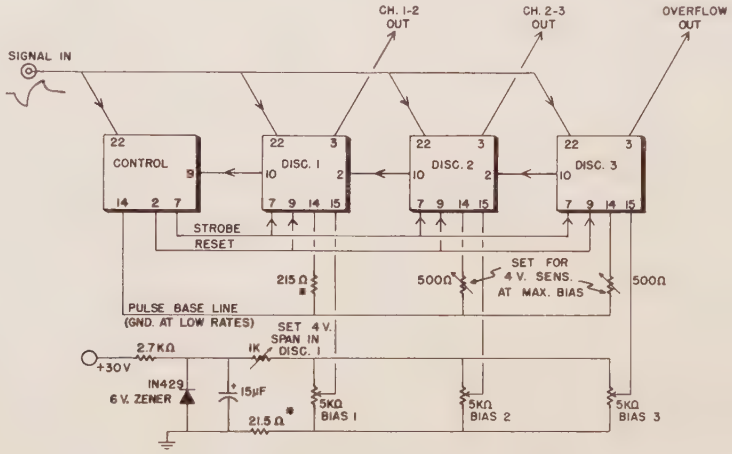

Fig. 9. Dual-channel analyzer wiring.

3.6. DUAL-CHANNEL ANALYZER (see fig. 9)

Many fast-slow coincidence systems use only a single-channel analyzer but occasions do arise when a dual-channel unit is useful and since sufficient space was available a dual-channel analyzer is included in the system. This uses three discriminators each with a bias control and a control unit which generates strobe and reset pulses for the discriminators. If double phase pulses are employed the preferred control unit is the crossover pick-off circuit described in section 3.4, while single-phase negative pulses require the baseline compensator unit described in section 3.5.

The connections shown in fig. 9 are almost self-explanatory. Bias for the discriminators is obtained from a Zener reference element and the 1 kΩ potentiometer in series with the 5 kΩ helical potentiometers serves to adjust the sensitivity of the discriminator 1 to — 4 V when different voltage drops in diodes in the various discriminators. When they are correctly made the discriminators track to within $\pm$ 0.2% of full-scale reading through their entire range.

3.7. LINEAR GATE CIRCUIT (see fig. 10)

The linear gate unit normally permits no input signals to pass through it but, on receipt of a gate trigger pulse, the gate connects signal input to signal output for a predetermined time.

All linear gates are imperfect in that a small pedestal is generated when the gate is open even though no signal is present at the signal input. To illustrate the importance of this many writers use the term "Pedestal-free gate" instead of "Linear gate" as used here. A second defect which occurs is break-through of signals from input to output when the gate is in its non-transmitting condition. These two defects are of

major importance in low level systems and, in a 4 V system as described here, both pedestal and signal breakthrough should be kept down to a few mV.

The block diagram (fig. 11) will be used in the following explanation of the operation of the linear gate. Q_5 and Q_6 are the gating elements; emitter in the non-conducting condition, signals fed to the collector of Q_5 are very highly attenuated by the gate before appearing at the output. Very small spikes appear at the output on fast signal edges but total break-through for 6 V signals is less than 10 mV.

When a gating trigger pulse is fed to its input

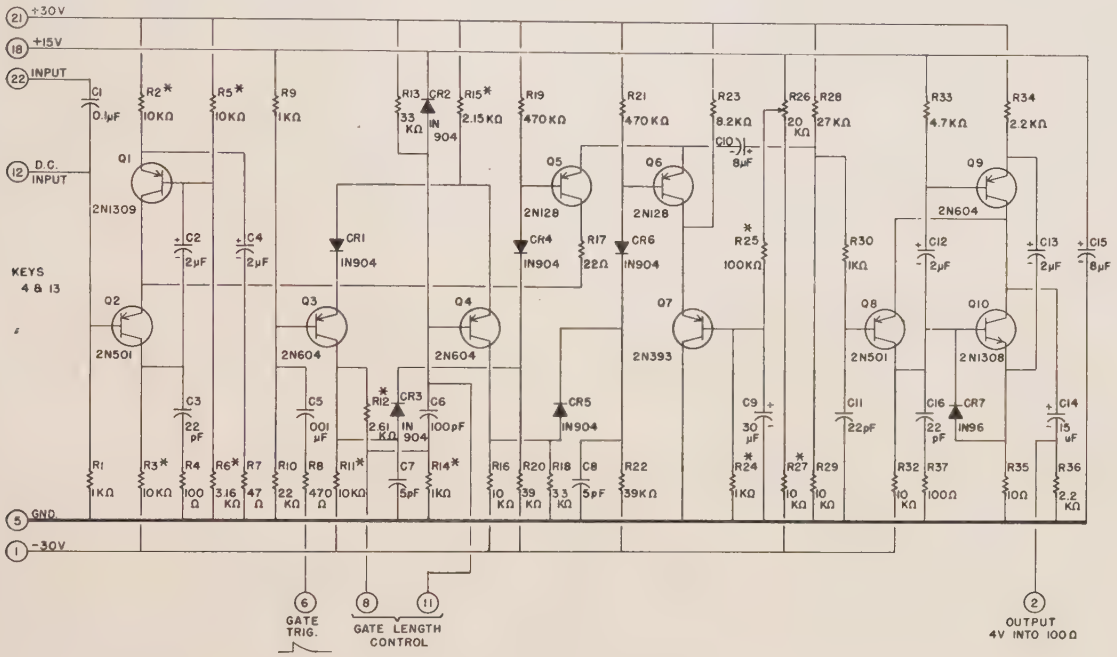

Fig. 10. Linear gate circuit.

the remainder of the circuit is incidental to the operation of the gate. In the rest condition of the circuit diode CR_3 is conducting so that the common cathode of CR_3 and CR_4 is held at + 7 V and, due to the 70 μA flowing in CR_4, the base of Q_5 is at approximately the same voltage. On the other hand CR_5 is non-conducting and CR_6 is passing 0.75 mA. The collector of Q_6 is connected to a low impedance voltage source whose output voltage is very close to ground. The current in CR_6 flows out of the base of Q_6 causing the collector of Q_6 to emit holes into the base and Q_6 acts as an inverted transistor. Since the emitter junction of Q_5 is reverse biased Q_6 is called upon to pass almost no emitter current and its emitter takes up almost the same potential as its collector. The effective impedance seen at the emitter of Q_6 is very low and since Q_5 behaves as a very high impedance between its collector and the gating pulse generator produces a narrow pulse which reverses the situation in transistors Q_5 and Q_6, Q_5 becoming a low impedance between collector and emitter while Q_6 becomes a high impedance. Thus, during the period of the gating pulse, the input signal suffers almost no attenuation in passing through the gate to the output of the unit. Note that a single transistor such as Q_5 or Q_6 with the other transistor replaced by a resistor acts as a good gate and, in fact, this arrangement is used in dc choppers[5]). However, using two transistors improves the transmission-attenuation ratio in the two conditions and also largely eliminates switching transients since one transistor comes into while the other one goes out of conduction.

The low impedance driver feeding the gate is

[5]) G. B. B. Chaplin and A. R. Owens, Proc. I.E.E. 105 B (1958) 258.

needed to prevent the collector current of Q_5 (when conducting) from producing a false signal. The low impedance output driver provides sufficient power to drive 100 Ω cable if required. Both drivers are similar to the output driver described in the previous article on the double delay line amplifier. The gating pulse generator is a normal Schmidt trigger circuit with coupling from the collector of Q_3 to the base of Q_4 via C_6. The gate duration can be changed by adding external capacity from pins 8 to 11 on the printed circuit socket. The low impedance variable voltage supply transistor Q_7 allows

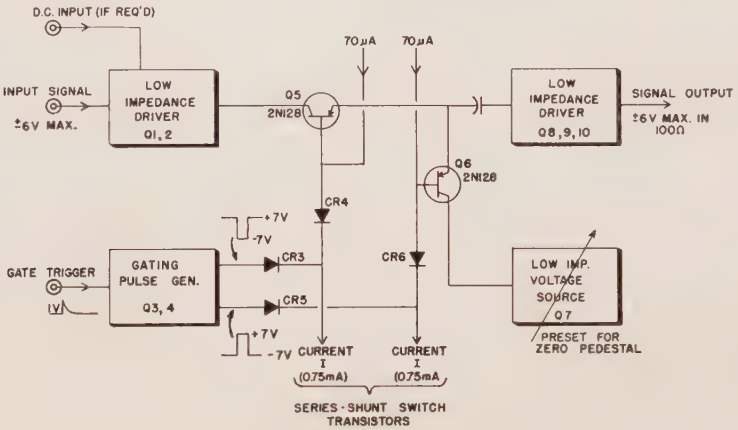

Fig. 11. Block diagram of linear gate unit.

adjustment of the pedestal to zero. The drop in the emitter-base junction of Q_7 compensates for that in the emitter-base junction of Q_2. Note that these voltages temperature compensate each other so that the pedestal is nearly independent of temperature.

Since the linear gate provides a good dc chopper, advantage can be taken of this to produce pulses of defined amplitude. With this in mind a dc input point is provided and application of trigger pulses to the gate generator while a dc potential is fed to the input produces pulses equal in amplitude to the dc input level. This facility is not used in the fast-slow coincidence system but has been used in other applications of the unit.

3.8. TIMING CONSIDERATIONS IN THE SYSTEM

Two cases must be considered according to whether the input pulses are single phase (negative) or double delay line pulses:

(a) *Single Phase Pulses* (using Base Line Compensator Unit)

In this case the triggering of discriminator 1 is used as the basic timing mark. A delay must then be provided to allow for the full rise time of the pulse in the "A" channel before strobing the state of the discriminators. This delay is made equal to the total pulse rise time T to cope with the case where discriminator 1 triggers from the very start of the pulse while the other discriminators may trigger at any point in the rise. Since, on the other hand, discriminator 1 may trigger on a small pulse very close to the end of the rise, the strobe timing can then be between as short as T and as long as $2T$ after the true start of a signal. Thus the linear gate will be instructed to open to allow signals through at any time between T and $2T$ after the start of a signal pulse. The linear gate requires 0.3 μsec to fully open so signals to be gated by it must be delayed by the delay line by a total time $2T + 0.3$ μsec if the gate is to allow through the start of the signal. In practice, the Chalk River kicksorter operates well from 0.3 μsec pulses and the open period of the linear gate need only bracket the signal for this time provided that the signal reaches its full amplitude during the gate open period. Clearly the ideal values of delay line length and of the durations of the various gates

and pulses depend upon the input signals and must be calculated for particular cases. However the following values have been chosen for NaI(Tl) pulses (rise time constant 0.3 μsec) shaped by a single 1 μsec delay line:

Strobe delay: 1.2 μsec
Strobe width: 0.5 μsec
Signal delay in "B" channel: 2 μsec
Gate duration: 2 μsec

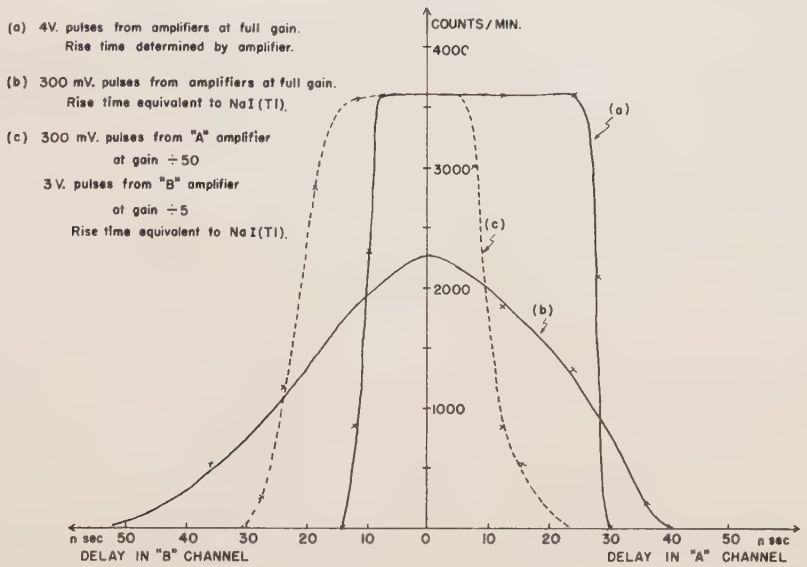
(a) 4V. pulses from amplifiers at full gain. Rise time determined by amplifier.
(b) 300 mV. pulses from amplifiers at full gain. Rise time equivalent to NaI(Tl).
(c) 300 mV. pulses from "A" amplifier at gain ÷50
3 V. pulses from "B" amplifier at gain ÷5
Rise time equivalent to NaI(Tl).
COUNTS / MIN.
4000
3000
2000
1000
(a)
(b)
(c)
n sec 50 40 30 20 10 0 10 20 30 40 50 n sec
DELAY IN "B" CHANNEL
DELAY IN "A" CHANNEL

Fig. 12. Resolution curves for system.

(b) *Double Phase Pulses* (using Crossover Pick-off Unit)

In this case the basic timing mark is the crossover from negative to positive phase in the pulse. Since this time is absolutely related to the start of the signal and also to the duration of the pulses it is possible to reduce all times as compared with the previous case. The strobe is automatically generated at the crossover time and the following times are suitable for operation with pulse lengths (negative phase) and rise times from 0.4 μsec to 1 μsec.

Strobe width: 0.5 μsec
Signal delay in "B" channel: 1 μsec
Gate duration: 0.5 μsec .

4. Performance

Tests on the instrument have shown that the whole system is quite capable of determining pulse amplitudes at rates up to 10^5 pulses/second and under all normal operating conditions with an accuracy of $\pm$ 5 mV. The time resolution has been measured by the usual method of inserting delay (100 Ω cable) in one channel relative to the other and the resulting resolution curve is seen in fig. 12. These curves were obtained with pulses from a pulse generator feeding two double delay line amplifiers and the remainder of the system. No attempt was made prior to the test to match delays in the two channels.

Curve (a) shows the resolution obtained with full size pulses (i.e. 4 V at the input to the coincidence system) having a rise-time solely determined by the amplifier (0.2 μsec from 10 to 90%). Curve (b) shows the degradation in resolution resulting from operation with small (300 mV) pulses of 0.3 μsec rise-time simulating NaI(Tl) scintillation pulses. Curve (c) is the result of operating with 4 V NaI(Tl) type pulses in the "A" channel and 300 mV similar pulses in the "B" channel. The spread in the resolution curves is entirely attributable to the effect of amplifier noise in producing jitter in the crossover time of the double-delay-line shaped pulses.

An example of the performance of the instrument used with NaI(Tl) pulses is shown in

fig. 13. The shaping delay lines in the amplifiers were 1 μsec long. The explanatory diagram in fig. 13 shows the set-up. γ-rays from a Cs^{137} source strike both crystals and 180° scattering occasionally occurs from one crystal into the other. The single-channel analyzer in the "A" channel is set to select the 200 keV scattered radiation in detector "A" and the spectrum of events in the photopeak at 660 keV are very prominent. Inclusion of the fast coincidence circuit cuts out nearly all the random coincidences as seen in curve (b). Curve (c) illustrates the effect of inserting 50 nsec delay in the "A" channel thereby eliminating nearly all true coincidences and leaving only the very low rate of chance coincidences at the output.

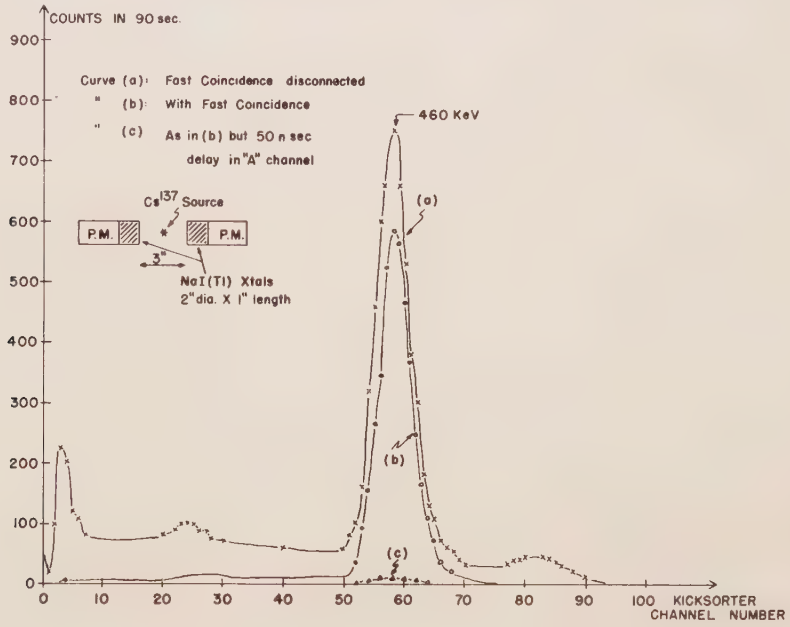

Fig. 13. Spectrum of γ rays in "B" channel in coincidence with 200 keV $\pm$ 20 keV events in "A" detector.

pulses in the "B" detector in coincidence with this is determined by the kicksorter. Curve (a) shows the result when the fast coincidence circuit is not connected. In this case random coincidences occurring in the 0.5 μsec resolution of the slow part of the system produce a general background for the peak and the random coincidences of

Acknowledgements

This work was carried out as part of the research programme of the Physics Division of Atomic Energy of Canada Limited. The authors wish to thank T. K. Alexander and L. B. Robinson for many useful comments and for their interest in this work.

NUCLEAR INSTRUMENTS AND METHODS 8 (1960) 297–303; NORTH-HOLLAND PUBLISHING CO.

A VERSATILE, HIGH EFFICIENCY 4π NEUTRON DETECTOR*†

J. B. MARION, R. J. A. LEVESQUE††, C. A. LUDEMANN and R. W. DETENBECK

Physics Department, University of Maryland, College Park, Maryland

Received 6 May 1960

A high efficiency 4π neutron detector has been constructed which consists of 12 $B^{10}F_3$ proportional counters imbedded in a two-foot cube of paraffin. The response of this detector as a function of neutron energy has been measured in the range 0.1 to 2.5 MeV by observing the yield curves for the T(p,n) and Li^7(p,n) reactions, the absolute total neutron production cross sections for which have been accurately measured by Macklin and Gibbons. These measurements indicate a detection efficiency of approximately 10 per cent and a response which is flat to within ± 5 per cent over the entire energy range studied. The efficiency for the detection of neutrons from a Ra-α-Be source (average neutron energy approximately 5 MeV) was found to be 6.5 per cent. The efficiency was observed to decrease for neutron energies below about 0.1 MeV by measuring the yield from the V^{51}(p,n) reaction. The efficiency for the detection of 50-keV neutrons is approximately 4 per cent. The detector has also been used to detect neutron thresholds for nuclear ground states and excited states by observing the slow threshold neutrons in the forward direction with a Li^6I scintillator surrounded by a B_4C shield. This "closed geometry" technique appears capable of only slightly less sensitivity than the "open geometry" method and is somewhat superior in energy resolution.

1. Introduction

The detection of neutrons in 4π geometry has long been a standard technique for the calibration of neutron source strengths in water-moderated baths containing, e.g., $MnSO_4$. These methods, although capable of high accuracy, require elaborate chemical techniques and therefore are not especially suited for the study of neutron production in nuclear reactions when the energy dependence of the neutron yield is desired. Several detectors have been constructed[1]) for the study of photoneutron processes in 4π geometry; however it appears that only two previous detectors have been designed specifically for the study of total neutron production cross sections from charged-particle induced reactions. The first of these detectors is the 5-foot diameter graphite sphere constructed at the Oak Ridge National Laboratory by R. L. Macklin[2]). This detector has been used extensively for the study of total neutron production cross sections from (p,n) and (α,n) reactions in the light nuclei[3,4]). Johnson, Galonsky, and Ulrich[5]) have constructed a paraffin-moderated assembly and have used this detector in the study of neutron strength functions from (p,n) reactions in the medium weight elements. The present detector was modeled after that constructed by Johnson *et al.*, but was designed to have a somewhat higher efficiency and a response that was more nearly flat with neutron energy. Experiments for which this detector was designed include the study of (α,n) and (p,n) reactions of extremely small cross section. One class of these experiments is the study of (α,n) reactions on the 4n + 1 nuclei (Be^9, C^{13}, O^{17}, and Ne^{21}) which have important astrophysical implications in that several of these reactions are considered to be likely sources of neutrons in stars. These

* Supported in part by the U.S. Atomic Energy Commission.

† A preliminary report of this work was given at the New York Meeting of the American Physical Society, January, 1960: C. A. Ludemann, R. J. A. Levesque and J. B. Marion, Bull. Am. Phys. Soc., Ser. II, **5** (1960) 16.

†† Now at the University of Montreal, Montreal, Quebec, Canada.

[1]) See, for example, R. Nathans and J. Halpern, Phys. Rev. **93** (1954) 437.

[2]) R. L. Macklin, Nucl. Instr. **1** (1957) 335.

[3]) J. H. Gibbons and R. L. Macklin, Phys. Rev. **114** (1959) 571.

[4]) R. L. Macklin and J. H. Gibbons, Phys. Rev. **109** (1958) 105.

[5]) Johnson, Galonsky and Ulrich, Phys. Rev. **109** (1958) 1243.

neutrons undergo capture reactions and thereby contribute to the formation of the heavier elements. Another class of experiments which can be studied with this detector is the investigation of neutron thresholds for nuclear ground states and excited states. The investigation of excited-state neutron thresholds in closed geometry has not previously been attempted.

2. Details of the Detector

2.1. CONSTRUCTION DETAILS

The details of the construction of the detector are shown in fig. 1. The outer shell of the detector is a two-foot cube of $\frac{1}{4}''$ steel plate. Within this steel shell is located an 18″ cube of $\frac{1}{4}''$ Boral (powdered B_4C pressed between 0.040-inch aluminum sheet). Prior to the filling of the shells with paraffin, hollow lucite rods were inserted through the shells for the purpose of supporting the detectors and the beam tube. The region between the steel and the Boral shells constitutes the outer paraffin shield. Neutrons which are incident on the detector from the outside are moderated in this outer shield and are then absorbed by the B^{10} in the Boral. The main paraffin block, which is an 18″ cube, constitutes the detector proper. The lucite rods which position the $B^{10}F_3$ detectors are arranged in two rings each containing 6 detectors. The counters in the inner ring are arranged on a pitch circle diameter of 6″ while the outer ring is on an 8″ diameter circle. This geometry differs from that employed by Johnson *et al.*[5]), in that there are more detectors located at a greater distance from the target position. This design change was made in order to increase the neutron detection efficiency for high energy neutrons. (Johnson's detector showed a decrease in efficiency of approximately 20 per cent between neutron energies of 0.1 and 0.7 MeV.)

The charged-particle beam enters the detector from the left in a beam tube which is inserted in the 1″ diameter hollow lucite cylinder; the target position is at the center of the detector. To the right of the target position is located a 4″ diameter hollow lucite tube. The object placed in this section depends upon the experiment; a polyethylene plug is used when total neutron production cross sections are being measured or a hollow B_4C cylinder is used as a shield for the threshold detector in measurements of neutron thresholds. When the charged-particle beam is on the target, cooling is accomplished by blowing air through the plastic target-cooling tube.

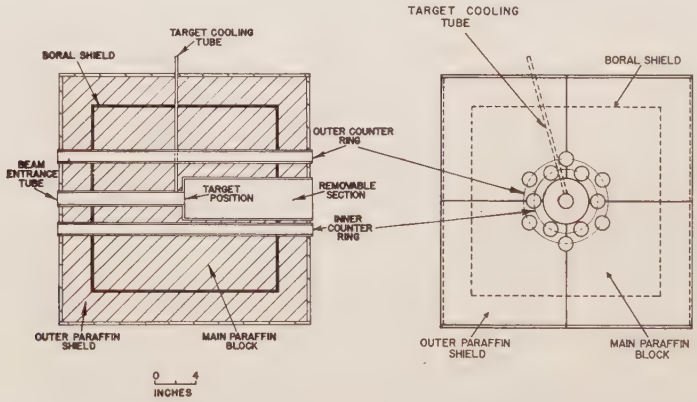

Fig. 1. Construction details of the 4π detecting system.

2.2. $B^{10}F_3$ PROPORTIONAL COUNTERS

The $B^{10}F_3$ proportional counters[6]) which were used in this detector were mounted in the two counter rings as shown in fig. 1. All counters in the inner ring were connected in parallel as were

[6]) Manufactured by Twentieth Century Electronics, Ltd. Croydon, Sussex, England. Distributed in U.S. by Hamner Electronics, Princeton, New Jersey.

all of those in the outer ring. The number of counts in each ring of counters was recorded separately. The pulse-height distribution obtained with six detectors connected in parallel is shown in fig. 2. This curve shows the excellent resolution and gain uniformity exhibited by

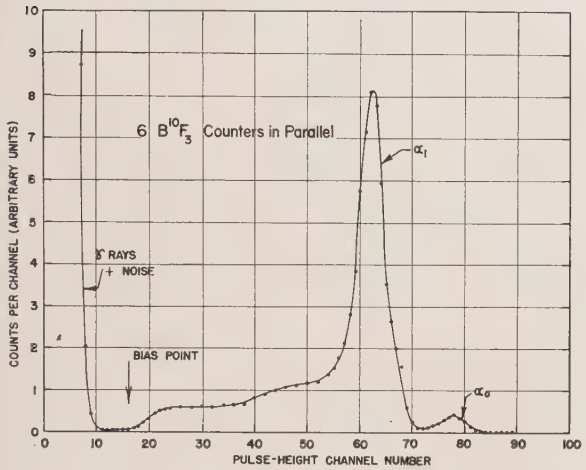

Fig. 2. Pulse-height distribution from 6 $B^{10}F_3$ detectors connected in parallel and irradiated with slow neutrons. The ground-state and first excited-state α-particle groups from the $B^{10}(n,\alpha)Li^7$ reaction are labeled α_0 and α_1, respectively. The resolution of the α_1 peak is 9.0 per cent.

these detectors. No adjustment of the high voltage was used in obtaining this pulse-height distribution; all detectors were connected directly in parallel. The two α-particle groups from the $B^{10}(n,\alpha)$ reaction are clearly resolved (α_0 and α_1 refer to the ground state and first excited state α-particle groups, respectively). Discrimination against γ rays and noise is readily achieved by biasing at channel 16. The detection efficiency of the counters used was found to be almost exactly equal to that of other commercially available detectors of similar size and with the same gas filling pressure[7]); the gain, however, was lower by about a factor of two but the resolution was far superior. When the detectors were operated singly the high voltage used was approximately 1600 volts. With six detectors operating in parallel it was necessary to increase the high voltage to approximately 1900 volts to compensate for the gain loss caused by the increased loading.

2.3. EFFICIENCY CALIBRATION

The efficiency of the detector as a function of neutron energy was measured by observing the yield curves for the $Li^7(p,n)$ and T(p,n) reactions, the absolute total neutron production cross sections for which have been accurately measured by Macklin and Gibbons[4]). The LiF target that was used for the efficiency calibration was obtained from Oak Ridge and was the same target that was used for the measurement of the absolute cross section for the $Li^7(p,n)$ reaction[8]). This target has a measured thickness of 387 ± 5 $\mu g/cm^2$. The tritium target which was used was also obtained from Oak Ridge[9]). During the course of the calibration runs it was found that if beam currents in excess of about 0.02 microamperes were used, then serious jamming of the detectors resulted. It was therefore decided to make the efficiency calibration by using only a single detector in each of the two counter rings. With this procedure, it was possible to use beam currents of approximately 0.2 μA. The use of these larger beam currents minimized instabilities in the regulation of the accelerator and also reduced the inaccuracies in the current integration system. Since all detectors are mounted symmetrically about the beam axis, the total efficiency of each ring was found by multiplying by six the efficiency for a single detector in that ring.

The absolute efficiency of the detector was measured with the Oak Ridge LiF target at a proton bombarding energy of 2.70 MeV. The $Li^7(p,n)$ cross section at this bombarding energy as given by Macklin and Gibbons[4]) is 285 mb. The average neutron energy (i.e., the energy of the neutrons emitted at 90° with respect to the beam axis) at this bombarding energy is 0.58 MeV. At this neutron energy, the detection efficiency of a single counter in the inner ring is

[7]) For example, those manufactured by N. Wood Counter Laboratory, Chicago, Illinois.

[8]) We are indebted to J. H. Gibbons of the Oak Ridge National Laboratory for supplying us with the LiF and V targets which were used in the cross section measurements of the $Li^7(p,n)$ and $V^{51}(p,n)$ reactions.

[9]) Obtained from the Stable Isotopes Division, Oak Ridge National Laboratory, Oak Ridge, Tennessee.

1.05 per cent while the efficiency for a single counter in the outer ring is 0.574 per cent. Therefore, with all twelve detectors connected the total efficiency for the detection of 0.58-MeV neutrons is 9.74 per cent.

A relative yield curve for the $Li^7(p,n)$ reaction was obtained with a target thinner than that used for the absolute calibration. The ratio of this yield curve to that measured by Macklin and Gibbons is shown in fig. 3. The efficiency is plotted as a function of the nominal neutron energy and is normalized to the numbers given

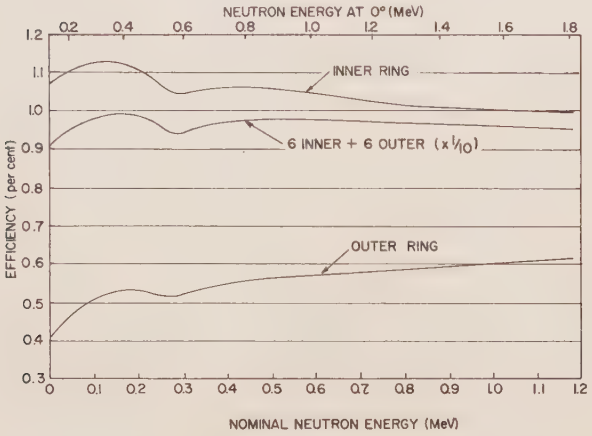

Fig. 3. Ratio of the neutron yield observed from the $Li^7(p,n)$ reaction with the 4π detecting system to that measured by Macklin and Gibbons (ref.[4]). The curves have been normalized at a nominal neutron energy (i.e., energy at 90° to the beam axis) of 0.58 MeV in the manner described in the text. The neutron energy at 0° to the beam axis is given on the upper scale for comparison. The curve marked "6 inner + 6 outer" gives the total detection efficiency of the system.

above for a neutron energy of 0.58 MeV. The curve marked "6 inner + 6 outer" gives the total efficiency of the detector. This curve is seen to exhibit a response which is flat to within about 3 per cent over the nominal neutron energy range from about 0.1 to at least 1.2 MeV.

With the counter geometry used in this detector the efficiency of neutron detection varies with the angle of emission of the neutron from the target relative to the beam axis. Therefore, the response of the detector will be, to some extent, dependent upon the angular distribution of the neutrons being studied. Fig. 3 shows this effect for the case of the $Li^7(p,n)$ reaction. All of the curves show rises and dips in the range of nominal neutron energy up to about 0.4 MeV. The most violent effect occurs between 0.2 and 0.3 MeV which corresponds to the proton bombarding energy range from 2.2 to 2.3 MeV; it is known that the neutron angular distribution changes rapidly with bombarding energy in this region[10]). The fact that large changes in the angular distribution give rise to only a few per cent effect in the detection efficiency indicates that the system can be relied upon to yield accurate total neutron production cross sections even for reactions which exhibit strong angular distributions.

Figure 4 shows the ratio of the measured yield from the T(p,n) reaction to the cross section obtained by Macklin and Gibbons[4]). The curves have been normalized to give a total detection efficiency of 9.74 per cent for a nominal neutron energy of 0.58 MeV. Again a response which is quite flat down to a nominal neutron energy of about 0.1 MeV is obtained. The variation of neutron energy with angle of emission is more rapid for the case of the T(p,n) reaction than for the $Li^7(p,n)$ reaction and at a proton bombarding energy of 3.2 MeV the nominal neutron energy

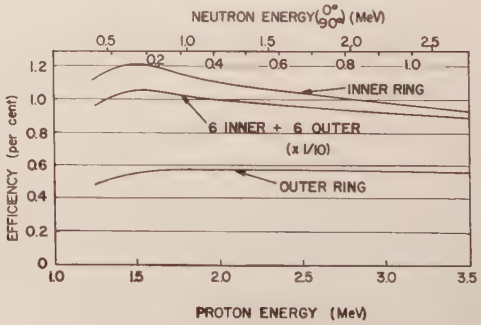

Fig. 4. Ratio of the neutron yield observed from the T(p,n) reaction with the 4π detecting system to that measured by Macklin and Gibbons (ref.[4]). The curves have been normalized at a nominal neutron energy (i.e., energy at 90° to the beam axis) of 0.58 MeV in the manner described in the text.

(i.e., the energy at 90°) is only 1.0 MeV whereas the neutron energy in the forward direction is approximately 2.4 MeV. If the response of the

[10]) R. Taschek and A. Hemmendinger, Phys. Rev. **74** (1948) 373.

detector were such that it decreased rapidly between neutron energies of 1.0 and 2.5 MeV then the response function as determined by measurements on the T(p,n) reaction would show the effect for proton bombarding energies above 3.0 MeV. It is therefore clear that the response cannot change drastically between 1.0 and 2.5 MeV and hence, we may state that the efficiency of the detector is constant to within about 5 per cent over the neutron energy range from about 0.1 to at least 2.5 MeV.

In order to determine the detection efficiency for neutrons of energy outside the range 0.1 to 2.5 MeV two additional measurements were made. A Ra-α-Be source which had been calibrated to an accuracy of better than 4 per cent at the National Bureau of Standards[11]) was used to obtain the efficiency for the detection of neutrons of approximately 5 MeV; a value of 6.5 per cent for the total detection efficiency was obtained. This confirms the previous statement that the efficiency cannot fall off rapidly as the neutron enrgy is increased in the 1.0 to 2.5 MeV. range. In order to obtain some indication of the response for low energy neutrons a measurement was made of the yield from the 1.607-MeV resonance in the $V^{51}(p,n)Cr^{51}$ reaction. The neutron energy at this resonance is 50 keV and the yield has been measured by Gibbons, Macklin and Schmitt[12]). A detection efficiency of approximately 4 per cent was obtained for 50-keV neutrons[8]).

When all of the uncertainties in the various measurements are taken into account it is considered that the absolute detection efficiency of this system is known to within 8 per cent for the neutron energy range from 0.1 to 5 MeV, and that the response is flat to within about 5 per cent over the neutron energy range from 0.1 to 2.5 MeV.

3. Threshold Measurements

The counter ratio method for the detection of thresholds for nuclear ground states and excited states was introduced by Bonner and Cook[13]) and has recently been summarized in detail[14,15]). The method utilizes two detectors mounted in tandem and in line with the charged-particle beam. The detector located nearer the target is designed to have a response function peaked for low energy neutrons while the second detector has a more or less flat response. The ratio of the counting rate in the slow neutron detector to

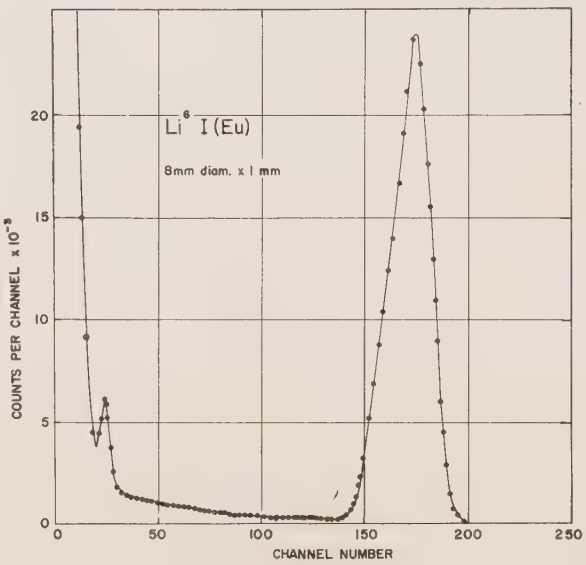

Fig. 5. Pulse-height distribution in the $Li^6I(Eu)$ crystal when irradiated with slow neutrons.

that in the fast neutron detector shows rapid increases when neutron threshold energies are reached. The geometry utilized in the detection of neutron thresholds with the 4π detecting system differs from the "open geometry" employed by the Rice group[13]) in that the fast neutron detector is replaced by the 4π system. The slow neutron detector employed in the present measurements consists of a $Li^6I(Eu)$ crystal (8 mm diam. $\times$ 1 mm thick) mounted on DuMont 6291 photomultiplier tube. This

[11]) We are indebted to the Neutron Physics Division of the National Bureau of Standards for supplying us with this calibrated source.

[12]) Gibbons, Macklin and Schmitt, Phys. Rev. **100** (1955) 167.

[13]) T. W. Bonner and C. F. Cook, Phys. Rev. **96** (1954) 122.

[14]) T. W. Bonner, in Nuclear Spectroscopy, ed. F. Ajzenberg-Selove (Academic Press, New York, 1960) Part A, p. 477.

[15]) J. B. Marion and T. W. Bonner, in Fast Neutron Physics, eds., J. B. Marlon and J. L. Fowler, (Interscience Publishers, Inc., New York, to be published 1960) Part II.

assembly is mounted at 0° with respect to the charged-particle beam. In order to supress detection of slow neutrons moderated in the paraffin of the 4π detector, the Li^6I crystal is mounted in a B_4C shield which is placed in the removable section indicated in fig. 1. The B_4C shield is a hollow cylinder of outside diameter 4″ and inside diameter 2″. The slow neutron detector is located within this cylinder and at a distance of approximately 2″ from the target. A $\frac{1}{8}$″ thick piece of paraffin is placed between the target and the Li^6I crystal in order to thermalize the forward neutrons and increase the detection efficiency of the crystal. This paraffin also serves to smooth out the intrinsic efficiency function of the Li^6I detector which otherwise would show a maximum at a neutron energy of 0.25 MeV due to the resonance in the $Li^6(n,\alpha)T$ reaction at that energy. Therefore, with a forward counter sensitive only to low energy threshold neutrons and with the 4π detector having a response sensitive to the fast neutron component, the basic requirements of the counter ratio method are met. The response to slow neutrons of the Li^6I crystal used as the slow detector is shown in fig. 5. It is evident that the $\alpha + T$ peak from the $Li^6(n,\alpha)T$ reaction is clearly resolved and that discrimination against γ rays and noise is relatively easy. The peak-to-valley ratio of the $\alpha + T$ peak is 100:1. As an illustration of the capabilities of this "closed geometry" system in the investigation of neutron thresholds fig. 6 shows the results for the first two thresholds (ground state and first excited state) in the $Li^7(p,n)Be^7$ reaction. The ratio of the yield in the forward counter to that in the 4π detector shows the peak at 1.881 MeV corresponding to the ground-state threshold energy for this reaction. The energy region near this threshold is shown in more detail in fig. 7. The ratio curve falls to half value in ap-

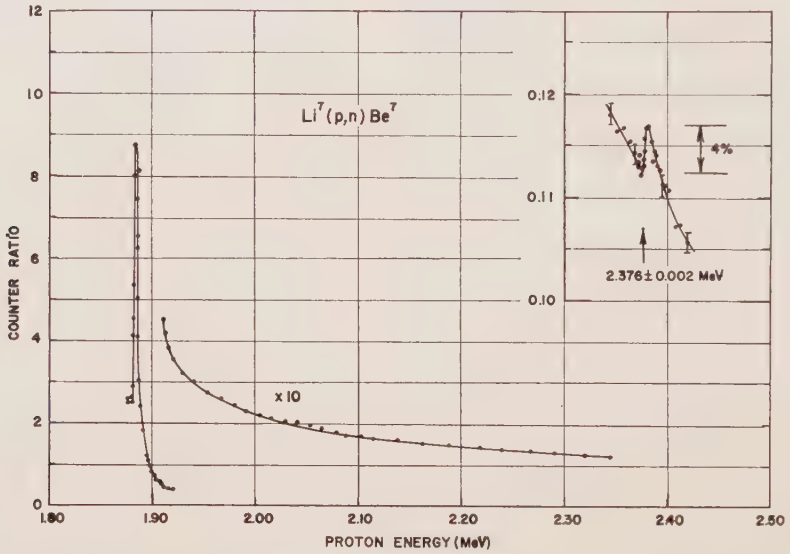

Fig. 6. Ratio of counting rate in the forward detector (Li^6I crystal) to that in the 4π system for the $Li^7(p,n)Be^7$ reaction.

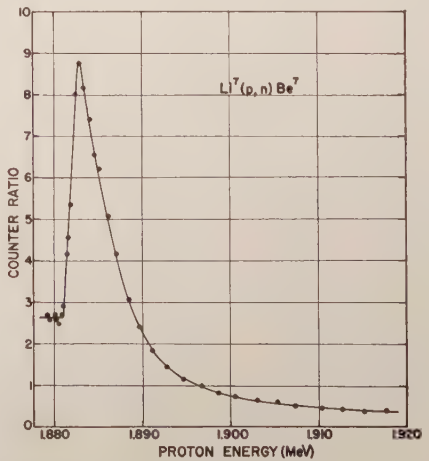

Fig. 7. Low energy region of fig. 6 for the $Li^7(p,n)Be^7$ reaction. The fall-off distances are given in the text.

proximately 5 keV and to 0.1 of the peak value in approximately 17 keV. The energy resolution as determined by these fall-off distances is superior to that obtained in open geometry experiments[16]) where the corresponding energy values are 20 and 200 keV, respectively. The threshold for the first excited state neutron group is extremely weak but is clearly shown in the ratio curve at a proton energy of 2.376 ± 0.002 MeV. (This gives as the energy for the first excited state of Be^7 433 ± 2 keV.) The magnitude of the effect observed at this excited-state threshold with the closed geometry system shows that this method is at present not as sensitive as the open geometry technique. The present results indicate a 4 per cent rise at the first excited state threshold whereas the Rice group[16]) has observed an 8 per cent effect. It is anticipated that by utilizing a somewhat larger Li^6I crystal and by placing this detector at a greater distance from the target the sensitivity can be materially increased.

[16]) T. W. Bonner and F. Gabbard; (1958) unpublished results.

NUCLEAR INSTRUMENTS AND METHODS 8 (1960) 304–312; NORTH-HOLLAND PUBLISHING CO.

H.F. POWER METER FOR OPERATION AT 2.5 MW PULSED POWER

E. ZACCHERONI†

CERN, *Proton Synchrotron Division, Geneva*

Received 11 February 1960

A description is given of an oil-cooled dummy load specially constructed to measure the output power of the 2.5 MW pulse amplifier of the CERN linear accelerator. The equipment can be used both as a dummy load and as a calorimetric power meter. Arrangements have been made to use it also as an attenuator of more than 30 db.

1. Introduction

The construction and the operation of the 2.5 MW pulsed power amplifier[1,2]) of the CERN linear accelerator raise the problem of dissipation and measurement of the output power.

The characteristics of the power pulse are as follows:

maximum pulsed power	2.5 MW
pulse length	200 μsec
radio-frequency	202.6 MHz
repetition frequency	1 pulse/sec .

A dummy load is needed which can withstand the high voltage corresponding to a 2.5 MW pulse and dissipate a mean power of the order of 500 W. It will be used both for the final installation and laboratory work. For installation a simple load is required. It will be connected to the power divider inserted between the drive stage and the final amplifier of the H.F. chain (fig. 1). The use of the power divider[3]) will not be discussed here. It is sufficient to note that the power divider regulates the drive to the final amplifier without affecting the output loading of the drive stage.

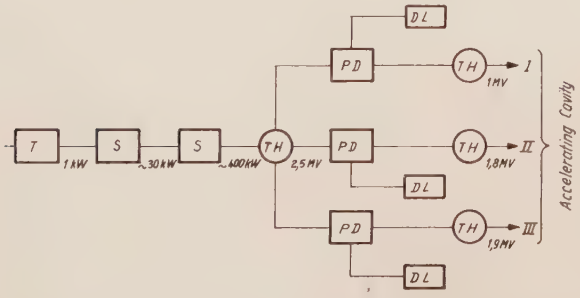

Fig. 1. T: transmitter (crystal controlled); S: pre-amplifiers; T.H.: drive and final amplifiers; P.D.: power dividers; D.L.: dummy loads.

The regulation is done by dividing the output power of the drive stage between the dummy load and the input to the final stage in any required ratio. If necessary the power can be diverted completely into the dummy load. The distribution of power can be measured by power flow monitors[4]), and no absolute power meter is required. For laboratory work, however, it is desirable to have a power meter of reasonable

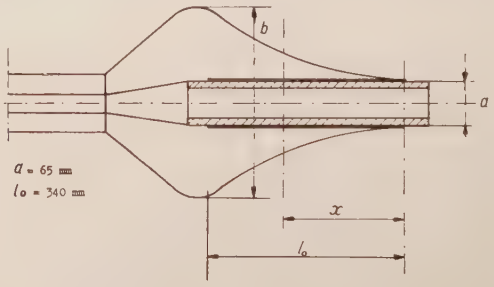

Fig. 2. $a = 65$ mm; $l_0 = 340$ mm.

† Present address: International Atomic Energy Agency, Vienna.

[1]) I. Afanassieff, Générateur à impulsion de 2 M.W. crête, Revue Technique CFTH (24.12.1956) p. 21.

[2]) E. Zaccheroni, The 2.5 M.W. amplifier of the CERN linear accelerator, CERN 58-22 LINAC/RF Group (September 1958).

[3]) P. Bramham, A coaxial line variable power divider and phase shifter for high power, CERN/PS Report (in preparation).

[4]) E. Zaccheroni, Power flow monitors for the LINAC H.F. system, CERN/PS report.

accuracy for checking the amplifier performance and calibrating the power flow monitors. The oil-cooling proposed for the dummy load suggested the idea of using the equipment also for calorimetric power measurement.

2. Coaxial Resistor Dummy Load

A "lossy line" consisting of a cylindrical resistor in a suitable outer conductor (fig. 2) has been used as reflection-free termination of the 50 Ω output line of the amplifier. The high peak

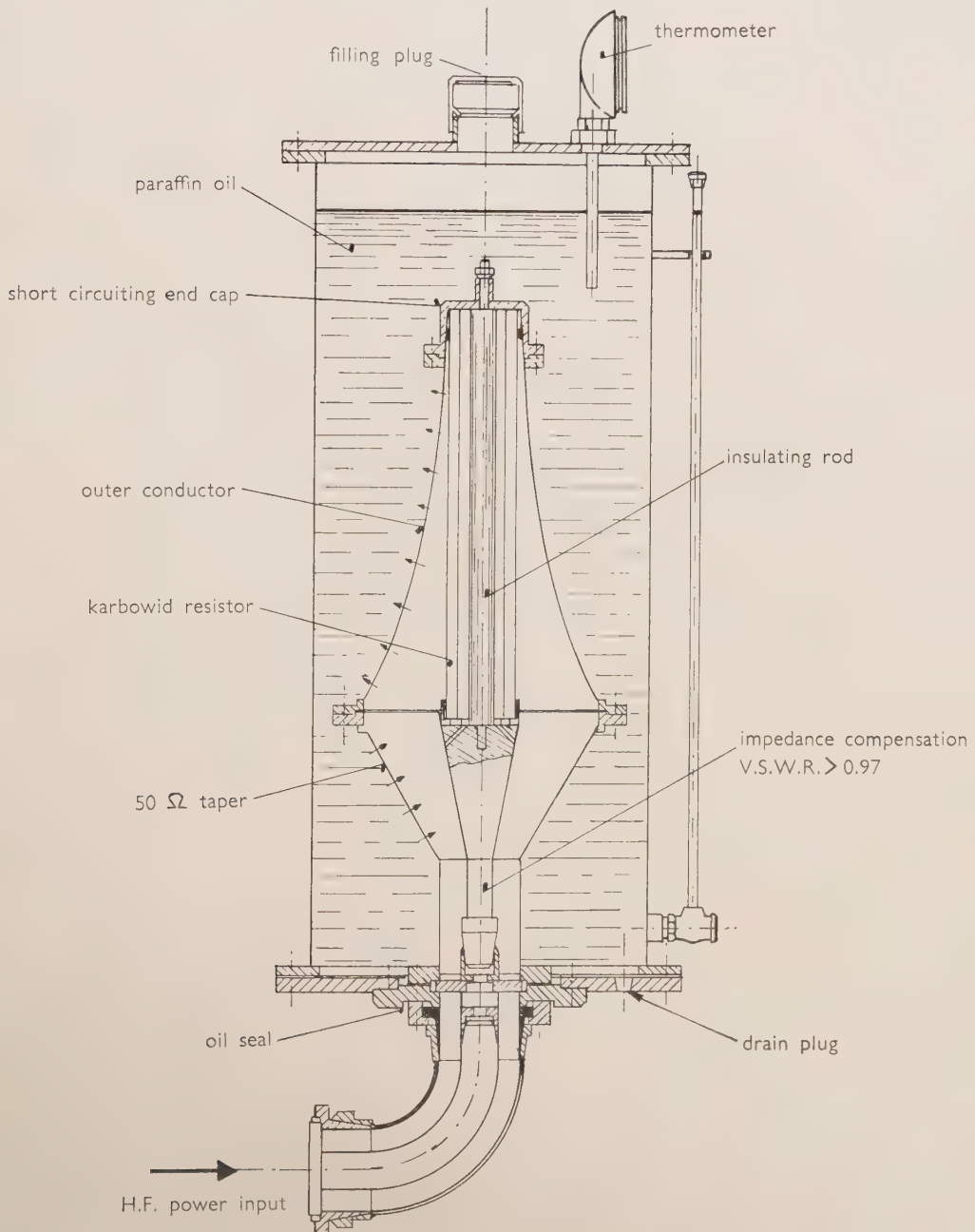

Fig. 3. Coaxial resistor dummy load.

power level raises surface breakdown problems on the inner conductor and fixes a minimum length for the resistor. The resistor used is the carbon coated Siemens Karbowid 50 ohm, 100 watt type. It stands easily the voltage corresponding to the 2.5 MW peak power if the pulse but it increases considerably the mean dissipation of the resistor.

The fixed frequency of operation makes it possible to choose between different shapes of outer conductor. The simplest form would be a cylindrical sleeve of any reasonable diameter

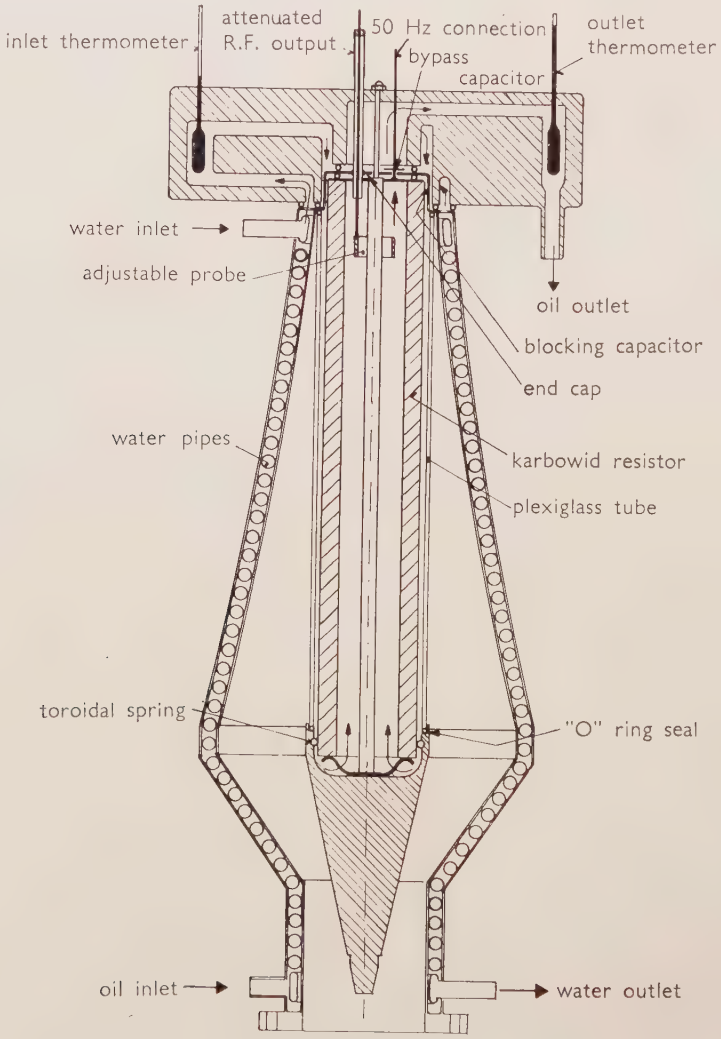

Fig. 4. Dummy load for power meter.

immersed in oil; when tested with water some breakdown was experienced. The heat during the 200 μsec pulse is carried away from the carbon layer by the ceramic former, so that the rise in temperature of the carbon at the end of the pulse is less than 150° C.

Oil cooling does not help appreciably during connected at one end to the resistor. It is easy in fact at any given frequency to compensate the reactive part of the load impedance and to transform the resistive part into the wanted value. However, the standing wave inside the dummy load and in the coaxial transformer cannot be avoided and the increased voltage at

the antinodes might cause trouble. Moreover the power is not uniformly dissipated along the carbon film. All these difficulties may be avoided by using an outer conductor of exponential shape.

It is shown in the Appendix that the input impedance of such a dummy load is equal to the resistance of the inner resistor and is independent of its length. The distribution of current along the resistor is uniform and no reflection will occur inside the dummy load. In principle, no coaxial transformer is needed. In practice, there may be some mismatch on the line; it will, however, be so small that the increase in voltage is negligible, and a very simple matching transformer can be used.

As illustrated in fig. 3 the outer conductor is connected to the extremity of the inner resistor by means of a brass cap. An insulating rod running along the axis fixes the inner conductor of the tapered line at the other end of the resistor. The impedance compensation is provided by adjusting the diameter of the inner conductor in the line that precedes the taper. The whole structure is contained in a box filled with paraffin oil (dielectric constant $\varepsilon = 2.17$), holes being provided in the outer shell to allow free circulation of the oil.

The maximum temperature reached during operation is about 50° C. The dielectric constant does not appreciably change over this range of temperature.

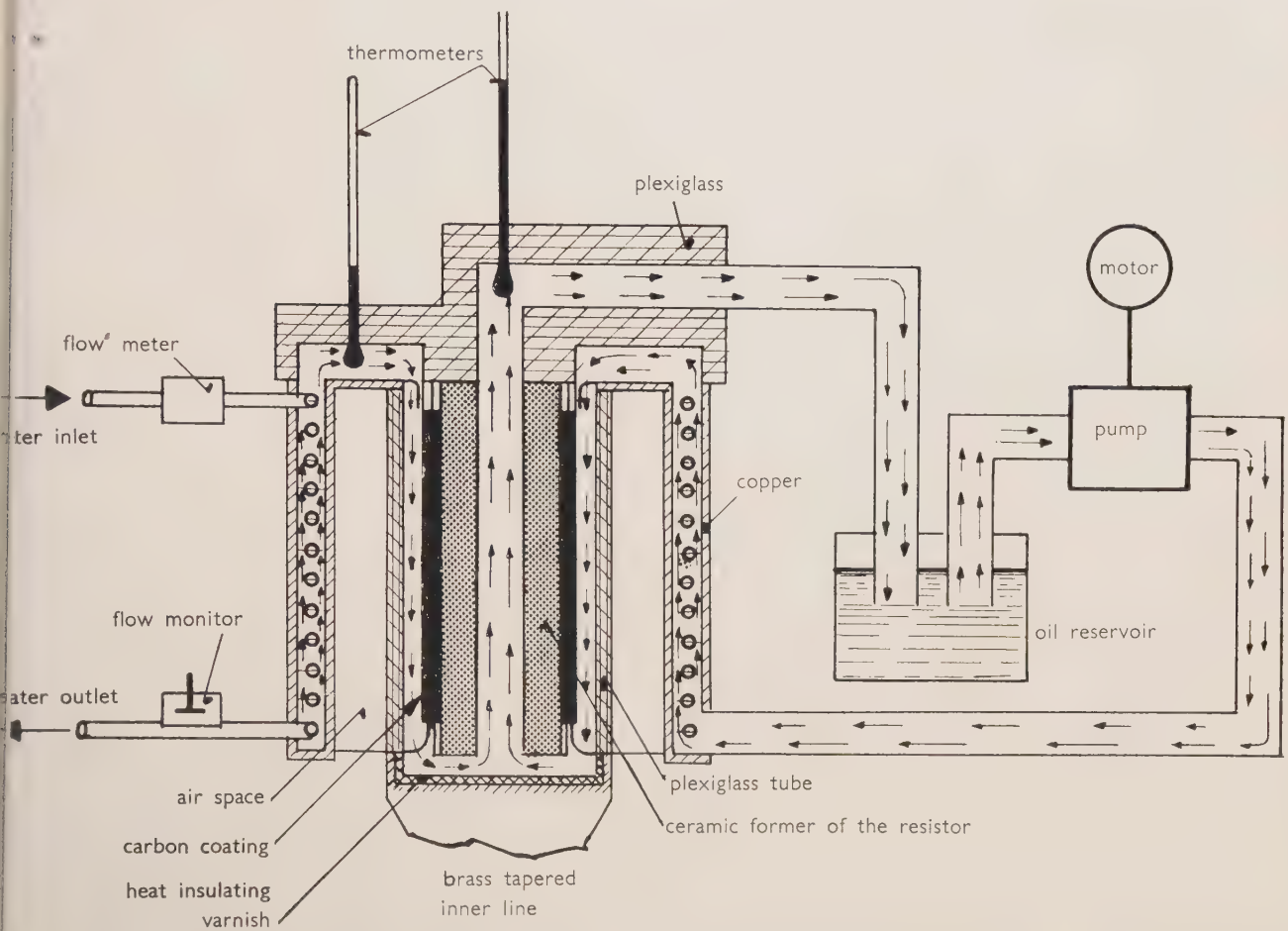

Fig. 5. Oil circulation of the power meter.

3. Dummy Load for Power Meter

The apparatus described above can work, in principle, as a calorimeter for measuring the power dissipated in the dummy load, if some precautions are taken to avoid heat leakage. The measurement, however, would be very inconvenient, because the heat capacity of the volume of oil is large and so the temperature rise would be very slow. In order to avoid this difficulty, the oil is confined by a plexiglass cylinder to a 2 mm annular space around the resistor (fig. 4). Sufficient cooling is obtained by circulating the oil at constant flow, and the power is calculated by measuring the difference in temperature of the oil between output and input. Constant flow through the system is maintained by a reciprocating pump driven by a synchronous motor (fig. 5). The stroke of the pump can be regulated to give any flow between zero and three l/min. Heat exchange with the surroundings is decreased by choosing a suitable sense of oil circulation and by keeping the mean oil temperature near to room temperature.

The dummy load is surrounded by an external jacket in which the oil flows from the bottom to the top around water cooling pipes. It goes then to the first thermometer and descends through annular space between the plexiglass tube and the resistor. Heat exchange between the resistor and the outer conductor is thus practically eliminated. The residual heat conduction along the end cap has been made very small by covering it with insulating varnish. The same has been done at the other end of the resistor along all the surface of the tapered line, which is in contact with the oil.

A further reduction in heat exchange has been obtained by adjustment of the oil flow so as to give a temperature difference of only a few degrees.

With $\Delta T = 1$ or 2° C the error in reading the thermometers becomes appreciable; a compromise has been reached by allowing a rise of the order of 5 degrees for 2.5 MW power. Arrangements have also been made to stir up the oil before it reaches the second thermometer so as to have a stream of uniform temperature. Air bubbles must be carefully avoided, because they can affect the measurements. The closed circuit of oil and the submerged pump produce a stream completely free of bubbles. Nevertheless valve points are provided to eliminate bubbles which may occur during filling.

4. Calibration of Power Meter

To calibrate the meter, 50 Hz power is applied to the resistor through an a.c. wattmeter and the power level adjusted by means of a Variac auto-transformer (fig. 6).

In principle, one calibration would suffice to determine once and for all the function $W = f(\Delta T)$ at constant flow (fig. 7). Nevertheless a substitution method is preferred because it allows the performance of the equipment to be checked continuously. The 50 Hz power is applied to the resistor during a time sufficient for the oil temperature to stabilise, then the H.F. power is applied and the 50 Hz power is decreased so as to keep the temperature rise unchanged. When equilibrium is reached a second reading of 50 Hz power is taken, the difference in reading giving the H.F. power applied. The H.F. and 50 Hz power are dissipated in the same part of the circuit with the same distribution, so errors due to heat exchange are avoided. Application of 50 Hz power to the resistor at the same time as H.F. power has been made possible by replacing the direct short circuit of the end piece by a capacitor of

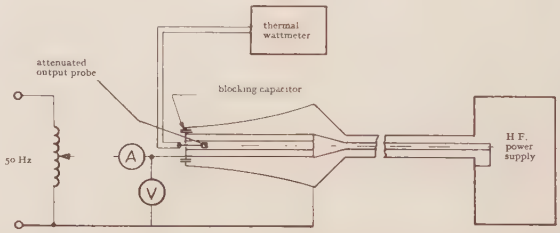

Fig. 6. Application of 50 Hz and H.F. power to the load.

[5]) J. K. Murray, U.H.F. Power meter for operation in the 200 Mc/s Communication Band, Electronic Engineering (May 1958) p. 345.

[6]) M. Geiger and E. Zaccheroni, A gated pulse voltmeter, CERN/PS Report LRF, 3 (March 1957).

negligible reactance (fig. 6). The capacitor consists of a 0.1 mm polyester film covering the silvered terminal of the cylindrical resistor and clamped under a copper strip fixed to the outer

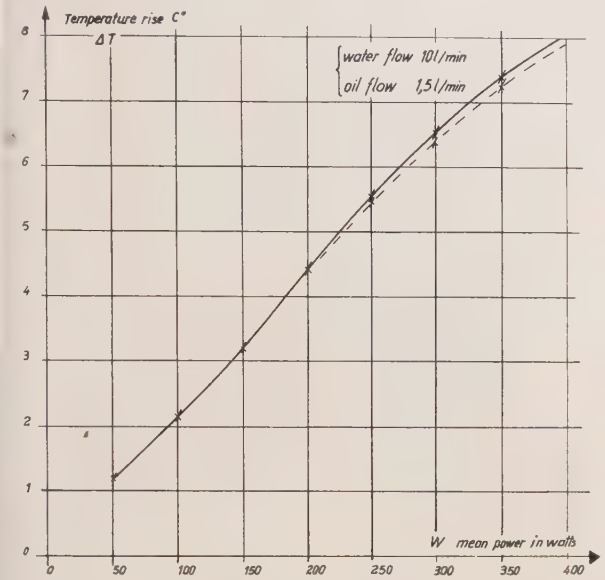

Fig. 7. Calibration curve of the power meter.
Broken line: check of calibration curve three months later.

conductor. The 50 Hz circuit is completed through the loop of the H.F. supply.

Accuracy of the measurement depends only on the accuracy of reading a fixed temperature rise from the two thermometers and the mean power on the a.c. wattmeter. Facilities are provided for connecting an external voltmeter and ammeter if higher precision is required. An accurate measurement by the substitution method takes about 40 minutes. A faster method using the dummy load as an attenuator has been developed, as described below.

5. Dummy Load as Attenuator

A fixed proportion of the power dissipated in the load can be measured directly by low-power equipment. As the frequency is fixed, the frequency sensitivity of the divider is not important, so that a single probe situated inside the resistor can be used. The coupling can be varied by adjusting the depth of insertion of the probe. The coupling must be loose enough not to affect the impedance matching of the dummy load. A 60 ohm coaxial line carries the attenuated power to a thermal wattmeter, the position of the probe being chosen to give a power ratio of 2000/1 (— 33 db). Five minutes is sufficient for a good measurement.

6. Conclusion

As already stated, the mean output power of the 2.5 MW pulse amplifier can be measured in three different ways:

(a) by observing temperature rise and reading the power from the calibration curve.

(b) By substitution of 50 Hz power for the H.F. power to be measured. The difference in reading of an a.c. wattmeter with and without the H.F. gives the amount of H.F. power.

(c) By reading on a low-power thermal wattmeter when the attenuation is known.

The most accurate of the three methods is (b). It forms the basis of the calibration for methods (a) and (c).

On the contrary the most practical is method (c) which allows a fairly accurate measurement in quite a short time. Once the mean power is measured, the pulse power can be calculated if the pulse length τ and repetition time τ' are known,

$$W_{\text{pulse}} = \frac{\tau'}{\tau} W_{\text{m}} .$$

If the pulse is rectangular there will be no uncertainty in measuring its length on the oscilloscope, but if the rise and fall times are not negligible the effective length is calculated from the expression

$$\tau = \frac{\int v^2(t)\, \mathrm{d}t}{V^2}$$

where V is the amplitude of the flat top.

The amplitude stability can be monitored with the accuracy of 0.5% by a "gated pulse voltmeter" connected to a power flow monitor.

The overall accuracy of the apparatus can be

[7]) D. R. Crosby and C. H. Pennypacker, R.F. resistor as uniform transmission lines, Proc. IRE **34** (1946) 62.

[8]) C. T. Kohn, The design of a radio frequency coaxial resistor, I.E.E. Proc. IV, 101 (1954) 146.

General view of coaxial resistor dummy load.

View of the dummy load partially opened, showing the exponential outer conductor.

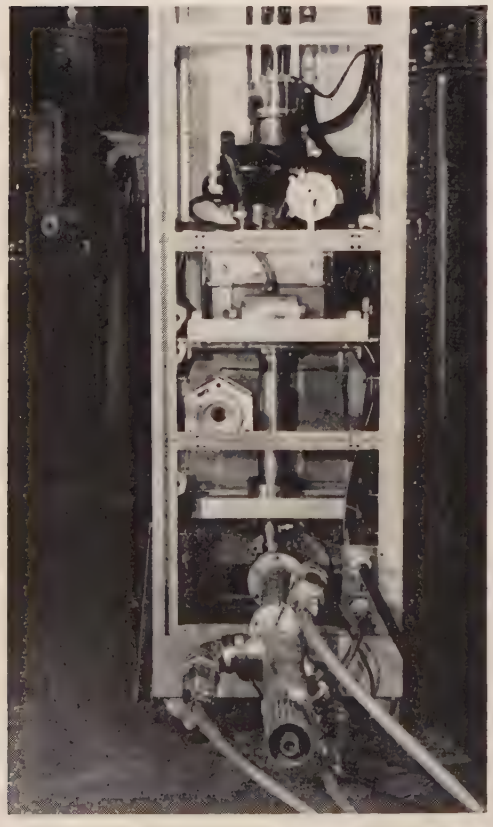

Rear view of power meter, showing the H.F. input, power flow monitor and constant flow pump.

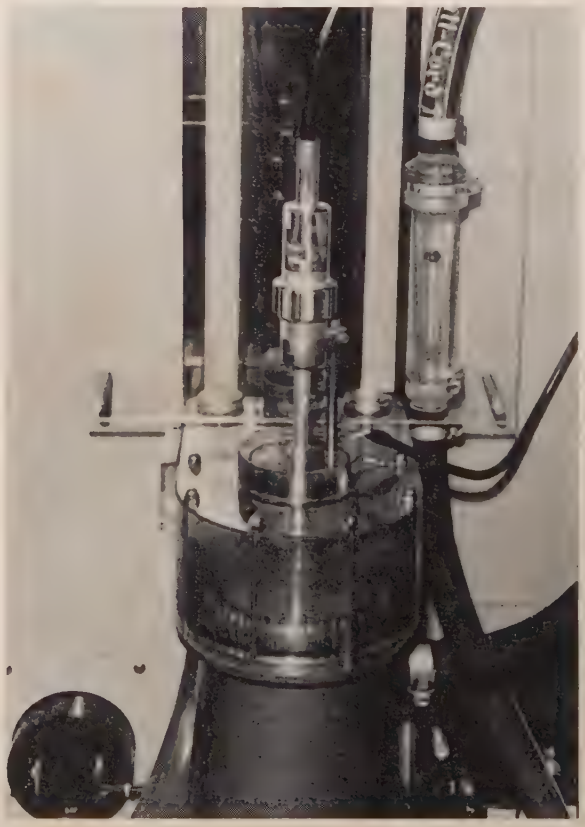

Head of dummy load for power meter, with thermometer holes, attenuated output probe and 50 Hz power input connexion.

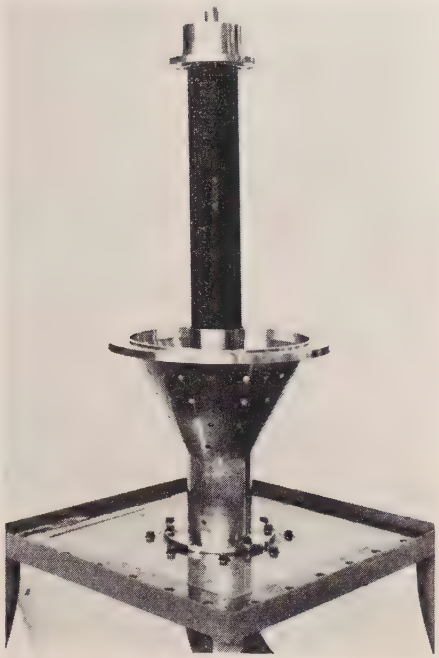

Coaxial resistor and tapered outer conductor.

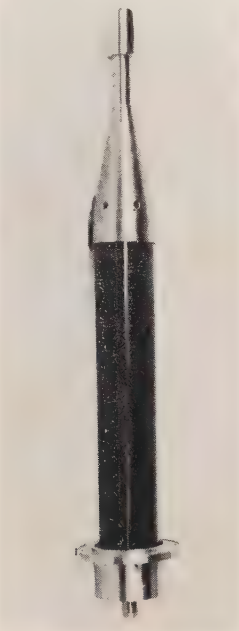

Brass end cap, coaxial resistor and tapered inner conductor.

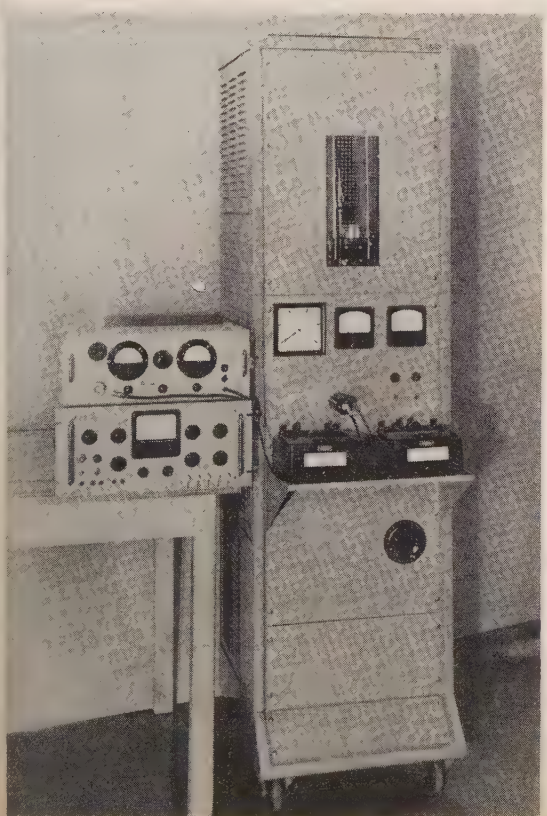

Front view of power meter with gated pulse voltmeter, thermal wattmeter and a.c. meters.

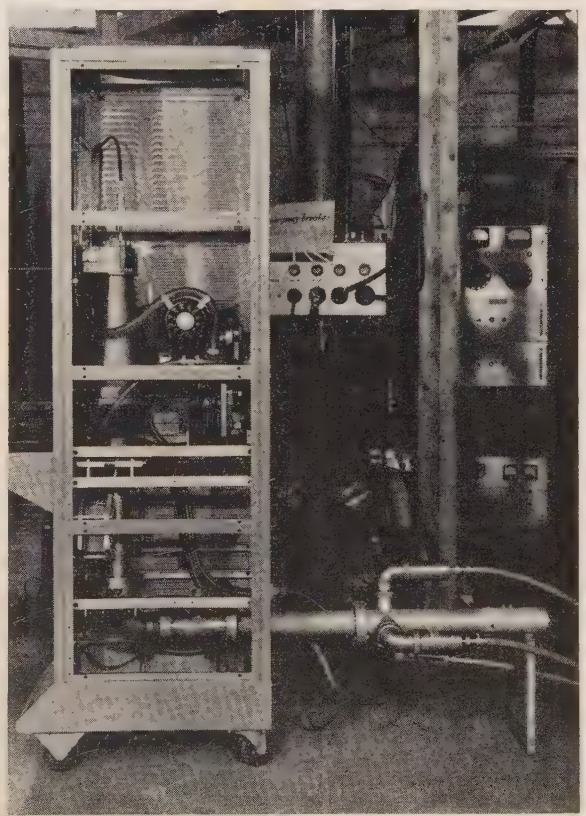

Side view of power meter.

kept better than 3% over the range from 100 kW to 2.5 MW by suitable choice of oil flow and attenuation.

I would like to thank Mr. Dind for his help in the design and construction of the dummy load, and I am particularly indebted to Mr. Stierlin for having adapted the original experimental design of the power meter to a convenient final construction.

Appendix[9])

Let us consider a coaxial line with a resistive inner conductor whose length is not negligible compared with the wave length (fig. 2). We can write the well-known transmission line equations:

$$\frac{\mathrm{d}I}{\mathrm{d}x} = (g + \mathrm{j}\omega c)\, V$$

$$\frac{\mathrm{d}V}{\mathrm{d}x} = (r + \mathrm{j}\omega l)\, I \qquad (1)$$

where r, l, g, c are the line constants and $I = I(x,t)$, $V = V(x,t)$ are the current and the voltage at a point x from the end of the line. Let Z be the characteristic impedance at the point x. From $Z = V/I$ it follows:

$$\frac{\mathrm{d}Z}{\mathrm{d}x} = \frac{1}{I}\frac{\mathrm{d}V}{\mathrm{d}x} - \frac{V}{I^2}\frac{\mathrm{d}I}{\mathrm{d}x} = (r + \mathrm{j}\omega l) - (g + \mathrm{j}\omega c)\, Z^2 . \qquad (2)$$

In this case we can assume $g = 0$. It follows that

$$\frac{\mathrm{d}Z}{\mathrm{d}x} = r + \mathrm{j}\omega\,(1 - cZ^2) . \qquad (3)$$

[9]) C. G. Montgomery, Technique of microwave measurements, Vol. II, MIT, Ch. 12, p. 721.

If we choose $cZ^2 = 1$, that is $Z = \sqrt{1/c}$ the above equation becomes:

$$\frac{\mathrm{d}Z}{\mathrm{d}x} = r , \qquad Z = rx + k . \qquad (4)$$

If the line is short circuited at the end

$$Z_{x=0} = 0 , \qquad \text{then} \qquad k = 0$$

and

$$Z = rx .$$

This means that the impedance at a point x from the end of the line should equal the resistance of the length x of the inner conductor.

But, as specified above $Z = \sqrt{1/c}$, so that the dimensions of the line in any point must be those of a non-dissipative line of impedance Z. It follows then, from the familiar

$$Z = \frac{60}{\sqrt{\varepsilon}} \ln \frac{b}{a}$$

and eq. (5) that

$$b = a \exp\,(rx\,\sqrt{\varepsilon}/60) .$$

The inner diameter a being constant, b must vary exponentially. At the point $x = l_0$, where l_0 is the length of the inner conductor,

$$Z = rl_0 = R .$$

The resistance R can be chosen to be equal to the characteristic impedance of the feeding line so that the dummy load can match the line directly. Although in this case it is not important it is worth noting that, if $cz^2 = 1$, the dummy load impedance is independent of frequency.

NUCLEAR INSTRUMENTS AND METHODS **8** (1960) 313–319; NORTH-HOLLAND PUBLISHING CO.

THE SPHERICAL CONDENSER AS A HIGH TRANSMISSION PARTICLE SPECTROMETER

II. DISC SOURCE

R. D. BIRKHOFF, J. M. KOHN†, H. B. ELDRIDGE and R. H. RITCHIE

Health Physics Division, Oak Ridge National Laboratory††, Oak Ridge, Tennessee

Received 10 May 1960

The inverse square electric field between the plates of a charged spherical condenser provides a focussing of charged particles leaving a source on the inner sphere. Part I of this paper dealt with the characteristics of such a spectrometer for the case where the source may be considered concentrated at a point on the axis of the instrument. The present analysis is concerned with the line profile, the transmission, and the resolution of the spectrometer for a distributed source. Where high transmission is important, a source on the inner sphere having a radius 30% of the radius of the inner sphere provides a transmission of 16% at an energy resolution of 7.7%.

In Part I of this paper[1]) the trace equation was considered of a non-relativistic charged particle in an inverse square electric field such as exists between two charged concentric spheres. It was shown that particles emitted isotropically from a point on the inner sphere may experience a focussing action after rotating through an angle ϕ ($> \frac{1}{2}\pi$) about the center of the spheres. (See Fig. 1.) An annular slit at the angle ϕ allows those particles in a certain radial band to pass into a region where they may be counted. The dependence of the transmission versus energy relation on the position and size of this annular slit has been examined. Very high transmissions are attainable in such a device without undue sacrifice of energy resolution, e.g., 25% transmission at 6% energy resolution is possible.

The present discussion concerns the effect of distributing the source over a spherical cap on the inner sphere centered about the instrument axis. The trace equation is obtained for a particle leaving the source off the axis, and the effect on the transmission-energy profile is examined in the small angle approximation used in Part I.

For generality we consider a source point P′ which is displaced from the on-axis point P a distance ξr_m parallel to the line OP, and a distance ηr_m perpendicular to this direction (see fig. 2). Here r_m is the radius of the inner sphere. The velocity vector $\bar{v}$ of a particle originating at

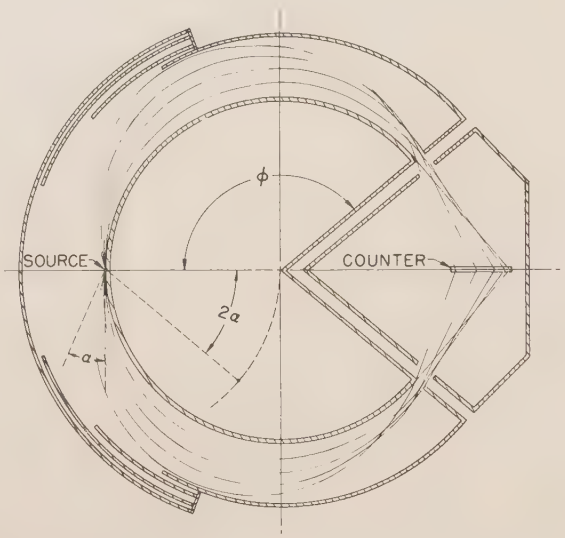

Fig. 1. Schematic of spherical condenser spectrometer with point source on the axis.

P′ is referred to a system of polar coordinates (θ', ψ') having polar axis parallel to the OP′ direction and to an unprimed system (θ, ψ) with polar axis parallel to OP. In both systems the aximuthal angles ψ and ψ' are measured from the

† Retired.

†† Operated by Union Carbide Corp. for the U.S. Atomic Energy Commission.

[1]) See Nuclear Instruments **6** (1960) 157–163.

plane containing the points O, P, and P′. We define $\alpha = \frac{1}{2}\pi - \theta$ and $\alpha' = \frac{1}{2}\pi - \theta'$. Suppose that after emission from the point P′, the charged particle travels in a focussing electric field and enters the plane of the selector gap at the point Q. The angle of rotation φ' is measured from the line OP′ in the plane containing OP′Q while the angle φ is measured from the line OP in the plane containing OPQ.

where we put $E = (1 + \delta)E_0$ as before. The constants A and B are evaluated from the given initial conditions (a) $[r]_{\phi' = 0} = r_m(1 + \xi)$; and (b) $[\mathrm{d}/\mathrm{d}\phi'\ (1/r)]_{\phi' = 0} = -[r_m(1 + \xi)]^{-1} \tan \alpha'$. One finds

$$(1 + \varepsilon) = \frac{(1 + \delta)(1 + \xi)^2 \cos^2 \alpha'}{1 - \cos\varphi' + (1 + \delta)(1 + \xi)\cos\alpha' \cos(\varphi' + \alpha')} \tag{3}$$

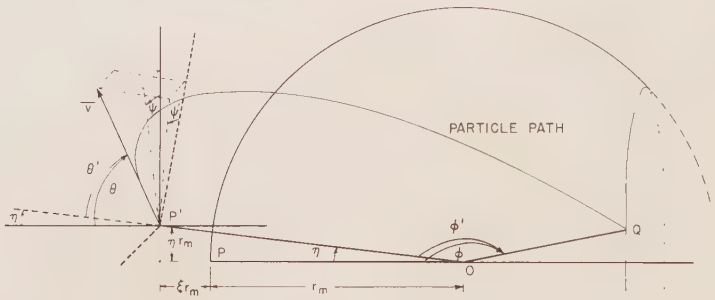

Fig. 2. Quantities describing the displacement of a point source off the axis of symmetry and inner sphere.

An orbit equation referring to the primed angles α' and φ' and containing the displacement parameters ξ and η will be derived. If one writes α' and φ' in terms of the unprimed angles the transmission-energy relation can be expressed in analytical form in the small-angle approximation.

As in Part I, we begin with the standard form of the particle path equation describing motion in the plane OP′Q:

$$u = \frac{1}{r} = \frac{mk}{l^2} + A \sin\varphi' + B \cos\varphi' \tag{1}$$

where, as before, r is the orbit radius and l is the angular momentum of the particle. It was shown in Part I that $k = 2r_m E_0$ (eq. (3)) where $E_0 = \frac{1}{2}mv_0^2$ is that energy which the particle must have in order to execute circular motion about O with radius r_m given the proper initial conditions. Also, the angular momentum l is given by $l = mv\, r_m(1 + \xi) \cos\alpha'$ if we assume $\xi \ll 1$. Then

$$u = \frac{1}{r} = \frac{1}{r_m(1 + \delta)(1 + \xi)^2 \cos^2\alpha'} + \\ + A \sin\varphi' + B \cos\varphi' \tag{2}$$

where $\varepsilon = r/r_m - 1$. We now write the relations between the primed and unprimed angles from fig. 2. Assuming $\eta, \xi \ll 1$, we have the following relationship from the vectors $\overline{v}$, $\overline{OP}$, and $\overline{OP'}$ (fig. 2).

$$\cos\theta' \cong \cos\theta + \eta \sin\theta \cos\psi \cong \cos(\theta - \eta\cos\psi)$$

or

$$\alpha' = \alpha + \eta\cos\psi \tag{4}$$

since $\alpha = \frac{1}{2}\pi - \theta$ and $\alpha' = \frac{1}{2}\pi - \theta'$. From the vectors $\overline{OP}$, $\overline{OP'}$ and $\overline{OQ}$, one finds

$$\cos\varphi \sim \cos\varphi' - \eta \sin\varphi' \cos\psi'$$

$$\varphi \sim \varphi' + \eta\cos\psi' \tag{5}$$

or

$$\chi - \chi' - \eta\cos\psi'$$

where χ and χ' are the supplementary angles of ϕ and ϕ' respectively.

The relation between ψ' and ψ may be seen from fig. 2 to be

$$\tan\psi' \cong \frac{\sin\theta \sin\psi}{\sin\theta\cos\psi - \eta\cos\theta}$$

or

$$\cos\psi' \cong \cos\psi - \psi \tan\alpha \sin^2\psi\,.$$

Since we shall retain only first order terms in η we may write

$$\alpha' = \alpha + \eta \cos\psi \qquad (4')$$

$$\chi' = \chi + \eta \cos\psi \,. \qquad (5')$$

We now return to the trace equation (eq. (3)) and expand it retaining only first powers of ξ, δ and η and up to second powers in α' and χ' $(= \pi - \varphi')$. We find

$$\varepsilon = 2\delta + 3\xi + \chi'\alpha' - 2\alpha'^2 \,.$$

Inserting the expression for α' and χ' from eqs. (4') and (5'), we have

$$\varepsilon = 2\delta + 3\xi + \alpha(\chi - 3\eta\cos\psi) + \chi\eta\cos\psi - 2\alpha^2 \,. \qquad (6)$$

From eq. (6) the radial displacement of the trace, ε, depends to a much smaller extent on the tangential displacement of the source point, η, than on the radial displacement ξ. That is, the coefficient of the former, $(\chi - 3\alpha)\cos\psi$, is always less than unity and tends to become smaller still when the integration over the azimuthal angle ψ is performed. In contrast the coefficient of the latter, 3, is obviously not reduced in this integration. Thus it appears advantageous to let $\xi = 0$ in the remainder of the calculation in the hope that the desirable characteristics found for a source on the axis will not be adversely affected by tangential displacements of the source. The trace equation may be transformed by the relations

$$d = \delta/\chi^2 \,, \qquad e = \varepsilon/\chi^2 \,, \qquad h = \eta/\chi \,,$$

$$a = \alpha/\chi \,, \qquad c = \xi/\chi^2$$

to eliminate the explicit dependence on χ and eq. (6) becomes

$$e = 2d + 3c + a\,(1 - 3h\cos\psi) + h\cos\psi - 2a^2 \,. \qquad (7)$$

The case $c = 0$ will be treated below.

In Part I the effect of varying the position and width of the energy-selecting annular gap at the angle φ for the on-axis source was examined. The optimum transmission-energy characteristic was obtained by choosing the inner gap radius r_i equal to r_m and the outer gap radius r_0 to be equal to $r_m(1 + \frac{1}{8}\chi^2)$ (see fig. 2 of Part I). Fig. 3 shows a plot of the relation between reduced energy d and reduced takeoff angle $a(= \alpha/\chi)$ for intercept with the outer gap radius, corresponding to $e = \varepsilon/\chi^2 = \frac{1}{8}$, as curve A. The intercept with the inner gap radius at $e = 0$ is shown as curve B. Particles emitted from the source in the range $a < 0$ are immediately intercepted by the inner sphere and need not be considered further. Particles emerging from the source at angles $a > \frac{1}{2}$ were assumed to intercept the outer sphere after rotating through a central angle φ of approximately $\frac{1}{2}\pi$ radians. The energy dependence

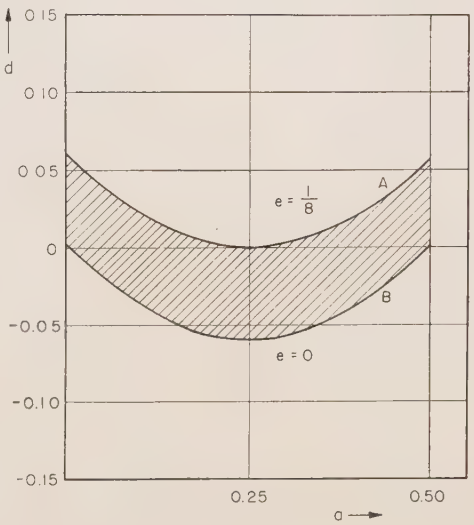

Fig. 3. Allowed region for take-off angles and energies for point source on the axis and inner sphere.

in this outer sphere interception was derived in Part I (eq. (16)), but for $\chi \ll 1$ it may be neglected. Thus the allowed region in fig. 3 was taken to be the cross-hatched area. Since the transmission is proportional to the length of the horizontal line lying inside this area at a given value of d, the expression for the transmission in this case is

$$T_{h=0}(d) = \tfrac{1}{4}\chi\sqrt{1 + 16d} \qquad 0 > d > -\tfrac{1}{16} \qquad (8)$$

$$= \tfrac{1}{4}\chi\,(1 - 4\sqrt{d}) \qquad \tfrac{1}{16} \geqslant d > 0 \qquad (9)$$

$$= 0 \qquad \tfrac{1}{16} \leqslant |\,d\,| \,. \qquad (10)$$

Comparison of this $T(d)$ relation obtained using the small angle approximation with that found from an exact orbit calculation showed very good agreement even for $\chi \approx 1$.

The case $h \neq 0$, $c = 0$ will now be considered

under the assumption that the inner and outer gap radii have the values chosen before, i.e., $r_i = r_m$ and $r_0 = r_m(1 + \frac{1}{8}\chi^2)$.

Analytical expressions for the transmission at given values of the azimuthal angle ψ, the displacement h and the energy d may be derived

The evaluation of the transmission now is considerably more complex than for the source on the axis, and the details are given in the appendix. It may be seen that the transmission at an azimuthal angle ψ, source displacement h, and energy d, may be expressed by various

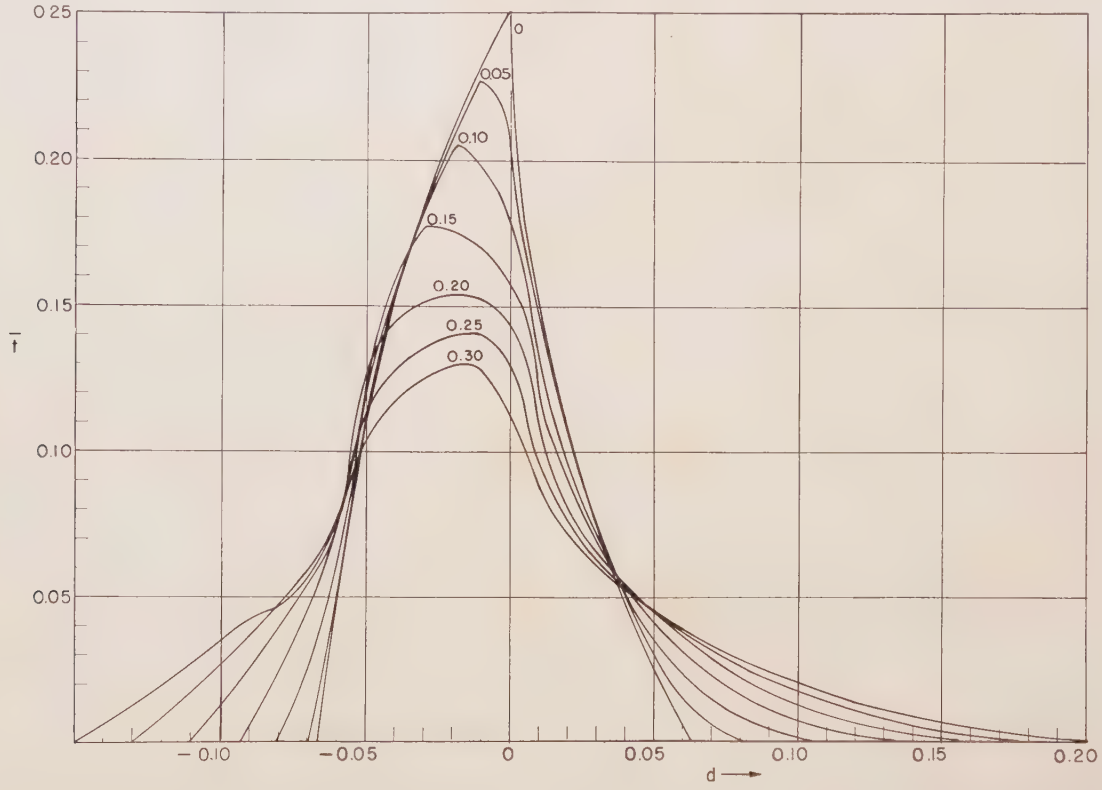

Fig. 4. Line profiles for a point source on the inner sphere but off the axis of symmetry. Numbers on curves are values of $h = \eta/\chi$ where η is the displacement of the source point from the axis of symmetry in units of the radius of the inner sphere.

easily if one assumes that the inner sphere and outer sphere intercepts are unchanged by the displacement of the source from the axis. This is clearly a good assumption if $\chi \ll 1$. Then, as before, the transmission at a given value of d is proportional to the horizontal intercept lying inside the area bounded by the lines $a = 0$, $a = \frac{1}{2}$, and the parabolas

$$2a^2 - a(1 - 3h\cos\psi) + \tfrac{1}{8} - h\cos\psi - 2d = 0 \quad (11)$$

and

$$2a^2 - a(1 - 3h\cos\psi) - h\cos\psi - 2d = 0\,. \quad (12)$$

The first of these parabolas represents the intercept of the trace with the outer gap radius while the second corresponds to the inner gap radius intercept.

functions of the quantities $(h\cos\psi)$ and d appropriate to the values of these parameters. One may define the transmission $t(h\cos\psi, d)$ with the understanding that the functional dependence of t on its arguments will be given by the equations in the Appendix. Then the average over ψ is given by

$$\bar{t}\,(h,d) = \frac{1}{\pi}\int_0^\pi t(h\cos\psi,d)\,d\psi\,. \quad (13)$$

Fig. 4 shows a plot of $\bar{t}(h,d)$ as a function of d for various values of h. These calculations of $\bar{t}(h,d)$ as well as those described below were made using an IBM-704 computer.

The transmission for a disc source of radius h_0 is given by

$$\bar{t}_D(h_0,d) = \frac{2}{\pi h_0^2}\int_0^{h_0} h\,dh \int_0^{\pi} t(h\cos\psi,d)\,d\psi \quad (14)$$

where the factor $2/h_0^2$ normalizes the total source intensity to unity. This may be simplified by setting $h = h_0 y$, and $y\cos\psi = \cos\omega$. One finds

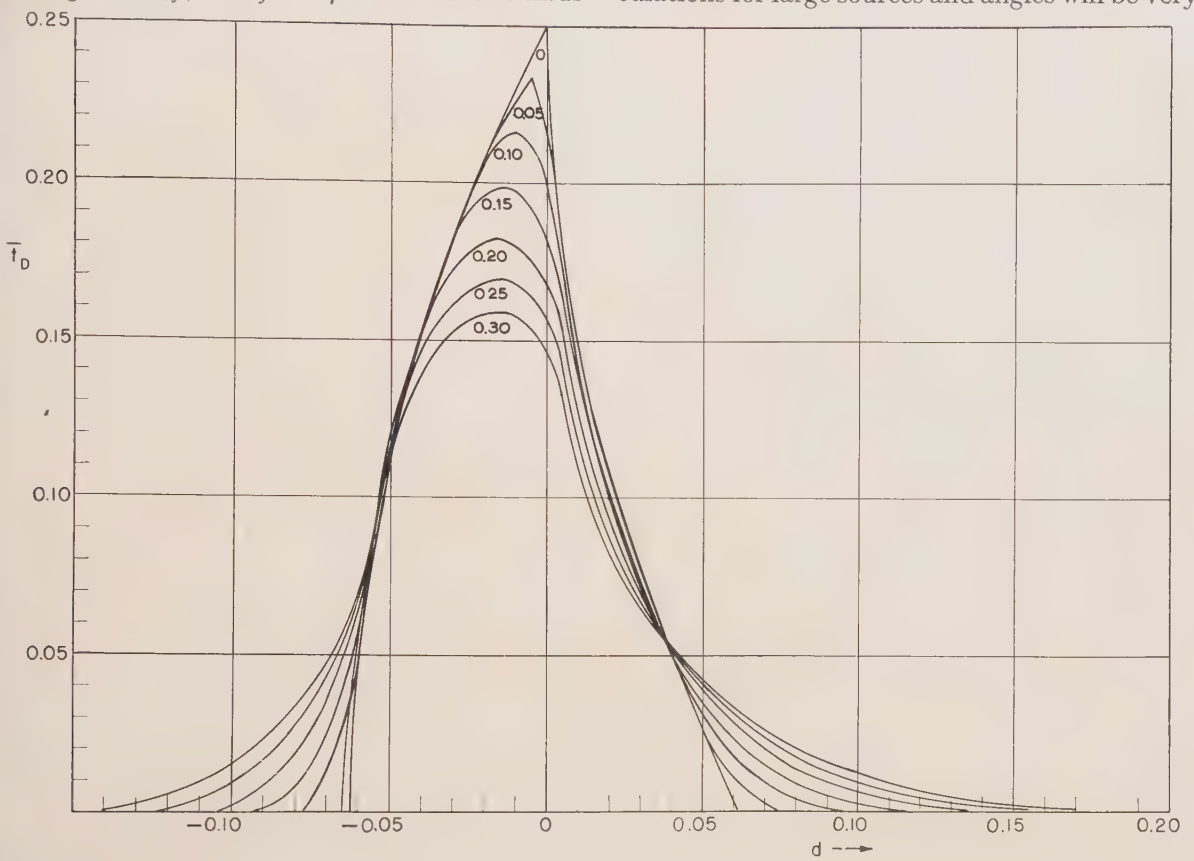

Fig. 5. Line profiles for a disc source on the inner sphere. Numbers on curves are values of $h_0 = \eta_0/\chi$ where η_0 is the source radius in units of the radius of the inner sphere.

$$\bar{t}_D(h_0,d) = \frac{2}{\pi}\int_0^1 y\,dy \int_{\cos^{-1}y}^{\cos^{-1}(-y)} t(h_0\cos\omega,d)\,\frac{\sin\omega\,d\omega}{\sqrt{y^2-\cos^2\omega}} \quad (15)$$

which may be further simplified by inverting the order of integration. The final result is

$$\bar{t}_D(h_0,d) = \frac{2}{\pi}\int_0^{\pi} \sin^2\omega\; t(h_0\cos\omega,d)\,d\omega\,. \quad (16)$$

Fig. 5 shows a plot of $\bar{t}_D(h_0,d)$ as a function of d for various values of h_0.

A calculation of instrument performance for the case of the largest source ($h = 0.3$) and highest transmission ($\chi = 1$) will serve to illustrate the use of the curves of fig. 5. It should be borne in mind that these values represent the extremes of the calculation where some error is inevitably present due to the small angle approximations used. In light of the good agreement between the calculations and graphical methods in Part I, it is thought that here also these calculations for large sources and angles will be very nearly correct. The above values of h and χ yield a source radius η of 0.3 in units of the radius of the inner sphere. The transmission and resolution are, from fig. 5, 0.16 and 0.077 respectively as compared with the corresponding values for the point source on the axis of symmetry of 0.25 and 0.063. Thus the transmission is reduced to 64% of its value for the point source and the resolution is impaired by the factor 1.22. Thus the ratio of transmission to resolution is reduced by about about a factor of two, a remarkably small change for a source radius which is 30% of the radius of the inner sphere. Use of such a large diameter source will permit a spreading of the radioactive material thinly enough to avoid

serious self-absorption problems. For use as a low-energy X-ray spectrometer, the spherical condenser instrument should allow use of broad beams of X-rays and extremely thin photoelectric radiators.

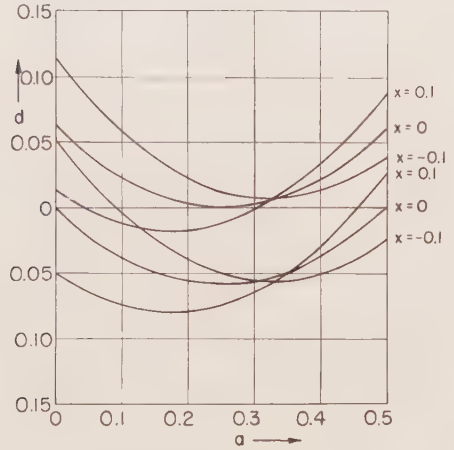

Fig. 6
Allowed region for take-off angles and energies for representative values of source displacement and azimuthal angle.

parameter x. The line $l_{\min}$ represents the variation with x of the position of the minimum of the lower parabola while l_0, and $l_{\frac{1}{2}}$ show the variation of the intercept of the lower parabola with the lines $a = 0$ and $a = \frac{1}{2}$, respectively, as a

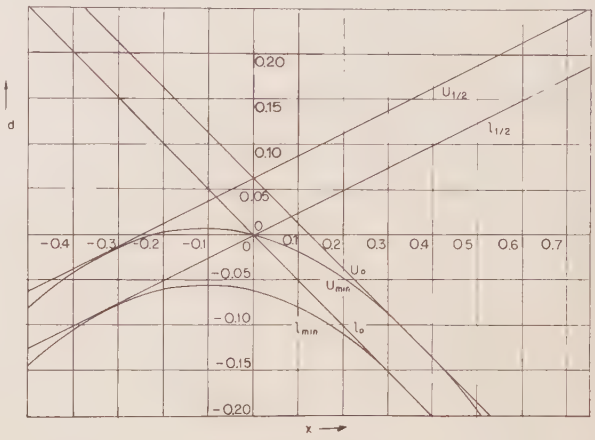

Fig. 7
Variation of critical boundary points with source displacement and azimuthal angle.

Appendix

Derivation of the $t(x,d) = \dfrac{1}{\chi} T(x,d)$ *relation*

It is helpful to consider the shape of the region of acceptance for a few values of the parameter $x = h \cos \psi$. In fig. 6 there are plotted the boundaries of this region for the values $x = (-0.1, 0, +0.1)$ in the d-a plane. One sees that as x increases in the positive direction, the region is depressed toward negative values of d in the left side of the region and raised toward larger positive values on the right side and that this skewing is reversed for decreasing values of x.

In obtaining the length of the horizontal intercept which lies inside the region of acceptance one must consider several different cases when $x \neq 0$; e.g., the intercept is clearly zero when d lies below the minimum in the lower parabola. Likewise, when d increases to the point where the value of a on the parabola is either greater than $\frac{1}{2}$ or less than zero one must change analytic representations for the length of the intercept.

Fig. 7 shows a plot of the variation in the position of these critical points in d versus the function of x. The lines designated by $u_{\min}$, u_0, and $u_{\frac{1}{2}}$ represent the corresponding quantities on the upper parabola. From an inspection of fig. 7 one may immediately write down expressions for $t(x,d)$. If one lets $a^l_{\pm}$ be the value of the larger $(+)$ or smaller $(-)$ solution of the equation (the lower parabola)

$$a^2 - \tfrac{1}{2}(1 - 3x)\, a - \tfrac{1}{2}(x + 2d) = 0$$

and $a^u_{\pm}$ be the larger $(+)$ or smaller $(-)$ solution of

$$a^2 - \tfrac{1}{2}(1 - 3x)\, a + \tfrac{1}{2}(\tfrac{1}{8} - x - 2d) = 0$$

then the transmission $t(x,d)$ may be written for the general case as

$$t(x,d) = \frac{1}{\chi} T(x,d) = \tfrac{1}{2}\Big[\{ \operatorname{Min}(\tfrac{1}{2}, a^l_+) - \operatorname{Max}(0, a^l_-) \} \operatorname{St}[-\operatorname{Im}(a^l_+)] - \{ \operatorname{Min}(\tfrac{1}{2}, a^u_+) - \operatorname{Max}(0, a^u_-) \} \operatorname{St}[-\operatorname{Im}(a^u_+)] \Big]$$

where

$$\operatorname{St}(z) \equiv 1 \qquad (z \geqslant 0)$$
$$\equiv 0 \qquad (z < 0)$$

and $\operatorname{Im}(z)$ is the imaginary part of the complex number z. Explicit representations for t may be written down as follows. When $x > 0$

$t = 0$ $\left(d \leqslant -\frac{1}{16} - \frac{1}{8}x - \frac{9}{16}x^2\right)$

$t = t_1 = \frac{1}{4}\sqrt{(1-3x)^2 + 8(x+2d)}$ $\left(-\frac{1}{16} - \frac{1}{8}x - \frac{9}{6}x^2 \leqslant d \leqslant -\frac{1}{2}x\right)$

$= t_2 = \frac{1}{8}\{(1-3x) + \sqrt{(1-3x)^2 + 8(x+2d)}\}$ $\left(-\frac{1}{2}x \leqslant d \leqslant -\frac{1}{8}x - \frac{9}{16}x^2\right)$

$= t_3 = \frac{1}{8}\{(1-3x) + \sqrt{(1-3x)^2 + 8(x+2d)}$

$-2\sqrt{(1-3x)^2 + 8(x+2d) - 1}\}$ $\left(-\frac{1}{8}x - \frac{9}{16}x^2 \leqslant d \leqslant \text{Min}\{\frac{1}{4}x, [\frac{1}{16} - \frac{1}{2}x]\}\right)$

$= t_4 = \frac{1}{4}\{1 - \sqrt{(1-3x)^2 + 8(x+2d) - 1}\}$ $\left(\frac{1}{2}x \leqslant d \leqslant \frac{1}{16} - \frac{1}{2}x\right)\left(x \leqslant \frac{1}{12}\right)$

$= t_5 = \frac{1}{8}\{\sqrt{(1-3x)^2 + 8(x+2d)}$ $\left(\frac{1}{16} - \frac{1}{2}x \leqslant d \leqslant \frac{1}{4}x\right)\left(x \geqslant \frac{1}{12}\right)$

$-\sqrt{(1-3x)^2 + 8(x+2d) - 1}\}$

$= t_6 = \frac{1}{8}\{1 + 3x - \sqrt{(1-3x)^2 + 8(x+2d) - 1}\}$ $\text{Max}[(\frac{1}{16} - \frac{1}{4}x), \frac{1}{4}x] \leqslant d \leqslant \frac{1}{16} + \frac{1}{4}x$

$= 0$ $\left(\frac{1}{16} + \frac{1}{4}x \leqslant d\right)$

For the case $x \leqslant 0$, the transmission takes a slightly different form

$t = 0$ $\left(d \leqslant -\frac{1}{16} - \frac{1}{8}x - \frac{9}{16}x^2\right)$

$= t_1$ $\left(-\frac{1}{16} - \frac{1}{8}x - \frac{9}{16}x^2 \leqslant d \leqslant \frac{1}{4}x\right)$

$t = \frac{1}{8}\{(1+3x) + \sqrt{(1-3x)^2 + 8(x+2d)}$ $\left(\frac{1}{4}x \leqslant d \leqslant -\frac{1}{8}x - \frac{9}{16}x^2\right)$

$= \frac{1}{8}\{(1+3x) + \sqrt{(1-3x)^2 + 8(x+2d)}$ $\left(-\frac{1}{4}x - \frac{9}{16}x^2 \leqslant d \leqslant \text{Min}[\frac{1}{2}x, (\frac{1}{16} + \frac{1}{4}x)]\right)$

$-2\sqrt{(1-3x)^2 + 8(x+2d) - 1}\}$

$= t_4$ $\left(-\frac{1}{2}x \leqslant d \leqslant \frac{1}{16} + \frac{1}{4}x\right), \left(-\frac{1}{12} \leqslant x\right)$

$= t_5$ $\left(\frac{1}{16} + \frac{1}{4}x \leqslant d \leqslant -\frac{1}{2}x\right), \left(x \leqslant -\frac{1}{12}\right)$

$= \frac{1}{8}\{(1-3x) - \sqrt{(1-3x)^2 + 8(x+2d) - 1}\}$ $\text{Max}(-\frac{1}{2}x, [\frac{1}{16} + \frac{1}{2}x]) \leqslant d \leqslant \frac{1}{16} - \frac{1}{2}x$

$= 0$ $\left(\frac{1}{16} - \frac{1}{2}x \leqslant d\right)$

NUCLEAR INSTRUMENTS AND METHODS 8 (1960) 320–326; NORTH-HOLLAND PUBLISHING CO.

CONTINUOUS MONITORING OF URANIUM LEACH SOLUTIONS

G. G. EICHHOLZ

Physics and Radiotracer Section, Mineral Sciences Division, Mines Branch, Department of Mines and Technical Surveys, Ottawa, Canada

Received 12 May 1960

A method for the determination of uranium content in leach solution by scintillation alpha-ray detection has been developed for possible application to the continuous monitoring and control of breakthrough in ion exchange colomns. The radioactive solution flows through a circular cell containing several thin disks of a plastic scintillation phosphor which respond to bombardment by alpha particles from uranium atoms in the solution. The fluorescence produced in the phosphor is observed and amplified by means of standard scintillation counter techniques. Breakthrough curves have been obtained by this method, and correlation with various alpha emitters has been attempted by the use of an alpha-ray spectrometer. Positive detection of activity to levels down to 0.2 g/l equivalent uranium content in solution seems possible on a continuous basis.

1. Introduction

In leach processes for the extraction of uranium from its ores and in subsequent chemical purification steps it would be advantageous if the actual uranium content of the various solutions could be monitored and recorded instantaneously and continuously. Such monitors might then be adapted to control the particular extraction process or to warn of excessive contamination in waste solutions. For this purpose it is tempting to turn to the radioactivity of uranium. The practical difficulty that one encounters, however, is that purified uranium with all its daughter elements removed emits only alpha particles. Though quite energetic (4.18 MeV), these particles have a short range in air and are easily absorbed in all solids and liquids, so that their range in water is only of the order of 25 microns.

For this reason attempts to monitor the uranium content of solutions continuously have not been very successful so far. The continuous monitoring of streams for fission products and other gamma emitters can be done fairly easily. (Wilson[1]), Wingfield[2]), and others), but for alpha emitters it has become customary to monitor by sampling the solution or stream automatically at fixed intervals. From these samples the uranium is extracted as an insoluble compound which is deposited on disks or filters and then counted with a zinc sulphide scintillation counter. Such methods have been described by Smales *et al.*[3]), Le France *et al.*[4]), and Wingfield[5]). The only equipment which has been described in the literature for direct continuous monitoring of alpha emitters in solution is that of Taylor and Abson[6]). Their apparatus consisted essentially of a rotating drum which dipped into the liquid and pulled up a thin liquid film by surface tension. This film passed under a zinc sulphide scintillation counter, in close proximity but without contact, and the alpha emission from the solution was thus determined. This ingenious method, however, did not work out too well in practice, as it was difficult to maintain

[1]) J. N. Wilson, Nucleonics **17**, No. 11 (1959) 140.

[2]) E. C. Wingfield, A Gamma Monitor for Liquid Streams, E. I. du Pont de Nemours and Co., Savannah River Laboratory, Report DP-342 (1958).

[3]) A. A. Smales, L. Airey, J. Woodward and D. Mapper, The Monitoring of Effluent for Alpha Emitters, A.E.R.E. Harwell Report C/R 2223 (1957).

[4]) J. D. LeFranc, P. Pottier and G. Roux, Énergie nucléaire **2**, No. 3 (1958) 195.

[5]) E. C. Wingfield, An Alpha Monitor for Waste Streams, E. I. du Pont de Nemours and Co., Savannah River Laboratory, Report DP-197 (1957).

[6]) D. Taylor and W. Abson, Proc. I.E.E. **98**, Part II (1951) 762.

uniform films on the drum under operating conditions and the sensitivity proved to be insufficient.

The work at the Mines Branch, Ottawa, arose principally from a desire to monitor the breakthrough of uranium in ion exchange columns used for the extraction of uranium in acid leach circuits, but the system developed may well have wider applications. Its main principle consists of detecting the alpha particles continuously by placing the detector in contact with the liquid. To compensate for the low sensitivity attainable, and because it is only the surface layer of the detector which responds to the alpha particles, it is important to increase the surface area used to detect the alpha particles. A further difficulty arises from the acidity of the leach solutions which attack unprotected inorganic scintillators and this requires careful design of the detector cell.

A first approach to this problem was attempted in 1951 by applying a thin coating to zinc sulphide films, the usual scintillating detector for alpha particles, to protect the zinc sulphide against corrosion from the solution[7]). This protective coating had to be uniform and free of pinholes, yet thin enough to permit easy passage of the alpha particles, while being fully resistant to strong sulphuric acid solutions. These requirements seemed to be mutually exclusive and this approach was abandoned in favour of one using thin plastic scintillation phosphors which at that time had just been developed[8,9]).

The advantage of the plastic scintillators lies in the fact that they may be made of polystyrene and are acid resistant and easy to manufacture in any desired shape or thickness. As plastic scintillators are also sensitive to gamma-rays, it is important to make them as thin as practicable to minimize counts from radium daughters and cosmic-ray background. The scintillation flashes produced by alpha particles are much smaller in plastic scintillators than in zinc sulphide, and good optical coupling is important. The remainder of the detection equipment consists of standard photomultiplier tubes, a pre-amplifier, a ratemeter and a recorder.

[7]) J. E. Wilson, Mines Branch Internal Report IR-42/51, Mines Branch, Department of Mines and Technical Surveys, Ottawa, Ont. (unpublished, 1951).

[8]) G. G. Eichholz and J. L. Horwood, Rev. Sci. Instr. **23** (1952) 305.

[9]) G. G. Eichholz, Phys. Rev. **89** (1953) 912.

2. Description of Apparatus

For test purposes, work with different detectors was carried out inside a large light-tight box which permitted maximum flexibility in changing detector types and configurations. The photomultiplier was supported vertically within its shield inside the box, and a detector cell rested on the light-sensitive photocathode of the photomultiplier. Depending on the nature of the tests either the scaler or the ratemeter was used as the count indicator.

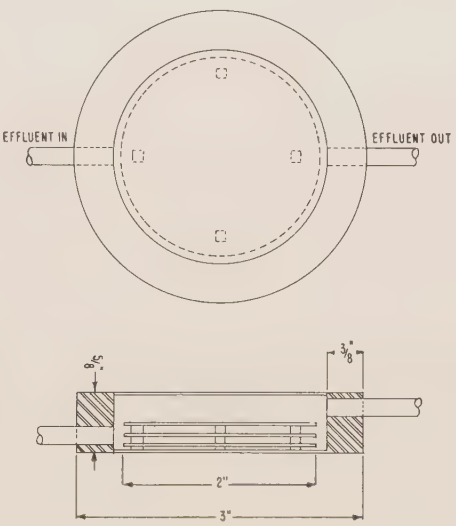

Fig. 1. Details of detector cells.

A 5-inch photomultiplier tube was used in some tests, but most of the test work was done with the cheaper 2-inch photomultiplier tube, type 6292, since, contrary to expectations, no appreciable increase in sensitivity and performance was obtained with either of two 5-inch photomultipliers, type 6364, which were tried.

The most critical operation is the preparation of the detector cells. Their assembly is presented diagrammatically in fig. 1 which shows an

all-plastic cell. All the plastic disks are made of scintillating plastic sheet having polystyrene beads as spacers. A similar cell was made with a stainless steel case, with the same type of plastic disk window and inner assembly. The stainless steel was painted with white Tygon paint to act as a light reflector.

The scintillator sheets were made on a laboratory press with polystyrene powder hot-moulded under pressure[8]). The hot platens were covered with aluminium foil and the thickness of the film could be adjusted by surrounding the powder with spacer rings of the appropriate thickness. Various scintillators were tried; a typical mixture would consist of 10g polystyrene (Dow No. 666), 400 mg p-terphenyl and 10 mg tetraphenyl butadiene. Diphenyl hexatriene was also used as a wave length shifter. For mechanical strength, slightly thicker sheets were chosen for the cell windows than those used in the inner detector assembly. The windows had to be mounted carefully since in operation they are subjected to considerable liquid pressure, and leaks could be disastrous. Absolute cleanliness is essential to avoid grease films on the detector disks. The disks were cut out with a sharp point around a heavy cylindrical guide. Similar commercial plastic scintillator sheets can also be employed, but no detailed tests have been carried out on these.

Calibration was carried out by circulating solutions of known uranium content in a closed circuit by means of a Sigma finger pump. All runs with test solutions from the ion exchange column were done with gravity feed only. It was found important to maintain the *p*H of the test solutions low, as in some early tests at near neutral *p*H a dense solid layer precipitated out on the plastic cell, which was later identified as silica from the leach solutions.

The photomultiplier was usually run at a potential of around 1100 volts. The ratemeter threshold level served as the only effective pulse height discriminator. Background levels were low, provided that the disk thicknesses were small enough to minimize gamma-ray detection.

3. Test Results

Owing to the intermittent nature of this project over the years 1954–1959, conditions varied from test to test and only typical results will be quoted here.

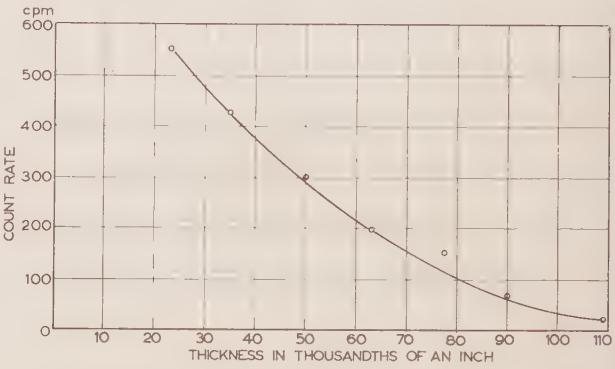

Fig. 2. Effect of phosphor thickness of alpha-ray detection.

3.1. DETECTOR TESTS

Experiments were carried out with various detector configurations and have been described more fully in a previous report[10]). Only the main conclusions will be summarized here. Fig. 2 shows the effect of scintillator thickness on count rate. It is seen that for thicker films there is considerable self-absorption of the fluorescent light, probably due to internal light scattering in the

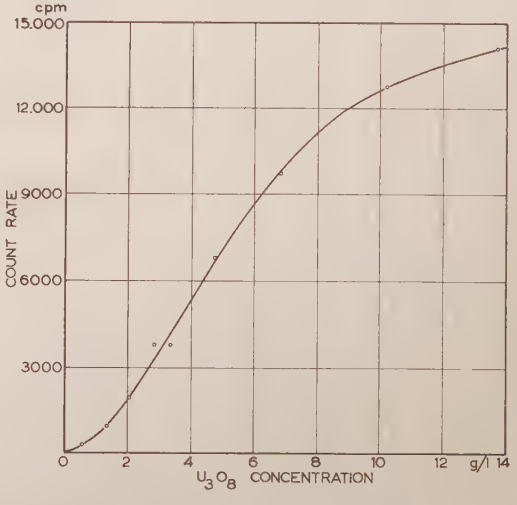

Fig. 3. Effect of uranium concentration on count rate.

[10]) H. H. Schwartz, Mines Branch Internal Report IR-219/56, Mines Branch, Department of Mines and Technical Surveys, Ottawa, Ont. (unpublished, 1956).

films. In practice, detector sheets were kept well below 15 mils.

Fig. 3 shows the response curve obtained with high grade solutions in a four-disk detector cell. The response is seen to be linear over most of the range. At the upper end it appears to level off, but this effect is ascribed to loss of light in passing through the solution, which was noticeably yellow at the higher concentrations. This light loss sets an upper limit to the total thickness of solution sampled, and hence to the number of disks that can usefully be employed. Table 1 presents results obtained in a typical case with different numbers of detectors, for a U_3O_8 concentration of 5 g/l.

TABLE 1

Effect of varying the number of detector disks (in a 7 cm diameter cell)

Number of detectors	Count rate (cpm)
1	3 437
2	7 345
3	11 958
4	14 743

It is seen that the count rate goes up steadily for all disk assemblies shown. In practice, four or five disks have been used for convenience. Larger assemblies pose problems in parallel mounting.

3.2. CALIBRATION

The system was calibrated by circulating synthetic uranium solutions through it. The solutions contained between 0.1 and 2 g/l U_3O_8, and fig. 4 is the corresponding calibration curve. It was seen that with the ratemeter time constant used, 0.1 g/l U_3O_8 is almost indistinguishable from background and represents the practical limit for the particular detector cell used. The recorder trace can be smoothed out by using a longer time constant in the ratemeter, and this is satisfactory when no abrupt changes in uranium content of the effluent are anticipated. The results shown in fig. 4 were obtained at a much later date and with a different detector cell than those shown in fig. 3, and this accounts for the better low-level discrimination obtained.

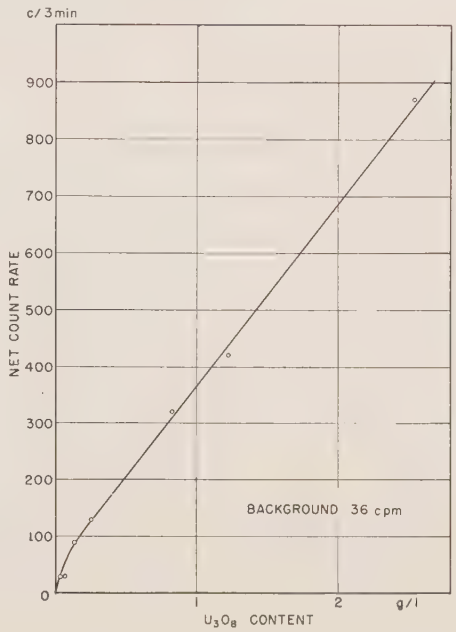

Fig. 4. Calibration for uranium solutions.

3.3. ION EXCHANGE EFFLUENT TESTS

Numerous tests were carried out on effluents from ion exchange columns for various pregnant uranium liquors. They all demonstrated plainly the steady rise in uranium content of the effluent and the absence of any abrupt change which could be pin-pointed as a definite breakthrough point. This is contrary to the experience gained by chemical determinations, where it was found that a fairly sharp increase in uranium content is observed in the effluent as the resin is loaded and breakthrough occurs. The difference may in part be due to the presence of other alpha emitters, and in part to a difference in scale. Most chemical loading curves pay little attention to the pre-breakthrough region. Fig. 5 shows a plot of the readings from two typical recorder traces for two different test runs. Some of the assays corresponding to these samples marked on run B are tabulated in table 2. This liquor contained some iron as well, and the iron assays are tabulated too, to show that the changes observed are not connected with the iron content.

TABLE 2
Solution monitor run B (Sept. 1959)

Sample number	U_3O_8 assay (g/l)	Fe assay (g/l)
Head sample	1.96	1.65
9	0.006	1.82
10	0.006	1.80
11	0.005	1.80
12	0.022	1.80
13	0.068	1.77
14	0.14	1.82
15	0.21	1.62

height analyser. This equipment is shown in fig. 7.

Figs. 8 and 9 show the alpha-ray spectra corresponding to some of the samples listed in table 2. According to the usual, arbitrary criterion used in uranium leach work, breakthrough was considered to take place when the uranium content in the effluent exceeded 0.1 g/l, i.e. between samples No. 13 and 14. Fig. 8 compares the alpha-ray spectrum of sample No. 12 with two spectrum curves obtained with pure uranium standards. It is seen that sample No. 12 consists almost entirely of thorium-230 with a

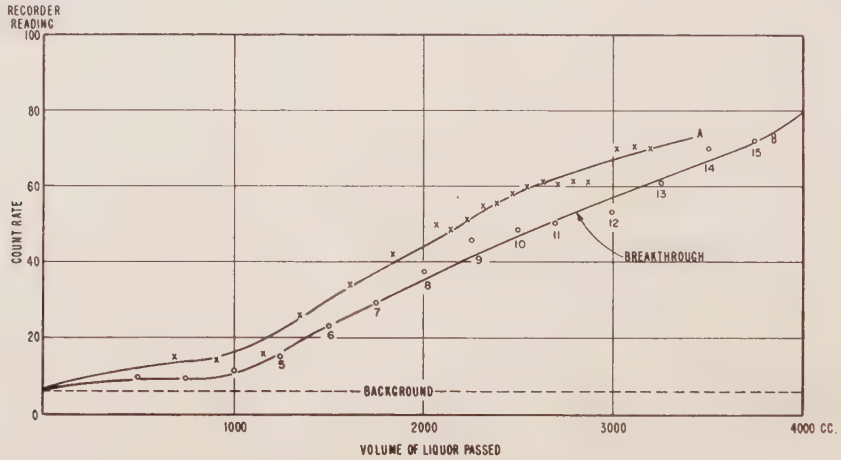

Fig. 5. Plot of typical ratemeter readings for two uranium leach liquors (ion-exchange column effluents). Feed rate 13 ml/min.

3.4. IDENTIFICATION OF EMITTING ISOTOPES

Some early runs with different pregnant leach liquors were characterised by a surprisingly rapid rise in detector indication. This is shown in fig. 6, in which the monitor indications for typical leach liquor effluents are plotted. The early rise was ascribed to the appearance of ionium (Th-230), which is replaced by uranium on the ion exchange resin. This was reportedly one of the difficulties encountered with Taylor and Abson's equipment[6]). To investigate this point, an alpha-ray spectrometer was set up as an aid in the identification of the alpha emitters in the various samples. The alpha-ray spectrometer consists of an ionization chamber of the type described by Harvey *et al.*[11]), followed by a linear amplifier, AEP type 1444, and a Marconi six-channel pulse peak at 4.68 MeV, clearly resolved from the uranium peaks at 4.76 MeV for uranium-234 and 4.18 MeV for uranium-238.

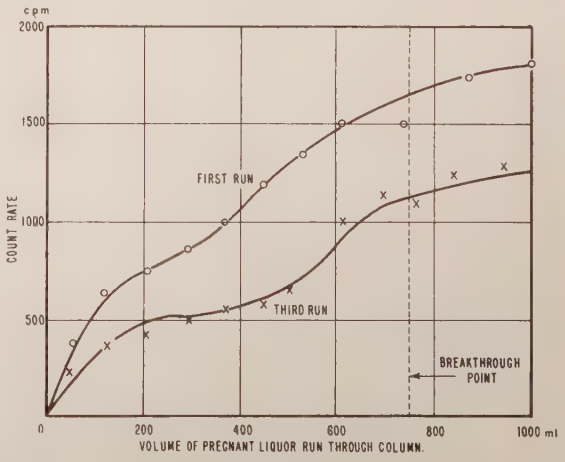

Fig. 6
Monitor indication of uranium content in two different test runs. (Breakthrough point determined colorimetrically.)

[11]) B. G. Harvey, H. G. Jackson, T. A. Eastwood and G. C. Hanna, Can. J. Phys. 35 (1957) 258.

Fig. 9 shows the progressive change in the alpha-spectra from sample to sample. It illustrates how thorium is adsorbed on the ion exchange resin first, to be replaced by uranium as breakthrough is approached, until for sample No. 16, long after breakthrough, uranium clearly predominates in the effluent. In this particular case, therefore, the appearance of ionium (Th-230) in the effluent and on the monitor records is linked so closely with the occurrence of breakthrough for uranium that it cannot be considered objectionable.

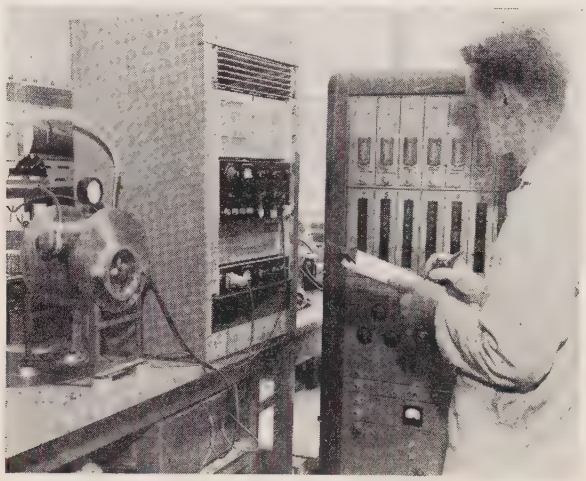

Fig. 7. Alpha-ray spectrometer.

3.5. OTHER URANIUM SOLUTIONS

To test the usefulness of the equipment in other applications, carbonate solutions from the leach plant of Eldorado Mining and Refining

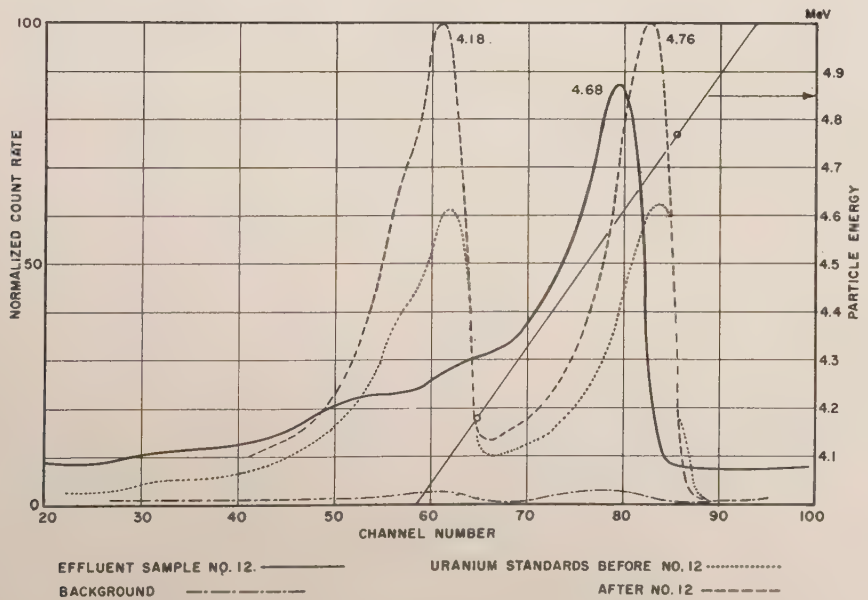

Fig. 8. Alpha-ray spectra of effluent samples (from Monitor Run B).

Limited at Beaverlodge, Sask., were run through the system. It was found that satisfactory monitor indications were obtained, provided that the liquors were filtered to remove all solid residues, for uranium contents above 0.15 g/l.

4. Conclusions

The tests indicate that it is possible to monitor uranium-bearing solutions continuously by the use of a plastic scintillator detector cell. While this method is less sensitive than methods using intermittent sampling and radiochemical purification, it is faster and more convenient. The limit in sensitivity for a given detector is set by the spontaneous fluctuations in count rate, which in turn depend on the time constant of the ratemeter. Where a slow response is adequate, a longer time constant of the order of 50 seconds, may be used to give a smoother output indication. For a sensitive, rapid response the fluctuations are too great and the variation in count rate too slow to permit actual control of the ion exchange column by breakthrough indication. However, the monitor can serve as a useful indicator of improper operation of the column or of premature breakthrough. It may also be useful in plutonium plants and in uranium refining.

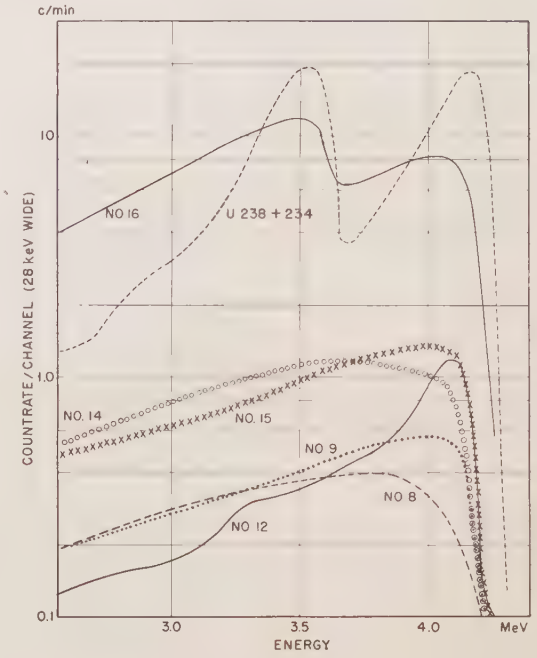

Fig. 9. Alpha-ray spectra of effluent samples showing uranium breakthrough.

Acknowledgments

It is a pleasure to record the patient and persevering assistance of J. M. Lefebvre who prepared all the detectors and carried out much of the test work, and the contributions of H. H. Schwartz and R. A. Wilkinson. Dr. J. D. Keys set up the alpha-ray spectrometer and C. McMahon and J. L. Horwood obtained the spectra. This project was suggested by the late Dr. E. A. Brown and the author owes much to discussions with him on various aspects of this work. This paper is published by permission of the Director, Mines Branch, Department of Mines and Technical Surveys, Ottawa, Canada.

NUCLEAR INSTRUMENTS AND METHODS 8 (1960) 327–330; NORTH-HOLLAND PUBLISHING CO.

DRIFT VELOCITIES OF ELECTRONS IN ARGON, NITROGEN AND ARGON MIXTURES

T. NAGY, L. NAGY and S. DÉSI

Central Research Institute for Physics, Budapest

Received 7 June 1960

Drift velocities of electrons produced by fission fragments in a parallel-plate ionization chamber have been measured in argon, nitrogen, and mixtures of gases, such as argon-nitrogen, argon-carbon dioxide and argon-methane. The results obtained are compared with data reported in the literature.

1. Introduction

For the operation of electron pulse ionization chambers it is necessary to know the drift velocities of electrons in the filling gas. In pure argon the drift velocity depends considerably on the presence of impurities and that is why the most careful purification of the gas is required in order to obtain reproducible results. This fact explains the discrepancies between data reported on this gas in the literature.

We repeated the experiments in pure argon and furthermore, measured the electron drift velocities in argon mixed with small amounts of contaminating gas.

2. Method of Measurement

Our measuring method was similar to that employed by Klema and Allen[1]) and Colli and Facchini[2]), that is we measured the collection times of electrons produced in a parallel-plate ionization chamber. But while these authors measured the collection times of electrons produced by α particles, in our experiments the rise times of pulses produced by fission fragments were photographed for investigation. The use of fission fragments instead of α particles has the advantage that the end of the pulse rise time becomes more definite. The end of the pulse is determined by the arrival of those electrons at the collecting electrode which are produced at the beginning of the track by the ionizing particle. As the specific ionization of the fission fragments is the greatest at the beginning of the track, that is the density of the electrons here is great, the rise of the pulse stops abruptly (fig. 1). The α particles on the other hand,

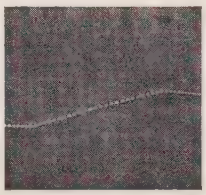

Fig. 1. Photograph of a pulse produced by a fission fragment. The marker has a duration of 0.5 μsec.

produce only few electrons at the beginning of their tracks, thus making determination of the end of the rise rather more uncertain than in case of fission fragments. A further advantage is the larger amplitude of pulses produced by fission fragments as compared with that of α particles.

The electrodes of the ionization chamber were 16 cm in diameter and were placed at a distance of 5 cm from each other. The 1 mg/cm^2 thick uranium layer deposited on the negative electrode had a diameter of 5 cm. With these dimensions and at the gas pressure applied, the electrons produced by the fission fragments move in a homogeneous electric field.

The chamber and a Po-Be neutron source were mounted in a paraffin container. By varying the distance between the source and the chamber, the number of fissions could be varied within wide limits.

[1]) E. D. Klema and J. S. Allen, Phys. Rev. **77** (1950) 661.
[2]) L. Colli and U. Facchini, Rev. Sci. Instr. **23** (1952) 39.

The chamber was connected to a purifying furnace 15 cm long and 5 cm in diameter containing 100 g of calcium chips. A motor was used to help the circulation of gas due to convection and in the case of gas mixtures also the mixing process. The rotor was provided with blades and the stator was mounted outside the gas system separated from the former by a glass tube.

Argon was purified as follows. The whole system was evacuated to 10^{-4} mm Hg pressure, then the furnace was heated up to 500°C in order to outgas the calcium. When the pressure decreased again below 10^{-4} mm Hg, the argon was let in through a trap containing liquid nitrogen.

Prior to the addition of molecular gases to the purified argon, the furnace was cooled in order to prevent the absorption of the small amounts of molecular gases by the calcium.

Gas pressures in the experiment ranged from 1000 to 2000 mm Hg, the potential difference between the electrodes could be varied from 0.1 to 7.5 kV.

In the course of each measurement the pressure was kept at a constant value, whereas the electrode potential was varied. The voltage pulses coming from the chamber were fed through a preamplifier and an amplifier to the vertical deflecting system of a synchroscope. The upper frequency limit of the amplifier chain was about 4 Mc/s, the clipping time 150 μsec. The pulses were fed from the amplifier to the synchroscope through a delay line in order to render visible the whole rising edge of the pulse, while the horizontal deflecting system was triggered by the non-delayed pulse.

The pulses were photographed as follows: the shutter of the camera was kept open until the appearance of a pulse. Since the camera was mounted on the synchroscope, the presence of the pulse was observed on the screen of a second synchroscope. A 25/10 DIN speed Agfa Rapid film and a lens with a relative opening of 1:1.5 was used.

The pulses obtained in the chamber were of various amplitudes depending on energies and directions of fission fragments. For a given pressure and field strength, however, the rise times are independent of the amplitudes.

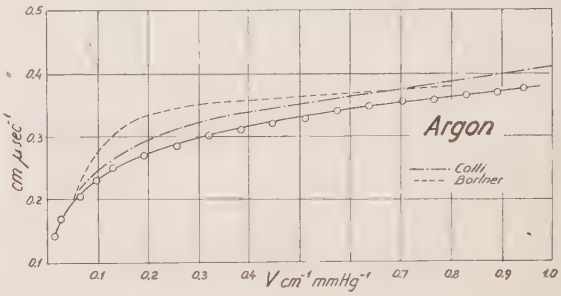

Fig. 2. Electron drift velocities in argon.

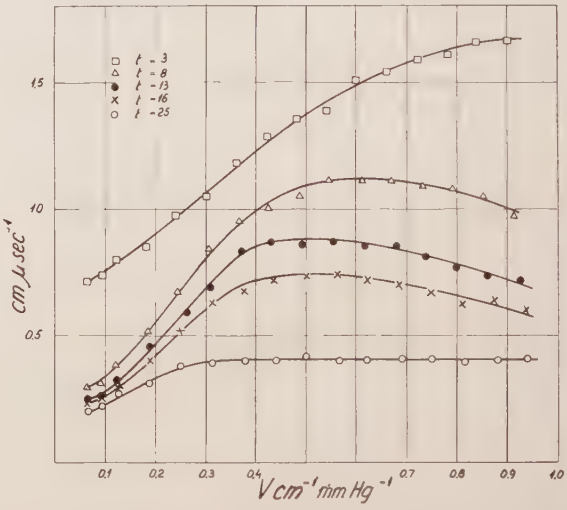

Fig. 3. Variation of electron drift velocity in argon with the time of purification if calcium was not outgassed. t denotes the purification time in hours.

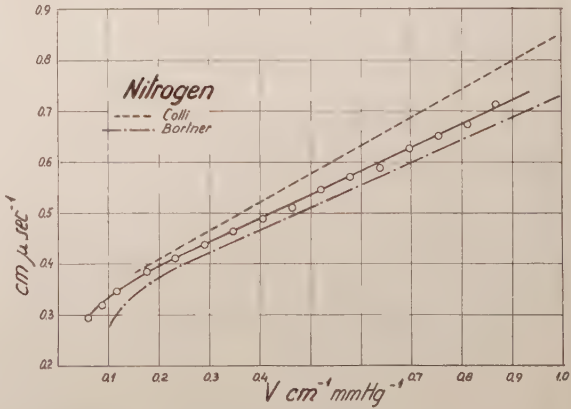

Fig. 4. Electron drift velocities in nitrogen. Our experimental points are marked by circles.

3. Results

3.1. ARGON

The results of our measurements of electron drift velocities in pure argon are shown in fig. 2, where the experimental points are marked by circles.

For comparison, the values obtained by Colli and Facchini[2]), and Bortner *et al.*[3]) were also plotted. These curves agree fairly well with our results. Nearly the same values were obtained by Nielsen[4]), Kirshner and Toffolo[5]). Several authors obtained much higher values for the drift velocity. This is probably due to the inadequate purity of the argon.

The purity of the tank argon used in our experiment was 99.7%. Using the above purifying procedure, the purification process was completed within 1–2 hours after the gas had been introduced. If the calcium was not outgassed, the purifying process was extremely retarded. For the latter case the values of the drift velocity are shown in fig. 3 with the purification time as parameter.

3.2. NITROGEN

The results obtained for nitrogen are seen in fig. 4. These data agree fairly well with those obtained by Klema and Allen[1]), Colli and Facchini[2]) and Bortner *et al.*[3]). The purity of the nitrogen used was better than 99.9% and for purification only a liquid nitrogen trap was used.

3.3. ARGON-NITROGEN GAS MIXTURES

The results are plotted in figs. 5 and 6. In the former we have shown also our curve for pure argon. It can be seen that even a small — 0.1%-nitrogen contamination considerably affects the value of the drift velocity. In both figures results of other authors are shown too.

In order to avoid overcrowding neither the curves of Colli and Facchini[2]) for 1% N_2 contamination nor those of English and

[3]) T. E. Bortner, G. S. Hurst and W. G. Stone, Rev. Sci. Instr. **28** (1957) 103.

[4]) R. A. Nielsen, Phys. Rev. **50** (1936) 950.

[5]) J. M. Kirshner and D. S. Toffolo, J. Appl. Phys. **23** (1952) 594.

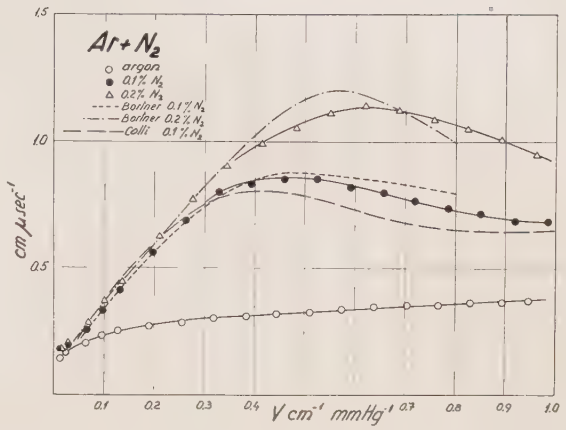

Fig. 5. Electron drift velocities in argon-nitrogen mixtures.

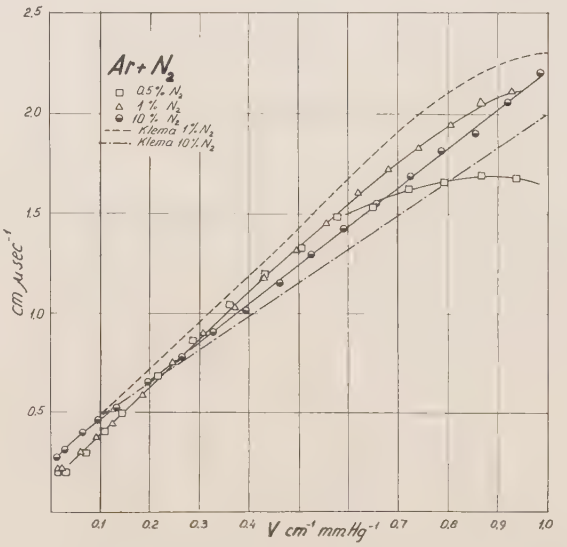

Fig. 6. Electron drift velocities in argon-nitrogen mixtures.

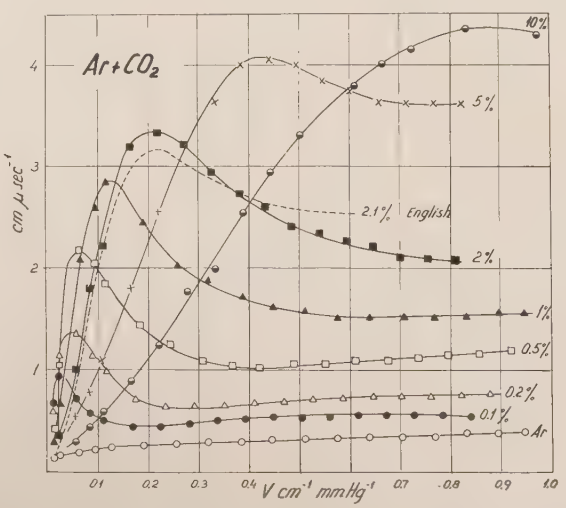

Fig. 7
Electron drift velocities in argon-carbon dioxide mixtures.

Hanna[6]) for 1% and 10% contamination are plotted in the figure, since they lie quite close to the curves which are shown. The curve of Kirshner and Toffolo[5]) obtained for 0.7% contamination which is not shown in the figure, lies much lower than our curve for 0.5% N_2, even lower than that of Bortner *et al.*[3]) for 0.2% N_2 contamination which incidentally shows a good agreement with our results.

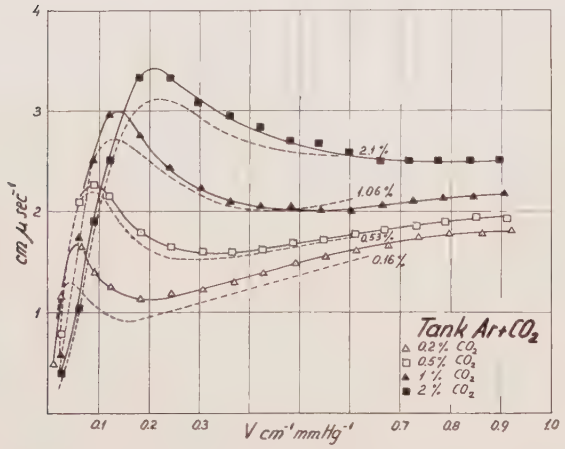

Fig. 8. Electron drift velocities in tank argon-carbon dioxide mixtures. The dashed curves represent values obtained by English and Hanna[6]).

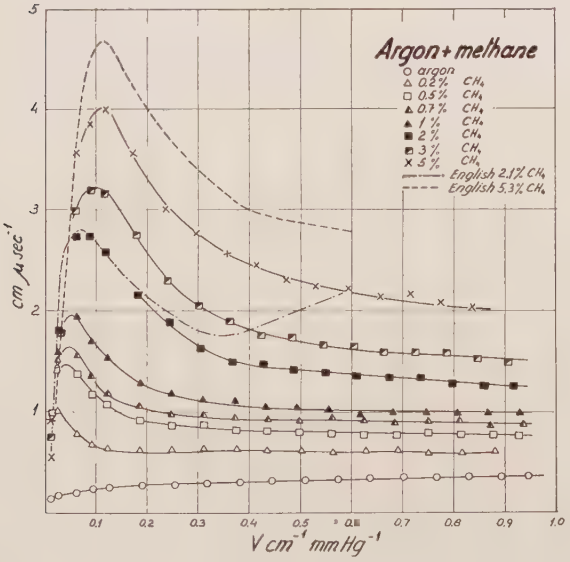

Fig. 9. Electron drift velocities in argon-methane mixtures. The asterisk* marks the coincident points of the 0.2, 0.7 and 2% contamination curves.

3.4. ARGON-CARBON DIOXIDE MIXTURES

In fig. 7 the drift velocities measured in purified argon slightly contaminated with various amounts of CO_2 are shown. For comparison, we have plotted English and Hanna's[6]) result obtained for argon with 2.1% CO_2 added. In their experiment, however, argon had not been purified and therefore, owing to the presence of some nitrogen contamination the tails of their curves show a stronger increase. The purity of argon used by the latter authors was 99.6%, thus nearly the same as that of our tank argon gas.

For comparison, measurements were carried out with a mixture of unpurified argon and carbon dioxide. The results are shown in fig. 8 and agree fairly well with those of English and Hanna[6]). From figs. 7 and 8 it is seen that the maxima of the curves obtained in both experiments lie nearly at the same abscissa value and for higher percentage contamination are shifted to the right.

The carbon dioxide was purified by repeated solidification and simultaneous desorption.

3.5. ARGON-METHANE GAS MIXTURES

Our results for pure argon to which some methane had been added are to be seen in fig. 9. For the purification of methane we used the same procedure as for carbon dioxide. For comparison, we plotted again results of English and Hanna[6]), however, as in the former case these authors here also used unpurified argon.

[6]) W. N. English and G. C. Hanna, Can. J. Phys. **31** (1953) 768.

NUCLEAR INSTRUMENTS AND METHODS **8** (1960) 331–338; NORTH-HOLLAND PUBLISHING CO.

EIN UNIVERSELLES VERFAHREN ZUR STABILISIERUNG VON SZINTILLATIONS-SPEKTROMETER-ANORDNUNGEN†

S. HAUN und D. KAMKE

Physikalisches Institut der Universität Marburg/L

Eingegangen am 22. Mai 1960

The gain of a scintillation-spectrometer can be held constant for long measuring times by including the spectrometer in a regulation circuit. All devices of this kind which have been described as yet are dependent on specific features of the spectrum and many situations arise where none of them can be used. The introduction of a pulsed source of light makes such stabilization devices universally applicable. This paper describes a light source and a suitable stabilization circuit with which a stability better than 0.5 per cent has been achieved for a 14 hour period, starting immediately after turning on the electronic circuits. The static and dynamic regulation properties are given as well as a method for evaluating all the effects due to the statistical character of the pulse height distribution produced by the light source and the photomultiplier.

1. Einleitung

Die Analyse eines elektrischen Impulshöhenspektrums, wie man es beim Szintillationsspektrometer mit Hilfe von Szintillationssubstanz und Photokathode (Photomultiplier) aus dem Energiespektrum einer Kernstrahlung herleitet, erfordert mit Amplituden-, Einkanal- oder Mehrkanaldiskriminator in vielen Fällen längere Messzeiten. Gutes energetisches Auflösungsvermögen genügt infolgedessen nicht, um mit einer bestimmten Apparatur zuverlässige Messergebnisse zu erhalten. Zusätzlich muss sichergestellt sein, dass man eine beliebige Energie innerhalb der untersuchten Kernstrahlung stets an derselben Stelle der Diskriminatorskala registriert. Dazu reichen elektronische Stabilisierung aller Versorgungsspannungen und Gegenkopplung im Impulsverstärker vielfach nicht aus.

Da die auftretenden Instabilitäten in erster Linie von Änderungen des Verstärkungsfaktors zwischen Photokathode und Verstärkerausgang herrühren, lässt sich folgendes Regelverfahren anwenden: Eine geeignete Stelle innerhalb des zu untersuchenden Impulshöhenspektrums wird ständig so kontrolliert, dass jede Verschiebung dieser Stelle gegenüber der Analysatorskala (und nur eine solche) eine entgegenwirkende Änderung der Hochspannung am Photomultiplier und damit der Gesamtverstärkung hervorruft.

Alle Stabilisierungseinrichtungen, die bisher nach diesem Prinzip praktisch ausgeführt wurden[1]), setzen eine hinreichend intensive Linie innerhalb des zu untersuchenden Energiespektrums voraus, deren Intensität oder Gestalt sich in einigen Fällen während der Messzeit nicht ändern darf. Bei vielen Messaufgaben, insbesondere bei allen Arbeiten an Beschleunigungsmaschinen, ist diese Voraussetzung nicht erfüllt. Der gelegentlich vorgeschlagene Ausweg, der zu untersuchenden Strahlungsquelle ein radioaktives Präparat hinzuzufügen, um die Stabilisierungseinrichtung an eine Linie innerhalb des Spektrums dieses Präparates anzuschliessen, kann nur selten beschritten werden,

† Eine ausführliche Beschreibung aller angestellten Untersuchungen findet man in No. 35 der "Rundberichte über unveröffentlichte Arbeiten aus dem Gebiete der Kernphysik und kosmischen Höhenstrahlung, herausgegeben im Auftrag des Fachausschusses für Kernphysik und kosmische Höhenstrahlung im Verband Deutscher Physikalischer Gesellschaften e.V. und der Kommission für Atomphysik". Sonderdrucke dieses "Rundberichtes" sind bei den Autoren der vorliegenden Arbeit verfügbar.

[1]) D. H. Wilkinson, J. Sci. Instr. **27** (1950) 36;
G. F. von Dardel, J. Sci. Instr. **32** (1955) 302;
H. de Waard, Nucleonics **13**, No. 7 (1955) 36;
U. Cappeller und R. Klingelhöfer, Z. f. Physik **150** (1958) 375.

ohne gleichzeitig das zu untersuchende Spektrum unerwünscht zu verändern.

Dagegen werden alle in der Literatur beschriebenen Stabilisierungsverfahren uneingeschränkt anwendbar, wenn man die benötigte scharfe Spektrallinie dadurch herstellt, dass man zugleich mit dem Fluoreszenzlicht der Szintillationssubstanz das Licht einer äusseren Impulslichtquelle (ILQ) auf die Photokathode nur in genau bekannter Weise verändert (besonders wertvoll bei der Untersuchung intensitätsschwacher Spektren).

Allerdings werden Schwankungen, die von Änderungen der Fluoreszenzausbeute der Szintillationssubstanz herrühren, von einer derartigen Stabilisierungseinrichtung nicht erfasst. Instabilitäten dieser Art gehen jedoch meistens mit erheblichen Änderungen der Szintillator-

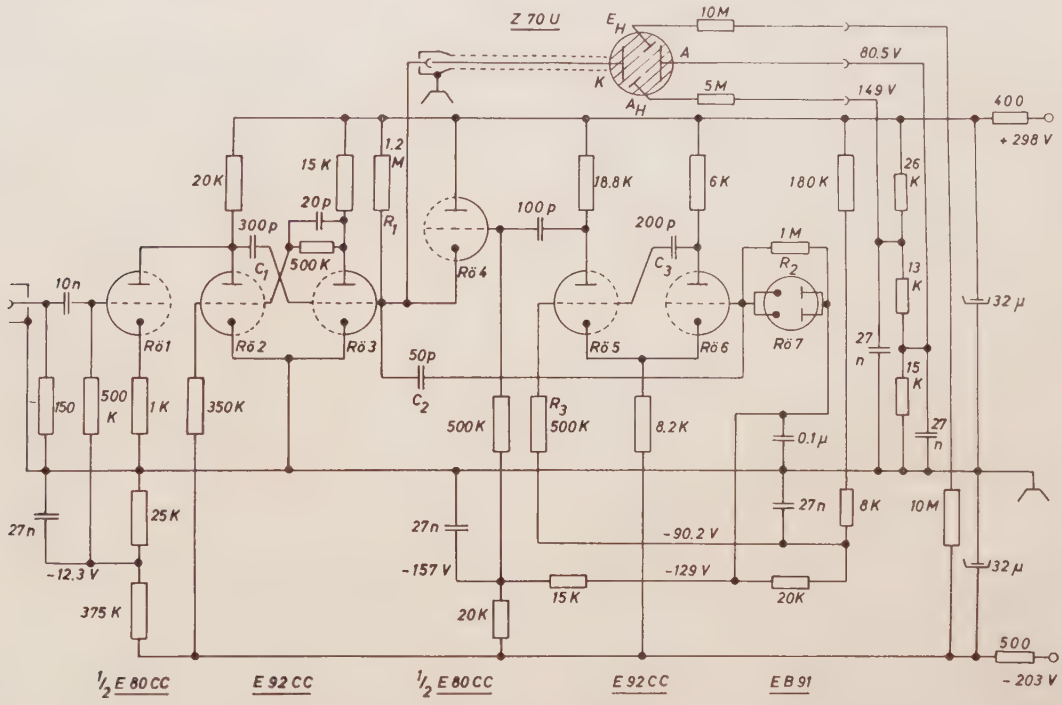

Fig. 1. Vollständiges Schaltbild der ILQ (Relaisröhre Z 70 U mit Zündgerät).

einfallen lässt. Dieses Verfahren bietet folgende Vorteile:

1. Die Lage der künstlichen Spektrallinie ("Lichtlinie") innerhalb des Spektrums (d.h. die Höhe der zugeordneten elektrischen Impulse) ist durch eine mechanische Blende vor der ILQ leicht einstellbar.

2. Eine solche Spektrallinie ist sehr scharf; daher sind Verschiebungen des Spektrums an ihr besonders deutlich wahrzunehmen.

3. Die Zahl der Lichtimpulse je Zeiteinheit ist beliebig wählbar und streut nicht statistisch. Dadurch wird das zu untersuchende Spektrum

eigenschaften einher, die ohnehin zum Abbruch der Messung zwingen.

2. Die Impulslichtquelle

Eine Impulslichtquelle (ILQ) zur Stabilisierung einer Szintillationsspektrometer-Anordnung muss folgende Eigenschaften besitzen:

1. Sie muss klein genug sein, um sich am Kopfteil eines Szintillations-Strahlungsdetektors mechanisch leicht anbringen zu lassen.

2. Sie soll Lichtimpulse liefern,

a. deren "Farbe" (Spektrum) mit der des Fluoreszenzlichtes der Szintillationssubstanz möglichst übereinstimmt;

b. deren Dauer von der Grössenordnung 1 μs ist;

c. die mit konstanter Frequenz (höchstens einige $10^2\,s^{-1}$) einander folgen;

d. deren Photonenzahl pro Impuls mit möglichst geringem mittlerem Schwankungsquadrat um einen Mittelwert streut; dieser Mittelwert muss über längere Messzeiten hinweg (10–20 Stunden) konstant bleiben.

Nach Vorversuchen mit einem Thyratron, der Gastriode EC 50[2]), wurden diese Eigenschaften schliesslich durch Verwendung der Röhre Z 70 U (Valvo), einer Relaisröhre mit kalter Kathode, erreicht. Diese Röhre bietet einige besondere Vorteile:

1. Sie ist ausserordentlich klein (10 mm ø, 25 mm Länge).

2. Ihr Entladungsleuchten ist sehr gut sichtbar.

3. Durch eine zusätzliche Hilfsentladung ist ihre Zündkennlinie von der äusseren Beleuchtung unabhängig, insbesondere arbeitet die Röhre auch in völliger Dunkelheit zuverlässig.

4. Bei der Konstruktion dieser Röhre ist besonderer Wert auf geringe Exemplarstreuung und gute Konstanz der Zündkennlinie während der – im übrigen sehr langen – Lebensdauer gelegt worden.

Figur 1 zeigt die Schaltung, mit der die Z 70 U als ILQ betrieben wird. Ihre wesentlichen Bestandteile sind zwei Univibratoren U_1 (Rö 2 und Rö 3) und U_2 (Rö 5 und Rö 6); beim Umklappen in den metastabilen Zustand bewirkt U_1 die Zündung, U_2 die Löschung der Relaisröhre. Die Schaltung hat folgende besondere Eigenschaften:

1. Die Frequenz der Lichtimpulse wird durch eine von aussen zugeführte Folge positiver Triggerimpulse bestimmt, deren Form und Höhe (etwa 6 V) nicht kritisch sind (vgl. Abschn. 5).

2. Zwischen zwei aufeinanderfolgenden Lichtimpulsen liegt an der Hauptentladungsstrecke der Z 70 U stets nur eine Spannung von rund 80 V, d.h. 33 V weniger als die minimale Brennspannung. Dadurch werden unbeabsichtigte Zündungen der Röhre sicher verhütet.

[2]) S. Haun und D. Kamke, Physikal. Verhandlgn. **9**, No. 2 (1958) 21.

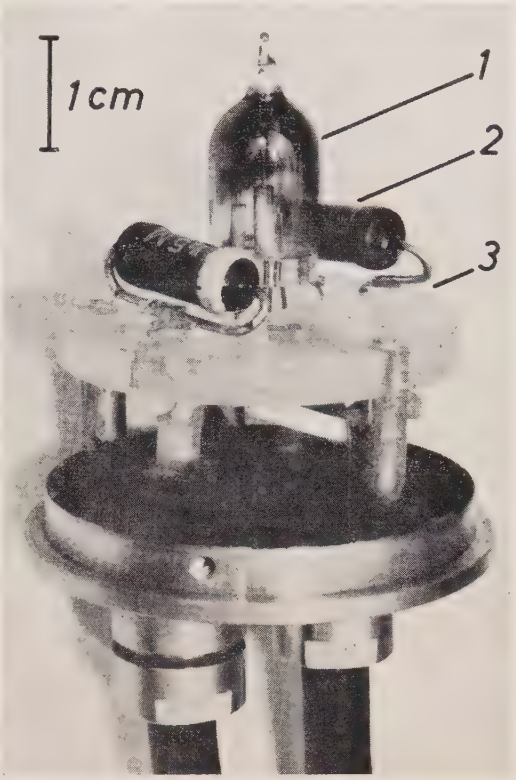

Fig. 2. Halterung der Relaisröhre im Innern des ILQ-Gehäuses.

3. Der Löschvorgang setzt erst ein, wenn Strom durch die Entladungsröhre fliesst. Dadurch wird ein Ausbleiben einzelner Zündungen trotz möglicher Zündverzögerung unmöglich gemacht.

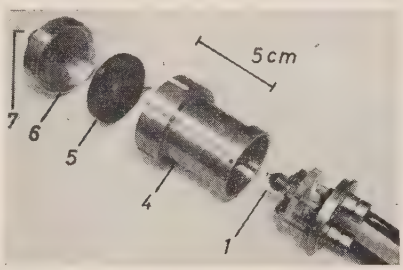

Fig. 3. ILQ, in ihre Einzelteile zerlegt.

4. Die je Lichtimpuls durch die Röhre fliessende Ladung, die die emittierte Lichtmenge bestimmt, hängt nur von wenigen Schaltelementen ab, nämlich im wesentlichen von Kondensator C_1 und der Differenz der Gitterpotentiale von Rö 5 und Rö 6.

Den mechanischen Aufbau dieser ILQ zeigen die Figuren 2 und 3.

Die Relaisröhre (1) besitzt anstelle von Sockelstiften etwa 32 mm lange Anschlussdrähte, mit denen sie neben Vorwiderständen (2) für Hilfselektrode und Hilfsanode auf einer Isolierscheibe (3) aus Plexiglas befestigt ist. Die ganze Anordnung befindet sich im Innern eines zylindrischen, lichtdichten Gehäuses (4), welches vor der Spitze der Entladungsröhre durch eine Irisblende (5) abgeschlossen wird. Die Fassung (6) dieser Blende läuft in einen Schraubansatz (7) aus, mit dem das ganze Gehäuse von der Seite in die Eisenabschirmung des Photomultipliers eingeschraubt wird, und zwar dort, wo ein Plexiglas-Lichtleiter den optischen Kontakt zwischen der Photokathode und dem Szintillator herstellt. Mit ihrem Zündgerät ist die Relaisröhre durch zwei 30 cm lange Kabel verbunden: Ein Koaxialkabel stellt die Verbindung zur Kathode her, ein dreiadriges Kabel versorgt Anode, Hilfsanode und Hilfselektrode mit den benötigten Gleichspannungen.

Die Figur 4 zeigt die bei den hier zu beschreibenden Untersuchungen ausschliesslich benutzte

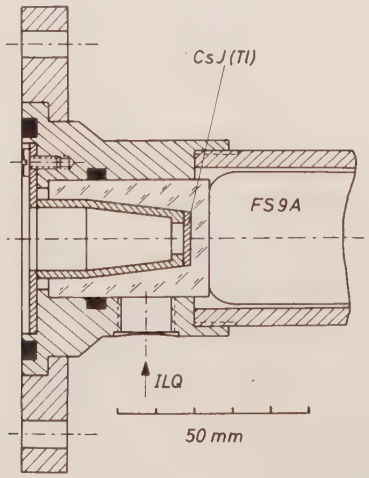

Fig. 4. Kopfstück des Strahlungsdetektors mit Gewindebohrung für die ILQ.

Anordnung im Kopfstück des Strahlungsdetektors: CsJ (Tl) als Szintillationssubstanz vor einem FS9A-Multiplier; der Lichtleiter (Plexiglas) führt das Licht der von unten einzuschraubenden ILQ der Photokathode zu und dient zugleich als Vakuum-Abschluss.

3. Der Regelkreis

Die *Regelstrecke* besteht aus Photomultiplier und Impulsverstärker des normalen Szintillationsspektrometers. Der Mittelwert V des für jeden Impuls anzugebenden Verhältnisses

$$\frac{\text{Höhe des elektrischen Ausgangsimpulses}}{\text{auf die Photokathode eingefallene Photonenzahl}}$$

stellt die Regelgrösse dar.

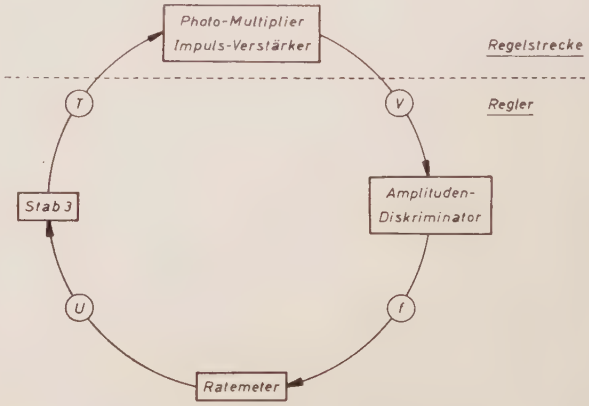

Fig. 5. Blockschaltbild des Regelkreises.

Der *Regler* setzt sich folgendermassen zusammen: An den Verstärker ist ein Amplitudendiskriminator (Schmitt-Trigger) angeschlossen. Ist die Irisblende vor der ILQ so eingestellt, dass die Lichtimpulse am Verstärkerausgang nur zu höheren Spannungsimpulsen führen als die Szintillationen des durch eine Kernstrahlung angeregten Szintillationskristalles, so ist bei passender Schwelleneinstellung des Diskriminators dessen Ausgangszählrate f eindeutig der Regelgrösse V zugeordnet (solange der Mittelwert der je Lichtimpuls auf die Photokathode einfallenden Photonenzahl sowie die Höhe der Diskriminatorschwelle unverändert bleiben). f wird daher als Mass für die Regelgrösse einem Ratemeter zugeführt, dessen Ausgangsspannung U die Multiplier-Hochspannung T und damit die Regelgrösse V beeinflusst.

Als Ratemeter dient eine gebräuchliche Zusammenstellung von Impulsformerstufe, *RC*-Integrierglied und Röhrenvoltmeter; zur Regulierung der Hochspannung wird "Stab 3" des

"Marburger Geräteprogrammes" verwendet, ein Hochspannungs-Stabilisierungsgerät (Differenzverstärker mit Querregelröhre), welches gestattet, die vorstabilisierte Hochspannung T mit Hilfe der Gleichspannung U kontinuierlich zu verändern.

Das statische Regelverhalten dieses Kreises ist durch den *Regelfaktor* zu beschreiben: Eine bestimmte Störung möge die Regelgrösse bei geöffnetem, also unwirksamem, Regelkreis um S, bei geschlossenem Regelkreis dagegen um q verändern. Dann wird das Verhältnis

$$\frac{S}{q} = \eta \qquad (1)$$

als Regelfaktor bezeichnet.

Um die Beiträge der einzelnen Kreisglieder zum Regelfaktor zu erkennen, ist für jedes Glied die Beziehung zwischen Änderungen von Eingangs- und Ausgangsgrösse aufzustellen. Solange diese Änderungen klein bleiben, sind sie bei jedem Glied einander proportional; dann ist der Regelfaktor im wesentlichen das Produkt aller Proportionalitätskonstanten. Insbesondere ist er der Intensität der "Lichtlinie" (Zahl der Lichtimpulse je Zeiteinheit) direkt und ihrer relativen Halbwertsbreite indirekt proportional.

Eine direkte Messung des Regelfaktors wurde folgendermassen ausgeführt: Durch Änderung der Verstärkungseinstellung am Impulsverstärker wurde eine bekannte Störung S innerhalb der Regelstrecke verursacht und die resultierende Änderung q der Regelgrösse bestimmt, indem ein einfaches Szintillationsspektrum mit einem zweiten Amplitudendiskriminator (parallel zum Diskriminator des Regelkreises angeschlossen) verfolgt wurde (Beschreibung der Apparatur siehe Abschnitt 5). Die Frequenz der Lichtimpulse betrug dabei 100 s^{-1}, die relative Halbwertsbreite der "Lichtlinie" 3%.

Aus der erhaltenen Kurve (Figur 6) ist der Regelfaktor als Koordinatenverhältnis jedes Kurvenpunktes zu entnehmen. Man liest für kleine Störungen $\eta = 35$ ab, ferner eine rasche Abnahme des Regelfaktors für Störungen $|S| > 5.5$ db.

Um das Verhalten des Regelkreises gegenüber zeitabhängigen Störungen zu untersuchen, wurden die Übergangsfunktionen aller Kreisglieder

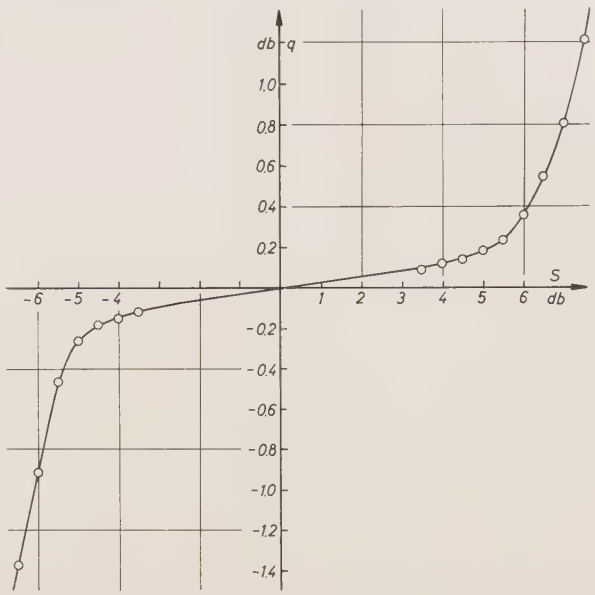

Fig. 6. Messung des Regelfaktors und des Regelbereiches.

ermittelt. Während bei Regelstrecke und Diskriminator die jeweilige Ausgangsgrösse einer Änderung der Eingangsgrösse spontan folgt, verlaufen die Ausgangsgrössen von Ratemeter und Stab 3 nach sprunghafter Änderung der Eingangsgrösse um K_f bzw. K_U nach Exponentialfunktionen. Diese Funktionen wurden oszillographisch aufgezeichnet und photographiert. Sie werden beschrieben durch die Ausdrücke

$$\Delta U(t) = -a\left(1 - \exp\left(-\frac{t}{D}\right)\right) K_f\,, \qquad (2)$$

$$\frac{\Delta T(t)}{T_0} = b\left(1 - \exp\left(-\frac{t}{d}\right)\right) K_U \qquad (3)$$

für $t \geq 0$ mit

$D = 17.6$ s, $\quad d = 2.15$ s, $\quad a > 0$, $\quad b > 0$.

(T_0 ist der zu $U = 0$ gehörige Wert von T.)

Daraus kann die Übergangsfunktion des geschlossenen Regelkreises nach bekannten Regeln ausgerechnet werden. Man findet, dass sich die Regelgrösse nach einer sprunghaft eingetretenen Störung K_V, die innerhalb des linearen Teils der Kurve von Figur 6 bleibt, gemäss einer gedämpften Sinusschwingung auf den neuen Regelzustand einstellt:

$$\Delta V(t) = \frac{K_V}{\eta}$$

$$\left[1 + (\eta - 1)\left(\cos \omega t + \frac{\delta}{\omega} \sin \omega t\right) \exp(-\delta t)\right] \quad (4)$$

mit

$$\delta = \frac{1}{2}\left(\frac{1}{d} + \frac{1}{D}\right), \qquad \omega = \sqrt{\frac{1}{dD}\eta - \delta^2}\,.$$

Hieran ist zu erkennen, dass man wenigstens eine der beiden Grössen d und D klein halten muss, um längere Einschwingdauer zu vermeiden.

4. Statistische Betrachtungen

Bei geschlossenem Regelkreis führt der statistische Charakter der Zählrate f (Ausgangsgrösse des Diskriminators) zu Schwankungen der Multiplier-Hochspannung T und damit der Regelgrösse V, so dass das zu untersuchende Impulshöhenspektrum auf der Skala des Analysiergerätes (Amplituden- oder Kanaldiskriminator) ständig um eine mittlere Lage hin und her wandert. Der Einfluss dieser Erscheinung auf die Genauigkeit, mit der das Spektrum einer Kernstrahlung ausgemessen werden kann, ist zu untersuchen.

Man denke sich bei fester Einstellung des Analysiergerätes dessen Ausgangsimpulse wiederholt eine bestimmte Zeit τ lang ausgezählt. Sind die Verschiebungen des Impulshöhenspektrums so klein, dass die Krümmung seiner Integral- bzw. Differentialkurve (je nachdem, ob ein Amplituden- oder Kanaldiskriminator als Analysiergerät dient) nicht spürbar ist, so streuen die Zählergebnisse ξ_i der einzelnen Zählperioden um denselben Mittelwert $\bar{\xi}_i$, wie es der Fall wäre, wenn das Spektrum seine mittlere Lage ständig beibehielte; jedoch ist das mittlere Schwankungsquadrat $\overline{(\xi_i - \bar{\xi}_i)^2}$ geändert. Man findet für diese Grösse †:

$$\overline{(\xi_i - \bar{\xi}_i)^2} = \bar{\xi}_i + \overline{\left(\frac{\mathrm{d}n}{\mathrm{d}T}\int_0^\tau \delta T(t)\mathrm{d}t\right)^2} \quad (5)$$

oder umgeformt:

$$\overline{(\xi_i - \bar{\xi}_i)^2} = \bar{\xi}_i + 2\left(\frac{\mathrm{d}n}{\mathrm{d}T}\right)^2 \int_0^\tau \mathrm{d}t \int_t^\tau \overline{\delta T(t)\cdot\delta T(t')}\,\mathrm{d}t'\,. \quad (6)$$

† Einzelheiten siehe "Rundbericht No. 35".

Hierin drückt $\mathrm{d}n/\mathrm{d}T$ die Abhängigkeit der Ausgangszählrate n von der Mulitplier-Hochspannung T aus; diese Grösse hängt vom verwendeten Multiplier, von der gewählten Beobachtungsstelle innerhalb des Spektrums und vom Analysiergerät ab. Mit $\delta T(t)$ ist die Abweichung der Hochspannung von ihrem Mittelwert $\overline{T}$ zum Zeitpunkt t bezeichnet gemäss der Beziehung

$$T(t) = \overline{T} + \delta T(t) \quad \text{mit} \quad \overline{\delta T(t)} = 0\,. \quad (7)$$

Der Querstrich schliesslich deutet Mittelbildung über viele Zählperioden von gleicher Länge τ an.

Treten dagegen grössere Verschiebungen des Impulshöhenspektrums auf, so streuen die Zählergebnisse ξ_i um einen anderen Mittelwert, als es bei konstanter Hochspannung $T(t) = \overline{T}$ der Fall wäre: Jede Spektrallinie wird verbreitert, das energetische Auflösungsvermögen der Spektrometer-Anordnung herabgesetzt. Für eine Spektrallinie, die bei konstanter Hochspannung $\overline{T}$ die relative Halbwertsbreite B hat, findet man, wenn die Hochspannung mit dem mittleren relativen Schwankungsquadrat $\overline{(\delta T/\overline{T})^2}$ um $\overline{T}$ als Mittelwert schwankt, die relative Halbwertsbreite B':

$$B'^2 = B^2 + c^2\overline{\left(\frac{\delta T}{\overline{T}}\right)^2} 8 \ln 2\,. \; [3] \quad (8)$$

Darin ist c die den Multiplier kennzeichnende Proportionalitätskonstante zwischen relativen Änderungen von Hochspannung und Verstärkungsfaktor. Es bleiben also das mittlere relative Schwankungsquadrat einer einzelnen Hochspannungsablesung, sowie die Korrelation zweier um eine bestimmte Zeitspanne getrennter Ablesungen bei geschlossenem Regelkreis zu bestimmen. Dazu geht man folgendermassen vor:

Zunächst wird aus den Übergangsfunktionen von Ratemeter und Stab 3 berechnet, welche Veränderung der Hochspannung T ein einzelner Impuls hervorruft, der zum Zeitpunkt t_i in das Ratemeter des Regelkreises einläuft. Man findet für Zeiten $t \geq t_i$:

[3] E. Breitenberger, Progress in Nucl. Phys., Vol. 4, (Pergamon Press, 1955) 56.

$$\Delta T(t) = A\left(\exp\left(-\frac{t-t_i}{d}\right) - \exp\left(-\frac{t-t_i}{D}\right)\right) \quad (9)$$

oder abgekürzt:

$$\Delta T(t) = A \cdot W(t-t_i)\,. \quad (10)$$

Hiermit lässt sich die Grösse $\delta T(t)$ als Summe der Wirkungen von Impulsen angeben, die vor dem Zeitpunkt t in das Ratemeter eingelaufen sind. Da am geschlossenen Regelkreis die Zahl der während eines kurzen Zeitintervalles Δt aus dem Amplitudendiskriminator in das Ratemeter einlaufenden Impulse um einen Mittelwert streut:

$$Z_i = \bar{f}\cdot\Delta t_i + \nu_i\,, \qquad \bar{\nu}_i = 0\,, \quad (11)$$

führt man $\delta T(t)$ auf frühere Zahlen ν_i zurück:

$$\delta T(t) = A \sum_{t_i<t} \nu_i W(t-t_i)\,. \quad (12)$$

Durch Quadratur und Mittelbildung ist hieraus die gesuchte Grösse $\overline{(\delta T)^2}$ zu finden. Diese Berechnung wird allerdings erschwert durch die den geschlossenen Regelkreis kennzeichnende Rückwirkung der in das Ratemeter einlaufenden Impulsfolge auf sich selbst. Diese Rückwirkung äussert sich in einer statistischen Abhängigkeit der Zahlen ν_i voneinander: Jede der Zahlen ν_i wird sowohl von statistischen Prozessen bei der Impulsbildung in ILQ und Photomultiplier als auch von der gerade herrschenden Hochspannung bestimmt, welche ihrerseits von früheren Zahlen ν_i abhängt. Für die Berechnung der Grösse $\overline{\nu_i^2}$, die bei der Quadratur des Summenausdruckes für $\delta T(t)$ auftritt, ist ausserdem zu beachten, dass die ILQ im Gegensatz zu jedem radioaktiven Strahler eine regelmässige Impulsfolge liefert. Es gelingt, alle diese Einflüsse exakt zu berücksichtigen, die auftretenden Integralgleichungen durch einfache Exponentialansätze zu lösen und schliesslich $\overline{(\delta T)^2}$ auszurechnen†. Die Grösse $\overline{\delta T(t)\cdot\delta T(t')}$ ergibt sich im Verlaufe dieser Rechnung. Das numerische Endergebnis steht in bester Übereinstimmung mit der direkten Beobachtung; man findet

$$\sqrt{\overline{\left(\frac{\delta T}{\bar{T}}\right)^2}} = 0.25 \times 10^{-3}\,.$$

† Vgl.: Rundbericht No. 35.

Das bedeutet, dass die beschriebene Stabilisierungseinrichtung keine merkliche Verringerung des energetischen Auflösungsvermögens verursacht, jedoch unter ungünstigen Umständen die statistische Genauigkeit einzelner Messungen spürbar vermindern kann, so dass man die Messzeit entsprechend zu verlängern hat.

5. Prüfung der stabilisierten Spektrometer-Anordnung

Die stabilisierte Spektrometer-Anordnung wurde durch Messungen des α-Teilchenspektrums von Po geprüft. Figur 7 zeigt das Blockschaltbild der vollständigen Apparatur.

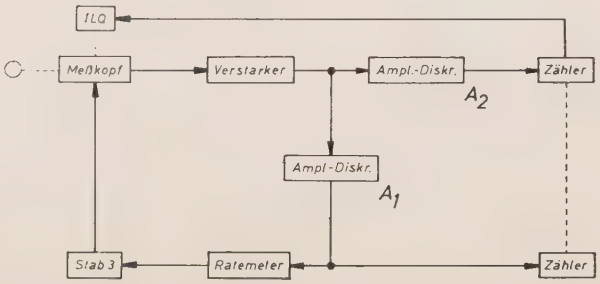

Fig. 7. Blockschaltbild der stabilisierten Spektrometer-Anordnung. Die gestrichelt gezeichnete Verbindung der beiden Zähler deutet synchrone Steuerung der Zählperioden an.

Der Aufbau des Messkopfes ist aus Figur 4 zu ersehen. An den Impulsverstärker (zweistufiger gegengekoppelter Pentodenverstärker mit zwei gleichen, parallel geschalteten Ausgangsstufen) sind die Regelkreisglieder und ein Amplitudendiskriminator A_2 als Messanalysator angeschlossen. Die Ausgangsimpulse der beiden Diskriminatoren A_1 und A_2 werden von zwei gleichen Berkeley "Eput and Timer"-Geräten gezählt. Eines dieser Geräte liefert unabhängig von seiner Funktion als Zähler an einem besonderen Ausgang eine quarzgesteuerte Impulsfolge, die gleichzeitig zur Zündung der ILQ und zur synchronen Festlegung der Zählperioden an beiden Zählern dient.

Die Messungen selbst wurden folgendermassen ausgeführt: Man wählt zunächst an der Irisblende der ILQ die je Lichtimpuls auf die Photokathode einfallende Lichtmenge so, dass im elektrischen Impulshöhenspektrum die "Lichtlinie" etwas höher liegt (dem Absolutbetrag der

Impulshöhe nach) als die 5.3 MeV-Linie des Po-α-Teilchenspektrums. Figur 8 zeigt die Photographie des Oszillographenschirmbildes dieses Impulshöhenspektrums; seine Analyse mit einem Amplitudendiskriminator liefert die entsprechende Integralkurve.

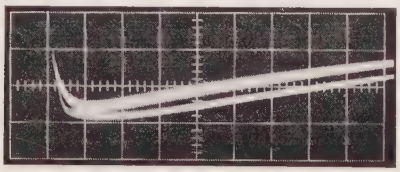

Fig. 8. Po-α-Spektrum mit "Lichtlinie" am Ausgang des Messkopfes; Massstab vertikal 0.5 V/Einheit, horizontal 2 μs/Einheit.

Man legt jetzt die Schwelle von A_1 auf den steilsten Teil der Integralkurve der "Lichtlinie", schaltet den Regelkreis ein und stellt dann die Schwelle von A_2 auf den steilsten Teil der Integralkurve der Po-α-Linie. Nun werden die Ausgangsimpulse von A_1 und A_2 fortlaufend 100 s lang gezählt, die Ergebnisse gedruckt und nach 10 s Pause automatisch eine neue 100 s-Zählperiode begonnen. Aus den Mittelwerten der beiden Zahlenfolgen, die man auf diese Weise erhält, lassen sich Änderungen des Verstärkungsfaktors von Multiplier und Impulsverstärker um 0.1% sicher erkennen. Gegensinnige oder verschieden starke Änderungen beider Mittelwerte deuten auf Einflüsse hin, denen Po-α- und "Lichtlinie" nicht in gleicher Weise unterliegen, denen die Regelung daher nicht entgegenwirken kann.

Zunächst wurde das Verhalten einzelner Teile der Apparatur gegenüber Änderungen der Umgebungstemperatur untersucht. Es zeigte sich, dass Änderungen von 5°–10° C nur dann die Po-α-Linie um mehr als 0.5% ihrer mittleren Impulshöhe verschieben, wenn sie die Photokathode treffen. Diese Erscheinung ist durch die Temperaturabhängigkeit der spektralen Empfindlichkeit der Photokathode zu erklären[4]), die sich deshalb in dieser Weise bemerkbar macht, weil die spektrale Zusammensetzung des Lichtes der ILQ (die Z 70 U ist mit reinem Neon gefüllt) wesentlich von der des Fluoreszenzleuchtens von CsJ[5]) abweicht. Daher wurden zusätzliche Vorkehrungen getroffen, um Temperaturänderungen von der Photokathode fernzuhalten: Durch eine Rohrschlange um den Abschirmzylinder des Multipliers strömt ständig die Badflüssigkeit eines Thermostaten. Mit dieser Anordnung wurde schliesslich erreicht, dass sich der Verstärkungsfaktor während 14 Stunden um weniger als 0.5% änderte, und zwar *vom Zeitpunkt des Einschaltens an* (d.h. ohne ein Anwärmen der Apparatur abzuwarten) und trotz Anstiegs der Raumtemperatur um 4° C.

Mit diesem Ergebnis ist die prinzipielle Grenze der Wirksamkeit einer solchen Stabilisierungseinrichtung erreicht. Entsprechende Versuche zeigten nämlich, dass langsame Schwellenverschiebungen an Amplitudendiskriminatoren und Instabilitäten, die nicht durch Veränderung des Verstärkungsfaktors auszugleichen sind, in derselben Grössenordnung liegen.

Wir danken Herrn Professor Walcher für das dieser Arbeit entgegengebrachte Interesse sowie für die Bereitstellung von Messgeräten der Deutschen Forschungsgemeinschaft und des Bundesministeriums für Atomkernenergie und Wasserwirtschaft.

[4]) N. Schaetti, W. Baumgartner, Helv. Phys. Acta **24** (1951) 614.

[5]) H. Knoepfel, E. Loepfe und P. Stoll, Helv. Phys. Acta **30** (1957) 521.

NUCLEAR INSTRUMENTS AND METHODS 8 (1960) 339–343; NORTH-HOLLAND PUBLISHING CO.

AN IMPROVED ANTI-COINCIDENCE SHIELD FOR USE IN LOW BACKGROUND COUNTING

R. P. PARKER

Physics Department, Institute of Cancer Research, Royal Cancer Hospital, London

Received 12 May 1960

A liquid scintillator is used as an anticoincidence shield for eliminating the cosmic ray component of the background of a Geiger-Müller (G.E.C. Type GM 4 LB) counter. The apparatus is described and its performance compared with that of a shield of Geiger counters. A reduction in background from approximately 0.8 cpm (as measured with the Geiger shield) to approximately 0.45 cpm, as measured with the scintillator shield, was obtained. Evidence is presented which suggests that the reduction is due to the detection of cosmic ray induced reactions in the material surrounding the counter.

1. Introduction

There are four main causes of the background counting-rate of a Geiger counter, namely external radiation from the environment, radiation from the counter itself, spurious counts and the contribution from cosmic rays. The first two effects may be reduced by careful choice of shielding and constructional materials (see, for example, Grummitt[1]). Good design of the counter and its associated electronic apparatus, with especial regard to avoiding pick-up of external electrical interference, should eliminate spurious counts. Whilst the primary soft cosmic ray component may be absorbed by approximately 15 cm lead or its equivalent[2]) it is not economically possible to shield against the hard component, which largely consists of the very penetrating μ-mesons. It is therefore normal to use a shield of cosmic ray counters in anticoincidence with the sample counter. An alternative method is to use a scintillation counter, as described below.

The properties required of an anticoincidence shield are

a. 100% efficiency to cosmic ray particles.
b. Complete screening of the sample counter.
c. Long life.
d. Reliability and robustness.
e. High efficiency to γ-radiation.

2. Types of Anti-Coincidence Shields

Cosmic-ray shields are normally made up from a number of Geiger counters, but proportional counters have also been used[3]).

In the Geiger counter shield the sample counter is surrounded by about twenty tubular cosmic ray counters arranged in such a manner that there is no gap between their active volumes. Such counters are very efficient detectors of the μ-meson component of cosmic rays[4]) but have a very low γ-efficiency. This system has the advantage that a number of different sample counters may be accommodated under one shield, but Geiger counters have a restricted life (approximately 10^8 counts) and need repeatedly checking to see that all the counters are operating on their respective plateaux. Thus the maintenance cost is quite high.

The use of scintillation counters both as cosmic-ray detectors[5,6]) and as anti-Compton shields suggested that they might form the basis

[1]) H. W. E. Grummitt, R. M. Brown, A. J. Cruikshank and I. L. Fowler, Canad. J. Chem. **34** (1956) 206.
[2]) B. Rossi, Rev. Mod. Phys. **20** (1948) 537.
[3]) A. Moljk, R. W. P. Drever and S. C. Curran, Proc. Roy. Soc. A **239** (1957) 433.
[4]) K. Greisen and N. Nereson, Phys. Rev. **62** (1942) 316.
[5]) M. M. Brennan, Nuovo Cimento **6** (1957) 216.
[6]) C. H. Millar, E. P. Hincks and G. O. Hanna, Canad. J. Phys. **36** (1958) 54.
[7]) C. C. Trail and Sol. Taboy, Rev. Sci. Instr. **30** (1959) 425.

of an anti-coincidence shield for a Geiger counter. It was decided to use a liquid luminophor since this has the advantage of being readily adaptable to any required shape. Such a technique also has the advantages of simplicity, reliability and robustness. The apparatus may be readily adapted to portable apparatus or to use as an anti-Compton screen in γ-spectrometry.

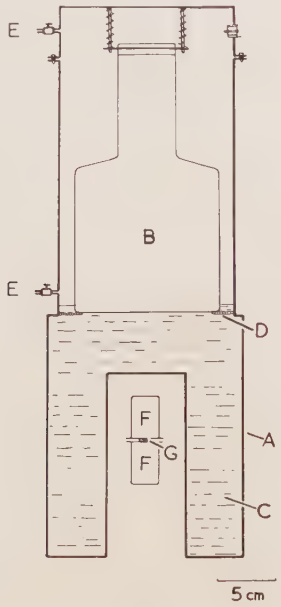

Fig. 1

Furthermore, any failure or change in efficiency of the system is immediately made apparent by monitoring the scintillator counting rate, whereas failure of one counter from a ring of twenty separate counters connected together could go unnoticed for some time.

The apparatus is shown in fig. 1 and consists of a vessel (A) made of commercial copper in the form of an inverted well, coated with "Group 37 enamel" pigmented with rutile titanium dioxide (by Courtesy of International Paints Ltd) to improve the reflectance of the wall surface. The photomultiplier (B) (EMI type 6099 B) dips into the luminophor (C) in order to obtain good optical contact, and is supported by polythene rods (D). This configuration does not give equal response for radiation incident from different directions, but has the advantage of greater detection efficiency in the vertical direction. In order to preserve the properties of the scintillator for long periods the space above it was filled with nitrogen by means of the gas taps (E). Sample counters (F), together with the sample (G), are contained in a perspex holder which can be inserted from below without disturbing the scintillator tank.

The liquid scintillator used was a solution of 3 g 2, 5-diphenyloxazole per litre of "Analar" toluene. The sample counter was surrounded by at least 5 cm of luminophor in order to provide a reasonable γ-efficiency. Since μ-mesons suffer an energy loss of 2.0 MeV cm^{-1} during passage through toluene they can be detected with 100% efficiency.

The whole assembly was surrounded by 5 cm of aged lead and placed on the floor of a pit excavated 2 metres deep into chalk, which has a low natural radioactive content and therefore serves as a good shielding material[8,9]). In later experiments the counters had the additional shielding of one metre of chalk directly above.

The photomultiplier was connected via a cathode follower to an amplifier and discriminator (Isotope Developments Ltd. Type 652). An EHT of 1700 V was used, with the discriminator set to approximately 100 keV. For a routine apparatus it is not necessary for the amplifier to be linear, and with a 13-stage photomultiplier any amplifier with a gain of approximately 30 db. would be suitable. The discriminator bias level need not be very stable, enabling a very simple circuit to be used.

The output pulse was lengthened to 200 μsec. and used as the blanking-off pulse in the anti-coincidence circuit. The sample pulse was delayed by 100 μsec, enabling the anti-coincidence circuit to be made simple and stable, with a coincidence resolving time of 200 μsec.

The total background counting rate of the sample counter (G.E.C. type GM4 LB) before

[8]) J. Vennart, Brit. J. Rad. **30** (1957) 55.

[9]) W. V. Mayneord, W. Anderson, R. E. Bentley, L. K. Burton, J. O. Crookall and N. G. Trott, Nature **182** (1959) 1473.

anti-coincidence cancellation was approximately 5 cpm, of which approximately 4.5 cpm are due to μ-mesons, and thus represent true coincidences. Only 0.5 cpm can cause random coincidences, and with a typical scintillator counting rate of 1000 cpm it follows that the random coincidence rate is only 0.002 cpm, which is negligible.

The long resolving time also avoids the necessity of an amplifier with good overload characteristics. Although a wide range of pulse heights has to be handled the amplifier is unlikely to be paralysed for more than 200 μsec following overload.

3. Results

The stability of the apparatus was checked by a series of 43 consecutive background readings of a GM 4 LB counter, carried out over a period of one month. Only one reading deviated from the mean value by more than two standard deviations. In two cases the interval distribution of the pulses was recorded and on analysis found to be exponential, indicating very few spurious pulses.

Owing to its height it has only recently become possible to place the apparatus under the chalk and not merely on the pit floor. A comparison with an orthodox Geiger counter shield has therefore to be made indirectly, and the results of different shielding arrangements are given in tables 1–3. The Geiger counter shield used was made up from twenty glass-wall counters (20th Century Electronics Type G 24). Unless otherwise stated 5 cm of aged lead was used as additional shielding.

4. Discussion

Table 1 indicates that the anticoincidence counting rate of a single GM4 LB end-window Geiger counter (General Electric Co.Ltd) is reduced by 0.2–0.3 cpm when the scintillator shield is used as opposed to the Geiger shield, even when the latter has the advantage of better shielding above the counter. This additional shielding of 1 metre of chalk is seen (table 2) to reduce the anticoincidence rate by a further 0.13 cpm presumably due to better shielding from environmental γ-radiation. Thus with identical shielding arrangements the anticoincidence rate with the Geiger shield is approximately 0.8 cpm (table 1) and with the liquid scintillator shield approximately 0.4 cpm (table 2).

From the last column of table 2 it is apparent that with the Geiger shield the rate of coincidence between the shield and the sample counter is unaltered by the addition of chalk shielding above the counters. This is to be expected if the coincidences are due to μ-mesons which are not appreciably attenuated by the chalk.

When the liquid scintillator is used (table 2, lower section) the additional chalk shielding again reduces the anticoincidence rate by 0.13 cpm, as with the Geiger shield. However, the performance of the scintillator shield is different in that the coincidence rate on the pit floor is

Table 1

Comparison between liquid scintillator shield on pit floor and Geiger shield under the chalk

Counter (GM4 LB)	Anticoincidence rate (cpm)			Coincidence rate† (cpm)		
	Geiger shield under chalk	Liquid scintillator on pit floor	Reduction	Geiger shield under chalk	Liquid scintillator on pit floor	Increase
A	0.86 ± 0.01	0.57 ± 0.01	0.29	4.38 ± 0.03	4.62 ± 0.02	0.24
B	0.81 ± 0.01	0.57 ± 0.01	0.24	3.24 ± 0.03	4.09 ± 0.02	0.85
C	0.77 ± 0.01	0.50 ± 0.01	0.27	3.18 ± 0.03	3.96 ± 0.02	0.78

† Corrected to 760 mm Hg atmospheric pressure.

TABLE 2

Counting rates on pit floor and under the chalk

Counter	Shield	Anticoincidence rate (cpm)			Coincidence rate† (cpm)		
		Pit floor	Under chalk	Reduction	Pit floor	Under chalk	Reduction
Pair of GM4 LB	Geiger	1.35 ± 0.01	1.05 ± 0.01	0.15 ††	6.96 ± 0.03	6.96 ± 0.03	—
Pair of GM4 LB	Geiger	1.29 ± 0.01	1.06 ± 0.01	0.12 ††	7.18 ± 0.03	7.22 ± 0.03	—
Single GM4 LB	Geiger	0.82 ± 0.01	0.60 ± 0.01	0.22	4.06 ± 0.03	4.04 ± 0.03	—
Single GM4 LB	Scintillator	0.50 ± 0.01	0.37 ± 0.01	0.13	3.75 ± 0.03	3.42 ± 0.03	0.33
Single GM4 LB	Scintillator	0.53 ± 0.01	0.40 ± 0.01	0.13	3.78 ± 0.03	3.45 ± 0.03	0.33

† Corrected to 760 mm Hg atmospheric pressure.
†† For a single GM counter.

now 0.33 cpm higher than it is under the chalk (table 2, right-hand column).

These results suggest that the scintillator shield is an efficient detector of a component of the background radiation which is inefficiently detected by the Geiger shield. This component is attenuated by the chalk, as shown in the last column of table 2. Various suggestions as to its nature may be considered.

(i) *Environmental γ-radiation.* This is improbable, since the reduction in anticoincidence rate by the chalk is approximately the same with each type of shield (table 2, column 5). Furthermore, the chalk is known to have a radioactive content of 1.2×10^{-12} α-ray curies g^{-1} [10]) and 6×10^{-8} $g^{40}K$ g^{-1} [11]). A calculation based on these values suggests that the environmental component of the background is approximately 0.3 cpm for the counter when shielded by chalk only. The addition of 5 cm aged lead would reduce this to less than 0.1 cpm. These figures agree with table 3, which indicates that an additional 5 cm aged lead shielding reduces the anticoincidence rate from 0.72 cpm to 0.37 cpm.

(ii) *Cosmic ray neutrons.* These are known to contribute to the background of the large counters used in ^{14}C estimation[12]). It is unlikely that the detection of secondary processes originating from these neutrons contribute significantly to the background of a small counter. Also, the anticoincidence rate (as measured with a Geiger shield) of these end-window counters shows no significant variation with atmospheric pressure. Such a variation would be expected if the component was due to neutrons, since the neutron flux in cosmic rays at sea-level varies

[10]) R. C. Turner, Private communication.
[11]) J. Vennart, Private communication.
[12]) Hl. de Vries, Nuclear Physics **1** (1956) 477.

TABLE 3

Counting rate of a GM4 LB counter in the liquid scintillator shield with various shielding arrangements

Shielding	Anticoincidence rate (cpm)	Coincidence rate† (cpm)
1 metre chalk all round	0.72 ± 0.01	3.60 ± 0.03
As above, but 5 cm Pb around sides	0.42 ± 0.01	3.54 ± 0.03
5 cm Pb + 1 metre chalk all round	0.37 ± 0.01	3.42 ± 0.03

† Corrected to 760 mm Hg atmospheric pressure.

inversely with barometric pressure to the extent of 1% per mm mercury pressure[13]).

(iii) *Other cosmic ray effects.* It is probable that the increased efficiency of the scintillator shield over the Geiger shield is due to the detection of the products of cosmic ray produced reactions in the material surrounding the counter, such as μ-meson decay, collision and capture processes. Presumably the products of a reaction outside the scintillator shield are detected by the sample counter, whilst the originating particle does not pass through the shield. The detection efficiency of the scintillator shield to low energy γ-radiation is much greater than that of a Geiger shield[5]), especially if the radiation is incident in the vertical direction, (as is probable if formed in a cosmic ray shower), due to the increased path length in the scintillator.

Independent evidence that a component of the background is due to the detection of uncharged radiation in the wall of the counter is given by Dixon *et al.*[14]) who detected strong characteristic X-radiation from the wall material of a proportional counter.

Acknowledgements

The author wishes to acknowledge the guidance and encouragement of Professor W. V. Mayneord throughout this work, and Dr. R. E. Bentley for many profitable discussions.

[13]) J. A. Simpson, W. Fonger and S. B. Treiman, Phys. Rev. **90** (1953) 934.

[14]) D. Dixon and A. Mcnair, Phil. Mag. **45** (1954) 1099.

NUCLEAR INSTRUMENTS AND METHODS 8 (1960) 344–347; NORTH-HOLLAND PUBLISHING CO.

A NEW METHOD OF MASS DISCRIMINATION

G. HREHUSS

Central Research Institute of Physics, Budapest, Nuclear Physics Laboratory

Received 14 May 1960

Emission spectra of CsI(Tl) scintillation crystals bombarded by heavy as well as light particles have been investigated. The results show the number of photons of shorter wavelength to be relatively higher in the case of excitation by light particles. This fact offers a new possibility for mass discrimination.

Mass discrimination with the use of scintillation detectors for the study of nuclear reactions is made possible by the recent discovery of the shape dependence of light pulses of scintillators on the mass of the exciting particles. Previous experiences in this field may be summarized as follows[1,2]).

The fluorescence of scintillators in general use is composed of two exponential components with half-lives differing from each other by about unit order of magnitude. Now, whereas the longer lived component is independent of the mass of the exciting particle, the component with a shorter half-life may show a difference in decay rate up to a factor of two depending on whether the excitation is induced by electrons or by α particles. For CsI(Tl) crystals the mean life of the longer lived component is 7 μsec, while that of the mass-dependent part is 0.43 μsec and 0.7 μsec for excitations initiated by α and β particles, respectively. For organic scintillators the case is similar with the difference, however, that for the latter the mean life is in general much shorter and also the mass-dependent component is faster for β-excitation. In the following, however, we shall restrict our considerations to the inorganic scintillator CsI(Tl).

Assuming that the mass-dependent component is due to the de-excitation of metastable states, it may be supposed that particles of different mass generate different metastable states with different probabilities, that is the emission spectra obtained from light particles can be expected to differ from those produced by heavy particles. If there is an appreciable difference, this will give a relatively simple method of mass discrimination: We have only to insert a colour filter between the photomultiplier and the phosphor permitting the transmission of either the spectrum range characteristic for the heavier or that for the lighter particles.

In order to verify this assumption the following measurements were performed:

1. Glass colour filters with known transmission characteristics were inserted between a CsI(Tl) scintillator 2.0 cm high and 3.0 cm in diameter (Harkovkij Zav. Chimreaktivov product) and an RCA 6342 photomultiplier. The phosphor was excited by Po α rays which struck the phosphor with an energy of 5.0 MeV, and by an annihilation radiation of 0.52 MeV as well as by direct γ radiation of 1,28 MeV from Na^{22}. By means of a single-channel amplitude analyzer the α and γ spectra were measured by using various colour filters. For both sources the number of scintillations was found to be about 10^3 sec^{-1}.

If the time constant of the anode circuit is sufficiently large, a voltage pulse proportional to the number of photons of the light pulse coming from the crystal is produced on the load resistance of the multiplier. Denoting now the number of photons per unit wave length by $f(\lambda)$,

[1]) R. S. Storey, W. Jack and A. Ward, Proc. Phys. Soc. (London) **72** (1958) 1.

[2]) R. B. Owen, Nucleonics **17** (1959) 92.

the function of spectral sensitivity of the multiplier by $\sigma(\lambda)$ and the transmission function of the colour filter by $\tau(\lambda)$, the voltage pulse of the multiplier for given particle energy is

$$S = K \int_{-\infty}^{+\infty} \tau(\lambda') \cdot \sigma(\lambda') \cdot f(\lambda') \, d\lambda' .$$

The transmission function of the colour filters is given by

$$\tau(\lambda') \approx \begin{cases} 0 \text{ for } \lambda' < \lambda \\ \text{constant for } \lambda' > \lambda . \end{cases}$$

Using the symbol Λ for denoting the red limit of the multiplier, we have

$$S = K' \int_{\lambda}^{\Lambda} \sigma(\lambda') \cdot f(\lambda') \, d\lambda'$$

and the spectral properties of the phosphor both for β and α excitation can be characterized by the ratio

$$s(\lambda) = \frac{S_\beta}{S_\alpha} = \frac{\int_{\lambda}^{\Lambda} \sigma(\lambda') \cdot f_\beta(\lambda') \, d\lambda'}{\int_{\lambda}^{\Lambda} \sigma(\lambda') \cdot f_\alpha(\lambda') \, d\lambda'} .$$

The measured ratios are shown in fig. 1 approximated by a straight line fitted to the points by the method of least squares. For each filter the α as well as the γ spectra were measured without altering the multiplier voltage. For better evaluation the photopeaks and the α peak were shifted to a convenient point of the measuring range of the amplitude analyzer by using the previously calibrated attenuator of the amplifier. Also an experiment was carried out to

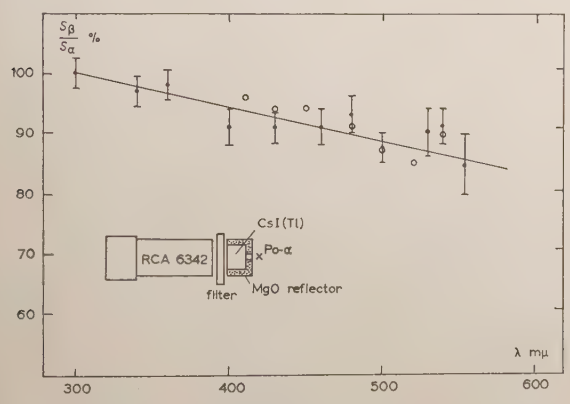

Fig. 1. The ratio of amplitudes S_β and S_α obtained with colour filters. The circles denote values of S_β/S_α calculated from the spectrographic measurements.

see whether saturation effect of the multiplier did not affect linearity and it was found that even within the applied voltage range (1000–1370 V) the deviation from linearity was less than 2.5%.

A similar effect may be caused also by a possible selective absorption of the CsI(Tl) crystal, for the path length of photons induced by α particles is longer than that of photons produced by β particles. Therefore the crystal was examined by means of a spectrophotometer, however, apart from surface reflection no wave length-dependent effects were found in the 400–600 mμ range and the surface reflection is negligible in this case.

2. The emission spectra of CsI(Tl) crystals excited successively by light and heavy particles were investigated by means of the arrangement shown in fig. 2. Since a continuous spectrum was

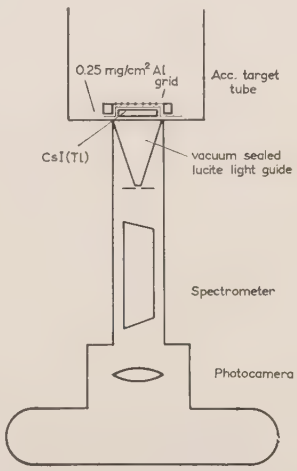

Fig. 2. Experimental arrangement for direct investigation of spectra.

expected, it was sufficient to use a spectroscope of low resolution in these experiments. The spectra were photographed by a Contax D camera on Agfa Isopan F film. The surface of the 1 mm thick crystal was about 1 cm² and a lucite wedge applied thereto directed the light to the spectroscope slit. The surface exposed to bombardment was covered by a 0.25 mg/cm² thick aluminium foil held down by a wire grid which served at the same time to carry away the charge collecting on the surface.

To induce excitation by electrons we made use of the 1 MeV Van de Graaf accelerator operating in our Institute. The bombarding electron beam passed through a 20 mg/cm² fredal foil, continued its flight through air for a distance of about 2 cm and then struck the crystal with an energy of 400 keV, the current density being about 1 μA/cm².

For heavy-particle bombardment the crystal was placed into the vacuum system of the 600 keV ion accelerator of the Institute in a way to be struck directly on the surface covered by the Al foil and the grid. It was bombarded by deuterons and α particles having energies of 300 keV and 500 keV for He^{++} ions and 250 keV for He^{+} ions, respectively. Taking into account the stopping power of the Al foil, the excitation energies were estimated to be 180 keV and 250 keV, respectively, while that produced by He^{+} ions was negligibly small. Current density on the crystal surface was invariably about 1 μA/cm².

After irradiation no damage could be observed on the crystal surface. The photographs of the spectra provided with a calibrated scale of wavelengths as well as with normal blackening were evaluated by MΦ-4 microphotometer after development. The spectra obtained and normalized to the same number of photons in the 410–580 mμ wave length range are seen in fig. 3.

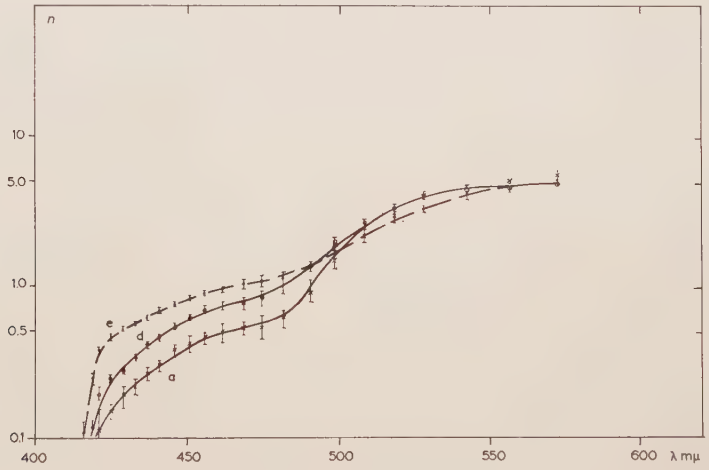

Fig. 3. Emission spectra of CsI(Tl) bombarded by electrons deuterons and α particles, not corrected for colour sensitivity of film.

Conclusion

In order to compare the results of the measurements performed by means of colour filters with those made by using a spectrometer the spectra obtained in the second experiment were analyzed as follows:

The ratios

$$\frac{\int_{\lambda}^{580} n_{\beta}(\lambda')\,\mathrm{d}\lambda'}{\int_{\lambda}^{580} n_{\alpha}(\lambda')\,\mathrm{d}\lambda'}$$

were computed for various values of λ within the range $410 < \lambda < 580$ mμ. Here $n_{\beta}(\lambda')$ and $n_{\alpha}(\lambda')$ mean the number of photons registered per unit wave length interval in the case of bombardment with β and α particles, respectively. Since in the given wave length range the colour sensitivity of the photomultiplier as well as that of the film were of about the same shape, the two measurements could be compared. Results of the comparison are seen in fig. 1, where the ratios computed from data of the second experiment are marked by circles.

Thus it is seen that the shape of the emission spectrum of CsI(Tl) depends on the mass – light or heavy—of the exciting particles. The number of photons emitted in the wave length range $410 < \lambda < 500$ mμ is the highest for β particle-induced excitation and decreases with increasing mass number.

The effect investigated above has been used for mass discrimination purposes in the following way. Two photomultipliers (DuMond 6292) equipped with a yellow ($\lambda_{rf} > 500$ mμ) and a blue colour filter ($\lambda_{rf} < 500$ mμ), respectively were attached to a CsI(Tl) scintillation crystal (1″ by $\frac{1}{2}$″). The total gain of each channel consisting of the photomultiplier and a non-overloading amplifier was adjusted in order to obtain the same pulse amplitude for an α particle of given energy at the output of both amplifiers. The pulses of both channels were transmitted to an analyzer each, and a coincidence circuit—scaler system counted the coincident pulses of the analyzers, which in addition were provided with a common bias. In the ideal case only the α particles can produce coincidences in such an arrangement for the response-energy functions of the two counters would be different for β particles according to the previous measurements.

Energy distributions of α and β particles, respectively are shown in fig. 4 measured by means of the method described. The energy of α particles emitted by a Po source was reduced in order to make the α spectrum comparable to the γ spectrum of Na^{22} serving as background by the use of thin Al absorption foils. Because of these foils the shape of the α spectrum became of course deformed.

Fig. 4 shows the pure α energy distribution without background, the α and β energy distributions obtained when the crystal was irradiated by α particles and at the same time γ radiation from Na^{22} was also present. The last two were obtained by means of the new mass discrimination method applied to α and β particles, respectively. The latter is at the same time the background of the α spectrum. We can see from these spectra that the background decreases by about an order of magnitude for α energies of less than 0.7 MeV and a mass discrimination of practically 100% can be achieved above 1.7 MeV. The lower limits of these energy values are determined by the

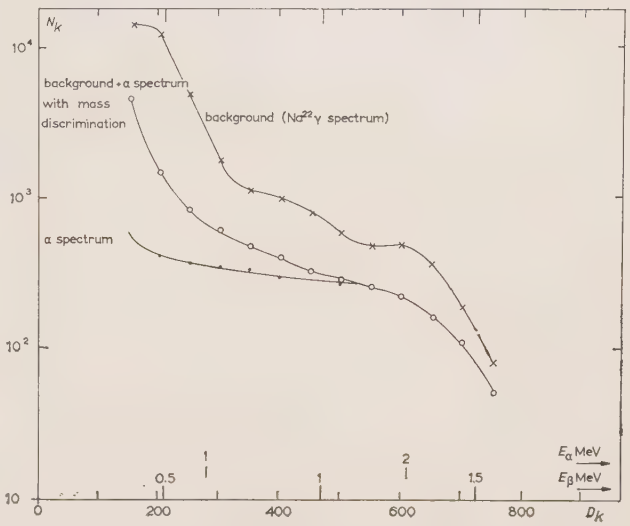

Fig. 4. α and β energy distributions measured by means of spectral mass discrimination.

statistical amplitude fluctuation of the multiplier pulses. In the case of low energy particles—because of the low number of photons produced—this amplitude fluctuation can be so big that the pair of analyzers adjusted for detecting only α particles detects β particles as well.

In order to illustrate the linearity of the effect made use of above the pulses of the yellow-and the blue-sensitive multipliers were—as usual—transmitted to the horizontal and vertical plates of an oscillograph. The shape of the impulses thus obtained can be seen on the photograph reproduced in fig. 5.

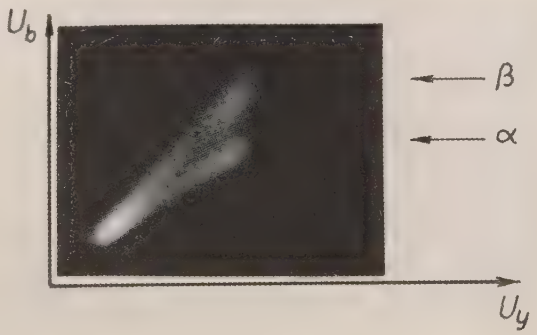

Fig. 5. The spacing and linearity of spectral mass discrimination for β and α particles, respectively.

NUCLEAR INSTRUMENTS AND METHODS 8 (1960) 348–353; NORTH-HOLLAND PUBLISHING CO.

AN IMPROVED INSTRUMENT FOR NUCLEAR EMULSION TRACK PHOTOMETRY

S. v. FRIESEN and B. PERSSON

Department of Physics, University of Lund, Lund

Received 3 June 1960

A description is given of a semi-automatic nuclear emulsion track photometer of high precision.

1. Introduction

A nuclear emulsion track photometer developed at Lund has been described in a number of papers[1–6]). The instrument has proved to be very useful in the determination of the masses of slow particles in nuclear emulsions. Recently, very satisfactory results have also been obtained in charge determinations on relativistic or nearly relativistic particles of the primary cosmic radiation[7–9]). The present paper describes an improved version of the photometer.

In the former instrument the mean track width, MTW, was determined by means of a modified Leitz microscope of type B. A Ks 100 objective combined with the lower lens of an eye-piece produces an image of the track. The tube length has been chosen in such a way as to give a magnification of exactly 100 times. At the position of the image there is a slit 3.0×0.25 mm^2. After passing through the slit the light falls on the cathode of a photomultiplier tube. The amplified output of the multiplier operates a Speedomax recorder. The recorded value x measures the amount of light which passes through the slit when it covers a section of the image of the track. This can be moved out of the slit by turning a plane parallel glass plate in the light path inside the tube. We now record a value y, which represents the amount of light passing through the slit when it is empty. When multiplied by the width of the slit, $(1 - x/y)$ gives the MTW of that segment of the track which is being measured. The MTW values which are obtained in this way must be corrected for depth in the emulsion, since with increasing depth the amount of scattered light increases. Also the effect of uneven development must be taken into account. We have always measured y on both sides of the track. This involves three measurements, three readings of the Speedomax chart and the calculation of $1 - x/y$.

A considerable gain in speed would be obtained if the three measurements could be made simultaneously and the calculations performed automatically. Such an arrangement would also to a large extent eliminate errors due to mistakes in reading the chart and in the calculations.

The new instrument includes the suggested improvements. It delivers directly an output voltage proportional to $(1 - x/y)$, which can be recorded by means of a digital voltmeter and a digital printer on a strip of paper.

[1]) S. v. Friesen and K. Kristiansson, Arkiv för Fysik **4** (1952) 505.

[2]) K. Kristiansson, Arkiv för Fysik **8** (1954) 311.

[3]) S. v. Friesen, Arkiv för Fysik **8** (1954) 305.

[4]) S. v. Friesen and L. Stigmark, Arkiv för Fysik **8** (1954) 121.

[5]) K. Kristiansson, Arkiv för Fysik **10** (1956) 447.

[6]) T. Johansson and K. Kristiansson, Arkiv för Fysik **11** (1957) 467.

[7]) B. Waldeskog and O. Mathiesen, Arkiv för Fysik **17** (1960) 427.

[8]) K. Kristiansson, O. Mathiesen and B. Waldeskog, Arkiv för Fysik **17** (1960) 455.

[9]) K. Kristiansson, O. Mathiesen and B. Waldeskog, Arkiv för Fysik **17** (1960) 485.

2. Description of the Instrument

Fig. 1 shows the principle of the photometer. The objective B and the lens C form an image of the track A on the middle one of three parallel

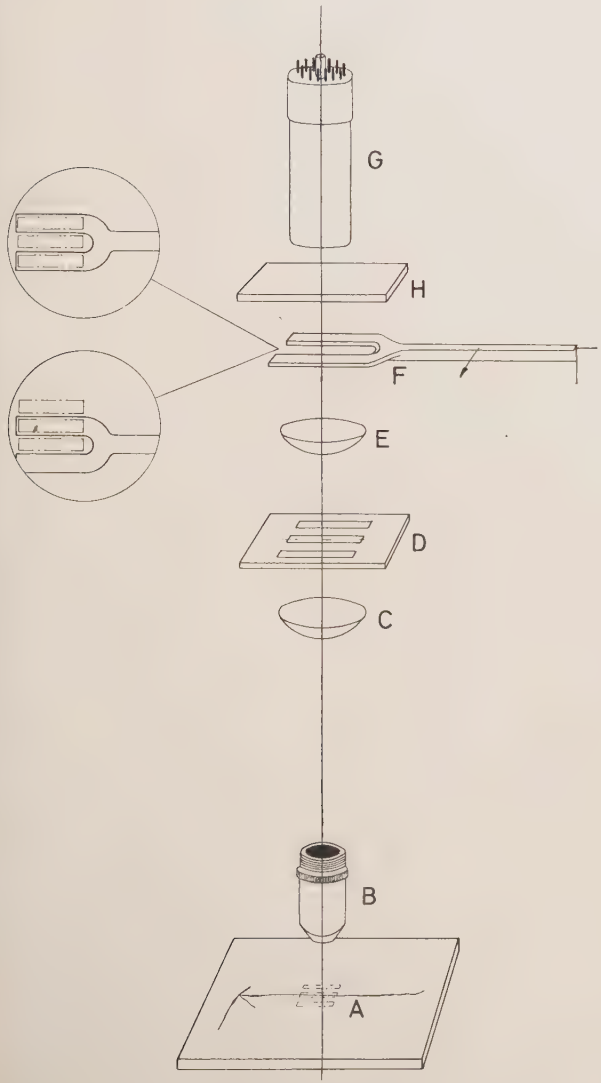

Fig. 1. Schematic diagram of the track photometer showing among other details the forked shutter, which lets the photomultiplier see either the track itself or the empty emulsion on both sides of the track.

slits at D. A second lens E produces a magnified image of the slits at the position F. A forked shutter normally covers the two outer slits, so that the photomultiplier G sees only a region of the emulsion defined by the middle slit and containing the track. By means of an electromagnet the shutter can be moved to a new position where it covers the middle slit and leaves the outer ones free. The photomultiplier now sees one region of the emulsion on each side of

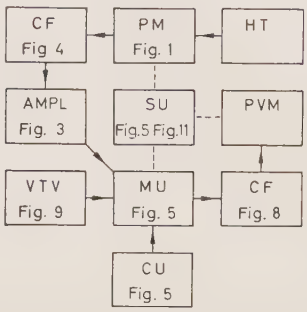

Fig. 2. Block diagram of the complete instrument. H.T. = High tension supply; P.M. = Photometer; C.F. = Cathode follower; Ampl. = Amplifier; M.U. = Main unit; S.U. = Steering unit; C.U. = Calibration unit; V.T.V. = Vacuum tube voltmeter; P.V.M. = Printing voltmeter.

the track and at the same depth in the emulsion. H is a milk glass plate which distributes the light more evenly over the cathode of the photomultiplier tube.

We thus measure two voltages x and $2y$, and need some means of comparing them in order to find $(1 - x/y)$. This can be achieved by means of an arrangement shown in fig. 2.

A perforated disc rotating in front of the microscope lamp gives 500 cycle AC output from the Du Mont 6467 photomultiplier. The AC goes to an amplifier (fig. 3) via a cathode follower (fig. 4). The final stage of the amplifier consists of another cathode follower. A built-in rectifier produces a DC voltage proportional to the amount of light hitting the photo cathode. Let x and $2y$ be the voltages which correspond to the middle slit (with the track) and the two outer slits, respectively. These voltages are used to charge the capacitors C_1 and C_2 to the voltages x and y (figs. 5 and 6a). In order to find the difference $-(y - x)$, we then disconnect point b and connect point c to ground (fig. 6b). The voltage $-(y - x)$ determines the input grid voltage of a Schmitt trigger circuit (fig. 7). Next we connect a resistor R across C_2, which starts to discharge, operating the trigger when its input grid reaches zero potential i.e. when $y = x$. At

exactly the same moment as we apply R across C_2 we also begin to charge a third capacitor C_3 through a circuit having the same time constant RC_2. The trigger impulse discontinues the

AR automatic DC digital voltmeter and a model H03-561 B digital recorder. In this way the MTW values come out of the instrument printed on a paper strip ready for analysis.

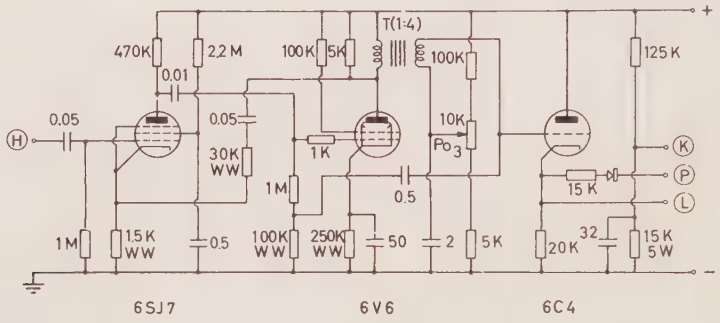

Fig. 3. Amplifier for the charging of the capacitors C_1 and C_2 (fig. 5).

charging of C_3, which has now reached a voltage U. The supply from which we charge C_3 gives U_0 volts. We call the discharging time T and get the following expressions:

$$x = y\, e^{-T/RC_2},$$

$$U = U_0\,(1 - e^{-T/RC_2}),$$

and

$$U = U_0\,(1 - x/y).$$

When multiplied by the width of the slit the voltage U, which is proportional to $(1 - x/y)$, measures the mean width of the track.

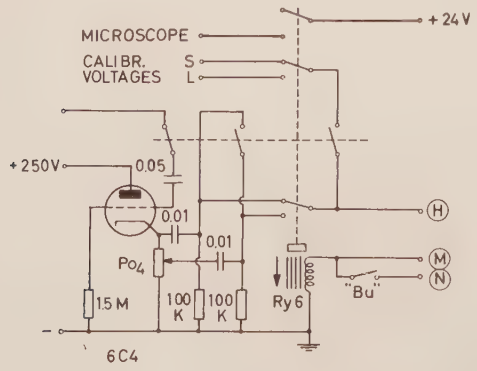

Fig. 4. Cathode follower operating on the input side of the amplifier.

The voltage U across C_3 goes to a cathode follower shown in fig. 8. The output of the cathode follower operates a Hewlett-Packard model 405

A special calibration unit (fig. 10) which gives 500 cycle signals in accurately known ratios, has been provided to enable the checking of the correct operation of the instrument. It gives the choice between two fixed ratios or ratios which can be adjusted at will by means of a calibrated Helipot potentiometer. For the adjustment of the instrument there is a built-in vacuum tube voltmeter (fig. 9).

3. Cycle of Operation

In the following an activated relay will be said to be closed.

On pushing the "start" button (fig. 5), relay Ry 1 closes, whereas all the others remain open. The instrument is now ready to receive information. The operator by means of a mirror and a lens (not shown) adjusts and focuses the track in the middle slit and then pushes the button "M". This starts a synchronous motor and the cycle of operation begins. The motor operates a number of micro switches MS 1–5 in a predetermined sequence by means of a series of cams on a shaft. MS 1 and MS 2 connect the capacitors C_1 and C_2, one after the other, to the output of the amplifier (fig. 3). MS 3 operates Ry 6 (fig. 4) so that the capacitors get the charge which corresponds to the correct position of the forked shutter. When C_1 and C_2 have reached their equilibrium voltages x and y MS 4 causes Ry 5 (fig. 5) to close. This results in the following:

1. Breaking of the ground connection of Ry 1, which opens this relay. The grid of the Schmitt trigger valve 6 SJ 7 (fig. 7) gets the potential $-(y-x)$ (too low to trigger).

2. After a short delay Ry 2 closes:

All this accomplished, Ry 5 opens. Meanwhile the discharging of C_2 continues to the point where $y = x$, i.e. until the trigger input gets zero potential. Triggering takes place and Ry 3 closes. The result will be that:

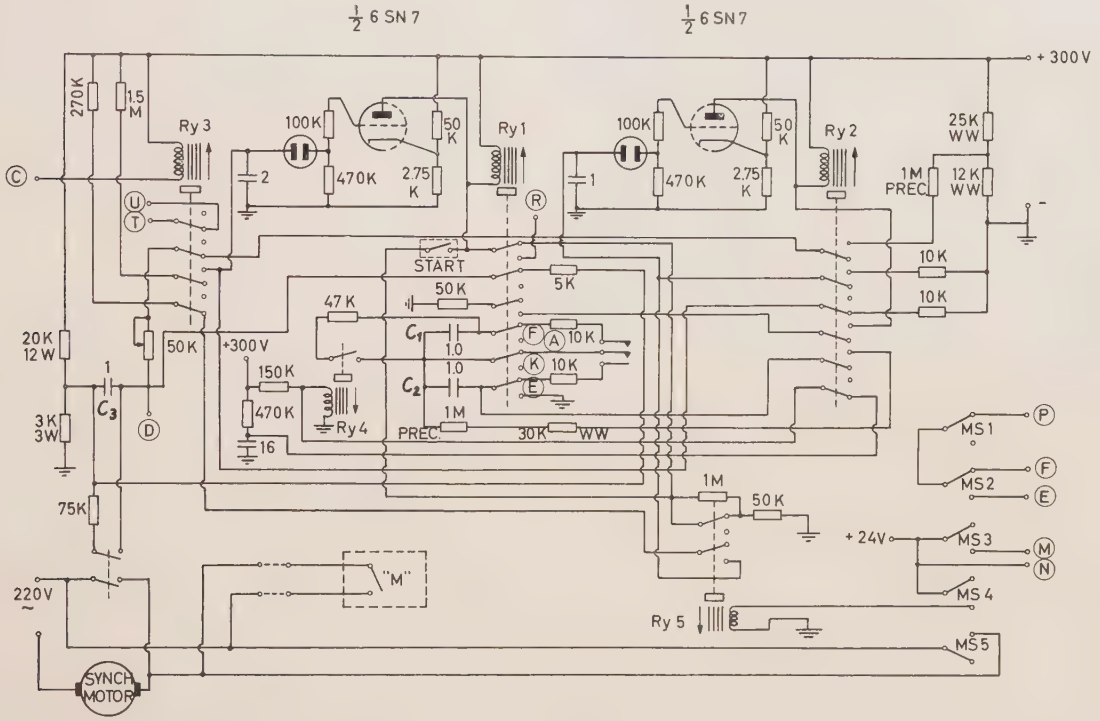

Fig. 5. Main unit including cam-operated microswitches and relays, which determine the cycle of operation and the arrangement including capacitors C_1, C_2, and C_3, which computes the mean track width.

(a) discharging C_2

(b) charging C_3

(c) breaking the ground connection of the 6 NS 7 circuit, which operates Ry 1, after a suitable delay.

(d) connecting that 6 SN 7 circuit to ground which operates Ry 2 and finally

(e) breaking the short circuit between the coil of Ry 4 and the 16 μF capacitor causing it to charge to 300 volts.

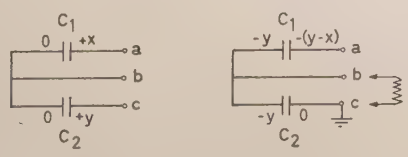

Fig. 6. The diagrams show the connection of the capacitors C_1 and C_2 a) being charged b) discharging.

(a) the charging of C_3 ceases.

(b) Ry 1 closes with a certain delay, discharging C_3 and opening Ry 2.

In its new position Ry 2 connects the 6 SN 7 circuit of Ry 1 to ground. It also makes the 16 μF capacitor discharge through the coil of

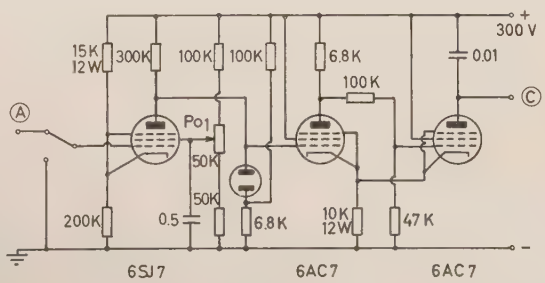

Fig. 7

Schmitt trigger circuit controlling by means of relays the discharging of the capacitors C_1 and C_2 and the charging of C_3.

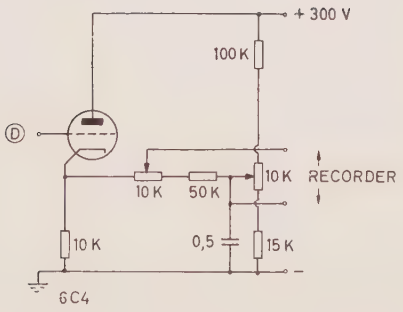

Fig. 8. Cathode follower on the output end of the main unit, feeding the printing voltmeter.

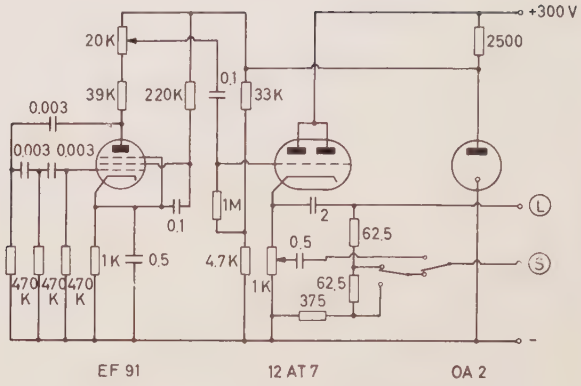

Fig. 10. Calibrating unit giving 500 c/s A.C. voltages in known ratios.

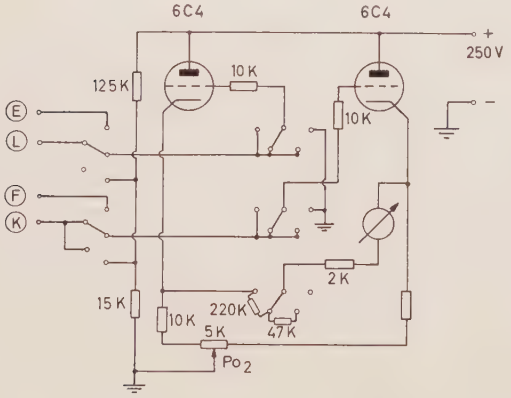

Fig. 9. Vacuum tube voltmeter for the adjustment of the instrument.

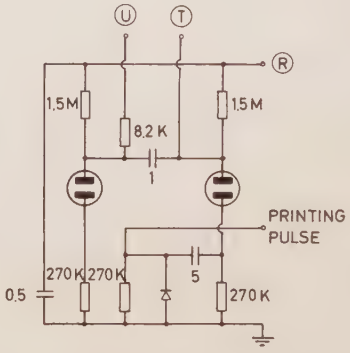

Fig. 11. Neon bulb circuit, which gives a printing pulse to the printing voltmeter at the correct time. The left hand neon bulb ignites at a lower voltage than the other one.

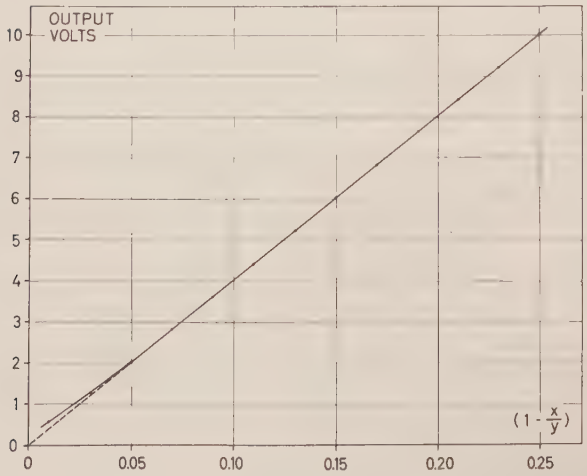

Fig. 12. Diagram showing the linearity of the relation between track width – slit width ratio ($1 - x/y$) and the output voltage of the instrument.

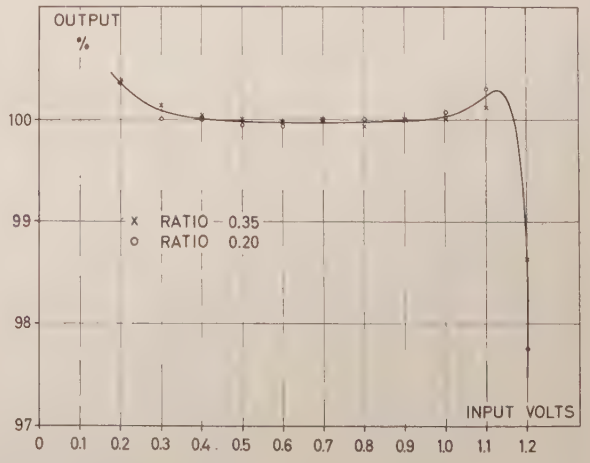

Fig. 13. Diagram showing that the output of the main unit is independent of the input voltage in the region 0.3–1.0 volts.

Ry 4 making this relay close temporarily to discharge C_1.

We are now back at the beginning of the cycle and ready for a new measurement.

4. Adjustments

In order to facilitate the adjustments a built in vacuum tube voltmeter has been provided (fig. 9).

The necessary adjustments are the following:

1. With the input grid of the Schmitt trigger grounded the 6 SJ 7 screen voltage is adjusted by means of the potentiometer Po_1 so that the circuit just triggers.

2. The vacuum tube voltmeter is set to read zero by means of the potentiometer Po_2.

3. The points K and L (fig. 3) are brought to the same potential by means of the potentiometer Po_3.

4. The level of the incoming signals is given a suitable value by varying the voltage on the photomultiplier or the intensity of the light source.

5. By pushing the button Bu (fig. 4) one can switch rapidly between observation of the middle slit and the outer slits, and adjust the potentiometer Po_4 for the same reading in both positions.

For each adjustment the VTV is connected to the proper circuit by means of a selector switch. During the measurements the VTV should be disconnected.

Fig. 14 shows the photometer and its auxiliary equipment.

5. Performance

The relation between $(1 - x/y)$ and the output of the instrument is shown in fig. 12. The linearity is good down to a value of $1 - x/y$ equal to 0.05. By choosing the width of the slit in a suitable way it will always be possible to work inside the linear region. Fig. 13 shows that the output of the machine is independent of the input voltage to better than one tenth of one per cent in the region from 0.3 to 1.0 volt.

The instrument has been in use for many months and has been proved to work in a very satisfactory manner. One of the tests made on slow singly charged particles in Ilford G 5 emulsions consisted in measuring an ending proton track 6000 microns in length. The average MTW value was calculated for 250 micron sections of the track. The sum of these averages was also calculated. One month later the same track was remeasured. It is obvious that the position of the track on the photometer cannot have been identical on the two occasions. Certain individual grains may have fallen at one time in a certain 31 micron section the next time in an adjacent section. The average diameter of a grain is 0.6 microns. The track being curved, due to scattering in the emulsion, its position in a direction at right angles to the slit must also have varied to some extent.

In spite of this the mean of the absolute values of the differences between the MTW-values found for the 250 micron sections amounted to only 0.88%, and the difference between the totals was not more than 0.13%. This error is inside the accuracy of $\pm$ 0.2% given by the manufacturer of the digital voltmeter.

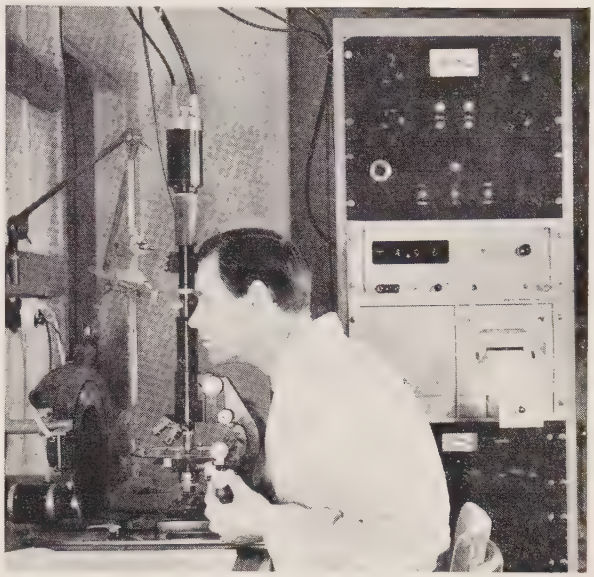

Fig. 14
Semi-automatic nuclear emulsion track photometer in use.

NUCLEAR INSTRUMENTS AND METHODS 8 (1960) 354; NORTH-HOLLAND PUBLISHING CO.

LETTER TO THE EDITOR

A METHOD FOR THE SEPARATION OF GOLD IRRADIATED MERCURY ISOTOPES

W. PARKER

Institute of Physics, University of Uppsala, Uppsala, Sweden

Received 6 July 1960

The purpose of this note is to make known the constructional details of an apparatus developed for the separation and consequent deposition of Hg isotopes from irradiated Au. The apparatus, which may be seen in the figure, functions as a vacuum evaporator and can be put together in a few hours by a machine shop and, when complete, may be relied upon to give reproducible results. Part of the apparatus forms a dewar flask constructed by placing a small brass cup, A, within a larger one, B. Cup A has a diameter of 40 mm's, the larger cup, B, 70 mm's. The bottom of A is drilled and tapped to take a threaded rod, C. Hard soldered to B are two half inch standard vacuum connections E and D. The male counterpart of D is fitted with a quartz tube, F, fastened by means of thermal cement† G, while the second vacuum connection E, is for evacuating the system.

The operating procedure is as follows: Part or all of the Au target is placed in the quartz tube. A gold spot, the diameter of which will depend on the source requirements, is vacuum deposited onto a suitable piece of mylar. The unthreaded end of the rod is smeared with vacuum grease and brought into contact with the uncoated side of mylar, the surplus mylar being pleated along the sides of the rod. The rod and quartz tube can now be screwed into their respective positions. After pumping for some minutes the rotary pump is isolated by means of a valve and the dewar filled with either dry ice and alcohol or liquid air. A bunsen burner is suitable as a heat source and only a small flame necessary.

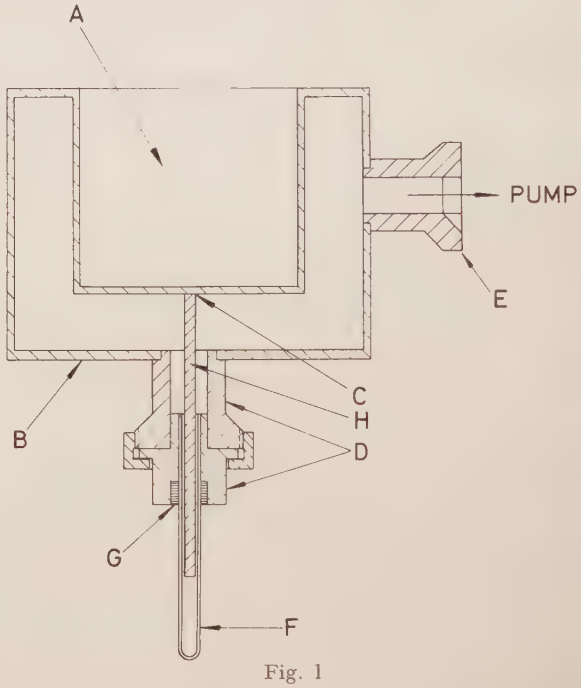

Fig. 1

Deposition times were from 15 to 60 minutes after which the mylar was removed and stretched over a suitable holder. Using the described apparatus efficient depositions have been carried out, and when necessary, 100% separation achieved.

† Alumina Thermal Cement.

AUTHOR INDEX

Alves, R. V. *see* Tochilin

Amsel, G., P. Baruch et O. Smulkowski, Détecteur de particules lourdes a jonction n-p au silicium . 92

Azuma, R. E., *see* Lewis

Baruch, P., *see* Amsel

Batchelor, R., W. B. Gilboy, A. D. Purnell and J. H. Towle, Improvements in the fast neutron time of flight technique using pulse shape discrimination in an organic phosphor 146

Bergström, I., E. C. O. Bonacalza, A. Jech, M. Perez and P. Thieberger, The oscilloscope method of measuring nuclear half-lives 151

Birkhoff, R. D., J. M. Kohn, H. B. Eldridge and R. H. Ritchie, The spherical condenser as a high transmission particle spectrometer II. Disc source 313

Blankenship, J. L., *see* Halbert

Bonacalza, E. C. O., *see* Bergström

Braams, C. M. and P. B. Smith, The Utrecht 850kV cascade generator. I. Beam deflection and energy control 27

Brini, D., A. Gandolfi and G. L. Tabellini, Transistorized apparatus for accumulation and binary-decimal conversion 46

Brucker, George J. and Kenneth C. Rogers, A kilovolt, kiloampere low pressure switch 236

Brugger, Robert M., *see* Tolk

Buczkó, M., *see* Csikai

Burgerjon, J. J. and W. Weidemann, The Pretoria cyclotron, Second Report 261

Butler, J. W., High-efficiency, long-lived vacuum cold trap 211

Csikai, J. and M. Buczkó, The effect of gamma-background on the BF_3 proportional counter 73

Day, P. Paul, *see* Melvin S. Freedman

Dési, S., *see* Nagy

Detenbeck, R. W., *see* J. B. Marion

De Vries, C. and A. H. Wapstra, A Siegbahn-Edvarson type ironfree doublefocusing beta-ray spectrometer 121

Ducros, G., *see* Sarazin

Dunaitzev, A. F., Yu. D. Prokoshkin and Tang Syao-Wei, π^-star detector 11

Eichholz, G. G., Continuous monitoring of uranium leach solutions 320

Eldridge, H. B., *see* Birkhoff

Engelhardt, H., I. Hauser and U. Krecker, Apparatus and laboratory for processing nuclear emulsion stacks. 55

Freedman, Melvin S., Frank Wagner, Jr., Fred T. Porter, John Terandy and Paul P. Day, Iron-free toroidal beta-beta coincidence spectrometer (Letter to the editor) 255

Gabathuler, E., *see* Lewis

Gandolfi, A., *see* Brini

Gat (Gutmann) J. R. and J. Gilat, A low background beta counter with a plastic scintillator anticoincidence shield 233

Giannelli, G. and L. Stanchi, Nonlinear operations on pulses by means of p-n junctions 79

Gilat, J., *see* Gat (Gutmann)

Gilboy, W. B., *see* Batchelor

Goulding, F. S., R. W. Nicholson and J. B. Waugh, A double-delay-line linear amplifier employing transistors I 272

Goulding, F. S. and R. A. McNaught, A transistorized fast-slow coincidence and pulse amplitude selecting system II 282

Gunnersen, E. M. and G. James, On the efficiency of the reaction $H^3(d,n)He^4$ in titanium tritide bombarded with deuterons. 173

Halbert, M. L. and J. L. Blankenship, Response of semiconductor suface-barrier counters to nitrogen ions and alpha particles 106

Haun, S. und D. Kamke, Ein universelles Verfahren zur Stabilisierung von Szintillations-Spektrometer-Anordnungen 331

Hauser, I., *see* Engelhardt

Hrehuss, G., A new method of mass discrimination . 344

James, G., *see* Gunnersen

Jech, A., *see* Bergström

Jongejans, B., *see* Tenner

Kamke, D., *see* Haun

Kohn, J. M., *see* Birkhoff

Krecker, U., *see* Engelhardt

Levesque, R. J. A., *see* J. B. Marion

Lewis, G. M., E. Gabathuler and R. E. Azuma, On the separation of π^+ mesons by a time of flight method 230

Luck, G., Zum Einfluss der Kristallform auf das energetische und zeitliche Auflösungsvermögen einer Szintillationsanordnung 249

Ludemann, C. A., *see* J. B. Marion

Marion, J. B., R. J. A. Levesque, C. A. Ludemann and R. W. Detenbeck, A. versatile, high efficiency 4π neutron detector 297

Mayer-Kuckuk, T. und R. Nierhaus, Über die Bestimmung der zufälligen Koinzidenzen in Schnell-Langsam-Koinzidenz-Anordnungen . . 76

McNaught, R. A., *see* Goulding

Moak, C. D., Space-charge effects in cylindrical beams with uniform acceleration 19

Mulot, P., R. Poussot, A. P. Schmitt et C. P. Zaleski, Appareil automatique pour la mesure des gradients locaux du flux de neutrons dans un réacteur 185

Nagy, L., *see* Nagy
Nagy, T., L. Nagy and S. Dési, Drift velocities of electrons in argon, nitrogen and argon mixtures 327
Nicholson, R. W., *see* Goulding
Nierhaus, R., *see* Mayer-Kuckuk

O'Conner, D. A., The theory and operation of the rotating crystal slow neutron chopper 244
Oselka, M., *see* Ramler

Parker, R. P., An improved anti-coincidence shield for use in low background counting 339
Parker, W., A method for the separation of gold irradiated mercury isotopes (Letter to the editor) 354
Perez, M., *see* Bergström
Persson, B., *see* v. Friesen
Porter, Fred T., *see* Melvin S. Freedman
Poussot, R., *see* Mulot
Prokoshkin, Yu. D., *see* Dunaitzev
Purnell, A. D. *see* Batchelor

Raimbault, P., *see* Sarazin
Ramler, W. J., J. L. Yntema and M. Oselka, Energy degrading-focusing of cyclotron beam 217
Ritchie, R. H. *see* Birkhoff
Rogers, Kenneth C., *see* Brucker
Rutherglen, J. G. and J. K. Walker, A scintillation counter system for the detection of positive and negative pions 239

Sakai, Mitsuo, Optimum conditions for double focusing beta ray spectrometers 61
Samueli, J., *see* Sarazin
Sarazin, A., J. Samueli, G. Ducros et P. Raimbault, Circuit allongeur d'impulsons rapides 70
Schmitt, A. P., *see* Mulot
Smith, P. B., *see* Braams
Smith, P. B., *see* Smulders
Smulders, P. J. M. and P. B. Smith, The Utrecht 850kV cascade generator. II. The beam integrator and galvanometer. 40
Smulkowski, O., *see* Amsel
Stanchi, L., *see* Giannelli

Stoker, P. H., On the construction and long-term performance of medium pressure BF_3 proportional counters used for cosmic-ray recording . 23

Tabellini, G. L., *see* Brini
Tang, Syao-Wei, *see* Dunaitzev
Tenner, A. G. C., B. Jongejans and H. Witteveld, An instrument facilitating the measurement of small-angle scattering in nuclear emulsion . . . 221
Terandy, John, *see* Melvin S. Freedman
Thieberger, P., *see* Bergström
Tiemeyer, J. C., A stabilizing system for a 700 kV cascade generator 117
Tochilin, E., and R. V. Alves, Neutron flux measurements from 100 keV to 4 MeV with a modified long counter 225
Tolk, Norman, H. and Robert M. Brugger, Calculated shapes for neutron bursts produced by phased chopper velocity selectors 203
Towle, J. H. *see* Batchelor

Van Bladel, J., Fields excited by beam currents in circular accelerators 1
Van de Graaff, R. J., Tandem electrostatic accelerators 195
v. Friesen, S. and B. Persson, An improved instrument for nuclear emulsion track photometry . 348

Wagner, Jr., Frank, *see* Melvin S. Freedman
Walker, J. K., *see* Rutherglen
Wapstra, A. H., *see* de Vries
Waugh, J. B. S., Bandwidths of the equal time-constant amplifier (Letter to the editor) 257
Waugh, J. B., *see* Goulding
Weidemann, W., *see* Burgerjon
Witteveld, H., *see* Tenner

Yntema, J. L., *see* Ramler

Zaccheroni, E., H. F. power meter for operation at 2.5 MW pulsed power 304
Zaleski, C. P., *see* Mulot

BOOK REVIEWS

Segré, E. (Editor), Experimental Nuclear Physics, Volume III (T. R. Gerholm) 258
Sommerville, J. L. (Editor), The Isotope Index, July 1959, International Edition (T. R. Gerholm) . . 258

SUBJECT INDEX

Accelerators and Reactors

Fields excited by beam currents in circular accelerators, J. VAN BLADEL 1
Space-charge effects in cylindrical beams with uniform acceleration, C. D. MOAK 19
The Utrecht 850 kV cascade generator I. Beam deflection and energy control, C. M. BRAAMS and P. B. SMITH . . . 27
The Utrecht 850 kV cascade generator II. The beam integrator and galvanometer, P. J. M. SMULDERS and P. B. SMITH 40
A stabilizing system for a 700 kV cascade generator, J. C. TIEMEYER 117
Appareil automatique pour la mesure des gradients locaux du flux de neutrons dans un réacteur, P. MULOT, R. POUSSOT, A. P. SCHMITT et C. P. ZALESKI 185
Tandem electrostatic accelerators, R. J. VAN DE GRAAFF 195
Energy degrading-focusing of cyclotron beam, W. J. RAMLER, J. L. YNTEMA and M. OSELKA 217
The Pretoria cyclotron, Second Report, J. J. BURGERJON and W. WEIDEMANN 261
H.F. power meter for operation at 2.5 MW pulsed power, E. ZACCHERONI 304
Continuous monitoring of uranium leach solutions, G. G. EICHHOLZ 320

Detectors

π-star detector, A. F. DUNAITZEV, YU D. PROKOSHKIN and TANG SYAO-WEI 11
On the construction and long-term performance of medium pressure BF_3 proportional counters used for cosmic-ray recording, P. H. STOKER 23
The effect of gamma-background on the BF_3 proportional counter, J. CSIKAI and M. BUCZKÓ 73
Détecteur de particules lourdes a jonction n-p au silicium, G. AMSEL, P. BARUCH et O. SMULKOWSKI 92
Response of semiconductor surface-barrier counters to nitrogen ions and alpha particles, M. L. HALBERT and J. L. BLANKENSHIP 106
Neutron flux measurements from 100 keV to 4 MeV with a modified long counter, E. TOCHILIN and R. V. ALVES . 225
A low background beta counter with a plastic scintillator anticoincidence shield, J. R. GAT (GUTMANN) and J. GILAT 233
A scintillation counter system for the detection of positive and negative pions, J. G. RUTHERGLEN and J. K. WALKER 239
Zum Einfluss der Kristallform auf das energetische und zeitliche Auflösungsvermögen einer Szintillationsanordnung, G. LUCK 249
A versatile, high efficiency 4π neutron detector, J. B. MARION, R. J. A. LEVESQUE, C. A. LUDEMANN and R. W. DETENBECK 297
Drift velocities of electrons in argon, nitrogen and argon mixtures, T. NAGY, L. NAGY and S. DÉSI 327

Instruments and Methods for Nuclear Spectroscopy

Optimum conditions for double focusing beta ray spectrometers, MITSUO SAKAI 61
A Siegbahn-Edvarson type ironfree double focusing beta-ray spectrometer, C. DE VRIES and A. H. WAPSTRA . . . 121
Improvements in the fast neutron time of flight technique using pulse shape discrimination in an organic phosphor, R. BATCHELOR, W. B. GILBOY, A. D. PURNELL and J. H. TOWLE 146
The oscilloscope method of measuring nuclear half-lives, I. BERGSTRÖM, E. C. O. BONACALZA, A. JECH, M. PEREZ and P. THIEBERGER 151
Calculated shapes for neutron bursts produced by phased chopper velocity selectors, NORMAN H. TOLK and ROBERT M. BRUGGER 203
On the separation of π^+ mesons by a time of flight method, G. M. LEWIS, E. GABATHULER and R. E. AZUMA . . . 230
The theory and operation of the rotating crystal slow neutron chopper, D. A. O'CONNOR 244
The spherical condenser as a high transmission particle spectrometer II. Disc source, R. D. BIRKHOFF, J. M. KOHN, H. B. ELDRIDGE and R. H. RITCHIE 313
Ein universelles Verfahren zur Stabilisierung von Szintillations-Spektrometer-Anordnungen, S. HAUN und D. KAMKE 331
An improved anti-coincidence shield for use in low background counting, R. P. PARKER 339
A new method of mass discrimination, G. HREHUSS 344

Instruments and Methods for High Energy Physics

On the construction and long-term performance of medium pressure BF_3 proportional counters used for cosmic-ray recording, P. H. Stoker 23
Apparatus and laboratory for processing nuclear emulsions stacks, H. Engelhardt, I. Hauser and U. Krecker 55
An instrument facilitating the measurement of small-angle scattering in nuclear emulsion, A. G. C. Tenner, B. Jongejans and H. Witteveld 221
An improved instrument for nuclear emulsion track photometry, S. v. Friesen and B. Persson 348

Letters to the Editor

Iron-free toroidal beta-beta coincidence spectrometer, Melvin, S. Freedman, Frank Wagner, Jr., Fred T. Porter, John Terandy and Paul, P. Day 255
Bandwidths of the equal time-constant amplifier, J. B. S. Waugh 257
A method for the separation of gold irradiated mercury isotopes, W. Parker 354

News Items

Accelerator Conference, sponsored by High Voltage Engineering Corporation, Amsterdam, Octorber 4–6, 1960 . . 259
Seminaire Internationale, International Seminar, organized by Institut Belge de Regulation et d'Automatisme, Brussels, November 21–23, 1960 260

Nuclear Electronics

Transistorized apparatus for accumulation and binary-decimal conversion, D. Brini, A. Gandolfi and G. L. Tabellini 46
Circuit allongeur d'impulsions rapides, A. Sarazin, J. Samueli, G. Ducros et P. Raimbault 70
Über die Bestimmung der zufälligen Koinzidenzen in Schnell-Langsam-Koinzidenz-Anordnungen, T. Mayer-Kuckuk und R. Nierhaus 76
Nonlinear operations on pulses by means of p-n junctions, G. Giannelli and L. Stanchi 79
A double-delay-line linear amplifier employing transistors I, F. S. Goulding, R. W. Nicholson and J. B. Waugh 272
A transistorized fast-slow coincidence and pulse amplitude selecting system II, F. S. Goulding and R. A. McNaught 282

Miscellaneous

On the efficiency of the reaction $H^3(d,n)He^4$ in titanium tritide bombarded with deuterons, E.M. Gunnersen and G. James 173
High-efficiency, long-lived vacuum cold trap, J. W. Butler 211
A kilovolt, kiloampere low pressure switch, George J. Brucker and Kenneth C. Rogers 236